



Black, Hannah Lucy (2016) *Impact of tyrosine phosphorylation of Syntaxin 4 and Munc18c on GLUT4 translocation*. PhD thesis.

<http://theses.gla.ac.uk/8181/>

Copyright and moral rights for this work are retained by the author

A copy can be downloaded for personal non-commercial research or study, without prior permission or charge

This work cannot be reproduced or quoted extensively from without first obtaining permission in writing from the author

The content must not be changed in any way or sold commercially in any format or medium without the formal permission of the author

When referring to this work, full bibliographic details including the author, title, awarding institution and date of the thesis must be given

Enlighten:Theses
<http://theses.gla.ac.uk/>
theses@gla.ac.uk

Impact of tyrosine phosphorylation of Syntaxin 4 and Munc18c on GLUT4 translocation

Hannah Lucy Black

BSc (Hons) MSc

Thesis submitted in fulfilment of the requirements for the Degree of

Doctor of Philosophy

September 2016

Institute of Molecular, Cell and Systems Biology

College of Medical, Veterinary and Life Sciences

University of Glasgow

Abstract

Insulin is an important regulator of glucose homeostasis. Insulin stimulation of fat and muscle cells results in the rapid translocation of the glucose transporter GLUT4 to the plasma membrane from its intracellular stores, allowing uptake of glucose into the cells from the blood. This tethering, docking and fusion event is driven by the formation of a SNARE complex at the plasma membrane consisting of the t-SNAREs Syntaxin 4 (Sx4) and SNAP23 and the v-SNARE VAMP2. The formation of this complex is regulated by the SM protein Munc18c. It has been shown that Sx4 is phosphorylated at residues Y115 and Y251 following insulin stimulation; however the effects of these phosphorylation events have yet to be studied. In addition phosphorylation of Y521 in Munc18c is also increased following insulin stimulation. This study aimed to first elucidate the effects of Sx4 phosphorylation on SNARE protein interactions and GLUT4 trafficking, then to begin to examine the impact of phosphorylation of both Sx4 and Munc18c.

I have used an *in vitro* approach to assess the affect Sx4 phosphorylation has on SNARE complex assembly. I have shown, using phospho-mimetic recombinant proteins, that the phosphorylation state of Sx4 affects the rate of SNARE complex assembly and its binary interactions with VAMP2 and SNAP23. Moreover, that this may be due to a conformational change in the protein. I have also shown, for the first time, that it is likely that Sx4 can be phosphorylated on Y115 and Y251 simultaneously. In addition I have used a HA-GLUT4-GFP expressing HeLa cell line to show that expression of phospho-mimetic Sx4 increases translocation of GLUT4 to the PM under basal conditions. Finally, I have begun to investigate the implications of both Sx4 and Munc18c phosphorylation on their *in vitro* interactions. This data provides insights into the direct regulation of membrane trafficking proteins by the insulin-signalling pathway. Increased understanding of the regulation of GLUT4 translocation could help to develop future therapies for type 2 diabetes, where GLUT4 trafficking is impaired.

Table of contents

Abstract	2
Table of contents	3
List of tables	9
List of figures	10
Acknowledgements	13
Author's Declaration	14
Abbreviations	15
1 Introduction	18
1.1 Membrane trafficking	18
1.1.1 The endocytic and secretory pathways.....	18
1.2 Membrane fusion	19
1.2.1 Vesicle tethering and docking.....	19
1.2.2 Membrane fusion.....	19
1.3 SNARE proteins and the SNARE hypothesis	20
1.3.1 The SNARE hypothesis.....	20
1.3.2 The SNARE core complex.....	22
1.3.3 Classification of SNARE proteins	25
1.3.3.1 Syntaxin family.....	25
1.3.3.2 SNAP family.....	27
1.3.3.3 VAMP family	28
1.3.4 Non-mammalian SNARE proteins	29
1.4 Regulation of SNARE-mediated membrane fusion	30
1.4.1 Sec1/Munc18 (SM) proteins	30
1.4.1.1 Interaction of Munc18 and syntaxin.....	31

1.4.2 Rab proteins.....	35
1.4.3 Tethering proteins and complexes.....	35
1.4.4 Phosphorylation.....	36
1.4.5 NSF and α -SNAP – SNARE complex disassembly.....	37
1.5 Glucose transport.....	38
1.5.1 Glucose homeostasis and type II diabetes mellitus	38
1.5.2 Glucose transporters and GLUT4.....	39
1.5.3 Insulin signalling	40
1.5.3.1 The PI3K pathway.....	40
1.5.3.2 The APS signalling pathway	41
1.5.4 The GLUT4 trafficking itinerary.....	42
1.5.4.1 GLUT4 storage vesicles.....	44
1.5.5 SNARE proteins in GLUT4 translocation	46
1.5.5.1 Sx4	47
1.5.5.2 SNAP23.....	48
1.5.5.3 VAMP2	48
1.5.6 Regulation of SNARE mediated GLUT4 trafficking	49
1.5.6.1 Munc18c.....	49
1.5.6.2 Synip.....	51
1.5.6.3 Tomosyn.....	51
1.5.6.4 AS160.....	51
1.5.6.5 Phosphorylation of Sx4 and Munc18c.....	52
1.6 Aims.....	56
2 Materials and Methods	58
2.1 Materials	58

2.1.1 General reagents.....	58
2.1.2 Solutions	59
2.1.3 Primary antibodies.....	62
2.1.4 Secondary antibodies	63
2.1.5 Mammalian cell lines	63
2.1.6 <i>E. coli</i> strains.....	63
2.1.7 Plasmids.....	64
2.1.8 Primers.....	66
2.2 General Molecular Biology Techniques	67
2.2.1 Small scale preparation of plasmid DNA	67
2.2.2 Large scale preparation of plasmid DNA	67
2.2.3 Agarose gel electrophoresis	67
2.2.4 PCR	68
2.2.5 Restriction endonuclease reactions	69
2.2.6 DNA ligase reactions	70
2.3 General Protein Techniques	71
2.3.1 Bacterial transformation.....	71
2.3.2 General expression and purification of recombinant proteins.....	71
2.3.3 Purification of GST-tagged proteins.....	72
2.3.4 Purification of His-tagged proteins	72
2.3.5 Purification of proteins with cleavable GST tags	72
2.3.6 Estimating protein concentration	73
2.3.7 SDS-PAGE.....	73
2.3.8 Coomassie staining and destaining	73
2.3.9 Semi-dry transfer	73

2.3.10 Immunoblotting.....	74
2.4 Complex Assembly Assay	74
2.5 Pull down assays with recombinant proteins.....	75
2.6 Chymotrypsin Assay	75
2.7 CIRK phosphorylation assay	75
2.8 Phos-tag based mobility shift SDS-PAGE.....	76
2.9 General cell culture techniques	76
2.9.1 Growth of HeLa cells	76
2.9.2 Growth of 3T3-L1 cells	77
2.9.3 Passage of cells	77
2.9.4 Freezing of cells	77
2.9.5 Resurrection of cells.....	78
2.9.6 Transfections.....	78
2.9.7 Differentiation of 3T3-L1 cells.....	78
2.9.8 Insulin stimulation of HeLa cells and adipocytes.....	79
2.10 Immunofluorescence	79
2.11 Generating mammalian cell lysates.....	80
2.12 Quantification of HA-GLUT4-GFP translocation by flow cytometry.....	80
2.13 Generating a CRISPR knockout cell line.....	81
2.14 Surface plasmon resonance	82
3 <i>In vitro</i> analyses of phospho-mimetic Sx4.....	85
3.1 Introduction.....	85
3.1.1 Regulation of GSV fusion at the plasma membrane	85
3.1.2 Phosphorylation as a regulator of SNARE proteins	86
3.2 Aims of this chapter	87

3.3 Results	88
3.3.1 Expression and purification of recombinant SNARE proteins.....	88
3.3.2 <i>In vitro</i> SNARE complex assembly assay	92
3.3.3 Limited proteolysis of Sx4 phospho-mimetic mutants	94
3.3.4 Investigating the binary interactions between Sx4 phospho-mimetic mutants and SNAP23/VAMP2 using <i>in vitro</i> pull down assays.....	98
3.3.5 Investigating the binary interactions between Sx4 phospho-mimetic mutants and SNAP23/VAMP2 using surface plasmon resonance (SPR).....	103
3.3.6 Analysing the phosphoprotein isoforms of CIRK phosphorylated Sx4.....	110
3.4 Discussion	118
4 Analyses of the effects of phospho-mimetic Sx4 on GLUT4 translocation	123
4.1 Introduction	123
4.1.1 Regulation of GLUT4 translocation.....	123
4.1.2 Cell systems used to study GLUT4 translocation.....	124
4.2 Aims of this chapter	125
4.3 Results	127
4.3.1 Characterising a Myc tagged Sx4 construct.....	127
4.3.2 The effect of Sx4(Myc) phospho-mimetic mutants on GLUT4 translocation in HeLa cells.....	131
4.3.3 Quantification of HA-GLUT4-GFP translocation in HeLa cells by flow cytometry	135
4.3.4 Generating Sx4 knockout 3T3 cell lines using CRISPR-Cas9 technology.....	141
4.3.5 Characterising Sx4 CRISPR knockout 3T3-L1 cell lines	146
4.4 Discussion	149
5 In vitro analyses of the interactions of phospho-mimetic Sx4 and Munc18c	154
5.1 Introduction	154
5.1.1 SM proteins	154

5.1.2 Sx4 and Munc18c interaction	154
5.1.3 Munc8c phosphorylation.....	155
5.2 Aims of this chapter	156
5.3 Results.....	156
5.3.1 Purification of His tagged Munc18c	156
5.3.2 The effect of Sx4 and Munc18c phospho-mimetic mutants on SNARE complex assembly.....	158
5.3.3 Binary interactions of phosphomimetic Sx4 and Munc18c	160
5.4 Discussion	162
6 Discussion	166
6.1 Discussion of results.....	166
6.2 Proposed model and future work	171
Appendix I: Summary of purified recombinant proteins used in this study.....	175
Appendix II: Raw SPR data	176
Appendix III: Raw data from flow cytometry analysis of cell surface HA-GLUT4-GFP antibody titration	179
Appendix IV: Raw data of the flow cytometry analysis of the effect of overexpressing Sx4 on cell surface HA-GLUT4-GFP levels	181
List of References.....	183

List of tables

Table 2.1: Primary antibodies used in this study	62
Table 2.2: Secondary antibodies used in this study	63
Table 2.3: Mammalian cell lines used in this study	63
Table 2.4: <i>E. coli</i> strains used in this study	63
Table 2.5 Summary of plasmids used in this study	64
Table 2.6: Oligonucleotides used in this study	66
Table 2.7: Transfection conditions	78
Table I: Summary of purified recombinant proteins used in this study.....	175
Table II Summary of K_D values of Sx4 binding to VAMP2/SNAP23 obtained by SPR	178

List of figures

Figure 1.1 Intracellular localisation of mammalian SNARE proteins in the secretory and endocytic pathways	21
Figure 1.2 The SNARE hypothesis	22
Figure 1.3 Structure of the SNARE core complex	24
Figure 1.4 Syntaxin proteins undergo a conformational shift	27
Figure 1.5 General domain structures of SNARE proteins	29
Figure 1.6 Binding modes of Munc18 to syntaxins	34
Figure 1.7 The insulin signalling cascade.....	42
Figure 1.8 A model of the GLUT4 trafficking itinerary.....	44
Figure 1.9: Sequence alignments of regions of selected Syntaxins and SM proteins	54
Figure 1.10: Predicted locations of the residues in Sx4 and Munc18c that are phosphorylated in response to insulin	55
Figure 3.1: Expression and purification of Sx4.	90
Figure 3.2: Expression and purification of Sx4 SNARE complex components.....	91
Figure 3.3: Sx4-Y115,251E forms more SNARE complex than Sx4-WT.	93
Figure 3.4: Phospho-mimetic Sx4 shows increased sensitivity to proteolysis when compared to WT.....	96
Figure 3.5: Sx4-Y115E and Sx4-Y115,251E show comparable sensitivity to limited proteolysis to the Sx4 open mutant.	97
Figure 3.6: Phosphomimetic Sx4 mutants bind more SNAP23 than WT Sx4.	99
Figure 3.7: Purification of thrombin cleaved VAMP2	100
Figure 3.8: Phosphomimetic Sx4 mutants show increased binding to VAMP2 compared to WT.....	102
Figure 3.9: Schematic of SPR ligand immobilisation and analyte binding.....	104
Figure 3.10: Sx4-WT and phospho-mutants binding to VAMP2 by SPR	106
Figure 3.11: Sx4-WT and phospho-mutants binding to SNAP23 by SPR	108

Figure 3.12: Summary of binding of Sx4 to SNAP23 and VAMP2 by SPR	109
Figure 3.13 Structure of acylamide-pendant Phos-tag ligand	111
Figure 3.14: Sx4-GST is phosphorylated by CIRK <i>in vitro</i>	114
Figure 3.15: Migration of Sx4-GST phospho-mimetic mutants is comparable to WT on Phos-tag SDS-PAGE gel	115
Figure 3.16: <i>In vitro</i> phosphorylated Sx4 is phosphorylated at more than one residue.....	117
Figure 4.1 Sx4(Myc) characterisation.....	129
Figure 4.2: Expression of Sx4(Myc) in HeLa cells	130
Figure 4.3: Insulin stimulates GLUT4 translocation in HeLa cells	132
Figure 4.4 Effect of Sx4 phosphomutant over expression in HA-GLUT4-GFP HeLa cells	134
Figure 4.5 Quantification of HA-GLUT4-GFP translocation in HeLa cells by flow cytometry	136
Figure 4.6 Expression of Sx4 phospho-mutants increases cell surface GLUT4	139
Figure 4.7 Histograms showing increase in basal cell surface GLUT4 in Sx4 phospho-mutant expressing HA-GLUT4-GFP HeLa cells	140
Figure 4.8 3T3-L1 and HA-GLUT4-GFP 3T3-L1 fibroblasts are successfully transfected	142
Figure 4.9 Fluorescence-activated cell sorting of CRISPR-Cas9 transfected 3T3-L1 cells	144
Figure 4.10 Immunoblots of 3T3-L1 Sx4 CRISPR knockout cell lines.....	145
Figure 4.11 Differentiation of Sx4 knockout 3T3-L1 fibroblasts to adipocytes	147
Figure 4.12 HA-GLUT4-GFP does not translocate to the cell surface in insulin-stimulated cells depleted of Sx4.....	148
Figure 5.1: Expression and purification of His-Munc18c.....	157
Figure 5.2 Sx4-Y115,251E pre-incubated with Munc18c-WT or -Y521E forms more SNARE complex than Sx4-WT	159
Figure 5.3 Sx4-WT pulls down more Munc18c than Sx4 phospho-mimetic mutants	161

Figure 6.1: Proposed model of the effects of insulin stimulated Sx4 phosphorylation at Y115 and Y251	171
Figure II.1 Raw data showing repeats of Sx4 binding to SNAP23 by SPR.....	176
Figure II.2 Raw data showing repeats of Sx4 binding to VAMP2 by SPR	177
Figure III.1 Summary of raw data from analysis of antibody titration of cell surface HA-GLUT4-GFP by flow cytometry	180
Figure IV.1 Summary of quantification of basal cell surface HA-GLUT4-GFP in cells expressing Sx4(Myc) phospho-mimetic mutants by flow cytometry	181
Figure IV.2 Summary of quantification of cell surface HA-GLUT4-GFP in insulin-stimulated cells expressing Sx4(Myc) phospho-mimetic mutants by flow cytometry	182

Acknowledgements

Firstly I would like to thank my supervisors Prof. Nia Bryant and Prof. Gwyn Gould for their guidance, understanding and support throughout the project. Thank you also to all the members of lab 241 in Glasgow and the cell biology labs in York for all your help. Thanks to Dr Dimitrios Kioumourtzoglou for helping me to get started and for always being interested in a chat about the project. I would also like to thank Dr Dani Ungar for his scientific advice.

Thank you to all my family and friends. I am especially grateful to my parents for their unwavering encouragement. Henry, thank you for your constant love and support.

Finally, I would like to thank the BBSRC for funding the project.

Author's Declaration

I declare that the work presented in this thesis is my own, unless otherwise cited or acknowledged. It is entirely of my own composition and has not, in whole or in part, been submitted for any other degree.

Hannah Lucy Black

September 2016

Abbreviations

(v/v)	Units volume per unit volume
(w/v)	Units weight per unit volume
°C	Degrees Celsius
~	Approximately
ADP	Adenosine diphosphate
Amp	Ampicillin
APS	Ammonium persulfate
AS160	Akt substrate of 160 kilodaltons
ATP	Adenosine 5'-triphosphate
bp	DNA base pair(s)
BSA	Bovine serum albumin
CAP	c-Cbl associated protein
dH ₂ O	Distilled water
DMEM	Dulbecco's modified Eagle's medium
DMSO	Dimethyl sulphoxide
DNA	Deoxyribonucleic acid
DNase I	Deoxyribonuclease I
dNTP	Deoxynucleoside (5')-triphosphate
<i>E. coli</i>	Escherichia coli
ECL	Enhanced chemiluminescence
EDTA	Ethylenediaminetetraacetic acid
ER	Endoplasmic reticulum
FBS	Foetal bovine serum
FRET	Förster resonance energy transfer
g	Gram
GDP	Guanosine-5'-diphosphate
GFP	Aequorea victoria green fluorescent protein
GLUT	Glucose transporter
GST	Glutathione S transferase
GSV	GLUT4 storage vesicle
GTP	Guanosine-5'-triphosphate
HA	Influenza haemagglutinin epitope tag
HCl	Hydrochloric acid
HEPES	2-[4-(2-Hydroxyethyl)-1-piperazine] ethanesulfonic acid
His	Six-histidine residue tag
HRP	Horse radish peroxidase
IB	Immunoblot
IF	Immunofluorescence
IgG	Immunoglobulin G
IP	Immunoprecipitation
IPTG	Isopropyl-β-D-thiogalactopyranoside
IR	insulin receptor
IRAP	insulin receptor-associated protein
IRS	insulin receptor substrate
Kan	Kanamycin
k	Kilo (prefix)
kb	Kilobase
kDa	Kilo daltons
L	Litre
LSB	Laemmli's sample buffer
m	Milli (prefix)
M	Molar
M18c	Munc18c

mA	Milliamp
mg	Milligram
min	Minute
ml	Millilitre
n	Nano (prefix)
N-terminal	Amino terminal
NCS	New-born calf serum
Ni-NTA	Nickel-nitrilotriacetic acid
NSF	N-ethylmaleimide sensitive factor
OD600	Optical density 600
p	Pico (prefix)
PAGE	Polyacrylamide gel electrophoresis
PBS	Phosphate buffered saline
PBS-T	Phosphate buffered saline plus Tween-20
PCR	Polymerase chain reaction
PFA	Paraformaldehyde
Pfu	Pyrococcus furiosus
PH	Pleckstrin homology domain
PI	Phosphatidylinositol
PI3K	Phosphatidylinositol 3-kinase
PIP2	Phosphatidylinositol 4,5-bisphosphate
PIP3	Phosphatidylinositol 3,4,5-triphosphate
PKB	Protein kinase B/Akt
PKC	Protein kinase C
PLA	Proximity ligation assay
PM	Plasma membrane
PMSF	Phenylmethylsulfonyl fluoride
psi	Pounds per square inch
RNA	Ribonucleic acid
rpm	Rotations per minute
<i>S. cerevisiae</i>	<i>Saccharomyces cerevisiae</i>
SDS	Sodium dodecyl sulfate
SDS-PAGE	Sodium dodecyl sulphate- polyacrylamide gel electrophoresis
SH2	Src homology 2
siRNA	Short interfering ribonucleic acid
SM	Sec1/Munc18
SNAP	Soluble NSF attachment protein
SNARE	Soluble NSF attachment protein receptor
SOC	Super Optimal Broth
Sx	Syntaxin
t-SNARE	Target SNARE
TAE	Tris acetate EDTA
Taq	<i>Thermus aquaticus</i>
TB	Terrific broth
TEMED	N, N, N', N' - tetramethylethylenediamine
TGN	<i>Tran</i> -Golgi network
TIRF	Total internal reflection fluorescent
Tris	2-Amino-2-(hydroxymethyl)-1,3-propanediol
Tween-20	Polyoxyethylene sorbitan monolaurate
v-SNARE	Vesicle SNARE
VAMP	Vesicle associated membrane protein
X-Gal	(5-bromo-4-chloro-3-indolyl-b-D-galacto-pyranoside) Yellow
μ	Micro (prefix)

Chapter One

Introduction

1 Introduction

1.1 Membrane trafficking

Eukaryotic cells are compartmentalised into a series of membrane bound organelles. These organelles consist of specific sets of proteins and other molecules and they are highly spatially and temporally regulated. Eukaryotes rely on membrane trafficking in order to regulate the functions of the cell and the organelles within it (Dacks and Field, 2007). There are two main types of membrane trafficking pathways that cells rely on: the endocytic and secretory pathways.

1.1.1 The endocytic and secretory pathways

Extracellular and plasma membrane (PM) proteins are internalised into cells by endocytosis. Defined regions of the PM invaginate and pinch off to form endocytic vesicles (Parkar et al., 2009). Proteins in the endocytic vesicles are then sorted in the early endosome where many of the vesicles are recycled back to the PM - thus maintaining and regulating the composition of the plasma membrane (Grant and Donaldson, 2009). Proteins that are not recycled are then transported to the lysosome, where they are degraded, or to late endosomes and the *trans*-Golgi network (Van Vliet et al., 2003).

In a seminal study, over 40 years ago, it was shown that newly synthesised proteins that were to be secreted first pass through a series of organelles; the endoplasmic reticulum (ER), Golgi apparatus and secretory vesicles (Palade, 1975). This corresponds to what is now termed the secretory or exocytic pathway. There are two types of secretory pathways – constitutive and regulated. The former delivers newly synthesised proteins to the PM via the Golgi apparatus in a constitutive manner. In the latter, proteins are stored in specialised secretory vesicles that are mobilised to their site of action, typically in response to an extracellular signal. Regulated exocytic events are mainly found in cells

specialised in secreting molecules such as hormones and neurotransmitters (Van Vliet et al., 2003).

1.2 Membrane fusion

Membrane trafficking relies on the formation of vesicles from a 'donor' compartment and their subsequent fusion with an 'acceptor' compartment. The process can involve two similar (homotypic) or two different (heterotypic) compartments. In order for the contents of these vesicles to be successfully delivered to their target membrane fusion must occur to allow for content and membrane lipid mixing of donor and acceptor compartments. The process of membrane fusion involves several distinct steps; tethering, docking and finally fusion. It is imperative that the correct donor vesicles fuse with the correct acceptor membranes and so the process is subject to multiple stages of regulation.

1.2.1 Vesicle tethering and docking

Prior to membrane fusion, vesicles are tethered to the appropriate membrane by often far-reaching tethering proteins or complexes (Dubuke and Munson, 2016) (discussed in more detail in section 1.4.3). The vesicles are then brought closer together into a more tightly bound docked state. It is thought these tethering and docking proteins represent an important point of regulation on membrane fusion (Pfeffer, 1999).

1.2.2 Membrane fusion

Membrane fusion occurs when two separate lipid bilayers come into close contact and fuse to become one lipid bilayer. Complete membrane fusion is now thought to occur via a hemifusion intermediate state (Chernomordik and Kozlov, 2003). The hemifusion hypothesis states that the two outer monolayers of compartments fuse, leaving the two inner monolayers of the compartments intact. A fusion pore then forms and complete fusion occurs, i.e. the inner monolayers fuse. More work is still needed on understanding the biophysical aspects of membrane fusion. The process is not energetically favourable

and so research into how the cells overcome energy barriers to allow fusion in of great importance (Weber et al., 1998). One family of proteins known to participate in nearly all membrane fusion events, and thought to be crucial to overcoming this energy barrier, are SNARE proteins. Indeed in an *in vitro* assay recapitulating membrane fusion, SNARE-mediated fusion was shown to transit through a hemifusion intermediate state (Xu et al., 2005).

1.3 SNARE proteins and the SNARE hypothesis

SNARE proteins are involved in all known membrane fusion events (Malsam et al., 2008). SNAREs were first identified in studies that sought to define membrane trafficking events using both genetic and biochemical approaches. NSF (N-ethylmaleimide Sensitive Factor) was first identified (Glick and Rothman, 1987) and found to be required for membrane fusion (Beckers et al., 1989; Diaz et al., 1989; Malhotra et al., 1988). Subsequently, NSF's binding partner α -SNAP (Soluble NSF Attachment protein) was discovered (Clary et al., 1990). Characterisation of these two proteins led to the discovery of SNARE proteins. An affinity column containing both NSF and α -SNAP was used to isolate binding partners from bovine brain lysates (Söllner et al., 1993). Four 'SNAP-receptors' (SNARE) proteins were identified, all of which localised to the synapse. These discoveries led to the hypothesis that the proteins were components of a universal fusion apparatus.

1.3.1 The SNARE hypothesis

Following the identification of the aforementioned SNARE proteins from bovine brain lysates, much research has been carried out in identifying more SNAREs. To date 36 SNARE proteins have been identified in *Homo sapiens* (Malsam et al., 2008). Furthermore, genome sequencing projects have unveiled SNARE proteins are a conserved family, with homologues in all eukaryotes (Bock et al., 2001). SNARE proteins are broadly split into two categories - t-SNAREs, which are present on the target membrane, and v-SNAREs, present on the donor vesicle membrane. The localisation of

SNARE proteins is thought to enhance fusion specificity and influence their function (Chen and Scheller, 2001). Figure 1.1 summarises the localisation of SNARE proteins in the secretory and endocytic pathways.

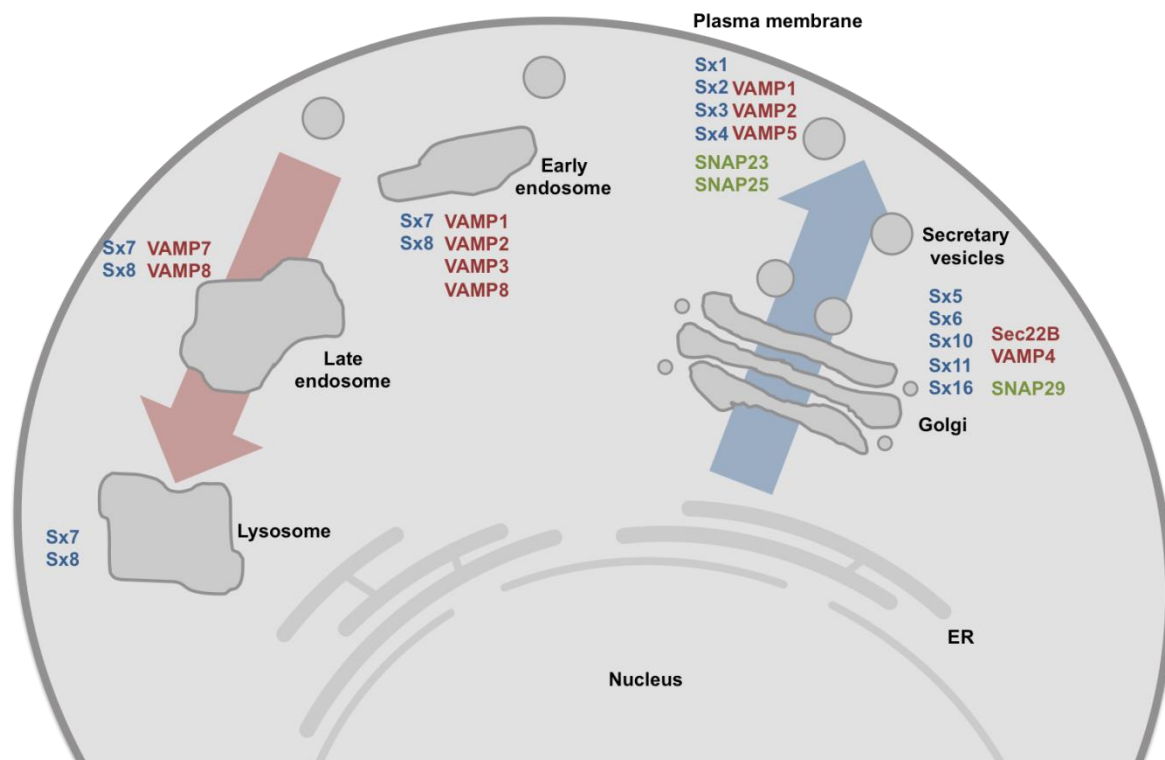


Figure 1.1 Intracellular localisation of mammalian SNARE proteins in the secretory and endocytic pathways

Schematic of the localisation of SNARE proteins in the secretory and endocytic pathways. Blue = syntaxin family members, green = SNAP family members, red = VAMP family members. Blue arrow represents the secretory pathway. Proteins are trafficked through the Golgi apparatus, *trans*-Golgi network and secretory vesicles. Red arrow represents the endocytic pathway. Proteins are endocytosed from the plasma membrane through early and late endosomes, and often to the lysosome where they are degraded.

The discovery of multiple SNARE proteins has led to the development of the SNARE hypothesis (Söllner et al., 1993). The SNARE hypothesis states that specific SNARE proteins from both donor and acceptor membranes form a complex that mediates docking of the membranes and leads to membrane fusion (Figure 1.2). The specificity of SNARE proteins has since been called into question as they have been shown to be promiscuous *in vitro* (Gagescu, 2000). However a study by McNew and colleagues in 2000

demonstrated that, when yeast SNARE proteins were reconstituted into liposomes only 5, out of a possible 33 combinations, resulted in fusion (McNew et al., 2000).

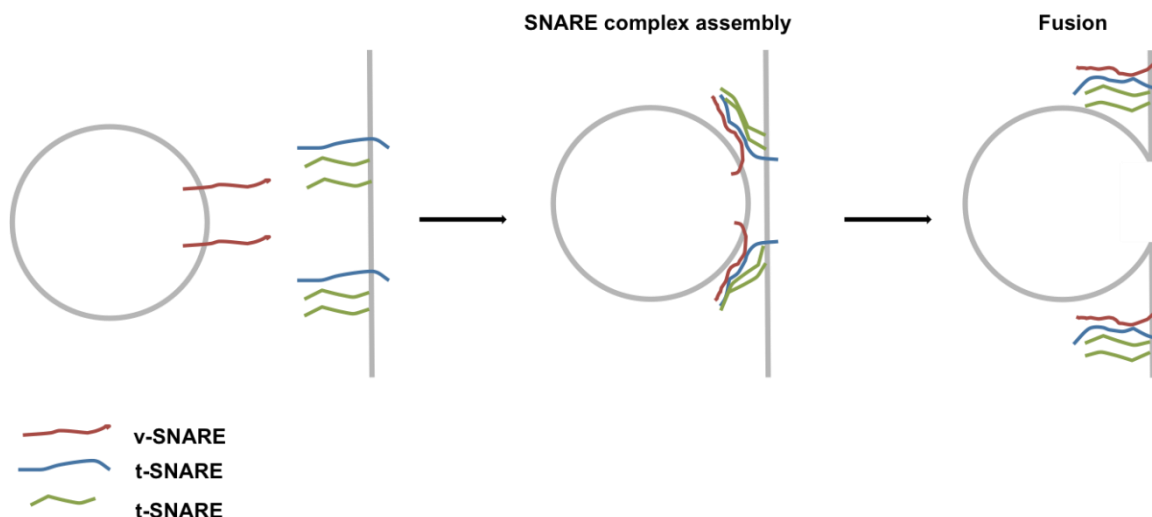


Figure 1.2 The SNARE hypothesis

A schematic of the SNARE hypothesis. V-SNAREs on the donor membrane come into close proximity to t-SNAREs on the target membrane. The proteins form the *trans*-SNARE complex, where the two families of SNARE proteins are on opposing membranes, providing the energy required for membrane fusion. Following fusion SNARE proteins remain in the *cis*-SNARE complex on the same membrane until the complex is dismantled.

1.3.2 The SNARE core complex

The SNARE complex is a helical bundle of four SNARE domains, three from t-SNAREs and one from the respective v-SNARE (Poirier et al., 1998a) (Figure 1.2). However since SNARE proteins are involved in homotypic fusion, fusion of two compartments of the same type, a more sophisticated classification system was required. SNARE proteins were therefore subsequently classified by the highly conserved structural features that contribute to the core SNARE complex (Fasshauer et al., 1998). SNAREs were therefore then categorised as Q- or R-SNAREs.

The SNARE complex formed by Sx1a, SNAP25 and VAMP2 is the most thoroughly characterised complex to date. In 1998, Sutton and colleagues reported the structure of this SNARE complex using x-ray crystallography at 2.4 Å resolution (Sutton et al., 1998). The structure revealed a highly twisted four helical bundle with an ionic layer at the centre comprised of one arginine and three glutamine residues from each of the four helices (Figure 1.3). Comparisons of sequences and subsequent structural analysis of the endosomal core SNARE complex consisting of syntaxin 7, syntaxin 8, vti1b and VAMP-8 suggests the core structure is a conserved assembly of SNARE complexes (Antonin et al., 2002).

The interactions of the SNARE complex have been shown to be extremely strong. The complexes are resistant to proteases, SDS and to cleavage by clostridial neurotoxin (Hayashi et al., 1994; Poirier et al., 1998b). In contrast to syntaxins, SNAP and VAMP proteins are unstructured prior to SNARE complex formation (Fasshauer et al., 1997). Circular dichroism (CD) analysis shows an increase in α -helicity and stability of the proteins upon assembly of SNARE complexes. It is thought this change from unstructured peptides to a highly-structured tightly packed complex is an energetically favourable process that assists in overcoming the energy barrier required for membrane fusion (Fasshauer et al., 1997).

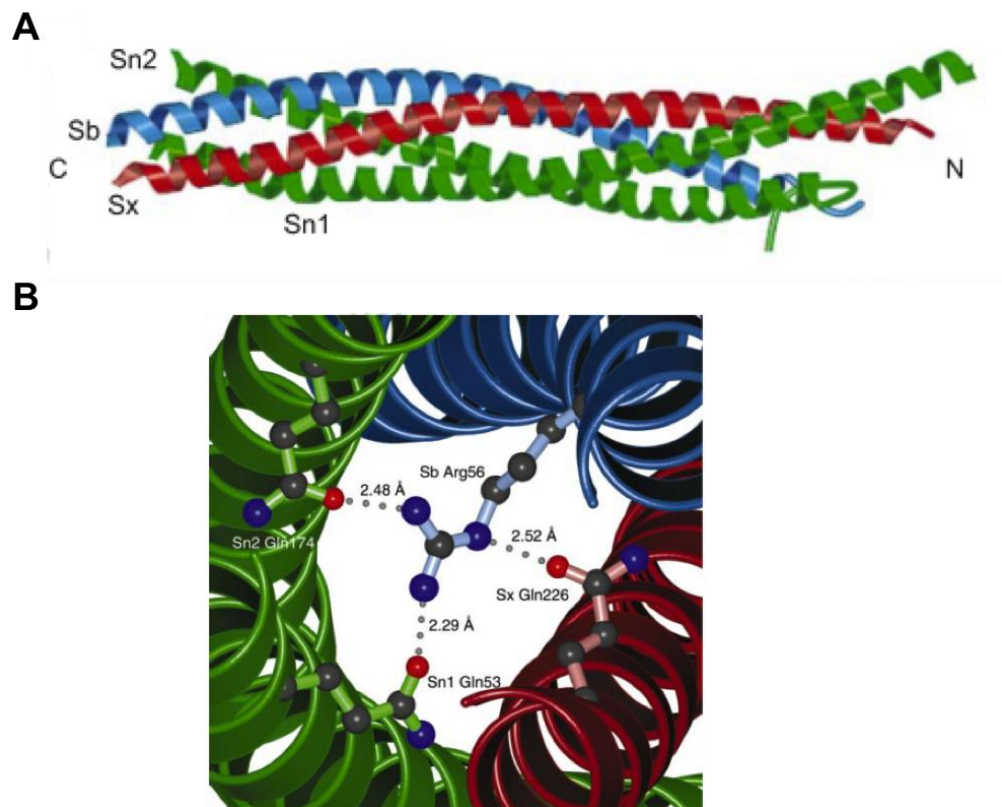


Figure 1.3 Structure of the SNARE core complex

A Ribbon drawing of the synaptic SNARE complex, helices from syntaxin1a (red), SNAP25 (green) and VAMP2 (blue). **B** The ionic '0' layer of the neuronal SNARE complex. An arginine residue from VAMP2 interacts with three glutamine residues from Syntaxin1a and SNAP25. Figure adapted from Sutton et al., 1998.

1.3.3 Classification of SNARE proteins

The defining feature of all SNARE proteins is the presence of a 60-70 amino acid region of heptad-repeats, termed the SNARE motif (Hong, 2005). This motif is critical for SNARE complex assembly and has been shown to be important for fusion specificity (Paumet et al., 2004). As stated previously, SNAREs were originally split into two categories – Q-SNAREs (t-SNAREs) or R-SNAREs (v-SNAREs).

Q-SNAREs are labelled as such due to the glutamine residue in their SNARE motifs that is crucial for formation of the core of the SNARE complex (Fasshauer et al., 1998) (Figure 1.3). Q-SNAREs generally correspond to t-SNAREs and have been further classified into Qa, Qb and Qc SNAREs depending on their position in the SNARE complex (Hong, 2005). In contrast R-SNAREs are named such due to the arginine residue that they contribute to the central layer of the SNARE complex (Fasshauer et al., 1998). R-SNAREs can typically also be classified as v-SNAREs.

Q and R-SNAREs can be further split into their respective protein family groups, which are introduced below.

1.3.3.1 Syntaxin family

The founding member of the syntaxin (Sx) family was first identified in neuronal cells. Syntaxin 1a is a 35 kDa protein and is localised to the plasma membrane in pre-synaptic neurons (Bennett et al., 1992). There are currently 15 known syntaxins in mammals and 8 in yeast. Syntaxins localise to multiple intracellular compartments (Figure 1.1). Syntaxins are cytosolically orientated and are between 288 and 301 amino acids in length (Bennett et al., 1993).

The syntaxin family of proteins are classed as Qa SNARE proteins. They are anchored to membranes by a transmembrane domain at the C-terminus (Bennett et al., 1993). The SNARE domain of syntaxin proteins lies adjacent to the C-terminus and is followed by an

N-terminal domain consisting of three anti-parallel alpha-helices (Bennett et al., 1993) (Figure 1.5). This N-terminal domain, called the Habc domain, links to the SNARE domain by a flexible region of the protein (Fernandez et al., 1998). This evolutionarily conserved feature is important for regulating syntaxin function. The Habc domain can fold back and bind to the SNARE motif, rendering the protein unable to form SNARE complexes (Dulubova et al., 1999) (Figure 1.4). Alleviating this intramolecular interaction exposes the SNARE motif allowing interaction with other SNARE domains and therefore formation of SNARE complexes. This molecular switch has been proposed to be an important regulatory feature of syntaxins (Dulubova et al., 1999). Indeed the feature is conserved in many syntaxin isoforms including Sx1a, Sx2, Sx3 and Sx4 (Bennett et al., 1992; Bock et al., 1996; Wong et al., 1998) and the yeast syntaxin Sso1p, a functional homologue of Sx1a (Fiebig et al., 1999).

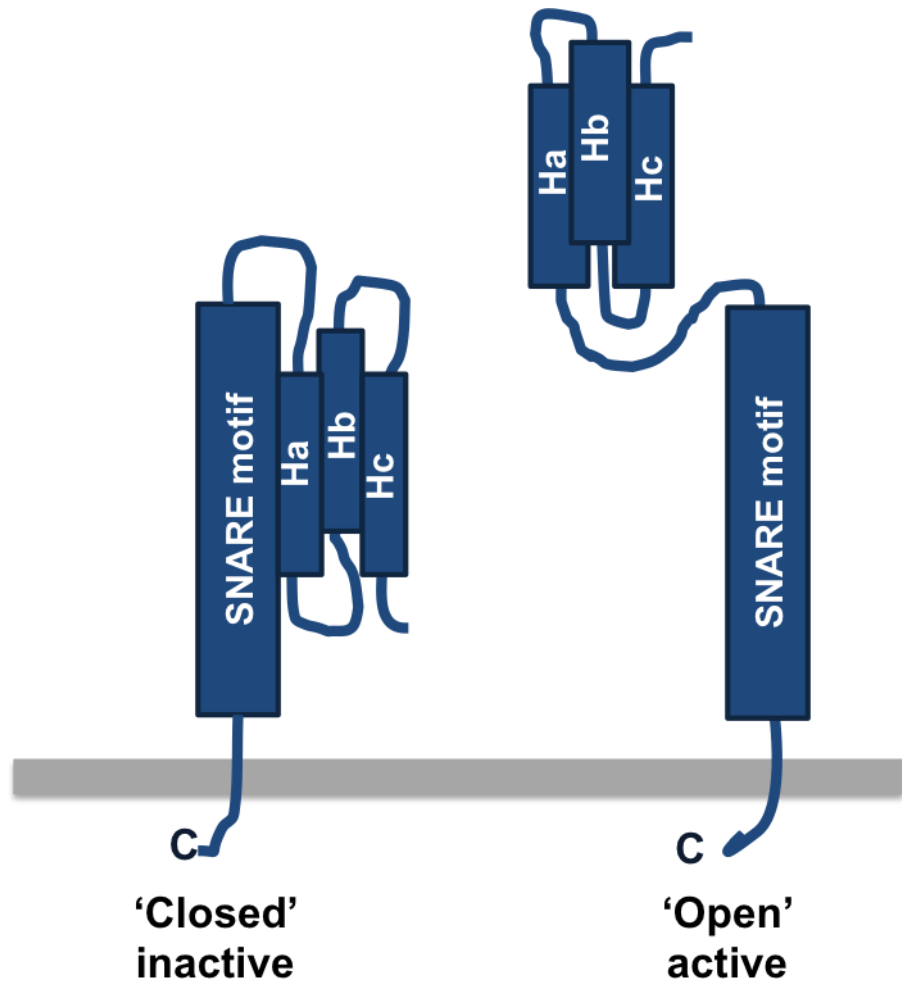


Figure 1.4 Syntaxin proteins undergo a conformational shift

The Habc domain of many syntaxin family members binds to the SNARE motif due to the flexible linker region. In this conformation the protein is 'closed' and unable to form SNARE complexes. When the interaction between the SNARE motif and the Habc domain is alleviated the SNARE motif is free to bind to others and form SNARE complexes, this is known as the open conformation.

1.3.3.2 SNAP family

SNAP family proteins are Qb and Qc SNAREs. As with syntaxins, the family was first identified in neuronal cells (Oyler et al., 1989). Other SNAP isoforms since have been identified, including SNAP23 (Ravichandran et al., 1996), SNAP29 (Steggmaier et al., 1998) and SNAP47 (Holt et al., 2006), and are ubiquitously expressed. The proteins contain two SNARE motifs that they contribute to the formation of SNARE complexes, hence their classification as Qb and Qc proteins (Chen and Scheller, 2001) (Figure 1.5).

Unlike other SNARE proteins SNAP family proteins don't have a transmembrane domain but associate with membrane post-translationally. Family members such as SNAP23 and SNAP25 are palmitoylated at cysteine residues in the linker region that connects the two SNARE motifs (Gonzalo and Linder, 1998). Alternatively, SNAP29 has been shown to associate with membranes due to its binary interactions with syntaxin (Steggmaier et al., 1998).

1.3.3.3 VAMP family

VAMPs (vesicle associated membrane proteins) (alternatively called synaptobrevins) are small proteins of around 120 amino acids. They were again first described in neuronal cells where they were shown to be components of synaptic vesicles (Trimble et al., 1988a). Like syntaxin family members they comprise three main domains - a hydrophobic c-terminal transmembrane domain, a SNARE domain and a proline-rich N-terminal domain (Trimble et al., 1988b) (Figure 1.5).

Seven members of the VAMP family have been identified thus far: VAMP1 (synaptobrevin 1), VAMP2 (synaptobrevin 2), VAMP3 (cellubrevin), VAMP4, VAMP5 (myobrevin), VAMP7 and VAMP8 (endobrevin) (Hong, 2005). The proteins are ubiquitously expressed, with the exception of VAMP1 which is neuronal specific (Lin and Scheller, 2000). VAMP proteins are expressed in multiple intracellular compartments and each VAMP isoform can be present in more than one. For example, VAMP7 is present in late endosomes and lysosomes (Advani et al., 1999) and at the PM (Williams and Pessin, 2008).

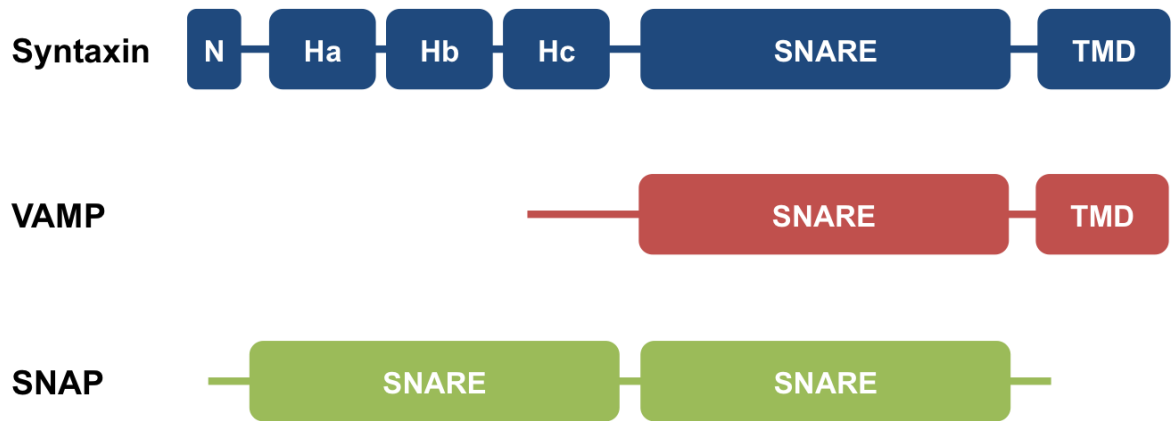


Figure 1.5 General domain structures of SNARE proteins

A comparison of the domain structures of syntaxin, VAMP and SNAP family SNARE proteins. Syntaxin proteins are composed of a C-terminal transmembrane domain (TMD), a SNARE motif (SNARE), a regulatory Habc domain (Hc, Hb and Ha) and an N-terminal domain. VAMP proteins contain a C-terminal transmembrane domain (TMD) and a SNARE motif. Whereas SNAP proteins contain two SNARE motifs joined by a linker region that can be post-translationally modified to associate the protein with membranes.

1.3.4 Non-mammalian SNARE proteins

Genome sequencing projects have shown that SNAREs are found in a wide range of organisms. One study showed that a basic set of 20 SNARE proteins are present in all eukaryotes, and that this set has diversified independently in different organisms to provide specificity and increased complexity in higher eukaryotes (Kloepper et al., 2007). Research on four species, whose sequenced genomes are readily available, has provided insight into the mechanisms of membrane trafficking: yeasts *Saccharomyces cerevisiae* and *Schizosaccharomyces pombe*, the nematode *Caenorhabditis elegans*, the fruitfly *Drosophila melanogaster* (Armstrong, 2000).

In particular, *Saccharomyces cerevisiae* has proved a very useful model for studying membrane trafficking. For example, an early study characterising the yeast SNARE complex consisting of Snc2, Sso1 and Sec9, used biochemical assays to show the importance of t-SNARE binary interactions to the formation of SNARE complexes, and noted striking similarities to the biochemistry of the neuronal SNARE complex (Rossi et al., 1997). Furthermore, functional homologues have been identified between mammalian and

yeast SNAREs. For example, expression of the mammalian t-SNARE syntaxin16 fully complements the phenotypes observed in yeast cells lacking the t-SNARE Tlg2 (Struthers et al., 2009).

Interestingly, compared to the genomes of other eukaryotes, the genomes of higher plant species encode a high number of SNARE proteins (Lipka et al., 2007). Indeed two plant specific subfamilies have been identified – NPSN (novel plant-specific SNARE) Qb- and SYP7 Qc-SNAREs (Sanderfoot et al., 2000). All plant R-SNAREs are so-called longins. Longins contain an extended N-terminal domain that, like with syntaxin family proteins, can form intramolecular interactions to regulate protein function (Rossi et al., 2004). Very few phenotypes have been observed in plant R-SNARE mutants suggesting that they, like mammalian R-SNAREs, exhibit some functional redundancy (Lipka et al., 2007).

1.4 Regulation of SNARE-mediated membrane fusion

Although SNARE proteins have been shown to be the minimal machinery required for bilayer fusion *in vitro* (Weber et al., 1998), membrane fusion is a rapid process that is essential for maintaining cellular integrity and therefore subject to extensive spatial and temporal regulation (Malsam et al., 2008). A number of protein families have been implicated in regulating SNARE mediated membrane fusion.

1.4.1 Sec1/Munc18 (SM) proteins

This family of proteins was originally identified in genetic studies performed in *C. elegans* that identified the UNC-18 gene (Brenner, 1974). Like SNARE proteins, homologues have now been found in all species. For example, the SEC1 gene was identified in yeast (Novick and Schekman, 1979). A temperature sensitive mutation of the gene results in the accumulation of intracellular vesicles, demonstrating its importance in vesicle exocytosis (Novick and Schekman, 1979). Indeed SM proteins have been implicated in all known membrane fusion events (Burgoyne and Morgan, 2007).

Seven mammalian SM proteins have been identified - Munc18a, b and c (mammalian unc-18), VPS33A and B, VPS45 and SLY1 (Hong, 2005; Jahn et al., 2003). Munc18a is predominantly expressed in the brain (Hata et al., 1993), whilst Munc18b and Munc18c are expressed ubiquitously (Tellam et al., 1995). SM proteins are hydrophilic proteins of 60-70 kDa and can be cytosolic or associate to membranes *via* their interaction with syntaxin proteins (this interaction is discussed in more detail in section 1.4.1.1) (Misura et al., 2000).

It is apparent SM proteins play a role in regulating more than one membrane trafficking event due to the small number of them in each species, whilst mammals express 7 SM proteins, only 4 have been identified in yeast (Jahn et al., 2003). However, despite the small number of SM proteins, they do not display functional redundancy. For example, synaptic transmission is abolished in mice lacking Munc18a, despite expression of Munc18b and Munc18c isoforms (Verhage et al., 2000). SM proteins were originally identified as syntaxin binding proteins, however interactions with other SNARE proteins have since been identified. For example, Munc18c directly interacts with the cytosolic domain of VAMP2 (Brandie et al., 2008). Elucidating the mechanism by which SM proteins regulate membrane fusion has proven to be complex and challenging. Characterising the binding between Munc18 and syntaxins has been the focus of intense research, often yielding confusing and contrasting results.

1.4.1.1 Interaction of Munc18 and syntaxin

SM proteins are known to be binding partners of syntaxins, with a high binding affinity (Smyth et al., 2010). One of the best characterised Munc18/syntaxin interactions is that of the neuronal proteins, Munc18a/syntaxin1a. The crystal structure of the interaction between Sx1a and Munc18a was solved (Misura et al., 2000). This study provided a detailed insight into the interactions between the two proteins. Both the Habc and SNARE domain of Sx1a were shown to interact with M18a. The SM protein has three domains that form an arch shape, with syntaxin1a in a closed conformation (see section 1.3.2.1)

binding to domains I and III of Munc18c in the central cavity (figure 1.6). This observation is consistent with biochemical and NMR data that showed that the closed conformation of Sx1a is essential for its interaction with Munc18a (Dulubova et al., 1999).

This mode of binding, termed mode 1, however, is proposed to be inhibitory for SNARE complex formation. In order to form SNARE complexes syntaxins must adopt an open conformation. These data suggest that Munc18a holds Sx1a in a closed and inactive form. However, numerous studies have shown that M18 is not inhibitory to membrane fusion (Carr et al., 1999; Scott et al., 2004); indeed its expression is required for synaptic transmission (Verhage et al., 2000).

In contrast to the Sx1a/Munc18a interaction, the yeast syntaxin Sed5 and the SM protein Sly1 have been shown to interact in a completely different manner. Biochemical studies showed that only the N-terminal 44 residues of Sed5 were required for interaction with Sly1 (Yamaguchi et al., 2002). Indeed, despite the structure of Sly1 being very similar to Munc18a, structural analysis of the Sly1/Sed5 interaction revealed a very different mode of binding (Bracher and Weissenhorn, 2002). Crystal structures solved in this study revealed that the N-terminal peptide of Sed5 binds to a hydrophobic pocket on the outer surface of Sly1. Similar modes of binding have been identified for other yeast and mammalian SNARE/SM protein interactions (Dulubova et al., 2002). Subsequent investigations have revealed that the extreme N-terminus of Sx1a also interacts with Munc18a (Khvotchev et al., 2007). Moreover, in an *in vitro* fusion assay, deletion of the N-terminus of Sx1a abolishes the stimulatory effect of Munc18a on membrane fusion, suggesting this interaction is important for SM protein function (Shen et al., 2007). In contrast to mode 1 binding, interaction between the syntaxin N-terminus and its cognate SM protein (mode 2 binding) is consistent with the protein being in an open or closed conformation and therefore not inhibitory to SNARE complex formation.

A third, and less well characterised, binding mode between SM and syntaxin proteins has also been reported. The yeast SM protein Sec1, which regulates fusion at the plasma membrane, was reported to bind to an assembled SNARE complex consisting of Sso1, Sec9p and Sncp (Carr et al., 1999). This study found that Sec1 not only coprecipitated with the syntaxin Sso1 but with the other proteins too. This study also showed that when a GFP tagged Sec1 protein is expressed in yeast mutants that exhibit impaired SNARE complex assembly, the protein is mislocalised. Moreover, in an *in vitro* binding assay using recombinant proteins, Sec1 was shown to have a strong interaction with both the t-SNARE and full ternary SNARE complex and a weaker interaction with free Sso1 (Scott et al., 2004). The yeast SM protein Vps45 exhibits multiple modes of binding, leading to the protein cycling on and off membranes (Bryant and James, 2003). Vps45 binds to the syntaxin protein Tlg2, before dissociating upon *trans*-complex formation, and then reassociates with the fully formed *cis*-complex. The highly studied Munc18a has also been shown to bind to assembled SNARE complexes containing syntaxin1a (Dulubova et al., 2007).

Figure 1.6 summarises the diverse binding modes identified between SM and syntaxin proteins. The multiple mode of interactions between SM and SNARE proteins suggest they may each have a different mode of action, however sequence and structural similarities between the family argue that they should have a common function (Toonen and Verhage, 2003). Defining the role of SM proteins in regulating SNARE mediated membrane fusion is therefore still on going.

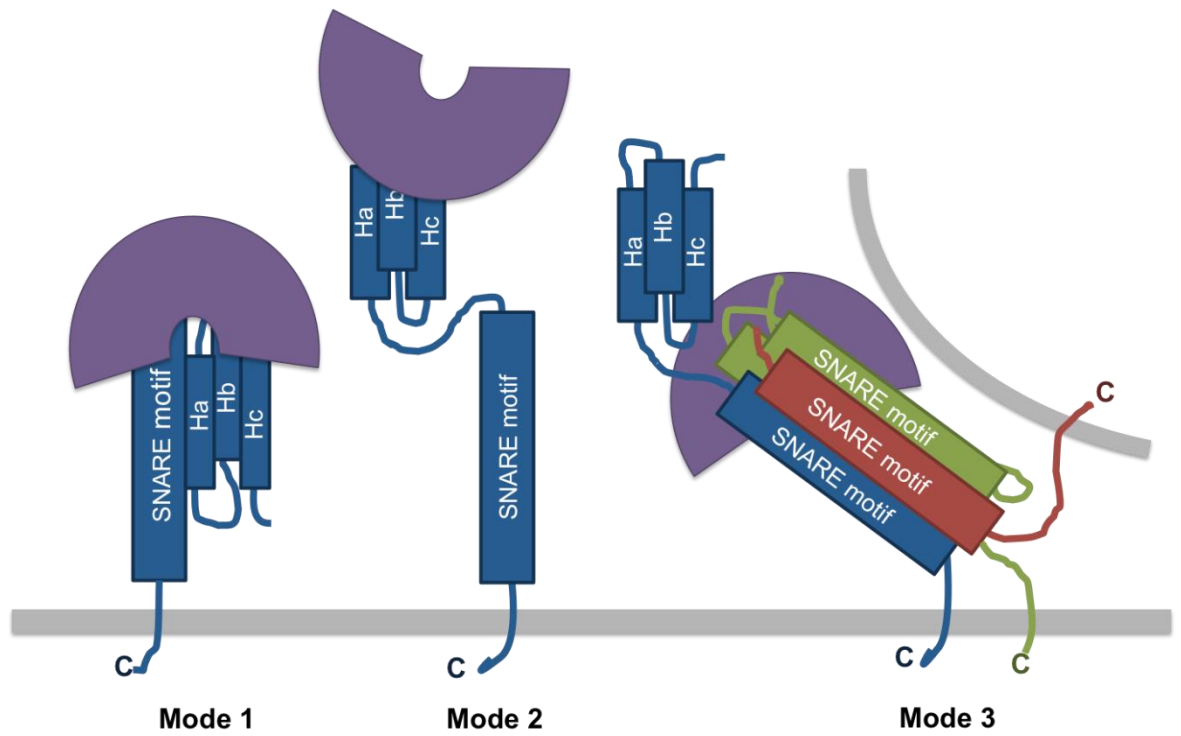


Figure 1.6 Binding modes of Munc18 to syntaxins

Munc18 proteins bind to syntaxins through three different binding modes. In mode 1 binding Munc18 binds to closed syntaxin *via* its central cavity. Munc18 also binds to the N-terminal of syntaxin through a hydrophobic pocket on its outer surface (mode 2 binding). In mode 3 binding Munc18c binds to the assembled SNARE complex.

1.4.2 Rab proteins

Ras-associated binding proteins are ubiquitously expressed small GTPases, 20-29 kDa in size (Hutagalung and Novick, 2011). They are a large family of proteins with 11 isoforms in yeast, 29 in *C. elegans* and more than 60 in humans and mice. Specific Rabs are associated with all organelles and transport vesicles, and they are thought to act as molecular switches to regulate membrane fusion throughout the cell (Hutagalung and Novick, 2011). Rabs exist in two states; an inactive GDP-bound state and an active GTP-bound state (Fukuda, 2008). This switch is controlled by guanine nucleotide exchange factors (GEFs) and GTPase activating proteins (GAPs). The GTP-bound activated Rabs are then recruited to transport vesicles where they regulate trafficking by interacting with specific effector proteins (Zerial and McBride, 2001).

Rabs are involved in almost all membrane fusion events (Stenmark, 2009). A study from 2009 by Ohya and colleagues used an *in vitro* fusion assay involving 'synthetic endosomes' containing Rabs and SNAREs (Ohya et al., 2009). This study reported that Rab and SNARE proteins act coordinately to increase the efficiency of membrane tethering and fusion.

1.4.3 Tethering proteins and complexes

Tethering proteins confer an increase in specificity to membrane trafficking by providing the first physical contact between trafficking vesicles and their target membrane (Pfeffer, 1999). Tethers can be split into two categories; long coiled-coil tethering proteins or multi-subunit tethering complexes (Whyte and Munro, 2002).

Long coiled-coil proteins are attached to target membranes and can span lengths several times the diameter of trafficking vesicles (Whyte and Munro, 2002). Electron microscopy studies have identified these structural features of the yeast tethering protein Uso1p (Yamakawa et al., 1996) and its mammalian homologue p115 (Sapperstein et al., 1996).

In addition to the coiled-coil proteins, seven multi-subunit tethering complexes have been identified along with their involvement at distinct trafficking steps. One such complex is the exocyst complex, which acts at the trans-Golgi network and plasma membrane (Yeaman et al., 2001). The exocyst complex consists of 8 components that were originally identified in genetic studies in yeast, where mutations in exocyst genes caused an accumulation of vesicles (Guo et al., 1999; TerBush et al., 1996). This complex has been shown to be an important regulator of proper membrane trafficking. For example, over expression of a mutated component of the mammalian exocyst complex, Exo70, resulted in inhibited insulin-stimulated glucose uptake in adipocytes (Inoue et al., 2003).

1.4.4 Phosphorylation

In addition to regulation by the accessory proteins discussed above, SNARE protein function can also be regulated by post-translational modification, such as phosphorylation (Snyder et al., 2006).

All three components of the much studied neuronal SNARE complex can be phosphorylated by different kinases. Syntaxin 1a is phosphorylated by casein kinase II (CKII) *in vitro* (Risinger and Bennett, 1999). Syntaxin 1a phosphorylated by CKII exhibits an increase in binding to the Ca²⁺ sensor synaptotagmin 1, suggesting this phosphorylation could directly regulate neurotransmitter release (Risinger and Bennett, 1999). Furthermore, Sx1 phosphorylated by CKII at serine 14 preferentially localises with SNAP25 in regions of the axon that are distinct from the localisation of synaptic vesicles (Foletti et al., 2000). These labelled regions in the axon may represent fusion sites for previously uncharacterised vesicles (Foletti et al., 2000). Phosphorylation of Sx1 at this residue has since been shown to regulate the interaction with Munc18a (Rickman and Duncan, 2010).

SNAP25 is phosphorylated by protein kinase A (PKA), however no effects of this phosphorylation have been reported in the binary or ternary interactions with Sx1 and/or

VAMP2 (Risinger and Bennett, 1999). However, another study has shown that phosphorylation of SNAP25 by protein kinase C (PKC) *in vitro* inhibits its interaction with syntaxin 1a (Shimazaki et al., 1996). VAMP2 is phosphorylated in synaptic vesicles by both CKII and calmodulin-dependent protein kinase II (CaMKII) (Nieler et al., 1995). However, the functional consequences of this phosphorylation are still unclear.

The effect of syntaxin phosphorylation has been shown to be important in other systems. For example, in yeast the t-SNARE Sso (a syntaxin 1 homologue) is dephosphorylated via a ceramide activated phosphatase (CAPP) Sit4, a process which increases its ability to form a complex with the t-SNARE Sec9 (Marash and Gerst 2001). Furthermore, the PKA (Protein Kinase A) pathway, which is involved in growth control, phosphorylates Sso inhibiting the assembly of SNARE complexes, highlighting the convergence of two signalling pathways on the control of t-SNAREs (Marash and Gerst 2001). Similarly, both the CAPP and PKA signalling pathways modulate endocytosis in yeast by modulating phosphorylation of Tlg t-SNAREs (Gurunathan et al. 2002). These studies suggest that phosphorylation of t-SNAREs plays a functional role and therefore further investigation is required into the consequences of such phosphorylation events.

1.4.5 NSF and α -SNAP – SNARE complex disassembly

Once SNARE complexes have formed and membrane fusion has occurred, the proteins remain in the *cis*-SNARE complex. It is therefore important that the complex be disassembled and the proteins made available to form new SNARE complexes. In order to disassemble the tightly bound SNARE complex, three molecules of α -SNAP bind to the SNARE core complex, this in turn recruits NSF (Hohl et al., 1998; Wimmer et al., 2001). NSF then uses ATP hydrolysis to disassemble the SNARE complex (Hayashi et al., 1995). Expression of temperature sensitive NSF in *Drosophila* resulted in the accumulation of SNARE complexes and inhibition of synaptic transmission when the protein was inactivated (Littleton et al., 1998).

1.5 Glucose transport

1.5.1 Glucose homeostasis and type II diabetes mellitus

Glucose is an essential source of energy for mammalian cells, however blood glucose levels that are too high or too low are damaging. The levels of blood glucose in humans are highly regulated and maintained at a concentration between 4 and 7 mM (Kahn et al., 2006). This maintenance is achieved by a balance of two hormones – glucagon, which is released in response to low blood glucose, and insulin, which is secreted in response to high blood glucose. Both hormones are secreted from cells in the islet of Langerhans in the pancreas, with insulin being secreted from beta cells and glucagon from alpha cells (Bell and Polonsky, 2001). Glucagon primarily acts to increase gluconeogenesis and glucose release from the liver. Insulin acts on the liver, skeletal muscle and adipose tissue to increase glucose uptake from the blood (Shepherd and Kahn, 1999). Skeletal muscle is responsible for around 90 % of glucose uptake (Kraegen et al., 1985). Although it only accounts for a small amount of glucose uptake, adipose tissue is essential for regulating whole-body energy homeostasis. Adipocytes detect the energy status and release hormones to regulate metabolism in the brain, muscle and liver (Leto and Saltiel, 2012). Indeed, mice in which the glucose transporter protein GLUT4 has been selectively depleted in adipose cells have been shown to develop insulin resistance in skeletal muscle and the liver (Abel et al., 2001).

Diabetes mellitus is a disease that can occur when glucose homeostasis becomes dysregulated. There are two types of diabetes; type I, in which insulin is not secreted from the beta islet cells in the pancreas, and type II, in which normally insulin responsive tissues become insulin resistant. Type I diabetes is normally treated by the administration of insulin. Type II diabetes, however is more complex and harder to treat. The world health organisation (WHO) estimates that 90 % of cases of diabetes are Type II. A sharp rise in the frequency of Type II diabetes has occurred in recent years, with the global prevalence in adults rising from 4.7 % in 1980 to 8.5 % in 2014 (World Health

Organization, 2016). In 2012 an estimated 1.5 million deaths were directly caused by diabetes (World Health Organization, 2016), demonstrating that understanding the development of this complex disease is of utmost importance.

Insulin resistance arises when insulin sensitive cells no longer mobilise a response to insulin, and therefore glucose is not absorbed from the blood. Insulin released from the pancreas binds to receptors on the surface of muscle and adipose cells, this triggers an intracellular signalling cascade. The culmination of this signalling cascade is the mobilisation of the glucose transporter protein, GLUT4, to the plasma membrane allowing glucose to enter the cells (Bryant and Gould, 2011). It is therefore imperative to understand the mobilisation and intracellular trafficking of GLUT4, in order to better understand the development of type II diabetes and to develop novel treatment for the disease.

1.5.2 Glucose transporters and GLUT4

Glucose transporters (GLUTs) are integral membrane proteins, with 12 predicted helical membrane-spanning domains and both termini exposed to the plasma membrane (Bryant et al., 2002). There are thirteen GLUTs in mammals split into three classes: class I (glucose transporters including GLUT1, 2, 3 and 4), class II (fructose transporters GLUT5, 7, 9 and 11) and class III (atypical members, GLUT6, 8, 10, 12 and the *myo*-inositol transporter HMIT1) (Bryant et al., 2002). GLUT1 and GLUT4 are expressed in insulin sensitive tissue, including skeletal and cardiac muscle and adipose. However, only GLUT4 shows a change in subcellular localisation in response to insulin (Douen et al., 1990).

In the early 1980s it was shown that adipocytes contain an intracellular pool of glucose transporters that, when the cells are stimulated with insulin, translocate to the plasma membrane (Cushman and Wardzala, 1980; Suzuki and Kono, 1980). This insulin response was subsequently identified in cardiac (Watanabe et al., 1984) and skeletal

muscle (Hirshman et al., 1990). The transporter responsible was later identified to be the unique insulin-sensitive GLUT4 (James et al., 1988). The GLUT4 gene was later identified (Bell et al., 1989; Birnbaum, 1989) and cloned (James et al., 1989).

1.5.3 Insulin signalling

Insulin binds to its receptors on the surface of insulin responsive cells triggering a downstream signalling cascade. Whilst much research has been carried out into the downstream effects of insulin in muscle and adipose tissue, the precise mechanism that leads to GLUT4 mobilisation to the plasma membrane is not yet fully understood.

The insulin receptor (IR) is a cell surface receptor with intrinsic kinase activity. The IR is comprised of two α -subunits and two β -subunits, linked with disulphide bonds (Gual et al., 2005). Insulin binds to the α -subunit resulting in tyrosine autophosphorylation of the β -subunit. There are two main signalling cascades that are triggered by insulin: the phosphoinositide 3-kinase (PI3K) pathway and the adaptor protein with pleckstrin homology and Src homology domains (APSH) pathway (Figure 1.7).

1.5.3.1 The PI3K pathway

Following phosphorylation of the IR, the insulin receptor substrate (IRS) is recruited, activating a PI3K dependent signalling cascade (Jewell et al., 2010). IRS then recruits and activates PI3K. Active PI3K phosphorylates phosphatidylinositol bisphosphate (PIP_2), yielding phosphatidylinositol trisphosphate (PIP_3). PIP_3 then recruits and activates the pleckstrin homology (PH) domain-containing serine/threonine kinase phosphoinositide-dependent kinase (PDK). Activated PDK then phosphorylates another serine/threonine kinase, protein kinase B (PKB, also known as Akt), which in turn phosphorylates the Rab-GTPase activating protein AS160. AS160 then signals downstream to Rab proteins, which are thought to coordinate membrane trafficking.

The steps that follow AS160 activation, including the Rab proteins recruited and mobilisation of GLUT4 from its intracellular stores are not yet fully elucidated. Inhibition of PI3K by both pharmacological inhibition using wortmannin (Okada et al., 1994) and competitive inhibition (Cheatham et al., 1994) block GLUT4 translocation.

1.5.3.2 The APS signalling pathway

Activation of the IR also results in the recruitment of the adaptor protein APS. APS recruits a complex of the proto-oncogene c-CBL and c-CBL-associated protein (CAP). This triggers the phosphorylation of c-CBL, which then interacts with the adaptor protein CRK. CRK is in a complex with the GEF C3G, which stimulates the GTPase activity of TC10, a Rho family small G-protein. Active TC10 then interacts with effector protein that regulate GLUT4 exocytosis.

Although over expression of mutant forms of TC10 or CAP reduce insulin stimulated GLUT4 translocation, the importance of this pathway has been questioned. siRNA depletion of numerous components of this pathway has no effect on insulin stimulated glucose transport in 3T3-L1 adipocytes.

Although the early stages of both the APS and PI3K pathways (section 1.5.3.1) are well defined, further research is needed to elucidate the mechanisms linking insulin signalling to GLUT4 trafficking.

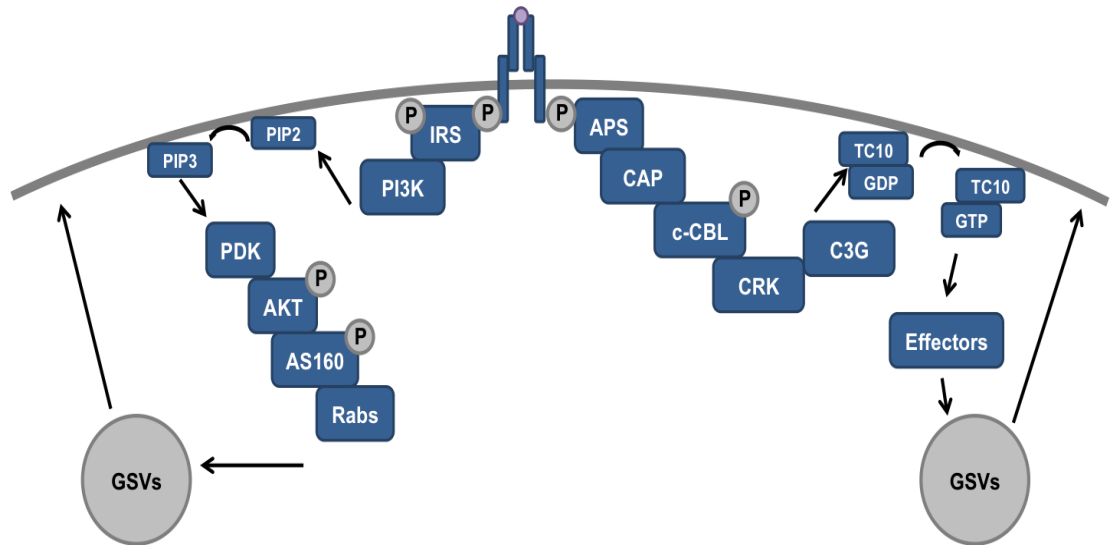


Figure 1.7 The insulin signalling cascade

Upon insulin binding to the insulin receptor, two downstream signalling cascades are triggered. The PI3K signalling pathway is initiated by the recruitment of IRS to the PM. Phosphorylated IRS then recruits PI3K, which converts PIP2 to PIP3. PIP3 then interacts with PDK and Akt. Akt binds to AS160 that then interacts with downstream Rabs resulting in GLUT4 translocation. Recruitment of APS to the insulin receptor triggers a different signalling cascade. APS recruits CAP and c-CBL, which then interact with the adaptor protein CRK. CRK then associates with C3G, which activates TC10. Active TC10 interact with downstream effector proteins, resulting in GSVs being mobilised to the PM.

1.5.4 The GLUT4 trafficking itinerary

Although the precise mechanisms by which insulin stimulates GLUT4 translocation to the PM are as yet unknown, a model has emerged for the trafficking itinerary of GLUT4 in the cell. GLUT4 is localised to numerous intracellular compartments including the PM, endosomes, the TGN and other intracellular vesicles (Slot et al., 1991). Figure 1.8 summarises the current proposed model of the GLUT4 trafficking itinerary. It is proposed that GLUT4 is rapidly trafficked through the endosomal system from the PM, before entering a slow recycling pathway between recycling endosomes, the TGN and a pool of

specialised GLUT4 storage vesicles (GSVs)(Bryant and Gould, 2011). It is from these GSVs that GLUT4 is immobilised to the PM in response to insulin.

GLUT4 is endocytosed from the plasma membrane via both clatherin and cholesterol dependent mechanisms (Blot and McGraw, 2006; Ros-Baro et al., 2001; Shigematsu et al., 2003). The connection between the endosomal GLUT4 pool and the TGN/GSV pool was established when Zeigerer and colleagues showed that when endosomal trafficking is blocked the amount of GLUT4 in the TGN/GSV pool is dramatically reduced (Zeigerer et al., 2002).

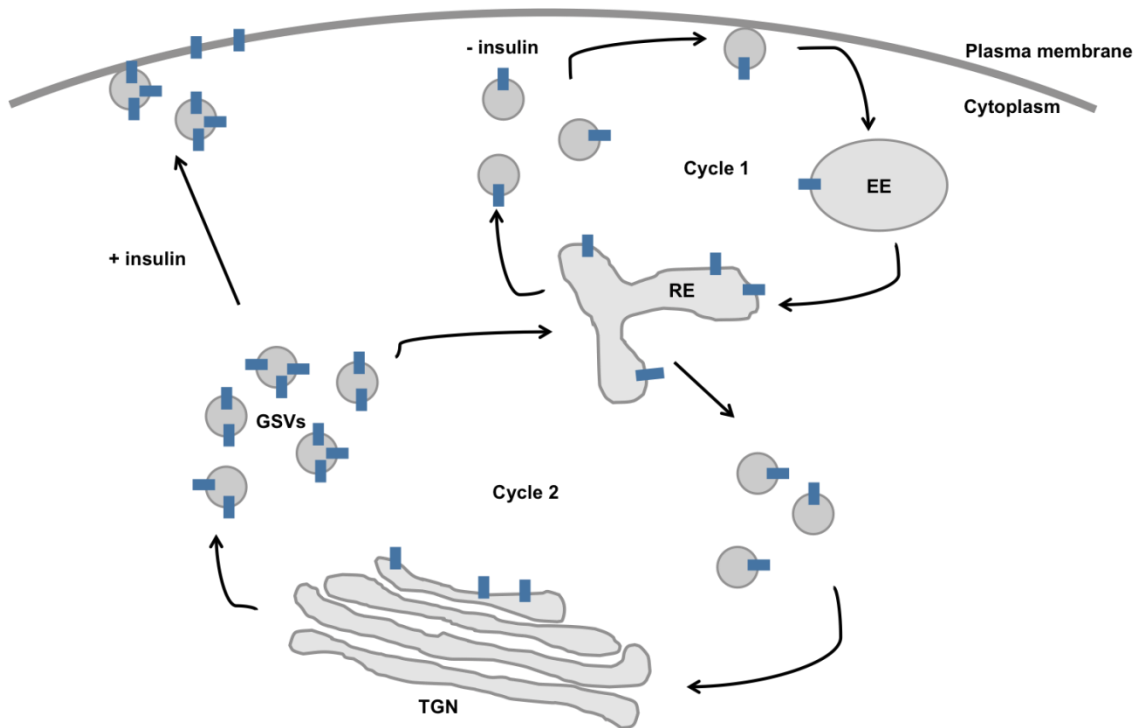


Figure 1.8 A model of the GLUT4 trafficking itinerary

A schematic of the current model for the trafficking itinerary of GLUT4. GLUT4 is continually trafficked through two interlinked trafficking cycles. In the first, GLUT4 is internalised into early endosomes (EE), through recycling endosomes (RE) and either back to the plasma membrane or into cycle 2. Cycle two is a slow moving cycle where GLUT4 moves through the *trans*-Golgi network (TGN) and is sorted into insulin responsive GLUT4 storage vesicles (GSVs). It is from these GSVs that GLUT4 is rapidly mobilised to the PM following insulin-stimulation.

1.5.4.1 GLUT4 storage vesicles

Studies have shown that the majority of intracellular GLUT4 is present in small (approximately 50 nm diameter) vesicles that cluster around, but are distinct from, the TGN (Kandror et al., 1995; Slot et al., 1991). These vesicles are named GLUT4 storage vesicles (GSVs) and have been shown to contain approximately 60 % of intracellular GLUT4 (Livingstone et al., 1996). GSVs are formed from either recycled endocytosed GLUT4 (Zeigerer et al., 2002) or newly synthesised protein (Watson et al., 2004). This study by Watson and colleagues utilised a tagged GLUT4 construct to show that newly synthesised GLUT4 becomes insulin responsive after between 9 and 12 hours,

suggesting that is when it is incorporated into GSVs. Moreover, they showed that this GLUT4 was not first trafficked to the PM before being sorted into GSVs. Proteomic analysis of immunopurified GSVs from rat adipocytes revealed around 100 proteins that associate with GSVs (Jedrychowski et al., 2010). Of these many proteins several have been the subject of further research and have been identified as important for the formation of GSVs or for their insulin responsiveness.

Sortilin has been identified as an important regulator of GSV formation. Sortilin expression increases with differentiation of 3T3-L1 adipocytes (Hatakeyama and Kanzaki, 2011). shRNA mediated knock-down of Sortilin decreases both GSV formation and insulin-induced glucose uptake (Shi and Kandror, 2005). Moreover, GLUT4 is degraded when expressed ectopically, however co-transfection of Sortilin and GLUT4 results in stable and co-localised expression of both proteins in functional GSVs (Shi and Kandror, 2005).

Whilst Sortilin has been shown to be important for GSV formation, IRAP (insulin-responsive aminopeptidase) is a protein that has been shown to be involved in the insulin responsiveness of GSVs. IRAP is present in GSVs and is translocated to the PM in response to insulin (Jedrychowski et al., 2010). Although whole body knockout of IRAP in mice had no effect on glucose homeostasis (Keller et al., 2002), siRNA knockdown of IRAP in 3T3-L1 adipocytes did impair GSV translocation to the PM (Yeh et al., 2007). The discrepancy in these results may result from the system used. In whole life, whole body knockout mice it is possible the organisms may have developed compensatory mechanisms that do not occur in cultured adipocytes transiently depleted of IRAP (Yeh et al., 2007). Interestingly, siRNA mediated knockdown of GLUT4 in this study did not effect insulin stimulated IRAP translocation, suggesting GLUT4 is not required for GSV translocation (Yeh et al., 2007).

A third protein that has been shown to be important for GSV function is LRP-1 (low density lipoprotein receptor- related protein 1). Depletion of LRP-1 in 3T3-L1 adipocytes

reduces GLUT4 expression and glucose uptake (Jedrychowski et al., 2010). Interestingly interactions between the Rab GAP AS160 and LRP-1 (Jedrychowski et al., 2010) and IRAP (Peck et al., 2006) have been reported, representing a potentially important interaction between the insulin signalling pathway and trafficking machinery.

1.5.5 SNARE proteins in GLUT4 translocation

The translocation of GLUT4, like all membrane trafficking events, is mediated by SNARE proteins. There are two main sites of SNARE protein action in GLUT4 trafficking – sorting GLUT4 into GSV and fusion of GSVs at the PM.

The t-SNAREs Sx6 and Sx16 have been implicated in sorting of GLUT4 into GSVs. Expression of a truncated mutant of Sx4 lacking the transmembrane domain, which acts as a dominant negative inhibitor, delays the reinternalisation of GLUT4 following the removal of insulin (Perera et al., 2003). Consistent with this observation, Sx6 has been shown to be required for recycling of IRAP from the PM to the GSVs (Watson et al., 2008). Syntaxin 16 forms a t-SNARE complex with syntaxin 6 (Perera et al., 2003). Sx16 shows a high co-localisation with GLUT4 (Shewan et al., 2003). Inhibition of Sx16, using morpholino antisense oligonucleotides (MAO) or expression of a dominant negative Sx16, reduces insulin-stimulated glucose transport (Proctor et al., 2006). Moreover, GLUT4 has been shown to be trafficked from the PM through a sub-domain of the TGN that is enriched in Sx6 and Sx16 (Shewan et al., 2003). Taken together these data provide good evidence that the t-SNAREs Sx6 and Sx16 facilitate trafficking of GLUT4 into GSVs.

In order to elucidate the role of VAMP proteins in GLUT4 translocation Williams and Pessin carried out systematic siRNA knockdown of VAMPs 2, 4 and 8 in 3T3-L1 adipocytes (Williams and Pessin, 2008). Depletion of VAMP8 results in elevated levels of GLUT4 at the plasma membrane under basal condition (in the absence of insulin) due to a decrease in GLUT4 endocytosis (Williams and Pessin, 2008). Whilst VAMP4 knockdown, a v-SNARE that is known to control traffic between endosomes and the TGN, causes the

redirection of a pool of GLUT4 to the plasma membrane under basal conditions (Williams and Pessin, 2008). These data suggest that VAMP8 is involved in the sorting of recycled GLUT4 to GSVs from the PM, whilst VAMP4 is involved in redirecting missorted GLUT4 from endosomes and/or the TGN.

Whilst relatively little is known about the sorting of GLUT4 into GSVs, much of the research into SNARE mediated translocation of GLUT4 has focused on GSV fusion with the plasma membrane. A SNARE complex consisting of Sx4, SNAP23 and VAMP2 has been implicated in this step.

1.5.5.1 Sx4

Sx4 is a Qa SNARE present at the plasma membrane and has been implicated in insulin mediated GLUT4 translocation in numerous studies. Introduction of anti-Sx4 antibodies into permeabilised adipocytes derived from 3T3-L1 cells results in a decrease in insulin stimulated glucose transport (Volchuk et al., 1996). The development of heterozygous Sx4 knockout mice has shown the importance of the protein for proper insulin mediated glucose uptake in skeletal muscle (Yang et al., 2001). Sx4 +/- knockout mice show a 50 % reduction in whole body insulin stimulated glucose uptake. This study attributed this to a similar reduction in GLUT4 translocation in skeletal muscle tissue. Consistent with this, mice overexpressing Sx4 in skeletal muscle display a two-fold increase of insulin stimulated GLUT4 translocation and glucose uptake (Spurlin et al., 2004).

In addition to its importance in skeletal muscle Sx4 has been shown to be important for GLUT4 translocation to the PM in adipocytes (Kawaguchi et al., 2010). This study showed depletion of Sx4 by siRNA results in a reduction of insulin stimulated glucose uptake. Moreover, when the effects of Sx4 knockdown were examined in more detail, its role in GSV tethering at the PM was demonstrated. In adipocytes expressing GLUT4 harbouring a GFP tag at its C-terminus as a Myc tag in the first exofacial loop, the cellular localisation of GLUT4 was examined using confocal microscopy. It was shown that siRNA knockdown

of Sx4 reduces the amount of GLUT4 in the plasma membrane, as shown by surface staining with anti-myc antibodies. Moreover, isolation of insulin stimulated PM lawns revealed reduced GLUT4 association with the membrane, suggesting a role for Sx4 in GSV tethering at the PM (Kawaguchi et al., 2010).

1.5.5.2 SNAP23

SNAP23 was originally identified as a none-neuronal SNAP protein, which binds to both syntaxin and VAMP proteins, in a yeast two-hybrid system (Ravichandran et al., 1996). Sx4 and SNAP23 colocalise at the PM in 3T3-L1 adipocytes (Tamori et al., 1998) and their interaction has been confirmed by co-immunoprecipitation studies in rat adipocytes (St-Denis et al., 1999). Inhibition of SNAP23 using a dominant negative truncated SNAP23 peptide results in reduced GLUT4 translocation to the cell surface in response to insulin (Rea et al., 1998).

1.5.5.3 VAMP2

Sx4 and SNAP23 have been shown to form an SDS-resistant SNARE complex with VAMP2 by surface plasmon resonance (SPR) (Rea et al., 1998). VAMP2 has since been implicated in insulin regulated GLUT4 translocation. Over expression of a SNAP23 mutant that was able to bind to Sx4 but not VAMP2 resulted in a reduction of insulin stimulated GLUT4 translocation (Kawanishi et al., 2000). However, VAMP2 is not the only v-SNARE that has been proposed to play a role in insulin stimulated GLUT4 translocation. Indeed, a recent study has shown that VAMPs 2, 3, 4, 5, 7 and 8 can form SDS-resistant SNARE complexes with Sx4 and SNAP23 *in vitro* (Sadler et al., 2015). Early studies showed that both VAMP2 and VAMP3 are present in GLUT4 containing vesicles and translocate to the PM in response to insulin stimulation of rat and 3T3-L1 adipocytes (Cain et al., 1992; Volchuk et al., 1995). Interestingly, when VAMP3 containing vesicles were immunoprecipitated they were found to contain GLUT4 but not VAMP2 (Volchuk et al.,

1995). This finding suggests that there are two pools of GLUT4 containing vesicle that are both insulin responsive.

Expression of the cytoplasmic domains of either VAMP2 or 3 (acting as dominant negative mutants) inhibits GLUT4 translocation in 3T3-L1 adipocytes (Olson et al., 1997). However, inhibition studies using tetanus toxin cleavage of either VAMP2 or VAMP3 did not impair insulin stimulated GLUT4 translocation in rat adipocytes (Hajduch et al., 1997). However, a contrasting study has shown that tetanus toxin cleavage of VAMP2 and VAMP3 in L6 myoblasts impairs GLUT4 translocation by 60-70 % (Randhawa et al., 2000). Moreover, this latter study showed that expression of a toxin resistant form of VAMP2 but not VAMP3 rescues the effect of tetanus toxin treatment in these cells.

More recent proteomic analysis of GSVs has shown that VAMPs 2, 3 and 8 are present on GSVs (Jedrychowski et al., 2010; Larance et al., 2005). Indeed one study using adipocytes derived from mouse embryonic fibroblasts showed that insulin stimulated GLUT4 translocation to the PM was only blocked when VAMP2, 3 and 8 were inhibited simultaneously (Zhao et al., 2009). This study also showed that reintroduction of only one of the VAMP isoforms is needed to rescue GLUT4 translocation highlighting potential redundancy in the pathway.

1.5.6 Regulation of SNARE mediated GLUT4 trafficking

1.5.6.1 Munc18c

The SM protein that has been implicated in regulating the Sx4/SNAP23/VAMP2 SNARE complex is Munc18c (Tamori et al., 1998). Munc18c binds to monomeric Sx4 *via* its N-terminus (mode 2 binding, figure 1.6) (Latham et al., 2006). The crystal structure of the Munc18c/Sx4 N-peptide complex was determined, confirming that the peptide bound to a hydrophobic pocket on the outer surface of Munc18c (Hu et al., 2007). This interaction is compatible with Sx4 in its open conformation, and therefore SNARE complex assembly. Systematic analysis of recombinant purified Sx4, tagged at either the N- or C-terminus,

and Munc18c revealed that the proteins interact *via* a second distinct binding mode, most likely through mode 1 binding (figure 1.6) (Aran et al., 2009). Indeed, homology modelling suggests that the residues required for the interaction of closed Sx1a and M18a are conserved in Sx4 (D'Andrea-Merrins et al., 2007). However, low-resolution structural analysis of the Sx4/Munc18c complex found that Sx4 was in the open conformation, and found no evidence for the proteins interacting when Sx4 is in the closed conformation (Christie et al., 2012). Munc18c also binds to binary t-SNARE complexes (Sx4/SNAP23) and to the assembled ternary SNARE complex (Latham et al., 2006). In addition, the SM protein has been shown to interact with the v-SNARE VAMP2, although with a lower affinity than Sx4 (Brandie et al., 2008).

Contradictory results have been found when assessing the effect of Munc18c on SNARE complex assembly and membrane fusion. One study has shown, using a *in vitro* complex assembly assay, that preincubation of Munc18c and Sx4 has been shown to inhibit ternary complex formation (Kioumourtzoglou et al., 2014). Whereas a similar assay has shown that preassembly of the Sx4/Munc18c complex accelerates complex assembly (Latham et al., 2006). Similarly contrasting results have been obtained when analysing the effect of Munc18c on membrane fusion. *In vitro* liposome fusion assays have shown that inclusion of Munc18c both inhibits (Brandie et al., 2008) and stimulates (Yu et al., 2013) membrane fusion. Heterozygous Munc18c knockout mice have reduced insulin sensitivity (Oh et al., 2005), suggesting a positive role for Munc18c in GLUT4 exocytosis. Whereas in adipocytes derived from mice embryonic fibroblasts of Munc18c knockout mice insulin-induced GLUT4 translocation is enhanced (Kanda et al., 2005). This is consistent with a negative role for the SM protein. The contrasting data on the role of Munc18c in insulin-stimulated GLUT4 translocation presents a complex picture of the mechanisms behind the process, and suggests that other proteins and regulatory systems may be important.

1.5.6.2 Synip

Synip was identified in a yeast-two hybrid screen as a novel Sx4 binding protein in 3T3-L1 adipocytes (Min et al., 1999). Association of Synip with Sx4 inhibits the interaction of Sx4 and VAMP2, but not Sx4 and SNAP23, suggesting the protein negatively regulates SNARE complex assembly (Min et al., 1999). Synip dissociates from Sx4 following insulin-stimulation and expression of a dominant-interfering C-terminal fragment of Synip inhibits GLUT4 translocation in 3T3-L1 adipocytes (Min et al., 1999). Synip is phosphorylated by Akt at serine 99 (Yamada et al., 2005). Overexpression of a phospho-resistant mutant of Synip acts as a dominant-negative and inhibits GLUT4 translocation to the PM in 3T3-L1 adipocytes (Yamada et al., 2014). As Akt is activated in the PI3K dependent insulin-signalling cascade, this mechanism could be a potentially important regulatory feature linking the signalling and trafficking machinery of GLUT4 transport.

1.5.6.3 Tomosyn

Tomosyn was originally identified as a syntaxin 1a binding protein from rat cerebral cytosol (Fujita et al., 1998). Subsequently, isoforms have been found in other tissues, including a splice variant of the syntaxin 1a binding protein called b-tomosyn that is present in adipocytes (Yokoyama et al., 1999). b-tomosyn binds to Sx4 and SNAP23 *via* its coiled-coil VAMP2-like region (Widberg et al., 2003). Overexpression of b-tomosyn in this study led to a reduction in insulin-stimulated translocation of GLUT4 to the PM, suggesting the protein plays an inhibitory role in regulating the trafficking of the glucose transporter.

1.5.6.4 AS160

The Rab GTPase activating protein AS160 is recruited and activated following insulin-stimulation (Sano et al., 2003). AS160 is associated with GSVs *via* its interaction with IRAP (Larance et al., 2005). Four Akt phosphorylation sites have been identified on AS160 and mutation of these residues inhibits insulin-stimulated GLUT4 translocation

(Sano et al., 2003). This observation led to the model whereby phosphorylation of AS160 by Akt inactivates the Rab GAP function of the protein, and that this is required for GLUT4 translocation (Larance et al., 2005). Indeed, siRNA knockdown of AS160 results in a partial relocalisation of GLUT4 to the plasma membrane under basal conditions, demonstrating that that protein is required for intracellular retention of GSVs (Eguez et al., 2005).

Detailed analysis of the function of AS160 has revealed it regulates GSV docking at the plasma membrane (Bai et al., 2007). This study by Bai and colleagues used total internal reflection microscopy (TIRF) to track and dissect the docking and fusion steps of GSVs at the plasma membrane. Expression of a phospho-resistant AS160 mutant, or treating cells with the PI3K inhibitor wortmannin, significantly decreases the docking frequency of GSVs whilst having no effect on fusion (Bai et al., 2007).

AS160 has been shown to display GTPase activity towards Rabs 2A, 3A, 10 and 14 *in vitro* (Mîinea et al., 2005). These Rab proteins also associate with GSVs (Larance et al., 2005; Mîinea et al., 2005) however their precise role in GLUT4 trafficking are as yet unclear.

1.5.6.5 Phosphorylation of Sx4 and Munc18c

Protein phosphorylation plays an important role in insulin signalling and in controlling some of the GLUT4 regulatory proteins discussed above (Jewell et al., 2010). Direct phosphorylation of SNARE proteins has been shown to be an important regulatory feature of the proteins, as discussed in section 1.4.4.

Munc18c is phosphorylated in response to insulin (Oh and Thurmond, 2006; Schmelzle et al., 2006). The study by Schmelzle and colleagues identified that phosphorylation of tyrosine 521 increased >10 fold in response to insulin-treatment of 3T3-L1 adipocytes. Subsequent analysis has shown that Munc18c is phosphorylated directly by the insulin

receptor kinase (CIRK) *in vitro* at Y521 (Aran et al., 2011). Moreover, both phosphomimetic and CIRK phosphorylated Munc18c no longer bind to Sx4 in an *in vitro* pull down assay (Aran et al., 2011). These data suggest that phosphorylation of Munc18c may alleviate its inhibition of Sx4. Indeed, in a complex assembly assay using recombinant proteins purified from bacteria, pre-incubating Sx4 with Y521E phosphomimetic Munc18c increases the amount of complex formed when compared to pre-incubation with WT Munc18c or experiments lacking the SM protein (Kioumourtzoglou et al., 2014).

A second study investigating Munc18c phosphorylation in response to insulin mapped a phosphorylation site to tyrosine residue 219 (Oh and Thurmond, 2006). Mutation of this phosphorylation site decreases the affinity of Munc18c for Sx4, suggesting that this is again a mechanism to relieve the inhibition of Munc18c on SNARE complex assembly (Oh and Thurmond, 2006). Furthermore, phosphorylation of Y219 of Munc18c causes a switch in binding specificity from Sx4 to the protein Doc2 β (Jewell et al., 2008). Doc2 β has been shown to bind to Munc18c and positively regulate insulin-stimulated GLUT4 translocation (Ke et al., 2007)

Schmelzle and colleagues also reported two sites in Sx4 that show an increase in phosphorylation in response to insulin-stimulation, Y115 and Y251 (Schmelzle et al., 2006). However the consequences of phosphorylation of Sx4 at these residues are as yet unknown.

A

		<u>H_{abc}</u>	
Sx4	101	LKAIEPQKEEA-DENYNSVNTRMRKTQHGVLSSQQFVELINKCNSMQSEYRE	150
Sx1A	94	LKSIEQSIEQEEGLNRSSADLRIRKTKHSTLSRKFVEVMSEYNATQSDYRE	143
Sx3	95	LKSMEKHIEEDE--VRSSADLRIRKTSQHSVLSRKFVEVMTKYNEAQVDFRE	143
Sx2	92	LKAIEQSFDQDESGNRTSVDLRIRRTQHSVLSRKFVEAMAAYNEAQTFLFRE	142
Sso1	94	LKNEIKS-----AQRDGIHDTNKQAQAENSRQRFLKLIQDYRIVDSNYKE	138
Sso2	98	LKADIKD-----AQRDGLHDSNKQAQAENCRQKFLKLIQDYRIIDSNYKE	142

		<u>SNARE</u>	
Sx4	246	LSSADYVERGQEHVKTALLENQKKARKKKVLI AICVSITV VLLAVI-IGVTV	295
Sx1A	238	EHAVDYVERAVSDTKKAVKYQSKARRKIMIIICCVILGVI IAST-VGGIF	287
Sx3	237	MHTVDHVEKARDETKKAVKYQSQARKKLI IIIIVLVV VLLGILALI-IGLSV	286
Sx2	237	MNATDYVEHAK EETKKAIKYQSKARRKWI IIIAVSVV LV AIIALI-IGLSV	286
Sso1	236	EDAQLDVEQGVGHTDKAVKSARKARKNKIRCWLIVFAI I VVVVVVVVPAV	286
Sso2	241	EDAQQDVEQGVGHTNKAVKSARKARKNKIRCLIIICFI IFAIVVVVVVPSV	290

B

Munc18c	485	-DAIDNRLDSKEWPYCSQCPAVWNGSGAVSARQKPR--ANYLEDRKNGSKLI	532
Munc18a	490	-DTIEDKLDTKHYPISTRSSASFSTTAVSARYGHW HKNKAPGEYRSGPRLI	538
Munc18b	487	-DAVEDRLDRNLWPFVSDPAPTASSQA AVSARFGHW HKNKAGIEARAGPRLI	535
Sly1	570	NSSQKNLETTDSYLYIDPKI--T-----RGS H---TRKPKRQSYNKSL	607
Vps45	492	TDL SKNALFRDRFKEIDT-----QGHRVIGN--QQSKDIPQDVI	528

Figure 1.9: Sequence alignments of regions of selected Syntaxins and SM proteins
 An alignment of numerous mammalian and yeast plasma membrane Syntaxins (A) and SM proteins (B) is shown. Tyrosine residues that have been shown to be phosphorylated in response to insulin in Sx4 and Munc18c are highlighted in blue. The regions of Sx4 that the sequences reside in are labelled in blue.

Figure 1.9 shows an alignment of regions of Sx4 and Munc18c with other PM syntaxins and SM proteins. The residues that are phosphorylated in response to insulin are highlighted. These residues do not appear to be highly conserved. It has been previously noted that residues responsible for forming interactions common to all SNARE proteins, such as regions of the SNARE domain that are crucial for SNARE complex formation are well conserved, however residues in SNARE and SM proteins that contribute to their specificity for their binding partners or their role in specific cellular functions are less well conserved (Misura et al., 2000). The lack of conservation of the tyrosine residues that are phosphorylated in response to insulin suggests that these residues may be important to the function of Sx4 and Munc18c in a manner that is specific to regulating an insulin response in these cells.

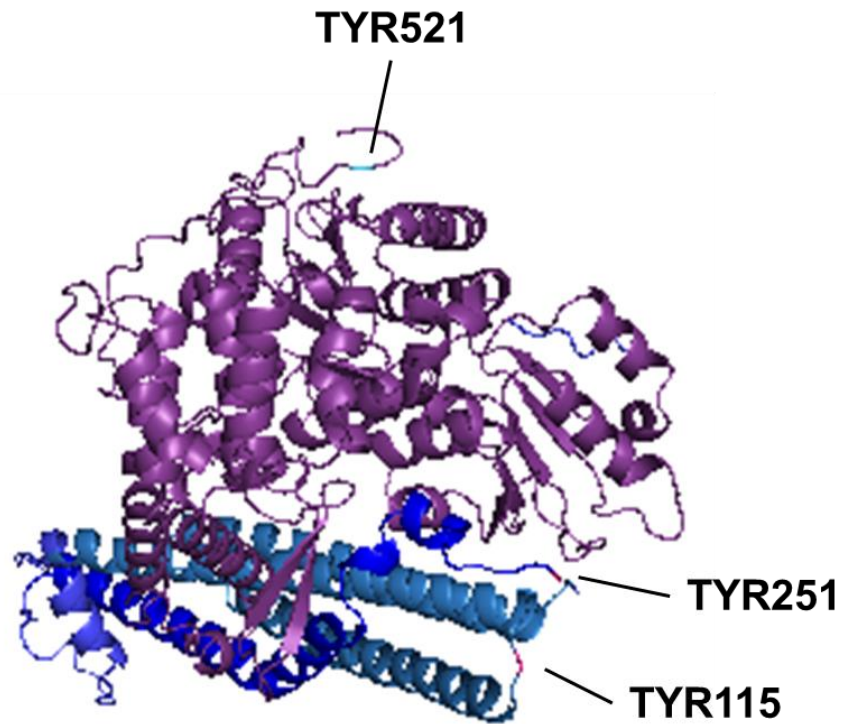


Figure 1.10: Predicted locations of the residues in Sx4 and Munc18c that are phosphorylated in response to insulin

The locations of the residues that have been shown to be phosphorylated on Sx4 and Munc18c were predicted based on the structure of the complex between closed Sx1A and Munc18a (PDB code 3C98). Syntaxin is shown in blue, the Habc domain is shown in light blue and the SNARE domain in dark blue. The predicted location for Y115 and Y251 are labelled and highlighted in pink. Munc18 is shown in purple. The predicted location of Y521 is labelled and highlighted in cyan.

Figure 1.10 shows a prediction of the sites of phosphorylation of Sx4 and Munc18c based on a structure of Sx1A and Munc18A (Burkhardt et al., 2008). In this structure the syntaxin in the closed conformation binds in the cleft of Munc18. The predictions for the locations of the phosphosites that this study focusses on are labelled. Though the phosphosites aren't predicted to be located in the regions of Munc18c or Sx4 that are likely to directly interact, the structure and conformation of both proteins are important for their function. The predicted location of these phosphosites indicates they may impact on the overall conformation, and therefore may affect the function, of Sx4 and Munc18c.

1.6 Aims

The aim of this thesis was to assess the effect of insulin-induced phosphorylation of Sx4 at Y115 and Y251 and of Munc18c at Y521 on SNARE complex assembly and GLUT4 translocation to the PM. Membrane trafficking is a complex and tightly regulated process. Phosphorylation of these two proteins could represent an important regulatory mechanism whereby SNARE proteins, and therefore SNARE complex assembly, are directly regulated by the insulin signalling cascade.

In chapter three, I examined the effect of phosphorylation of Sx4 *in vitro* using recombinant phospho-mimetic Sx4 mutants. Complex assembly assays, pull down assays and surface plasmon resonance was used to analyse the effect of the phospho-mutants on both binary and ternary SNARE complex interactions. Limited proteolysis experiments were also carried out to examine any conformational changes of the phospho-mimetic mutant proteins. Finally, a Phos-tag SDS-PAGE based mobility shift assay was carried out to analyse the phospho-isoforms present following *in vitro* phosphorylation of Sx4.

I then examined the effect of phospho-mimetic Sx4 mutants on the translocation of GLUT4 in HeLa cells in chapter 4. A HA-GLUT4-GFP reporter construct was used to assess the effect of over expression of Myc tagged Sx4 phospho-mutants on GLUT4 translocation by both microscopy and flow cytometry. I also generated Sx4 knockout 3T3-L1 cell lines; with the view to differentiating these into Sx4 depleted 3T3-L1 adipocytes.

Finally, in chapter 5, the effect of both phosphorylation of both Sx4 and Munc18c on their interactions is examined. Recombinant phospho-mimetic Sx4 and Munc18c were used in pull down and complex assembly assays in order to assess the effect of phosphorylation of both proteins on binary and ternary SNARE interactions.

Chapter Two

Materials and Methods

2 Materials and Methods

2.1 Materials

2.1.1 General reagents

General laboratory kits and reagents were obtained from the following suppliers:

- Ambion, Austin, USA
- BD Biosciences, Oxford, UK
- BioRad Laboratories Ltd, Hertfordshire, UK
- Clontech Laboratories Inc, California, USA
- Fisher Scientific Ltd, Loughborough, Leicestershire, UK
- FormediumTM, Norfolk, UK
- GE Healthcare Bio-Sciences Ltd, Buckinghamshire, UK
- Invitrogen Ltd, Paisley, UK
- New England Biolabs UK Ltd, Hertfordshire, UK
- Melford Laboratories Ltd, Ipswich, Suffolk, UK
- Merck Chemicals Ltd, Nottingham, UK
- Millipore Ltd, Livingston, UK
- New England Biolabs, Ipswich, USA
- Pierce, Perbio Science UK Ltd, Cheshire, UK

- Promega Ltd, Southampton, UK
- Roche Diagnostics Ltd, Burgess Hill, UK
- Severn Biotech Ltd, Worcestershire, UK
- Sigma Aldrich Company Ltd, Dorset, UK
- Spectrum Laboratories Inc, Netherlands
- Stratagene Technologies, California, USA
- Synaptic Systems, Göttingen, Germany
- VWR UK Ltd, Leicestershire, UK
- Whatman Plc, Kent, UK

2.1.2 Solutions

High quality pure sterile water was used as the dissolving agent in all solutions in this study unless otherwise stated.

2x Laemmli Sample Buffer (LSB): 100mM Tris, HCl pH 6.8, 4 % (w/v) SDS, 20 % (v/v) glycerol, 0.2 % (w/v) bromophenol blue, 10 % (v/v) β -mercaptoethanol

Buffer C: 25 mM HEPES, 0.4 M KCl, 10 % (w/v) glycerol, pH 7.4

Coomassie: 0.05 % (w/v) Coomassie brilliant blue R-250, 50 % (v/v) methanol, 10 % (v/v) acetic acid

Coomassie Destain: 15 % (v/v) methanol, 15 % (v/v) acetic acid

GST-Elution Buffer: 50 mM Tris base pH 8.0, 25 mM reduced glutathione, 10 % (w/v) glycerol

GST-Preparation Buffer: 100 mM HEPES, 500 mM NaCl, 5 mM MgCl₂, 5mM β-mercaptoethanol, 10 % (w/v) glycerol, 1 tablet of complete protease inhibitor mix per 100 ml (Roche)

LB media: 1 % (w/v) peptone, 0.5 % (w/v) yeast extract, 1 % (w/v) NaCl, 1.2 % (w/v) Agar (optional)

PBS: 85 mM NaCl, 1.7 mM KCl, 5 mM Na₂HPO₄, 0.9 mM KH₂PO₄, pH 7.4

PBST: 85 mM NaCl, 1.7 mM KCl, 5 mM Na₂HPO₄, 0.9mM KH₂PO₄, 0.1 % (v/v) Tween-20, pH 7.4

Ponceau Stain: 0.2 % (w/v) Ponceau Stain, 1 % (v/v) glacial acetic acid

SDS-PAGE resolving buffer: 75mM Tris-HCl, pH 8.8, 0.2% (w/v) SDS

SDS-PAGE stacking buffer: 25mM Tris-HCl, pH 6.8, 0.2% (w/v) SDS

SDS-PAGE running Buffer: 20mM glycine, 62mM Tris-Base, 0.1% (w/v) SDS

Semi-dry transfer Buffer: 24mM Tris base, 20mM glycine, 0.1% (w/v) SDS, 20% (v/v) methanol

SOC media: 2% (w/v) tryptone, 0.5% (w/v) yeast extract, 10 mM NaCl, 2.5 mM KCl, 10 mM MgCl₂, 10 mM MgSO₄, and 20 mM glucose

TAE: 40 mM Tris-Acetate pH 8, 1mM EDTA

Terrific Broth (TB): 1.2% (w/v) tryptone, 2.4% (w/v) yeast extract, 0.4% (v/v) glycerol, 17mM KH_2PO_4 , 72mM K_2HPO_4 (obtained from Melford Labs Ltd)

TST: 50 mM Tris-HCl pH 7.6, 150 mM NaCl, 0.05% (v/v) Tween-20

YPD yeast media: 1% (w/v) yeast extract, 2% (w/v) peptone, 2% (w/v) glucose, 2% (w/v) Agar (optional)

2.1.3 Primary antibodies

Table 2.1: Primary antibodies used in this study

Antigen	Working dilution	Description	Source
HA	IF: 1:100	Rat, monoclonal, clone 3F10	Roche applied sciences (11 867 423 001)
His ₆	IB: 1:10000	Mouse, monoclonal	Sigma-Aldrich (H1029)
GAPDH	IB: 1:10000	Mouse, monoclonal	Applied Biosystems (AM4300)
VAMP2/ Synaptobrevin	IB: 1:2000	Mouse, monoclonal	Synaptic Systems (104 211)
Syntaxin 4	IB: 1:1000-1:5000	Rabbit, polyclonal antiserum	Synaptic Systems (110 042)
BiP (GRP78)	IB: 1:1000	Rabbit, polyclonal	Abcam (ab21685)
Myc	IB: 1:1000 IF: 1:300	Mouse, monoclonal, clone 9E10	Sigma-Aldrich (M4439)
Phosphotyrosine (PY20)	IB: 1:1000	Mouse, purified	BD Biosciences (610000)

2.1.4 Secondary antibodies

Table 2.2: Secondary antibodies used in this study

Antigen	Working dilution	Description	Source
Anti-mouse IgG	IB: 1:2000-5000	Peroxidase conjugate, produced in goat	Sigma-Aldrich (A4416)
Anti-rabbit IgG	IB:1:2000-5000	Peroxidase conjugate, produced in goat	Sigma-Aldrich (A0545)
Anti-rat AlexaFluor 647	IF/FACS: 1:300	Produced in goat, purified, whole IgG	LifeTechnologies (A-21247)
Anti-mouse DyLight 405	IF/FACS: 1:300	Produced in Goat, whole IgG affinity purified	Jackson ImmunoResearch (115-475-003)

2.1.5 Mammalian cell lines

Table 2.3: Mammalian cell lines used in this study

Cell line	Source
3T3-L1	American Type Culture Collection (ATCC)
HeLa	American Type Culture Collection (ATCC)

2.1.6 *E. coli* strains

Table 2.4: *E. coli* strains used in this study

Strain	Genotype	Source
BL21 (DE3)	F-ompT hsdSB(rB-mB-) gal dcm (DE3)	Invitrogen Ltd
Top10	F- mcrA _(mrr-hsdRMS-mcrBC) ϕ 80lacZ_M15 _lacX74 nupG recA1 araD139 _(ara-leu)7697 galE15 galK16 rpsL(StrR) endA1 λ -	Invitrogen Ltd

2.1.7 Plasmids

Table 2.5 Summary of plasmids used in this study

Plasmid	Description	Source
pETDuet-1:GST	<i>E. coli</i> expression vector encoding GST	Constructed by Dr Fiona Brandie
pETDuet:Sx4-GST	<i>E. coli</i> expression vector encoding C-terminally GST tagged Sx4 cytosolic domain	Constructed by Dr Fiona Brandie
pETDuet:Sx4-GST (Open)	<i>E. coli</i> expression vector encoding C-terminally GST tagged Sx4 cytosolic domain. Contains two mutations in the hinge region (L173A/E174A)	Constructed by Dr Veronica Aran-Ponte
pETDuet:Sx4-GST (Y115E)	<i>E. coli</i> expression vector encoding C-terminally GST tagged Sx4 cytosolic domain. Contains a phosphomimetic mutation (Y115E)	Constructed by Dr Veronica Aran-Ponte
pETDuet:Sx4-GST (Y251E)	<i>E. coli</i> expression vector encoding C-terminally GST tagged Sx4 cytosolic domain. Contains a phosphomimetic mutation (Y251E)	Constructed by Dr Veronica Aran-Ponte
pETDuet:Sx4-GST (Y115,251E)	<i>E. coli</i> expression vector encoding C-terminally GST tagged Sx4 cytosolic domain. Containing two phosphomimetic mutations (Y115,251E)	Constructed by Dr Veronica Aran-Ponte
pGEX-4T-1:GST-VAMP2	<i>E. coli</i> expression vector encoding N-terminally GST tagged VAMP2 cytosolic	Constructed by Dr Dimitrios Kioumourtzoglou

pQE30:His-SNAP23	domain (Thrombin cleavable) <i>E. coli</i> expression vector encoding N-terminally His tagged SNAP23	Constructed by Dr Fiona Brandie
pETDuet:Sx4(Myc)-GST	<i>E. coli</i> expression vector encoding C-terminally GST tagged Sx4 cytosolic domain. Contains Myc tag positioned between the N-terminus and Habc domain	Cytoplasmic domain of Sx4 was amplified from pCR3.1:Sx4(Myc). The PCR product was cloned into TA TOPO cloning vector pCR2.1-TOPO before being excised by restriction enzyme digest with <i>NheI</i> and <i>ApaI</i>
pCR3.1	Mammalian expression vector	GenScript, Piscataway, NJ, USA
pCR3.1:Sx4(Myc)	Mammalian expression vector encoding full length syntaxin 4. Contains Myc tag positioned between the N-terminus and Habc domain	Constructed using the custom gene synthesis service from GenScript, Piscataway, NJ, USA
pCR3.1:Sx4(Myc)-Y115E	Mammalian expression vector encoding full length syntaxin 4 with a tyrosine to glutamic acid mutation at residue 115. Contains Myc tag positioned between the N-terminus and Habc domain.	Constructed using the custom gene synthesis service from GenScript, Piscataway, NJ, USA
pCR3.1:Sx4(Myc)-Y251E	Mammalian expression vector encoding full length syntaxin 4 with a tyrosine to glutamic acid mutation at residue 251. Contains Myc tag positioned between the N-terminus and Habc domain	Constructed using the custom gene synthesis service from GenScript, Piscataway, NJ, USA

pCR3.1:Sx4(Myc)- Y115,251E	Mammalian expression vector encoding full length syntaxin 4 with a tyrosine to glutamic acid mutation at residue 115 and 251. Contains Myc tag positioned between the N-terminus and Habc domain	Constructed using the custom gene synthesis service from GenScript, Piscataway, NJ, USA
pCMV-Cas9-RFP	CRISPR plasmid containing syntaxin 4 target guide RNA sequence, Cas9 and RFP	Purchased from Sigma- Aldrich, St Louis, MO, USA

2.1.8 Primers

Oligonucleotides were purchased from Integrated DNA Technologies. Each primer pair was diluted to a concentration of 100µM and stored at -20°C.

Table 2.6: Oligonucleotides used in this study

Primer	Sequence (5'-3')
Sx4-Myc ΔTMD Forward	CGG GGC ATA TGC GCG ACA GGA CCC AT
Sx4-Myc ΔTMD Reverse	GGC TCG AGG ACC TTT TTC TTC CTC GCC TTC TTC TG

2.2 General Molecular Biology Techniques

2.2.1 Small scale preparation of plasmid DNA

A single colony of newly transformed bacteria (section 2.3.1) was used to inoculate 10ml sterile LB supplemented with the appropriate antibiotic for selection (section 2.1.3) and grown overnight at 37°C in a shaking incubator. Bacteria were pelleted by centrifugation (2500 rpm, 10 minutes) and plasmid DNA was extracted using the Promega Ltd Wizard Plus SV mini-prep kit following the manufacturer's instructions. The concentration of DNA was determined using a NanoDrop (ThermoScientific) and was examined by agarose gel electrophoresis (section 2.2.2).

2.2.2 Large scale preparation of plasmid DNA

A single colony of newly transformed bacteria (section 2.3.1) was used to inoculate 50 ml of sterile LB media supplemented with the appropriate antibiotic for selection (section 2.1.3) and grown overnight at 37°C in a shaking incubator. Bacteria were pelleted by centrifugation at 2500 rpm for 10 minutes and plasmid DNA was extracted using the Qiagen HiSpeed Plasmid Purification midi-prep kit as per manufacturer's instructions. The concentration of DNA was determined using a NanoDrop (ThermoScientific) and was examined by agarose gel electrophoresis (section 2.2.2).

2.2.3 Agarose gel electrophoresis

DNA samples were routinely visualised by agarose gel electrophoresis. Agarose powder (0.8 - 1.5% (w/v)) was dissolved in TAE buffer (40 mM Tris Acetate, 1 mM EDTA, pH 8.0) by heating in a microwave. The solution was allowed to cool before SYBR safe DNA gel stain was added at a 1:10000 dilution. DNA samples were prepared by addition of 6x DNA loading buffer (40% (w/v) ficoll, 0.25% (w/v), bromophenol blue). Samples were loaded onto the gel, alongside a 100 bp or 1 kb DNA marker (New England Biolabs Ltd). The gel was then run at 100 V in TAE buffer and DNA samples were visualised with a blue light

box Syngene U:Genius 3 gel documentation system (Syngene). DNA was extracted from agarose gels using a GeneJET Gel Extraction Kit (ThermoScientific).

2.2.4 PCR

Forward and reverse oligonucleotide primers were designed and purchased from Integrated DNA Technologies. The high fidelity DNA polymerase *Pfu* was routinely used and purchased from Promega UK. Reactions were carried out in PCR tubes in a volume of 50µl of sterile dH₂O. A typical reaction would be as follows:

Template DNA (~1 µg/µl)	1µl
10X <i>Pfu</i> buffer	5µl
Forward primer (5 pM)	1.5µl
Reverse primer (5 pM)	1.5µl
dNTPs (10 mM)	1µl
<i>Pfu</i> polymerase	1µl (5 units)

Reactions were carried out in a thermocycler using the following standard conditions:

Initial denaturation	95°C	5 mins	
Denaturation	95°C	1 min	} 30 cycles
Primer annealing	~55°C*	1 min	
Elongation	72°C	1 min/kb+1 min	
Final elongation	72°C	10 mins	

2.2.6 DNA ligase reactions

Linearised parental vector and DNA fragment inserts were ligated using T4 DNA ligase (New England Biolabs Inc). A typical ligase reaction was as follows;

Linearised vector DNA (1mg/ml)	2 μ l
Fragment DNA (1mg/ml)	6 μ l
10 x T4 DNA ligase buffer	1 μ l
T4 DNA ligase	1 μ l (10 units)

Reactions were carried out at room temperature overnight before being transformed into TOP10 cells (Section 2.3.1).

2.3 General Protein Techniques

2.3.1 Bacterial transformation

15-50µl of the appropriate chemically competent bacterial cell stock was thawed and mixed with 3µl of mini-prepped DNA. The mixture was on ice for 30 minutes before being heat shocked at 42°C for 30 seconds. The cells were then returned to ice for 2 minutes. 200µl of SOC media was added and the cells were incubated at 37°C in a shaking incubator for 1 hour. 50µl of the culture was spread onto LB agar plates containing the appropriate antibiotic for selection and incubated overnight at 37°C.

2.3.2 General expression and purification of recombinant proteins

10ml of sterile LB media was inoculated with a single colony of freshly transformed BL21-DE3 bacteria and grown in a shaking incubator at 37°C overnight. The appropriate volume of TB (1-12 L) was then inoculated and cultures grown to an OD₆₀₀ of 0.6 at 37°C with shaking. Protein production was then induced with 0.5mM of IPTG and cultures were left to grow overnight at 19-22°C with shaking. Bacteria was harvested by centrifugation at 5000 rpm for 20 minutes and resuspended in the appropriate buffer (section 2.3.3 and 2.3.4). Bacteria were lysed using sonication. Lysate was then cleared by centrifugation at 15000 rpm for 45 minutes. The cleared lysate was incubated with 300µl of the appropriate beads, which had been preequilibrated with lysis buffer, overnight at 4°C. Following incubation, beads were washed three times by resuspending in wash buffer and centrifuging at 1000rpm for 1 minute. Protein bound to the beads was eluted by incubating the beads with 1-3ml of elution buffer with rotation at 4°C for 1.5 hours; eluted protein was then collected by centrifugation at 1000rpm for 1 minute and the supernatant was collected. This elution step was repeated as desired up to three times. Samples from each step of the process were analysed by SDS PAGE and Coomassie staining or immunoblotting. Eluted protein was dialysed overnight at 4°C using Float-a-Lyzer (SpectrumLabs) columns with 20kDa pores against 5L PBS plus 5% glycerol. Purified

protein was then aliquoted and snap frozen in liquid nitrogen before being stored at -80°C. For details of culture and elution volumes used for each protein see Appendix I.

2.3.3 Purification of GST-tagged proteins

To immobilise GST tagged fusion proteins glutathione Sepharose 4 Fast Flow affinity medium (GE Healthcare) was used. Bacteria were resuspended in GST preparation buffer (100 mM HEPES, 500mM NaCl, 5mM MgCl₂, 5mM β-mercaptoethanol, 10% (w/v) glycerol, 1 tablet of complete protease inhibitor mix (EDTA free) per 100ml (Roche)). Beads were also equilibrated with this buffer prior to incubation with cleared lysate. Once protein was bound, the beads were washed with PBS, with the last wash being PBS plus 0.5M NaCl. Protein was eluted using GST elution buffer (50mM Tris base pH 8.0, 25mM reduced glutathione, 10% (w/v) glycerol).

2.3.4 Purification of His-tagged proteins

Ni-NTA Agarose (Qiagen) was used to purify His₆ tagged fusion proteins. The lysis buffer used was Buffer C supplemented with 4 mM imidazole, 5 mM β-mercaptoethanol, 1 tablet of complete protease inhibitor mix (EDTA free) per 100ml (Roche). Beads were washed with Buffer C supplemented with 20 mM imidazole, 5 mM β-mercaptoethanol. Protein was eluted using Buffer C supplemented with 250 mM imidazole, 5 mM β-mercaptoethanol.

2.3.5 Purification of proteins with cleavable GST tags

Proteins were purified as per section 2.3.3, however proteins were cleaved from the beads and GST tag using thrombin in replace of eluting. Glutathione Sepharose beads with protein bound were resuspended in 2ml PBS and 5 units of thrombin was added. The beads were incubated with the thrombin for 3 hours at room temperature with rotation. Once cleavage was complete thrombin action was inhibited with the addition of 1mM phenylmethylsulfonyl fluoride (PMSF) protease inhibitor. Protein was collected by centrifuging at 1000 rpm for 1 minute and collecting the supernatant.

2.3.6 Estimating protein concentration

Purified protein samples were thawed on ice. Once thawed samples were diluted in PBS by a factor of 1:5 and/or 1:10. Samples were then diluted 1:2 in 2 x Laemmli Sample Buffer (LSB) and run on 15% SDS-PAGE gels alongside BSA standards (0.1 µg, 0.2 µg, 0.4 µg, 1µg, 2µg). Gels were Coomassie stained (Section 2.3.8) and protein concentrations were estimated with the aid of densitometry using Image J software.

2.3.7 SDS-PAGE

Sodium dodecyl sulfate polyacrylamide gel electrophoresis (SDS-PAGE) was carried out using a Bio Rad Mini-PROTEAN Tetra cell gel apparatus (Bio-Rad Laboratories Ltd) according to the manufacturer's protocol. Precision Plus Protein Standards from BioRad were run along with protein samples. Gels were prepared with either 7.5,12 or 15% (v/v) acrylamide resolving gel (75 mM Tris.HCl, pH 8.8, 0.1 % (w/v) SDS, 7.5, 12 or 15% v/v acrylamide, 0.05 % (v/v) Ammonium persulfate and 0.01 % (v/v) TEMED) with 4 % stacking gel (25 mM Tris.HCl, pH 6.8, 0.1 % (w/v) SDS, 4 % (v/v) acrylamide, 0.05 % (v/v) Ammonium persulfate and 0.01 % (v/v) TEMED). Gels were run in SDS running buffer (25 mM Tris, 190mM glycine and 0.1 % (w/v) SDS) at 120 V.

2.3.8 Coomassie staining and destaining

Following SDS-PAGE gels were immersed in Coomassie stain for around 30 minutes. Gels were then destained in Coomassie destaining buffer for as long as necessary, the buffer was periodically changed during destaining.

2.3.9 Semi-dry transfer

Following SDS-PAGE (section 2.3.7) proteins were transferred onto phenylmethylsulfonyl fluoride (PVDF) membranes. PVDF was first activated by soaking in methanol. The membrane, acrylamide gel and 1.5mm filter paper were then soaked in semi-dry transfer buffer (24mM Tris, 20mM glycine, 0.1% (w/v) SDS, 20% (v/v) ethanol). The membrane

and gel were sandwiched between two sheets of filter paper in a BioRad Trans-Blot SD semi-dry electrophoretic transfer cell, taking care to remove any air bubbles. A constant current of 300mA was applied to carry out the transfer for 60 minutes. Transfer efficiency was routinely checked by Ponceau S staining (0.1% (w/v) Ponceau S, 5% (v/v) acetic acid).

2.3.10 Immunoblotting

Following protein transfer (section 2.3.9), the PVDF membrane was blocked for 1 hour in 5% milk powder in PBST (85mM NaCl, 1.7mM KCl, 5mM Na₂HPO₄, 0.9mM KH₂PO₄, 0.1% (v/v) Tween-20, pH 7.4). Primary antibodies were diluted to the appropriate concentration in 1% milk PBST and incubated with the membrane overnight at 4°C. Membranes were then washed three times for 10 minutes in PBST. Horseradish peroxidase (HRP) linked secondary antibodies were diluted to the appropriate concentration in 5% milk PBST and applied to the membrane for 1 hour at room temperature. The membranes were again washed three times in PBST for 10 minutes. The blots were visualised using enhanced chemiluminescence (ECL).

Equal amounts of ECL solutions A and B (Merck Millipore) were mixed and applied to the surface of the membrane. The membrane was incubated with the ECL for 2 minutes before the excess was removed. The blot was then visualised using a Syngene GeneGenius gel documentation system (Syngene).

2.4 Complex Assembly Assay

Equimolar concentrations of (approximately 5 µM) Sx4, SNAP23 and VAMP2 (or GST controls) were combined in a volume of 500µl of Buffer C plus 100µg/ml BSA and incubated at 4°C, with rotation, for between 15 and 60 minutes. Samples were then immediately mixed with 2X LSB and boiled at 95°C for 5 minutes. Samples were analysed using SDS-PAGE (section 2.3.7), Coomassie staining (section 2.3.8) and immunoblotting (section 2.3.10).

2.5 Pull down assays with recombinant proteins

GST tagged Sx4 was purified and left immobilised to glutathione Sepharose beads (section 2.3.3). Alternatively purified Sx4-GST was immobilised to washed glutathione Sepharose beads by incubating 200 μ l of Sx4 with 60 μ l of beads for 3 hours at 4°C with rotation. Beads were then washed three times in PBS to remove any unbound protein. A sample of the beads was analysed by SDS-PAGE and Coomassie staining to check immobilisation.

Once immobilised 1-5 μ g Sx4-GST was incubated with an excess of either His-SNAP23, His-Munc18c or thrombin cleaved VAMP2 in 500 μ l binding buffer (PBS, 5mM β -mercaptoethanol, 100 μ /ml BSA). Reactions were carried out by incubating at 4°C with rotation for 30, 60 or 120 minutes. Following incubation beads were collected by centrifugation at 1000 rpm for 1 minute at 4°C. The beads were then washed at least six times in binding buffer to remove any unbound protein. Once washed, beads were resuspended in 50 μ l 2X LSB and boiled for 95°C for 5 minutes. Samples were then analysed by SDS-PAGE (section 2.3.7) and immunoblotting (section 2.3.10). Ponceau staining was carried out to analyse Sx4 input.

2.6 Chymotrypsin Assay

30 ng/ μ l of chymotrypsin (Sigma-Aldrich) was incubated with roughly 0.3mg/ml of protein in PBS at room temperature for 0-30 minutes. Samples were taken at the desired time point and immediately mixed with 2X LSB and boiled at 95°C for 5 minutes. Samples were then analysed by SDS-PAGE (section 2.3.7) and Coomassie blue staining (section 2.3.8).

2.7 CIRK phosphorylation assay

Autophosphorylated CIRK and Sx4 were mixed and made up to a final volume of 50 μ l in filter sterilised reaction buffer (50 mM HEPES pH 7.5, 4 mM MnCl₂, 0.2 mM DTT, 100 μ M ATP Na-salt). Samples were incubated at 30 °C in a water bath for 150 min. The reaction

was stopped by the addition of sample buffer. Phosphorylation was analysed by immunoblotting.

2.8 Phos-tag based mobility shift SDS-PAGE

Phos-tag™ Acrylamide SDS-PAGE was carried out using a Bio Rad Mini-PROTEAN Tetra cell gel apparatus (Bio-Rad Laboratories Ltd, Hemel Hempstead, UK) according to the manufacturer's protocol. Precision Plus Protein Standards from BioRad were run along with protein samples. Resolving gels were prepared with 50µM Phos-tag, 100µM MnCl₂, 75 mM Tris.HCl, pH 8.8, 0.1 % (w/v) SDS, 10 % v/v acrylamide, 0.05 % (v/v) Ammonium persulfate and 0.01 % (v/v) TEMED, and were left to set for 30 minutes. A 4 % stacking gel was then prepared (25 mM Tris.HCl, pH 6.8, 0.1 % (w/v) SDS, 4 % (v/v) acrylamide, 0.05 % (v/v) Ammonium persulfate and 0.01 % (v/v) TEMED). Gels were run in SDS running buffer (25 mM Tris, 190mM glycine and 0.1 % (w/v) SDS) at 100 V for 210 minutes.

Once gels were run they were incubated in semi-dry transfer buffer (24mM Tris, 20mM glycine, 0.1% (w/v) SDS, 20% (v/v) ethanol) plus 1 mM EDTA for 10 minutes with agitation. Gels were washed twice in semi-dry transfer buffer before proteins were transferred onto phenylmethylsulfonyl fluoride (PVDF) membranes (section 2.6.9). The membranes were then subject to immunoblot analysis (section 2.6.10).

2.9 General cell culture techniques

2.9.1 Growth of HeLa cells

HeLa cells were purchased from ATCC (USA). A HeLa cell line stably expressing HA-GLUT4-GFP had been previously generated in the laboratory. HeLa cells were cultured in DMEM (Dulbecco's Modified Eagle's Medium) supplemented with 10% (v/v) Foetal Calf Serum (FCS), 1% Glutamax (ThermoFisher Scientific) (v/v) at 37°C in a humid

atmosphere of 5% CO₂. Media was changed every other day and cells were passaged when confluent.

2.9.2 Growth of 3T3-L1 cells

3T3-L1 cells were purchased from ATCC (USA). A 3T3-L1 cell line stably expressing HA-GLUT4-GFP was previously generated in the lab. 3T3 cells were cultured in DMEM supplemented with 10% (v/v) New-born Calf Serum (NCS), 1% Glutamax (v/v) at 37°C in a humid atmosphere of 5% CO₂. Media was changed every other day and cells passaged when 70-80% confluent.

2.9.3 Passage of cells

Cells were passaged when they reached the appropriate confluency. Media was aspirated and cells washed with 5-10 ml of pre-warmed serum-free media. 5mls of 0.05 % (w/v) Trypsin (Invitrogen) was then added and cells returned to the incubator for between 5 and 10 minutes, until all cells were dissociated. 1 ml of the cell suspension was then added to 14 ml of media in a 75 cm² tissue culture flask for continued culture. Alternatively, suspended cells were counted, using a haemocytometer, and plated at the appropriate density in 6 or 24 well plates.

2.9.4 Freezing of cells

Cells were frozen at 70-80 % confluency. Cells were washed and trypsinised as described in section 2.7.3. 10 ml of cell culture media was then added the cell suspension and cells were pelleted by centrifugation at 800 rpm for 5 minutes. Pelleted cells were then resuspended in 1-4 ml of cell freezing media (FBS + 10% (v/v) DMSO, filter sterilized). 1 ml aliquots of the cell suspension were then frozen in a Nalgene "Mr Frosty" containing isopropanol in 1.8 ml cryo-vials and stored at -80 °C for 24 hours, before being transferred to liquid nitrogen for long term storage.

2.9.5 Resurrection of cells

Cells were resurrected from liquid nitrogen storage by incubation in a 37°C water bath until thawed. Cells were then transferred to a 75 cm² cell culture flask containing 14 ml of the appropriate cell culture media. Cells were left to adhere to the flask for 24 hours before the culture media was changed to remove DMSO.

2.9.6 Transfections

GeneCellin DNA transfection reagent (Eurobio Lifesciences) was used for all transfections as per manufacturer's instructions, the standard transfection conditions used are summarised in table 2.8. Cells were seeded onto the appropriate plate 24 hours prior to transfection. Midi-prepped plasmid DNA was combined with serum free DMEM and GeneCellin, lightly mixed and incubated for 15 minutes at room temperature. The transfection mixture was then added to the cells dropwise and transgene expression was analysed 24 hours later.

Table 2.7: Transfection conditions

Tissue culture vessel	Number of cells seeded	Volume of cell culture medium (µl)	Amount of DNA (µg)	Volume of DNA solution (µl)	Volume of genecellin (µl)
24 well	50000	500	0.5	100	2
6 well	250000	2000	2	200	8
100mm	2000000	10000	10	500	30

2.9.7 Differentiation of 3T3-L1 cells

Low passage number 3T3-L1 cells were plated at 60-70 % confluence in DMEM supplemented with 10 % NCS and 1 % Glutamax. The cells were then grown to full confluence, with the media changed every two days. Two days post confluence the media

was changed for DMEM supplemented with 10 % FBS, 1 % Glutamax, 1 µg/ml insulin, 5 µM troglitazone, 0.25 µM dexamethasone, 0.5 mM IBMX. This was considered day 0. On day 3 media was changed to DMEM supplemented with 10 % FBS, 1 % Glutamax, 1 µg/ml insulin, 5 µM troglitazone. On day 6 the media was changed to DMEM supplemented with 10 % FBS and 1 % Glutamax. Adipocytes were cultured in this media until use. The media was changed every two days. Experiments were carried out on day 8-10.

2.9.8 Insulin stimulation of HeLa cells and adipocytes

Cells were washed two times before being serum starved for 2 hours in serum-free DMEM. Culture media was then changed to serum-free DMEM with or without 170 nM insulin for 20 minutes at 37°C.

2.10 Immunofluorescence

Cells were seeded at the appropriate density onto sterilised 13 mm coverslips in 24 well plates. Coverslips were sterilised by first autoclaving, then by dipping twice in 70 % (v/v) ethanol before being air dried in a cell culture hood for 1 hour. Once the appropriate transfections or treatments had been carried out, cells were subject to indirect immunofluorescence. Cells were washed three times in PBS before being fixed in 3 % (w/v) paraformaldehyde (PFA) for 20 minutes. Cells were then washed three times in PBS + 20mM Glycine to quench the PFA before being blocked for 30 minutes in staining solution (PBS + 20mM glycine, 2% (w/v) BSA) supplemented with 5 % (v/v) goat serum (Sigma). Where required staining solution also contained 0.1% saponin to permeabilise the cells. For subsequent staining and washing coverslips were removed from the wells and placed, cell side down, onto 40µl drops of the appropriate solution on clean nescofilm that had been fixed to the lab bench with water. Cells were incubated with primary antibody in staining solution for 45 minutes. The cells were then washed four times in staining solution before being incubated with the appropriate secondary antibody, diluted

in staining solution, for 30 minutes. Cells were then washed three times with PBS + 20 mM glycine. Where required, coverslips were then incubated with 1µg/ml DAPI (4',6-diamidino-2-phenylindole) in PBS for 5 minutes to stain cell nuclei. Finally cells were dipped in PBS, air dried and mounted onto slides using ImmunoMount (GeneTex). Slides were stored in the dark at 4°C for a minimum of 24 hours before being imaged using a Zeiss LSM 880 with Airyscan confocal microscope.

2.11 Generating mammalian cell lysates

Cells were plated and treated as desired before being washed three times in ice-cold PBS. Cells were then scraped in 150 µl PBS containing EDTA free protease inhibitor cocktail (Roche) and 2X LSB. Cells were then homogenised by passing through a 26 ½ gauge needle 10-15 times. The lysates were boiled at 95°C for 5 minutes. Samples were then stored at -20°C before being analysed by SDS-PAGE (section 2.3.7).

2.12 Quantification of HA-GLUT4-GFP translocation by flow cytometry

Translocation of HA-GLUT4-GFP in HeLa cells was analysed by flow cytometry. Roughly 150000 cells were seeded into a 6 well plate 48-72 hours before analysis. Where cells were transfected this was carried out using the standard protocol (section 2.7.6) 24 hours prior to analysis. Cells were serum starved for two hours prior to being treated with or without 170nM insulin for 20 minutes at 37°C. The plates were then placed on ice and all subsequent steps used ice cold solutions. Cells were washed three times with PBS before being fixed with 1% (w/v) electron microscopy grade, methanol free PFA for 20 minutes. Cells were again washed twice in PBS before non-specific epitopes were blocked with 2 % (w/v) BSA in PBS for 45 minutes. GLUT4 was then surface stained with 1:200 anti-HA primary antibody in PBS supplemented with 2 % (w/v) BSA for 45 minutes. Cells were washed again three times in PBS. Alexa Fluor 647 (ThermoFisher) coupled secondary

antibody was then applied in 2 % (w/v) BSA in PBS and incubated for 45 minutes. Cells were then washed 3 times in 2 % (w/v) BSA in PBS.

When required, cells were then fixed again using 4 % electron microscopy grade, methanol free PFA for 20 minutes to fix anti-HA antibodies in place. Cells were washed three times and then permeabilised and blocked with PBS plus 0.1 % saponin in 2 % BSA for 45 minutes. The cells were then stained for Sx4(Myc) expression using an anti-Myc antibody in PBS plus 2 % BSA for 45 minutes. Cells were then washed three times in PBS plus 2 % BSA. Secondary anti-body was applied, diluted in PBS plus 2 % BSA, for 30 minutes. Cells were then washed three times in PSB.

The cells were then dissociated from the tissue culture dish using a cell lifter. Dissociated cells were collected and centrifuged at 600 g for 8 minutes at 4°C. The resulting pellet of cells was suspended in 350µl of 2 % (w/v) BSA in PBS. Samples were then analysed on a Beckman Coulter CyAn ADPs flow cytometer. Data was collected and analysed using Summit Software v4.3.

2.13 Generating a CRISPR knockout cell line

3T3-L1 and HA-GLUT4-GFP 3T3-L1 cells were plated in 10cm dishes. The cells were transfected with Sx4 CRISPR plasmid using GeneCellin as per manufacturers instructions (section 2.7.6). 24 hours after transfection cells were washed in pre-warmed serum free DMEM and dissociated from the cell culture dish using 4 ml of 0.05 % (w/v) Trypsin (Invitrogen) and incubated for 5 minutes at 37 °C. They were then collected, and pelleted by centrifugation at 800 rpm for 5 minutes. Cells were resuspended in 1 ml of PBS before being sorted based on the presence of RFP fluorescence using a Beckman Coulter MoFlo Astrios flow cytometer and Summit 6.2 software. RFP positive cells were serially diluted and plated in both 10 cm dishes and 6 well plates. The cells were cultured in DMEM supplemented with 10 % NCS and 1 % Glutamax until single colony units were formed. During this time the media was changed every 3 days.

Individual colonies were then selected, firstly the medium was removed and cells were carefully washed three times with prewarmed serum free DMEM. Colonies were isolated using autoclave sterilized wide ends of 1 mL pipette tips attached to the plate using autoclaved silicon grease. Selected colonies were then incubated with 100 μ L trypsin for around one minute before being suspended by trituration with the trypsin. The selected colonies were then expanded and either frozen in aliquots (section 2.7.4) or lysed for immunoblot analysis (section 2.9).

2.14 Surface plasmon resonance

Surface plasmon resonance experiments were carried out on a Biacore T100 (GE Healthcare). All experiments used a Series S Sensor Chip CM5 (GE Healthcare). Proteins were expressed and purified as described previously (section 2.3.2). Sensor chips were docked and equilibrated to SPR running buffer (filter sterilised PBS + 5 % glycerol, 0.05 % (v/v) Tween-20) for at least 1.5 hours. All binding experiments were carried out at 25 °C at a flow rate of 10 μ L/min.

Ligands were immobilised using thiol coupling. This chip surface was activated by injecting an equal mix of EDC (1-ethyl-3-(3-dimethylaminopropyl) carbodiimide) and NHS (N-hydroxysuccinimide) for 420 seconds at a flow rate of 30 μ L/min. The ligand was then diluted to between 0.1 and 0.5 μ M in 10 mM sodium acetate, pH 4.5 and flowed over the activated chip for between 120 and 480 seconds until roughly 900 units of ligand were immobilised. Running buffer was then run over the chip for 180 seconds to remove any unbound ligand. Finally, the remaining uncoupled active groups on the sensor chip were deactivating by injecting 1M ethanolamine hydrochloride pH8.5 for 420 seconds.

All binding experiments were carried out at 25 °C at a flow rate of 10 μ L/min, in running buffer. Sx4-GST analyte proteins were dialysed into SPR running buffer before being diluted to concentrations between 1.2 and 20 μ M. Injections of each concentration were carried out in duplicate, moving from the lowest concentration to the highest and back

down to the lowest. The order of protein mutants injected was randomised. Sx4 proteins were injected for 180 seconds, 120 seconds later the chip surface was regenerated by injecting 1M ethanolamine hydrochloride pH8.5 for 30 seconds.

The data obtained was analysed using the affinity analysis functions in BIAevaluation Software (GE Healthcare).

Chapter Three

***In vitro* analyses of phospho-mimetic Sx4**

3 *In vitro* analyses of phospho-mimetic Sx4

3.1 Introduction

3.1.1 Regulation of GSV fusion at the plasma membrane

Insulin is an important regulator of whole body glucose homeostasis. In order to maintain blood glucose levels insulin binds to its receptor on adipocyte and muscle cells, resulting in a downstream signalling cascade (Leto and Saltiel, 2012). The result of this signalling cascade is the rapid translocation of GLUT4 containing vesicles to the plasma membrane, where they fuse with the PM, allowing glucose to enter the cells (Olson and Pessin, 1996). This specialised trafficking event, as with all membrane trafficking, is regulated by SNARE proteins. The SNARE complex that has been shown to be responsible for GSV fusion with the plasma membrane is comprised of Sx4, SNAP23 and VAMP2 (Kawanishi et al., 2000; St-Denis et al., 1999). A functional SNARE complex consisting of the three proteins has been shown to form, *in vitro* (Brandie et al., 2008; Kioumourtzoglou et al., 2014) and in 3T3-L1 adipocytes and muscle cells (Randhawa et al., 2000; Rea et al., 1998).

Numerous studies have been carried out that show the importance of Sx4/SNAP23 in insulin-stimulated GLUT4 translocation. Sx4 heterozygous knock-out mice show a 50% reduction in glucose uptake in insulin stimulated skeletal muscle (Yang et al., 2001). Similarly, siRNA depletion of both Sx4 and SNAP23 in adipocytes showed they were essential for GLUT4 translocation following insulin stimulation (Kawaguchi et al., 2010)

Whilst there are a number of studies suggesting that VAMP2 is the v-SNARE responsible for fusion of GSVs with the plasma membrane, there is evidence to suggest some redundancy in the v-SNARE required. Early studies used competitive inhibition to show that introduction of the VAMP2 N-terminus (Martin et al., 1998) or cytosolic domain (Millar et al., 1999) inhibits insulin-stimulated GLUT4 translocation. However, it is important to note that while these studies saw a reduction in GLUT4 translocation, it was not completely blocked. Indeed other studies have found addition of tetanus neurotoxin, which

cleaves both VAMP 2 and 3, is not sufficient to block insulin-stimulated glucose uptake (Hajduch et al., 1997). A study by Zhao and colleagues showed that GLUT4 translocation is only blocked in adipocytes that lacked functional VAMP 2, 3 and 8 (Zhao et al., 2009). Proteomic analysis has revealed that VAMP 2, 3 and 8 are all present in GSVs (Jedrychowski et al., 2010). Furthermore, it has been suggested that all three of these v-SNAREs are able to form a functional SNARE complex with Sx4/SNAP23 (Polgar et al., 2002). Although these studies demonstrate that further investigation is needed to establish the role of VAMP proteins in insulin-stimulated GLUT4 translocation, this is discussed in more detail in section 1.5.5.3. For this study I have chosen to focus on VAMP2 as this is the best characterised and has been consistently shown to play a role in insulin stimulated GLUT4 translocation (Bryant and Gould, 2011).

3.1.2 Phosphorylation as a regulator of SNARE proteins

Phosphorylation is a vital regulator of cell signalling pathways, including the insulin signalling cascade. Upon insulin binding to the insulin receptor a signalling cascade is triggered, involving numerous phosphorylation steps, resulting in the fusion of GLUT4 storage vesicles with the plasma membrane (Olson and Pessin, 1996). The interaction between the insulin-mediated signalling cascade and the trafficking machinery required for fusion at the plasma membrane could represent an important regulatory point in this pathway.

A number of studies have shown that SNARE proteins can be phosphorylated, and that their phosphorylation state can affect their interactions with other SNARE proteins (Gerst, 2003). Sx4 has been shown to be phosphorylated by cAMP-dependent protein kinase (PKA) (Foster et al., 1998). *In vitro* binding assays showed that PKA phosphorylated Sx4 displays reduced binding to SNAP23, whereas its interactions with VAMP2 are not affected. Another study showed that syntaxin 1A and Sx4 can be phosphorylated by the serine/threonine kinase casein kinase II (CKII) *in vitro* (Risinger and Bennett, 1999).

Biochemical analysis carried out in this study showed a reduced interaction between Sx4 and SNAP25 when Sx4 is phosphorylated. Similarly, it has been shown that, the predominantly ER localised, syntaxin17 can be phosphorylated in CHO and MIN6 cells (Muppirala et al., 2012). This phosphorylation results in reduced interaction with COPI vesicles, suggesting it plays a role in regulating trafficking through the early secretory pathway.

Similar phosphorylation events have been observed in yeast. Research carried out by Marash and colleagues showed that dephosphorylation of the yeast t-SNARE Sso1 increases its assembly in to complexes with the t-SNARE Sec9 both *in vitro* and *in vivo* (Marash and Gerst, 2001). The role of phosphorylation in regulating SNARE protein function is discussed in more detail in section 1.4.4.

A study by Schmelzle and colleagues in 2006, used quantitative mass spectrometry to identify insulin-induced tyrosine phosphorylation sites in 3T3-L1 adipocytes. The study found 89 tyrosine phosphorylation sites that changed at least 1.3 fold following insulin stimulation, only 20 of these had previously been identified (Schmelzle et al., 2006). Amongst the newly identified phosphorylation sites it was found that two residues on Sx4, Y115 and Y251, both show a ≥ 3 fold increase in phosphorylation in response to insulin. The consequences of this phosphorylation are as yet unknown; however it may represent an important step in the communication between signalling and trafficking pathways of insulin action.

3.2 Aims of this chapter

Sx4 has been shown to be phosphorylated in response to insulin (Schmelzle et al., 2006). This may be an important regulatory step in the insulin-stimulated translocation of GLUT4; however the consequences of this phosphorylation are unknown. Here I have carried out *in vitro* complex assembly assays, limited proteolysis and pull down assays in order to systematically assess the effects of phospho-mimetic mutant forms of Sx4 on both their

binary and tertiary interactions with other SNARE proteins. I have further studied the binary interactions of Sx4 with SNAP23 and VAMP2 using the more quantitative technique of surface plasmon resonance (SPR). Finally, I have begun to investigate the different phosphoprotein isoforms of Sx4 using an *in vitro* phosphorylation assay and Phos-tag based mobility shift SDS-PAGE analysis.

3.3 Results

3.3.1 Expression and purification of recombinant SNARE proteins

In order to study the effect of phosphorylation on SNARE protein interactions, I first expressed and purified recombinant tagged forms of the proteins of interest. Sx4 phospho-mimetic mutant plasmids had been made previously by Dr Veronica Aran-Ponte (University of Glasgow). The constructs contained mutations in the tyrosine residues that have been shown to be phosphorylated in response to insulin. Tyrosine residues 115 and 251 were mutated to glutamic acid, chosen due to its bulkiness and negative charge to mimic phosphorylation. The resulting mutant proteins have been subject to circular dichroism (CD) to analyse their secondary structure (Aran-Ponte, 2009). No significant change in the secondary structure was seen in the proteins containing the glutamic acid mutations.

The cytosolic domain of Sx4 (residues 1-273) tagged at the C-terminus with GST (Sx4-GST) was expressed and purified from *E. coli* (section 2.3.2). Figure 3.1 shows coomassie stained SDS-PAGE gels that were typical for Sx4 purifications (See appendix I for culture volume details). Wild type Sx4 (Figure 3.1 A) was purified along with phospho-mimetic mutant forms of the protein; Y115E (B), Y251E (C) and Y115,251E (D). Recombinant proteins that make up the other components of the SNARE complex responsible for GLUT4 vesicle fusion at the PM were also purified from *E. coli* (2.3.2). Figure 3.2 shows coomassie stained gels from typical purifications of SNAP23 tagged at the N-terminus with His (His-SNAP23, A) and VAMP2 (residues 1-91) with a GST tag at

the N-terminus (GST-VAMP2, B). Purified GST only was used as a negative control protein and was provided by Dr Dimitrios Kioumourtzoglou (University of York). Following purification, protein concentration was estimated as described in section 2.3.6.

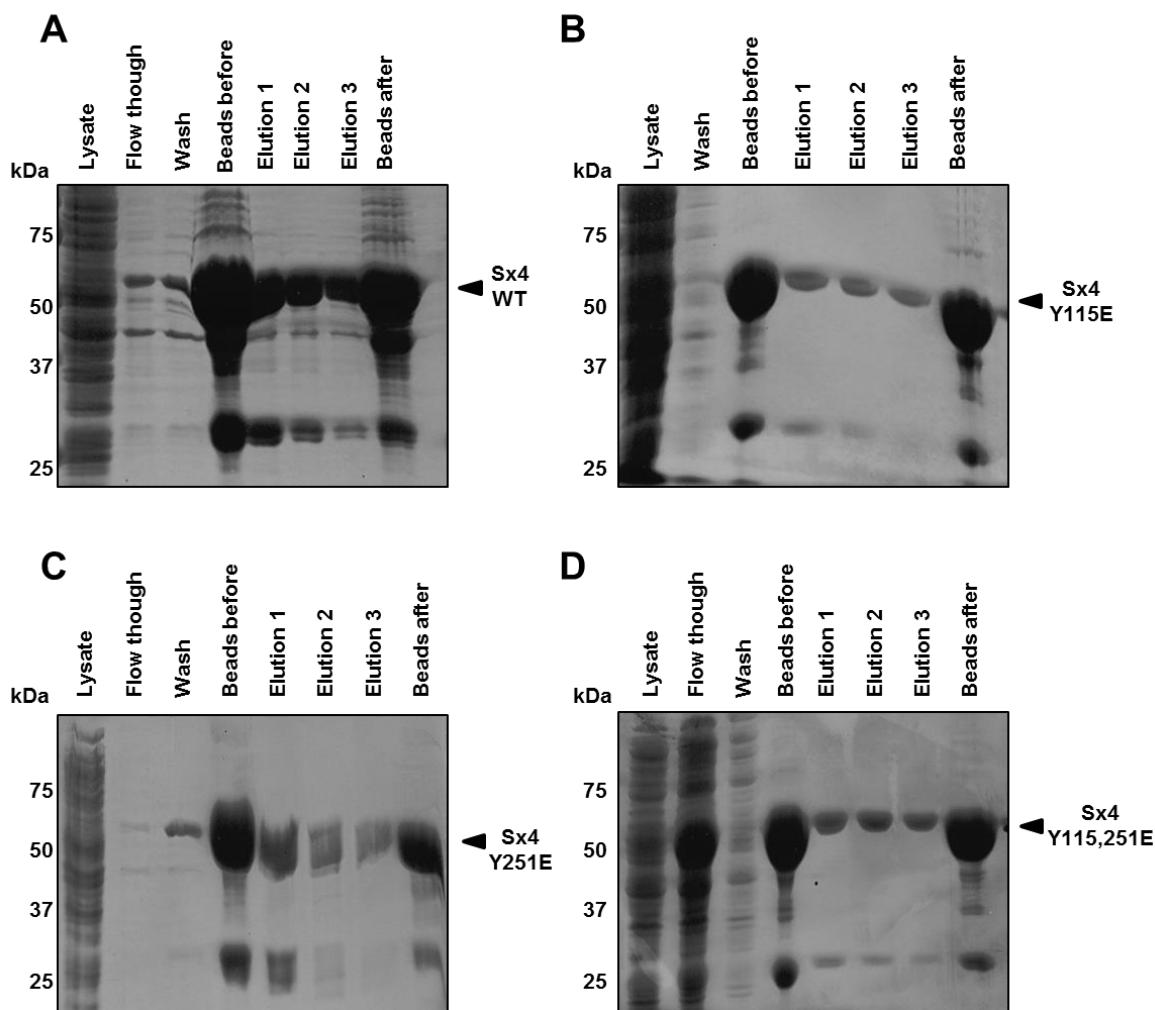


Figure 3.1: Expression and purification of Sx4.

Sx4-GST was expressed and purified from BL21 (DE3) *E. coli* as described in section 2.3.2. 10 μ l of samples taken during purification were run on 12% SDS-PAGE gels and coomassie stained. Shown are examples of typical purifications for Sx4-GST WT **A**, Y115E **B**, Y251E **C** and Y115,251E **D**. Samples corresponding to bacterial lysate (lysate), unbound proteins following glutathione Sepharose incubation (flow through), beads wash sample (wash), Sx4-GST bound to glutathione Sepharose (beads before), each of the three elutions and proteins that remained bound to beads following elution (beads after) were run. Elution samples represent 0.25% of total elution. See Appendix I, Table I for details of culture and elution volumes.

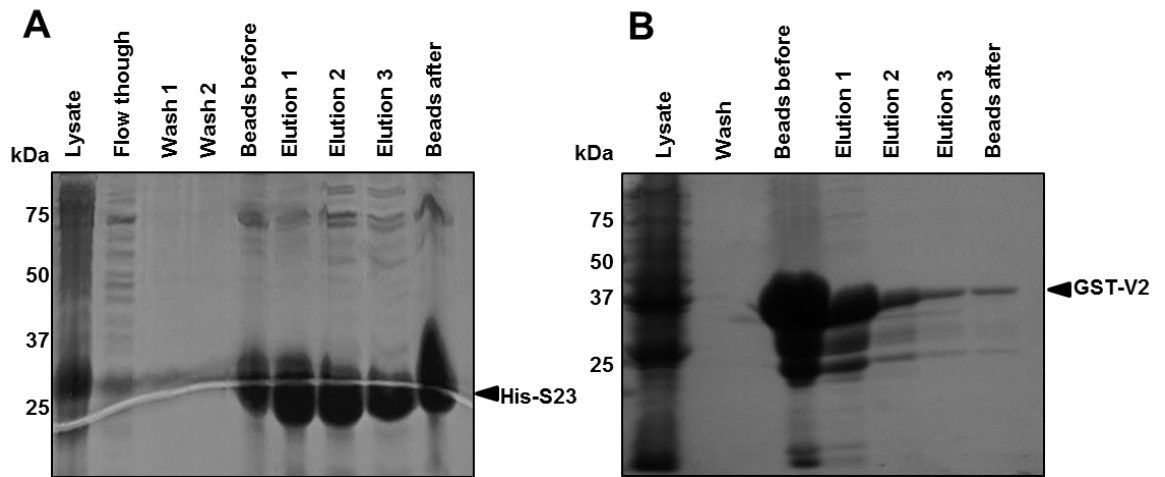


Figure 3.2: Expression and purification of Sx4 SNARE complex components.

His-SNAP23 **A** and GST-VAMP2 **B** were purified from BL21 (DE3) *E. coli* as described in section 2.3.2. 10 μ l of samples taken during purification were run on an SDS-PAGE gel and coomassie stained, shown are examples of typical purifications. Samples corresponding to bacterial lysate (lysate), unbound proteins following incubation with beads (flow through), beads wash sample (wash), proteins immobilised to beads (beads before), each of the three elutions and proteins that remained bound to beads following elution (beads after) were run. Elution samples represent 0.25% of total elution for His-SNAP23 and GST-VAMP2. See Appendix I, Table I for details of culture and elution volumes.

3.3.2 *In vitro* SNARE complex assembly assay

It has been previously shown that bacterially-produced, tagged versions of the cytosolic domains of Sx4 and VAMP2 can form an SDS-resistant complex with SNAP23 *in vitro* (Kioumourtzoglou et al., 2014). I utilised this *in vitro* assay to examine the consequences of Sx4 phosphorylation on ternary complex formation. Approximately equimolar amounts of Sx4-GST, His-SNAP23 and GST-VAMP2 were incubated for 15 minutes at 4°C before the amount of complex formed was assessed by SDS-PAGE, coomassie staining and immunoblot analysis (section 2.4). Figure 3.3A shows that an SDS-resistant complex is only formed when all of the components of the complex are present. Figure 3.3 shows that when phospho-mimetic mutant Sx4 proteins were used in the assay Sx4-Y115,251E showed a 28% increase in the amount of complex formed than the WT ($p=0.035$, pairwise t-test comparison). A one way analysis of variance statistical test was carried out to compare the mean amount of complex formed for each mutant, finding a P value of 0.18.

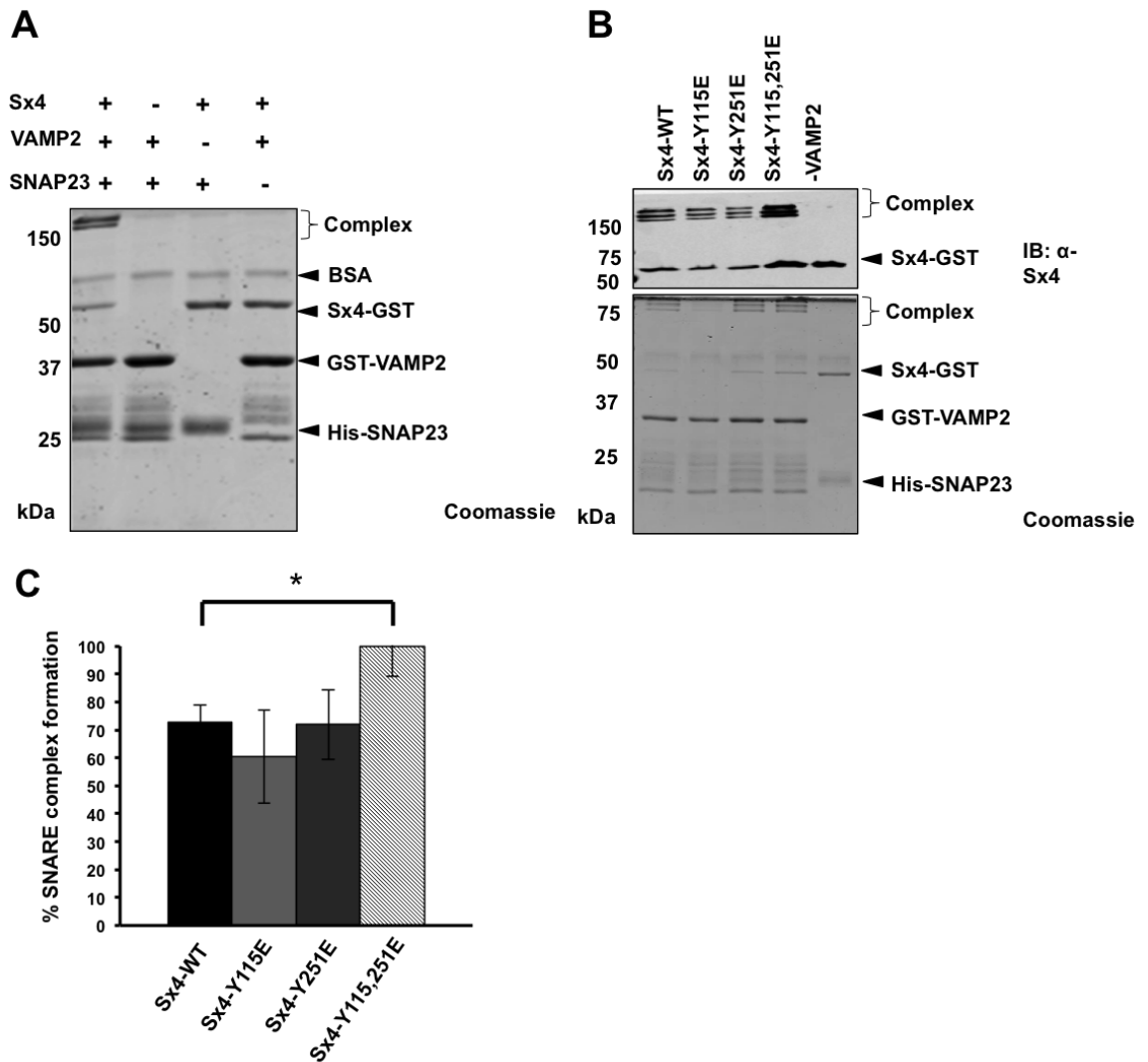


Figure 3.3: Sx4-Y115,251E forms more SNARE complex than Sx4-WT.

Roughly equal amount of Sx4-GST, GST-VAMP2, His-SNAP23 were incubated for 15 minutes at 4°C with rotation, the reaction was stopped by the addition of 2xLSB and boiled at 95°C for 5 minutes (methods section 2.4). The amount of SDS-resistant SNARE complex formed was analysed by SDS-PAGE. **A** Coomassie staining shows that the complex is only formed when all three components are present. **B** Representative anti-Sx4 immunoblot and coomassie stained gel are shown from complex assembly assays using phosphomimetic syntaxin proteins. **C** The amount of complex formed in four independent experiments was analysed by densitometry from anti-Sx4 immunoblot using ImageJ software. Error bars show standard error of the mean. Statistical analysis between Sx4-WT and Sx4-Y115,251E was assessed using a t-test, $*=p<0.05$.

3.3.3 Limited proteolysis of Sx4 phospho-mimetic mutants

Figure 3.3 shows that the Sx4-Y115,251E protein formed more complex in an *in vitro* assay than the WT or single phospho-mimetic mutant forms. Given that phosphomimetic mutants showed an increase in ternary complex formation the effects of tyrosine phosphorylation at residues 115 and 251 was further dissected. An important regulatory feature of syntaxins is their ability to adopt an 'open' or 'closed' conformation. In the 'closed' conformation the Habc domain of the protein can interact with the SNARE domain, rendering the protein unable to form SNARE complexes, whilst the 'open' form renders the SNARE domain available to bind to other proteins (Aran et al., 2009; Dulubova et al., 1999).

The effect of phosphorylation on the conformation of Sx4 was therefore investigated using limited proteolysis. Previous studies have shown that mutating Sx4 residues L165 and E166, which are in the linker region, to alanine results in the protein maintaining an 'open' conformation that is more susceptible to proteolysis than the WT (Aran et al., 2009). Limited proteolysis experiments are based on the principle that the more unstructured, or in this case open, a protein is the more susceptible they are to cleavage by the protease (Hubbard, 1998).

Initially, Sx4 WT or phosphomimetic mutants were incubated with chymotrypsin at room temperature for between 0-30 minutes before being analysed by SDS-PAGE (methods section 2.6). The amount of full length Sx4 remaining after incubation with chymotrypsin was analysed by densitometry using ImageJ software. This data was analysed for statistical significance using one-way ANOVA (Figure 3.4B) and t-test (Figure 3.4D). Figure 3.4A+B shows that Sx4-Y115E was cleaved faster than both Sx4-WT and Sx4-Y251E after 1 minute ($p = 0.025$ and 0.032 respectively). After 5 minutes, both Sx4-Y115E and Sx4-Y251E were degraded faster than Sx4-WT ($p = 0.038$ and 0.022 respectively).

Similarly, figure 3.4C+D shows that Sx4-Y115,251E was cleaved faster than Sx4-WT after 1 minute of incubation with chymotrypsin ($p = 0.041$).

The rate of proteolysis of phospho-mimetic Sx4 mutants was then compared to that of the 'open' Sx4 mutant. The cytosolic region of Sx4 (residues 1-273) tagged at the C-terminus with GST and including L165A, E166A mutations (Sx4-Open) was purified from *E. coli* (as described in section 2.3.2). A limited proteolysis experiment was then carried out as before (section 2.6). Figure 3.5 shows that Sx4-Y115E and Sx4-Y115,251E were digested by chymotrypsin at a comparable rate to that of the open mutant. One way ANOVA statistical analysis was carried out. This found a statistically significant difference in the proportion of Sx4 remaining between Sx4-WT and Sx4-Y115,251E (63 % and 30 % respectively, $p = 0.024$) and between Sx4-Y251 (68 % remaining) and both Sx4-Y115,251E and Sx4-Open (39 % remaining) ($p = 0.010$ and 0.044 respectively). This data suggests that phosphorylation of Sx4 may alter the conformation of the protein.

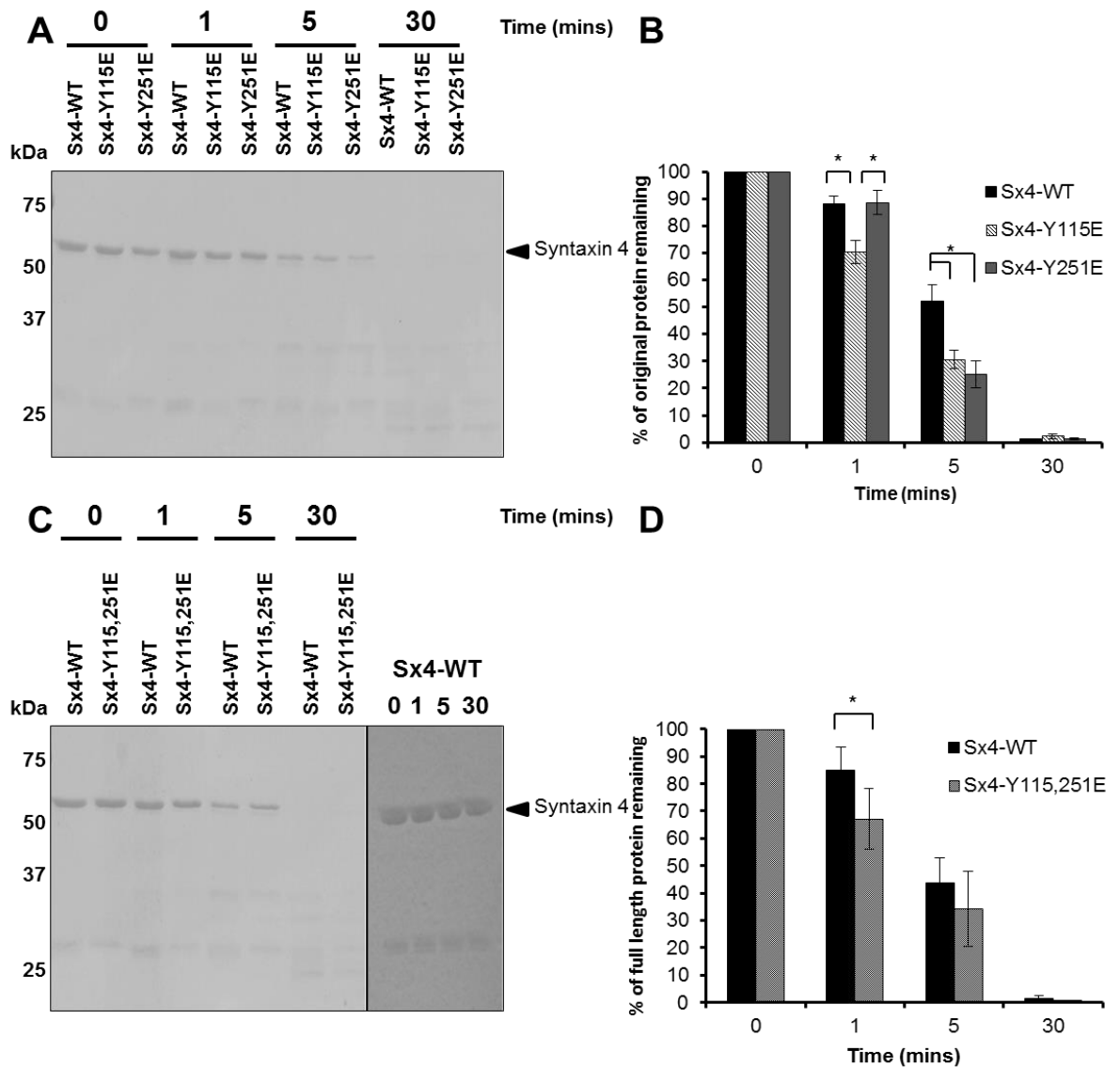


Figure 3.4: Phospho-mimetic Sx4 shows increased sensitivity to proteolysis when compared to WT.

Equal amounts of Sx4 WT, Y115E, Y251E and Y115,251E were incubated with chymotrypsin at room temperature for various time points before the reaction was stopped by the addition of 2xLSB and samples boiled at 95°C for 5 minutes (section 2.6). Samples were analysed by SDS-PAGE and coomassie staining. **A** and **C** show representative gels. A negative control of Sx4 incubated at room temperature with no chymotrypsin is included in **C**. **B** and **D** show densitometry analysis of the amount of full length protein remaining when compared to the amount at 0. n=3, error bars show standard error of the mean. Statistical significance was calculated using one-way ANOVA with a post-hoc Tukey test (**B**) and t-test (**D**), * p < 0.05.

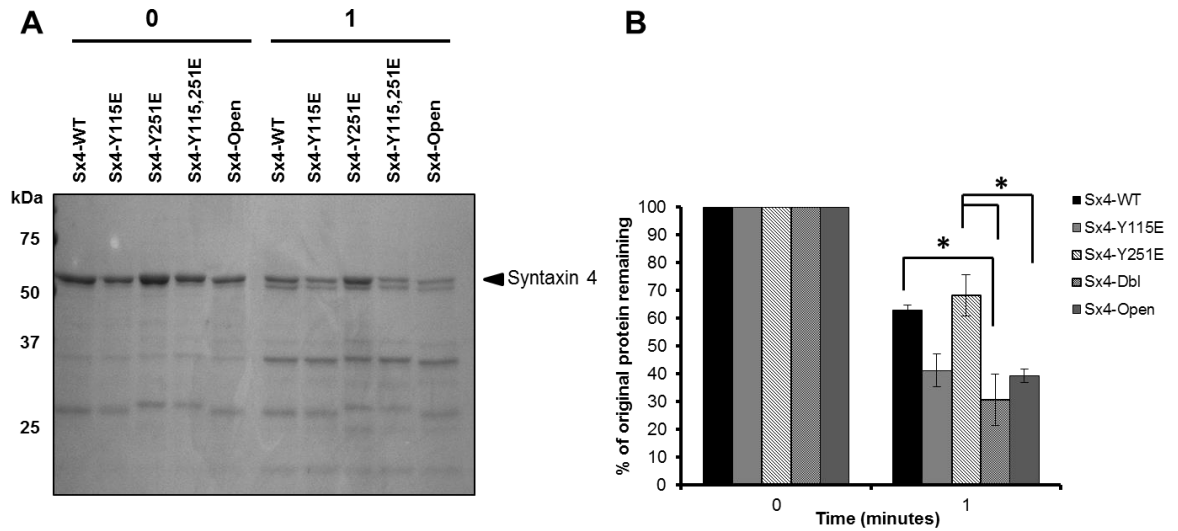


Figure 3.5: Sx4-Y115E and Sx4-Y115,251E show comparable sensitivity to limited proteolysis to the Sx4 open mutant.

Equal amounts of Sx4 WT, Y115E, Y251E, Y115,251E and Sx4-Open were incubated with chymotrypsin at room temperature for 0 and 1 minutes before the reaction was stopped by the addition of 2xLSB and samples boiled at 95°C for 5 minutes (section 2.6). Samples were analysed by SDS-PAGE and coomassie staining. **A** shows a representative coomassie stained gel. **B** Data was analysed using densitometry to calculate the amount of full length protein remaining compared to the protein at 0 minutes. n=3, error bars show standard error of the mean. Statistical significance was calculated using one-way ANOVA with a post-hoc Tukey test, * p < 0.05.

3.3.4 Investigating the binary interactions between Sx4 phospho-mimetic mutants and SNAP23/VAMP2 using *in vitro* pull down assays

The data presented thus far suggests that Sx4 phosphorylation at tyrosine residues 115 and/or 251 increases the propensity of Sx4 to form SDS-resistant complexes and has an effect on protein conformation. The consequences of Sx4-phosphorylation on the binary interactions between Sx4 and the other components of the SNARE complex, SNAP23 and VAMP2 were then investigated.

First the interaction between Sx4 and SNAP23 was investigated using an *in vitro* pull down assay. Sx4-GST and His-SNAP23 were expressed and purified as described previously (Figure 3.1 and 3.2). Equimolar amounts of Sx4-GST WT, Y115E, Y251E, Y115,251E, Sx4-Open and GST only were immobilised to glutathione Sepharose beads and incubated with His-SNAP23 for 30 or 60 minutes (section 2.5). The beads were then extensively washed to remove any unbound protein before being analysed by SDS-PAGE. Figure 3.6A shows a representative immunoblot of the amount of SNAP23 pulled down by Sx4. Pull down assays were quantified by densitometry using ImageJ software. The amount of SNAP23 pulled down was calculated relative to the amount of Sx4 in that sample. Figures 3.6 B + C show the relative amount of SNAP23 bound to Sx4 plotted against time. The data show that Sx4-Y115,251E and Sx4-Open display a two fold increase in binding to SNAP23 after 60 minutes, compared to WT (figure 3.6C). Both single phospho-mimetic mutants showed around a 50% increase (Figure 3.6B). Undetectable amounts of SNAP23 were pulled down with the GST control protein, demonstrating that any observed interaction was not due to the presence of the GST tag. One way analysis of variance statistical analysis was carried out and p values were found to be 0.2 when comparing means at 30 minutes, and 0.5 after 60 minutes.

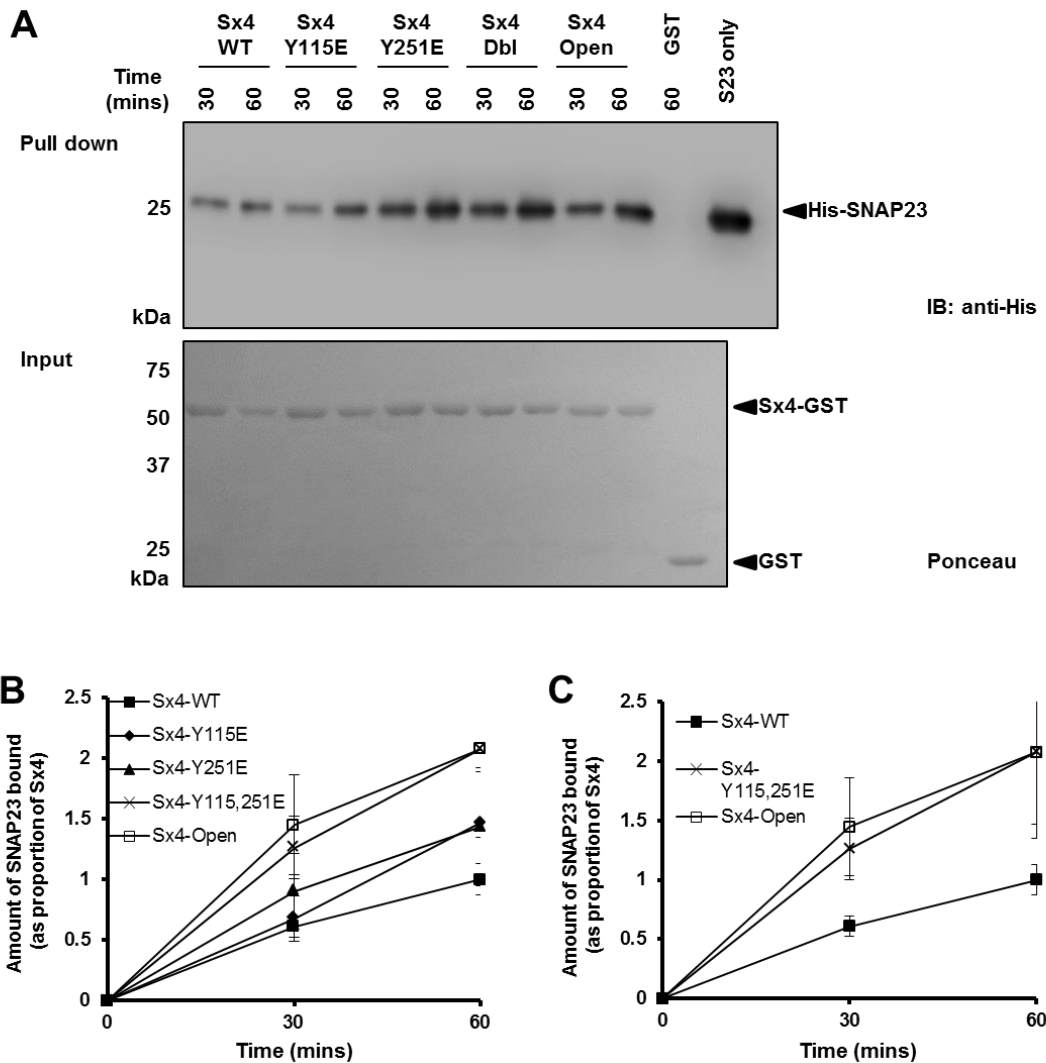


Figure 3.6: Phosphomimetic Sx4 mutants bind more SNAP23 than WT Sx4.

Immobilised Sx4-GST was incubated with His-SNAP23 for up to 60 minutes at 4°C with rotation. Beads were collected and washed extensively before being subject to SDS-PAGE and immunoblotting to analyse the amount of SNAP23 bound (section 2.5). **A** Representative anti-His immunoblot and ponceau stained membrane. The amount of bound protein was quantified using densitometry and expressed as a proportion of Sx4 (from the same sample). **B** Sx4-phosphomutants and the Open mutant showed an increase in SNAP23 binding compared to the WT protein, **C** A simplified graph demonstrating the difference between the Sx4-Y115,251E and Sx4-Open mutant and the WT protein.

Next the interaction between Sx4-phosphomutants and the v-SNARE VAMP2 was investigated. For this assay VAMP2 that had been cleaved from the N terminal GST tag using thrombin was used (section 2.3.5), as the GST tag would interact with the glutathione Sepharose to which Sx4 is immobilised. Figure 3.7 shows an example of cleaved VAMP2 purification.

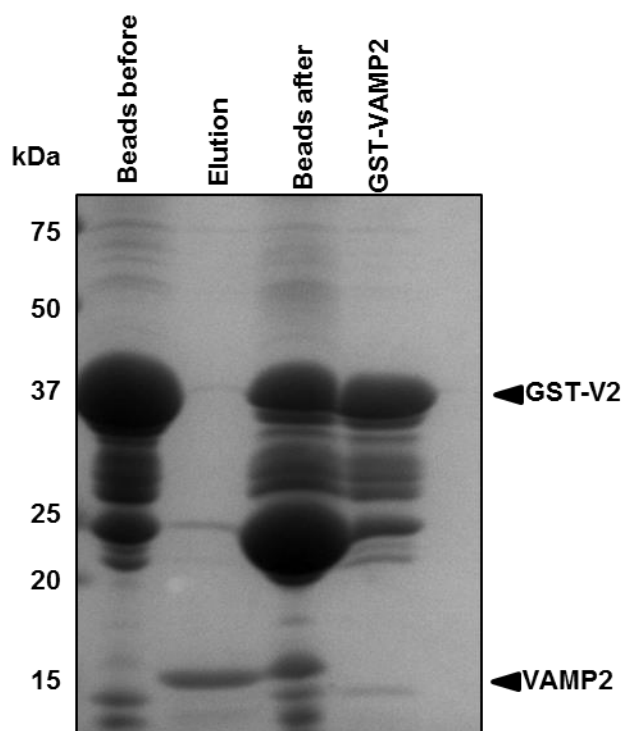


Figure 3.7: Purification of thrombin cleaved VAMP2

N-terminally GST tagged VAMP2 was expressed in BL21 (DE3) *E. coli* before being immobilised to glutathione Sepharose beads (beads before sample). VAMP2 was then cleaved from the beads by incubating with 5 units of thrombin in 3 ml PBS (section 2.3.5). Elution sample corresponds to 0.3% of the total elution (See Appendix I for details of culture and elution volume). The beads after the elution were run (beads after) along with previously purified GST-VAMP2 (0.5% of total elution) for comparison.

A pull down assay using immobilised Sx4-GST and VAMP2 was then carried out, as described previously (section 2.5). A representative immunoblot of VAMP2 pull down by Sx4 is shown in figure 3.8A. The negative GST only control pulled down very little VAMP2. The amount of VAMP2 bound was again calculated relative to the amount of Sx4 in that sample by densitometry using ImageJ software. As with the previous SNAP23 pull down experiment (figure 3.6), Sx4-Y115,251E showed a 2 fold increase in VAMP2 bound when compared to WT. In contrast, the Sx4-Open mutant, although it showed a 50 % increase when compared to WT, pulled down less VAMP2 after 60 minutes than the Sx4-Y115,251E mutant. Furthermore, the Sx4-Y251E phospho-mutant pulled down the most VAMP2, with a 2.5 fold increase over WT. One way analysis of variance statistical analysis was carried out to assess significance; P values were found to be 0.19 when comparing means at 30 minutes, and 0.24 after 60 minutes.

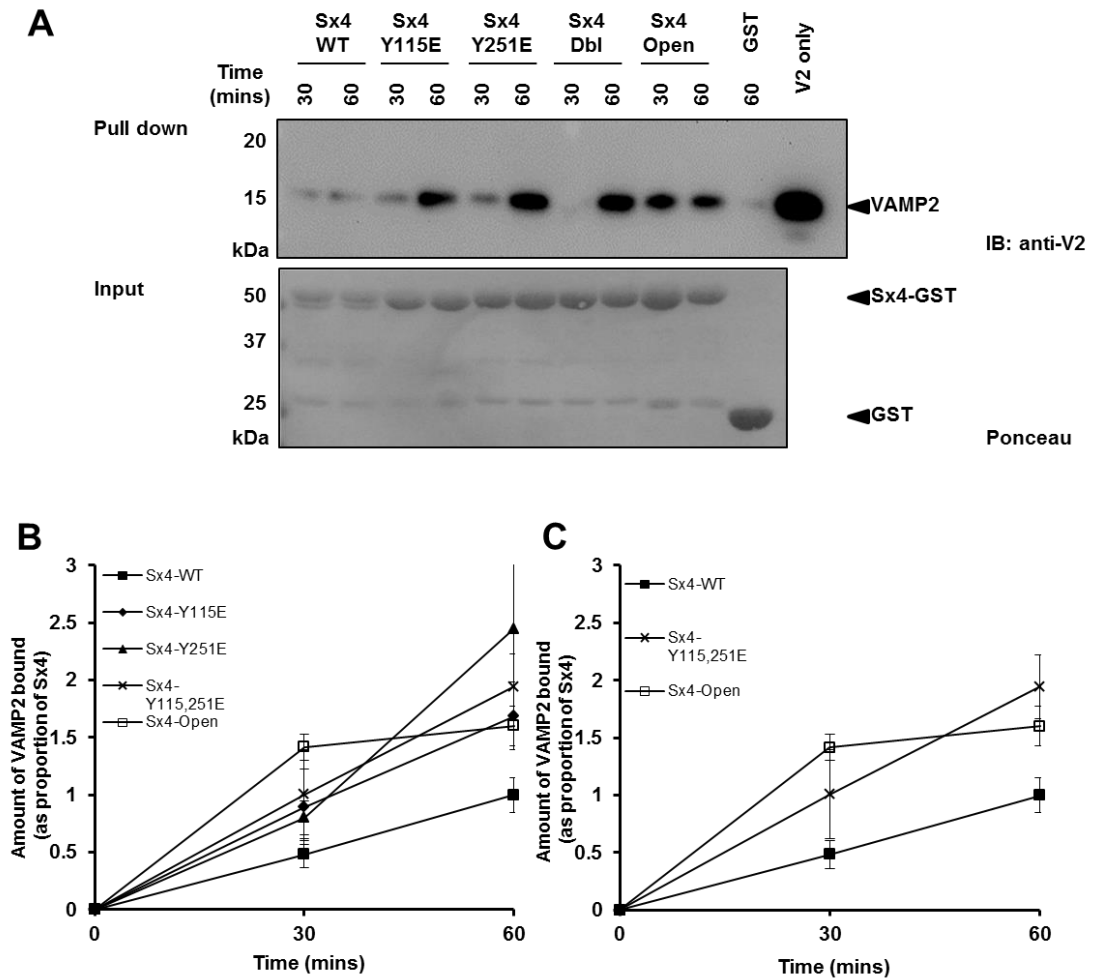


Figure 3.8: Phosphomimetic Sx4 mutants show increased binding to VAMP2 compared to WT

Immobilised Sx4-GST was incubated with VAMP2 for up to 60 minutes at 4°C with rotation. Beads were collected and washed extensively before being subject to SDS-PAGE and immunoblotting to analyse the amount of VAMP2 bound (section 2.5). **A** Representative anti-VAMP2 immunoblot and ponceau stain. The amount of bound protein was quantified using densitometry and expressed as a proportion of Sx4 (from the equivalent sample). **B** Quantification of Sx4 binding to VAMP2. Sx4 mutant proteins show increased binding to VAMP2 when compared to WT **C** A simplified graph demonstrating the difference between the Sx4-Y115,251E and Sx4-Open mutant and the WT protein. n=3, error bars show standard error of the mean.

3.3.5 Investigating the binary interactions between Sx4 phospho-mimetic mutants and SNAP23/VAMP2 using surface plasmon resonance (SPR)

Data presented in figure 3.6 and 3.8 suggest that the phosphorylation state of Sx4 does affect its binary interactions with VAMP2 and SNAP23. These interactions were then examined using a more quantitative technique. Figures 3.6 and 3.8 demonstrate that Sx4 phospho-mutants consistently pulled down more SNAP23 and VAMP2 than the WT protein however the numbers obtained from densitometry quantification showed some variability; hence the large error bars representing standard error of the mean and large p values when calculating statistical significance. The interactions between phospho-mimetic Sx4 and SNAP23 or VAMP2 were therefore examined further using surface plasmon resonance (SPR).

SPR measures protein interactions in a quantitative manner by detecting a change in mass near a surface by measuring changes in the refractive index. Experiments are carried out with one reactant (ligand) immobilised to the surface, another molecule (analyte) is passed over in solution and the binding is measured (Torreri et al., 2005). A number of different sensor chips are available for SPR. For this study I used a CM5 chip. The CM5 sensor chip consists of a matrix of carboxymethylated dextran covalently linked to a thin gold layer. The ligand is immobilised by first activating the dextran matrix by flowing over an equal mix of EDC (1-ethyl-3-(3-dimethylaminopropyl) carbodiimide) and NHS (N-hydroxysuccinimide). This creates reactive succinimide esters on the chip surface. The chip surface carries a negative charge at a pH >3.5, and so the ligand is then passed over the activated chip surface in a buffer with a pH higher than 3.5 but lower than the PI of the protein. This gives the protein a positive charge, whilst the chip carries a negative charge, the protein is therefore attracted to the chip surface allowing the activated dextran to spontaneously react with amine groups on the protein, covalently coupling the ligand to the chip surface (Figure 3.9A). Once any unlinked ligand has been washed away by buffer, the remaining uncoupled active groups on the chip surface are deactivated using 1M ethanolamine hydrochloride pH8.5.

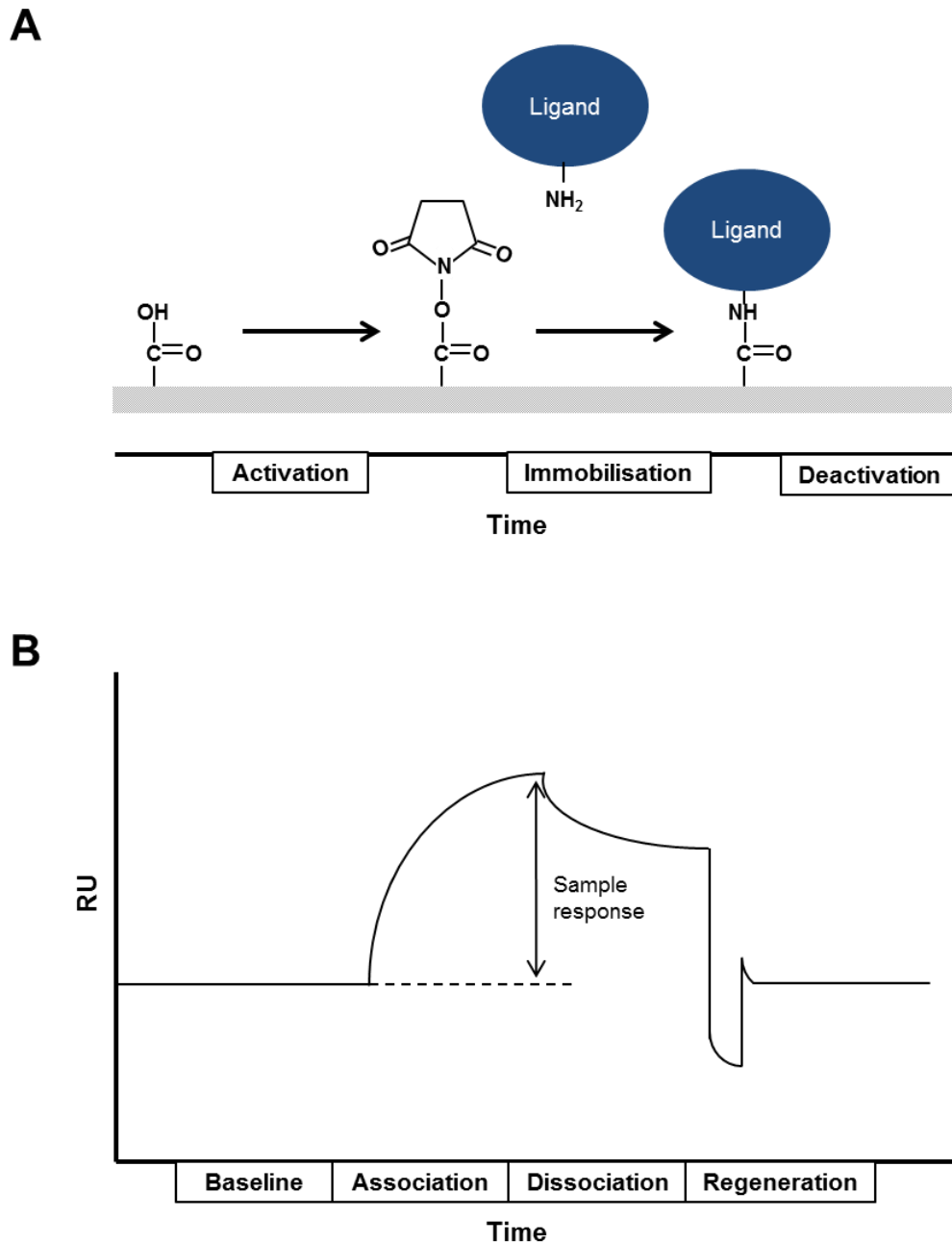


Figure 3.9: Schematic of SPR ligand immobilisation and analyte binding

A Schematic of ligand immobilisation. An activation reagent is passed over the chip surface; the ligand is then passed over the activated surface until a sufficient amount has bound. The remaining activated groups on the chip surface are then deactivated with a different reagent. The level of the base line after deactivation shows how many units of ligand have been immobilised. **B** Schematic of analyte/ligand binding. Analyte is flowed over the chip surface and association with the ligand is measured by a change in the refractive index, measured in response units (RU). The dissociation is then measured, seen by a reduction in RU. If the analyte doesn't fully dissociate with buffer alone, a regeneration reagent is passed over to remove the bound analyte. Following the regeneration the baseline should return to its pre-binding level.

First, the binding of Sx4 mutants to immobilised VAMP2 was examined. Around 900 response units of GST-VAMP2 were immobilised (section 2.14). Sx4-GST WT, Y115E, Y251E, Y115,251E, Open and GST alone were then flowed over the immobilised VAMP2 at a flow rate of 10 μ l/minute for 300 seconds (section 2.14). Figure 3.9B shows a schematic of a typical binding curve obtained using SPR. A control cell with no bound ligand was used and so binding sensorgrams produced show the response from the experimental cell minus any background detected in the control cell. Figure 3.10 shows binding curve sensorgrams for Sx4 phospho-mutants binding to VAMP2. Sensorgrams show that Sx4 binding to VAMP2 increases with increasing Sx4 concentration. GST alone shows very little binding to VAMP2 even at high concentrations. Interestingly, Sx4-WT and Sx4-Open exhibited very similar binding to VAMP2 at each concentration; both in the shape of the binding curves and the point at which binding reached saturation. Contrastingly, the binding curves from Sx4-Y115E, Sx4-Y251E and Sx4-Y115,251E show a clear difference in binding compared with both WT and Open Sx4, particularly at higher concentrations. Sensorgrams show that unlike the WT and Open Sx4 measurements the Sx4 phospho-mutants did not reach saturation levels at concentrations up to 20 μ M. Both the association and dissociation curves of Sx4 binding to VAMP2 appear to be biphasic. The gradient of the binding curves suggests that there might be two modes of binding that are detected. However it is important to note that this may be an experimental artefact (discussed in more detail in section 3.4).

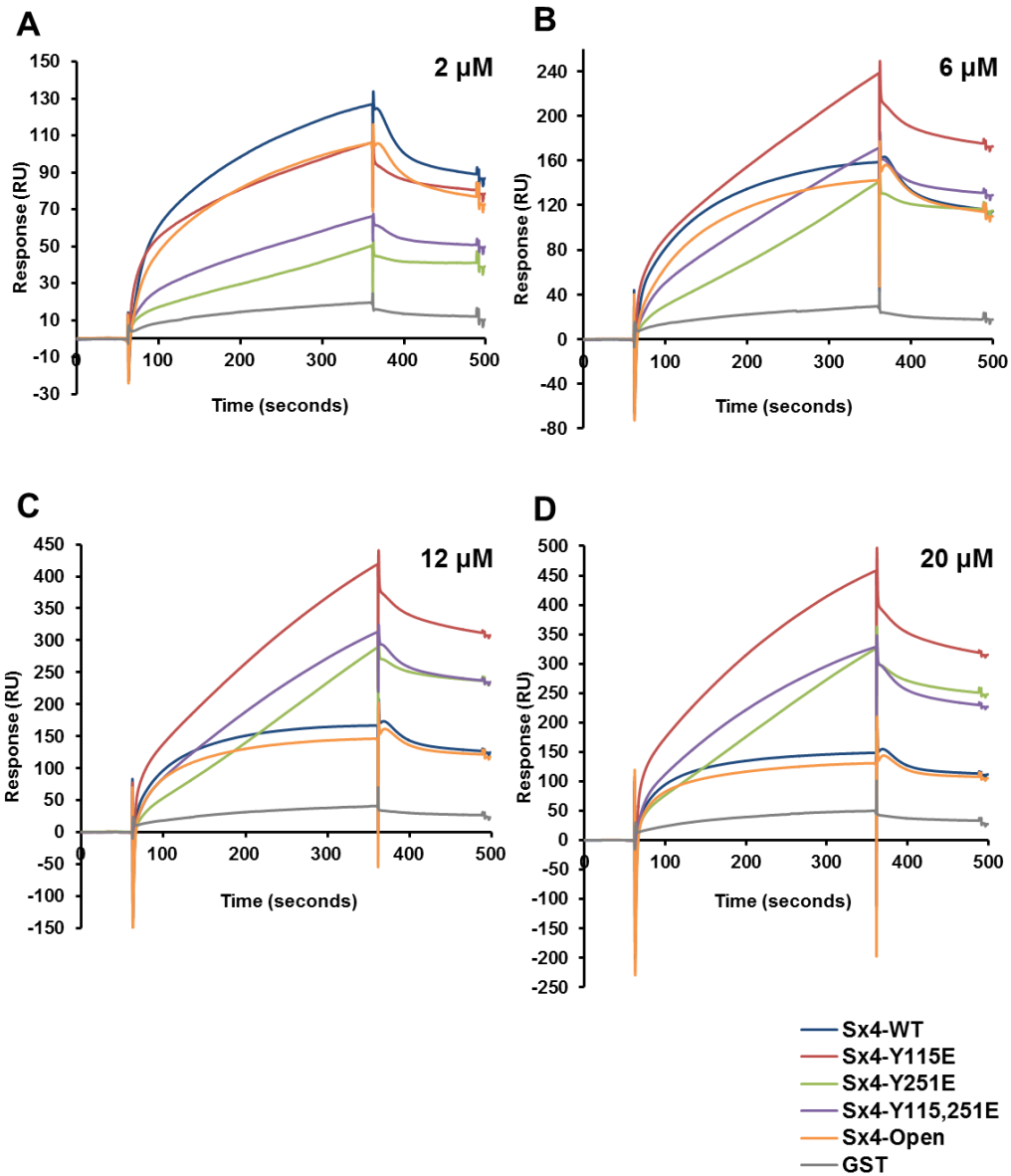


Figure 3.10: Sx4-WT and phospho-mutants binding to VAMP2 by SPR

Approximately 900 units of GST-VAMP2 was immobilised to a CM5 sensor chip via amine coupling. Sx4-GST was then flowed over the chip surface at 10 $\mu\text{l}/\text{minute}$ (section 2.14). Sx4-WT, Sx4-Y115E, Sx4-Y251E, Sx4-Y115,251E, Sx4-Open or GST only at 2 (A), 6 (B), 12 (C) or 20 (D) μM were injected for 300 seconds. All samples were injected in duplicate, shown are representative sensograms. For raw data see Appendix II.

SPR was then used to assess Sx4 binding to SNAP23. Figure 3.10 shows that as Sx4 is injected a sharp dip in the response units is seen, resulting in a spike below 0. This is likely due to slight differences between the protein buffer and the running buffer. Although both were in the same buffer (PBS, 5 % (v/v) Glycerol and 0.05 % (v/v) Tween-20), two separate batches of buffers were used and so some slight discrepancies are likely. Sx4 proteins were therefore dialysed into fresh buffer, and this same buffer was used as running buffer in subsequent experiments.

Approximately 900 units of His-SNAP23 was immobilised by amine coupling (section 2.14). Again GST tagged Sx4-WT, Sx4-Y115E, Sx4-Y251E, Sx4-Y115,251E, Sx4-Open and GST only were flowed over the chip surface at 10 μ l/minute for 300 seconds. All Sx4 samples were injected in duplicate. Figure 3.11 shows representative binding sensorgrams. Again, GST showed very little binding to VAMP2. In contrast to data presented in figure 3.10, figure 3.11 shows that Sx4-Open binds to more SNAP23 than the other Sx4 proteins. In addition, the initial binding rates (shown by the gradient of the binding curve) of both Sx4-WT and Sx4-Open are faster than the Sx4 phospho-mutants. Moreover, the peak binding points for both Sx4-WT and Sx4-Open are higher than those of the Sx4 phospho-mutants (with the exception of 20 μ M Sx4-Y115E).

Figure 3.12 shows a summary of the peak binding points of Sx4 binding to both VAMP2 (Figure 3.12A) and SNAP23 (Figure 3.12B) as obtained from SPR analysis. Figure 3.12A shows that the peak binding response to VAMP2 of Sx4 phospho-mimetic mutants was higher than both the WT and Open mutant. In contrast, figure 3.12B shows the peak SNAP23 binding response of Sx4-Open was greater than the other Sx4 mutants. Affinity analysis of Sx4 binding to both VAMP2 and SNAP23 was carried out using Biacore T200 evaluation software. The resulting equilibrium dissociation constant (KD) values are summarised in appendix II table II.1.

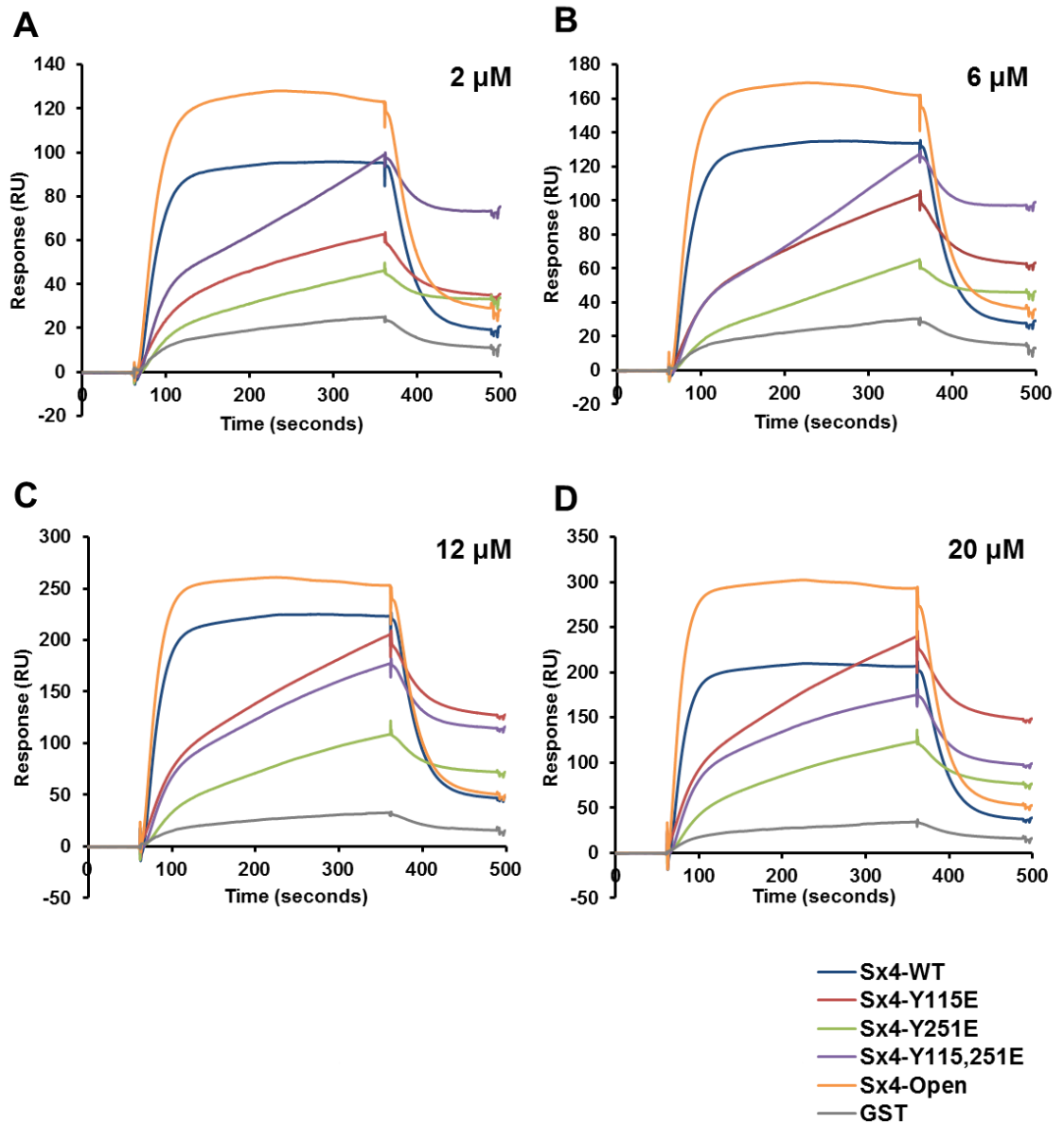


Figure 3.11: Sx4-WT and phospho-mutants binding to SNAP23 by SPR

Approximately 900 units of His-SNAP23 was immobilised to a CM5 sensor chip via amine coupling. Sx4-GST was then flowed over the chip surface at 10 $\mu\text{l}/\text{minute}$ (section 2.14). Sx4-WT, Sx4-Y115E, Sx4-Y251E, Sx4-Y115,251E, Sx4-Open or GST only at 2 (A), 6 (B), 12 (C) or 20 (D) μM were injected for 300 seconds. All samples were injected in duplicate, shown are representative sensograms. For raw data see Appendix II.

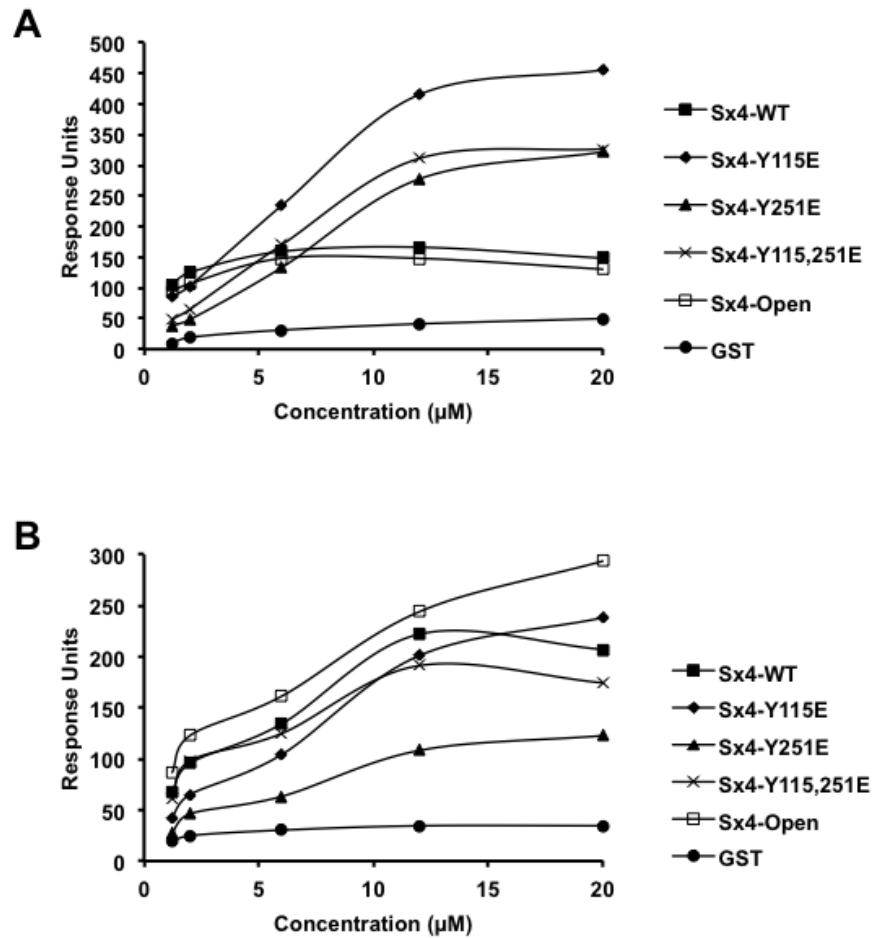


Figure 3.12: Summary of binding of Sx4 to SNAP23 and VAMP2 by SPR

Approximately 900 units of GST-VAMP2 (**A**) or His-SNAP23 (**B**) were immobilised to a CM5 sensor chip via amine coupling. Sx4-GST was then flowed over the chip surface at 10 μ l/minute (section 2.14). Sx4-WT, Sx4-Y115E, Sx4-Y251E, Sx4-Y115,251E, Sx4-Open or GST only at 1.2, 2, 6, 12 or 20 μ M were injected for 300 seconds. All samples were injected in duplicate. Shown are plots of the mean peak binding response for each Sx4 mutant.

3.3.6 Analysing the phosphoprotein isoforms of CIRK phosphorylated Sx4

The data presented in this chapter thus far suggests that the phosphorylation state of Sx4 affects both its ability to form a SNARE complex with SNAP23 and VAMP2 and the binary interactions between the proteins. Moreover, limited proteolysis experiments suggests that phosphorylation effects the conformation of Sx4, resulting in the protein being in a more open conformation. In the majority of the experiments carried out in this chapter, the double phosphomimetic Sx4 mutant has shown the biggest change when compared to the WT protein. However, whilst mass spectrometry analysis has identified both Y115 and Y251 are phosphorylated in response to insulin (Schmelzle et al., 2006), the analysis was carried out on fragmented proteins and so it is not yet known whether one molecule of Sx4 can be phosphorylated on both residues simultaneously. In order to investigate this Phos-tag based SDS-PAGE analysis to detect mobility shifts of *in vitro* phosphorylated Sx4 was utilised.

In 2003, Koike and colleagues at Hiroshima University reported their finding of a selective phosphate-binding tag molecule, Phos-tag (1,3-bis[bis(pyridin-2-ylmethyl)amino]propan-2-olato dizinc(II) complex) (Takeda et al., 2003). It has since been shown that a polyacrylamide bound Mn^{2+} -Phos-tag can be used to separate phosphoprotein isoforms by simple SDS-PAGE (Kinoshita et al., 2006). Figure 3.13 shows the structure of polyacrylamide bound Mn^{2+} -Phos-tag and how this interacts with phosphate groups.

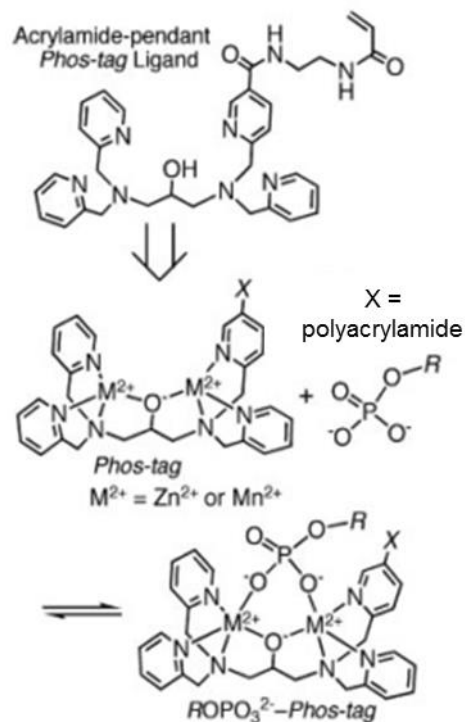


Figure 3.13 Structure of acrylamide-pendant Phos-tag ligand

Phosphate groups on proteins form stable complex interactions with Mn^{2+} -Phos-tag in the polyacrylamide gel.

In order to assess the phosphorylation state of Sx4 *in vitro* phosphorylation assay was first carried out using cytosolic insulin receptor kinase. Whilst investigating phosphatases involved in insulin signalling, Kuhné and colleagues produced a recombinant cytosolic insulin receptor kinase (CIRK), consisting of residues 941-1343 of the β subunit of the insulin receptor, and containing the intrinsic tyrosine kinase domain (Kuhné et al., 1994). CIRK was purified from the insect cell line Sf9 using baculovirus infection, following a protocol developed by Villalba and colleagues (Villalba et al., 1989), and was kindly gifted to the lab by Prof Gustav E. Lienhard (Dartmouth University, USA). Previous work in the laboratory by Dr Veronica Aran-Ponte has shown that Sx4 is phosphorylated by CIRK *in vitro* (Aran-Ponte, 2009).

In order to be active CIRK needs to first be autophosphorylated, this had been previously carried out by Dr Veronica Aran-Ponte (University of Glasgow) (Aran et al., 2011). Activated CIRK was then incubated with WT Sx4-GST at 30 °C for 150 minutes, and Sx4 phosphorylation analysed by SDS-PAGE and immunoblot using an anti-phosphotyrosine (PY20); the assay was carried out in duplicate (section 2.7). Sx4 only, CIRK only and Sx4/CIRK –ATP negative controls were included to be sure any phosphorylated bands seen are Sx4. Figure 3.14A shows that Sx4-GST is phosphorylated by CIRK *in vitro*. The no ATP control shows low background levels of Sx4 phosphorylation, seen in the upper band in the PY20 blot. This phosphorylation is increased by the inclusion of ATP in the reaction. The samples from the kinase assay were then run on a Mn²⁺-Phos-tag SDS-PAGE gel (50µM Phos-tag, 100µM MnCl₂) (Figure 3.14B). Proteins on Phos-tag gels do not run at their expected molecular weights. Figure 3.14B shows that the CIRK kinase does not run at the same rate as Sx4, as demonstrated by the lack of PY20 signal in the CIRK only samples. The α-PY20 blot in figure 3.14B shows multiple phosphorylated Sx4-GST bands, suggesting the protein is phosphorylated at numerous residues as expected.

In order to further dissect the phosphoprotein isoforms of Sx4 phospho-resistant mutant forms of the protein were used to analyse the migratory patterns of these proteins once they are phosphorylated. Typically, phospho-resistant mutants are made by mutating the phosphorylated tyrosine residues to phenylalanine. However, for this purpose I have used the existing phospho-mimetic Y to E mutant proteins. These phospho-mutants will be unable to be phosphorylated on the mutated residue. As the function of the protein is not crucial for this experiment the effects of the phospho-mimetic mutations should not affect any conclusions relating to which residues are phosphorylated. The migratory pattern of Sx4 phospho-mutants was first examined to ensure they are comparable to WT, and that the negative charge of the glutamic acid does not affect migration of the protein through the gel. Samples of Sx4-WT, Sx4-Y115E, Sx4-Y251E and Sx4-Y115,251E were run on a 10 % SDS-PAGE, and 10 % SDS-PAGE 50 µM Phos-tag gel, before being stained with

coomassie. Figure 3.15 shows very little difference in the migration of the Sx4 phosphomimetic mutants on a standard SDS-PAGE gel (top panel). This difference in migration is no more pronounced on the Phos-tag gel (bottom panel).

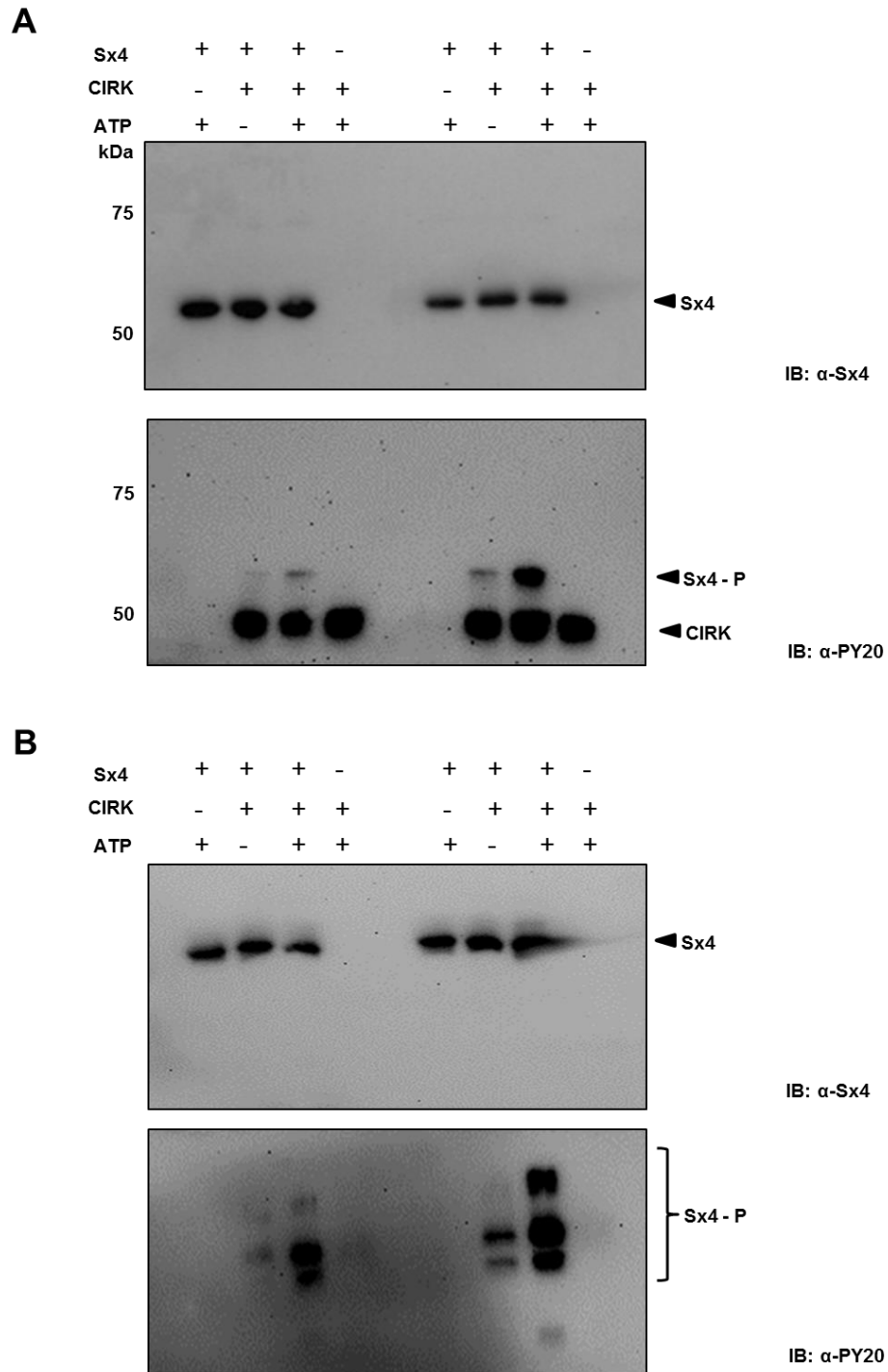


Figure 3.14: Sx4-GST is phosphorylated by CIRK *in vitro*

Sx4 was incubated with activated CIRK with or without 100 μ M ATP at 30°C for 150 minutes (methods section 2.7). **A** Samples were run on a 10% SDS-PAGE gel and blotted for Sx4 (top panel) or phospho-tyrosine (PY20, bottom panel). Autophosphorylated CIRK is detected just below the 50 kDa marker, whereas phosphorylated Sx4 can be seen just above the 50 kDa protein marker. **B** The same samples were ran on a Phos-tag gel (100 μ M Phos-tag) and blotted for Sx4 (top panel) or phosphotyrosine (PY20, bottom panel). Autophosphorylated CIRK is not detected on the Phos-tag gel. Multiple phosphorylated Sx4 bands can be seen. Assays were run in duplicate.

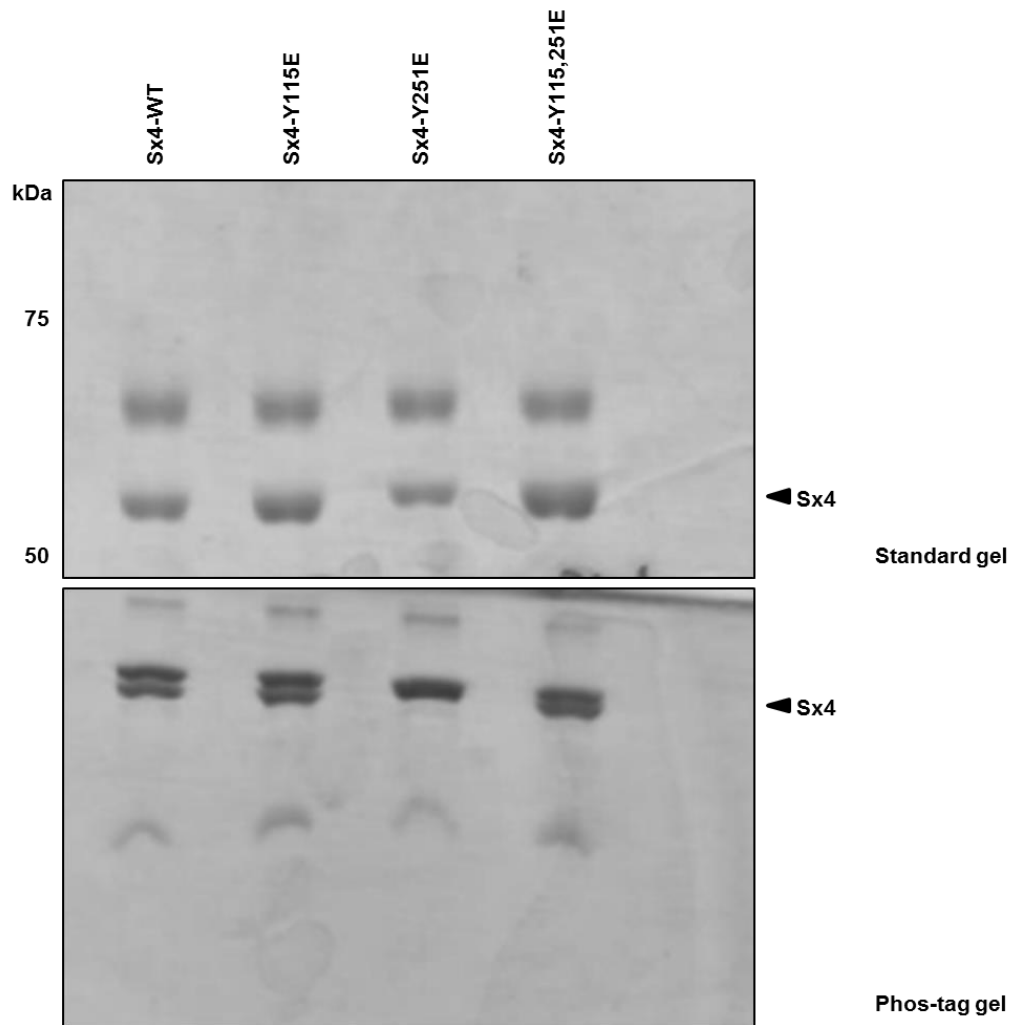


Figure 3.15: Migration of Sx4-GST phospho-mimetic mutants is comparable to WT on Phos-tag SDS-PAGE gel

Sx4 WT and phosphomimetic mutants were run on a 10% SDS-PAGE gel (top panel) and a Phos-tag gel (50 μ M Phos-tag). Proteins were visualised by coomassie staining. Both gels show little difference in the migration of all Sx4 proteins.

Given that the migration of Sx4 phospho-mutants were comparable to Sx4-WT a CIRK phosphorylation assay was carried using Sx4 WT, Y115E, Y251E and Y115,251E. The proteins were incubated with or without CIRK for 150 minutes at 30 °C, along with a CIRK only control (section 2.7). The samples were then analysed by SDS-PAGE. Figure 3.16A shows that Sx4-WT, Y115E and Y251E are phosphorylated by CIRK, whereas the Sx4-Y115,251E phospho-mutant is not phosphorylated (anti-PY20 blot). This is as expected as both of the known phosphorylated tyrosine residues in Sx4-Y115,251E have been mutated. The amount of phosphorylation of the single phospho-mutants is less than the WT protein. Again this is as expected as one of the phosphorylated residues has been mutated.

The samples were then analysed by 50 μ M Phos-tag SDS-PAGE. Figure 3.16B shows several different mobility shift patterns of phosphorylated Sx4. In samples of Sx4-Y115E incubated with CIRK a phosphotyrosine positive band (corresponding to phosphorylated Y251) that runs lower through the gel than the phosphotyrosine band seen in the Sx4-Y251E sample (corresponding to phosphorylated Y115) is detected. The Sx4-WT sample has both of these bands present, as expected. In addition a higher phospho-tyrosine positive band can be seen in the WT sample that is not present in any of the mutant protein samples. This band is likely to correspond to Sx4 that has been phosphorylated on both Y115 and Y251.

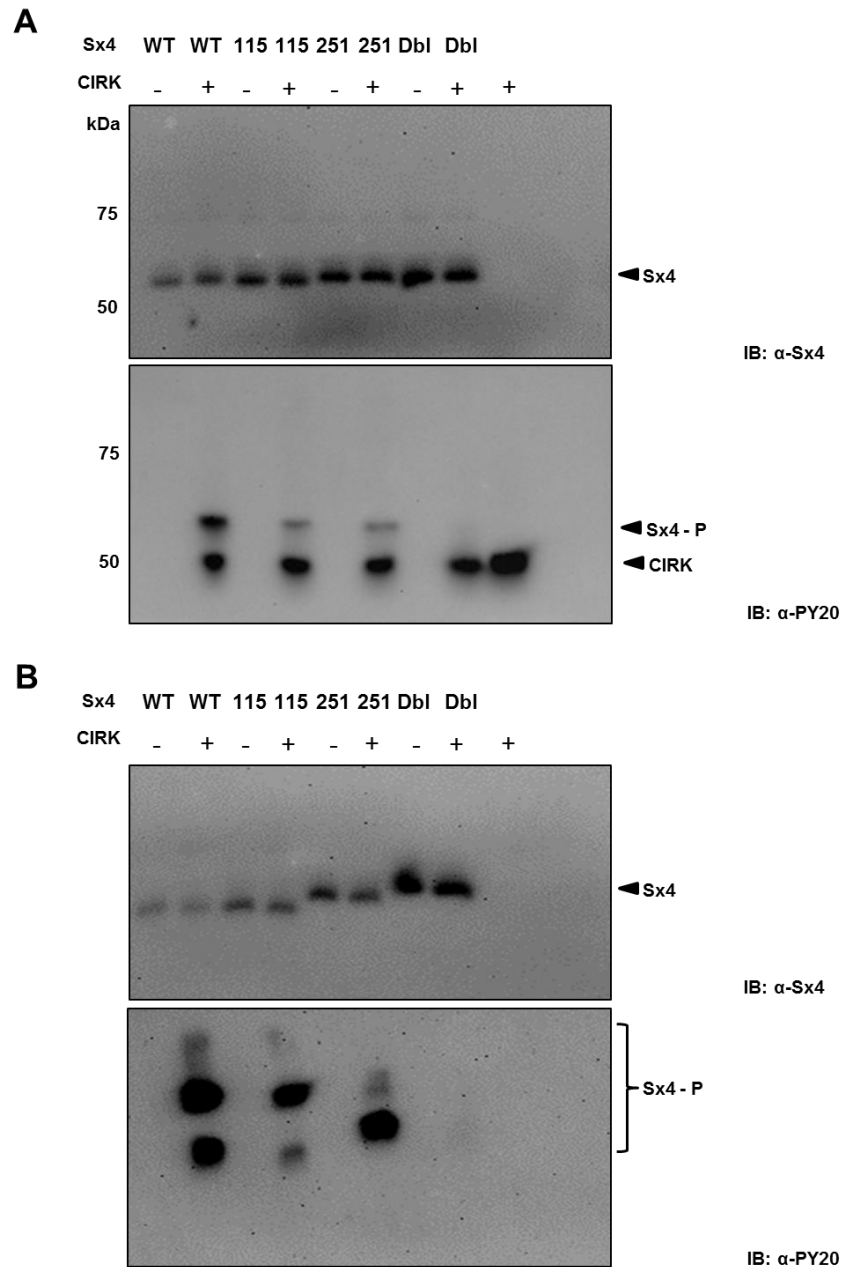


Figure 3.16: *In vitro* phosphorylated Sx4 is phosphorylated at more than one residue

Sx4-GST WT, Y115E, Y215E and Y115,251E were phosphorylated *in vitro* by incubating with activated CIRK for 150 minutes at 30 °C (section 2.7). **A** Samples of phosphorylated Sx4 were run on 10 % SDS-PAGE gels and analysed by immunoblotting (section 2.3.10). Anti-Sx4 blot (top panel) shows that Sx4 was present in all samples. Anti-PY20 blot (bottom panel) shows that Sx4-WT, Y115E and Y251E were phosphorylated by CIRK, whereas the Sx4-Y115,251E mutant was not phosphorylated. Autophosphorylated CIRK can be detected in all samples where it was present (bottom band). **B** Samples of phosphorylated Sx4 were run on 10 % Phos-tag SDS-PAGE gels (section 2.8). Top panel shows that the Sx4 mutants run at roughly the same rate, with the Y251E and Y115,251E mutant showing a slight shift in mobility. Bottom panel shows that multiple phosphorylated forms of Sx4 are present in the WT sample. Shown are representative immunoblots from three separate experiments.

3.4 Discussion

Translocation of GLUT4 is a regulated membrane trafficking event. As with all membrane trafficking events it is regulated by SNARE proteins. The SNARE complex that has been implicated in regulating GLUT4 translocation at the PM consists of Sx4, SNAP23 and VAMP2 (Bryant and Gould, 2011). Sx4 is phosphorylated in response to insulin in 3T3-L1 adipocytes (Schmelzle et al., 2006), however the consequences of this phosphorylation are unknown. This chapter aimed to elucidate the effects of phosphorylation of Sx4 at Y115 and Y251 on its interactions with SNAP23 and VAMP2 *in vitro*.

First, a complex assembly assay was carried. I showed that Sx4-Y115,251E had an increased ability to form SNARE complexes when compared to Sx4-WT (figure 3.3). However, although SNARE complex assembly consistently increased in assays using the Y115,251E mutant assessing the statistical significance of this increase was challenging. Variability in the intensity of immunoblot images between experiments meant that densitometry quantification resulted in a large standard deviation. A comparison between the amount of complex formed by Sx4-WT and Sx4-Y115,251E using a t-test showed that the difference was significant. In order to make more direct measurements of the effect of the phospho-mimetic mutants on SNARE complex assembly, SPR could be used. SPR has been previously used to examine SNARE complex assembly (Rea et al., 1998), and would negate the need to carry out immunoblots and therefore result in more quantitative results.

I then showed using limited proteolysis, that phosphorylation of Sx4 may affect protein conformation (figure 3.5). The ability to adopt an 'open' or 'closed' conformation is an important regulatory feature of syntaxins (Dulubova et al., 1999; MacDonald et al., 2010). Phosphorylation of the yeast syntaxin Sso1 is known to regulate its ability to form SNARE complexes (Marash and Gerst, 2001) and it has been suggested this

occurs by altering the conformation of the protein (Marash and Gerst, 2003). Data presented in figure 3.5 suggests that phosphorylation of Sx4 at Y115 and Y251 may stabilise the open form of the protein, leading to an increased ability of the protein to form SNARE complexes (figure 3.3).

I next sought to investigate the effect of Sx4 phosphorylation on its binary interactions with SNAP23 and VAMP2. Initially, this was investigated using pull down assays (figure 3.6 and 3.8). Pull down assays suggested that Sx4 phospho-mutants bound to more SNAP23 and VAMP2 than Sx4-WT. Again this data was hard to quantify accurately and so these interactions were further investigated using SPR. Figures 3.10 and 3.11 show that Sx4-WT, Open and phosphomutants bound to both SNAP23 and VAMP2 with differing affinities. Interestingly the off rates of Sx4-WT and –Open are faster than for the phosphomutants (shown by the gradient of the curve following binding). A slower off rate suggests that the complex formed between Sx4-phosphomutants and SNAP23/VAMP2 is more stable than with WT or Open. Moreover, Sx4-phosphomutant binding to VAMP2 exceeds both the WT and Open mutant (figure 3.10 and 3.12) whereas both Sx4-WT and Open exhibit more binding to SNAP23 than the phospho-mutants (figure 3.11 and 3.12). It is important to note however that these binding curves have not yet reached equilibrium, therefore more thorough characterisation of the interactions between VAMP2/SNAP23 and the syntaxin mutants could be carried out. Immobilising less ligand to the sensor chip and increasing the flow rate would improve the chance of the reaction reaching equilibrium.

SPR experiments also suggested there may be more than one binding mode or site between VAMP2 and Sx4. The binding curves for Sx4 phospho-mutants were biphasic (Figure 3.10). Whilst this may indicate there may be more than one binding mode between Sx4 and VAMP2, it would be important to confirm this with further experiments. There can be several reasons for biphasic binding curves including: conformational change; sample heterogeneity; steric hindrance or non-specific binding

events (Hulme and Trevethick, 2010). The nature of the immobilisation used here means there could be two populations of VAMP2 on the chip surface. Amine coupling results in random immobilisation of the ligand in potentially different orientations, and so the availability of the binding domain for the analyte may vary. Previous studies have shown that the SNARE domain of VAMP2 is essential for interaction with Sx4 (Kioumourtzoglou, 2012). It may therefore be that the SNARE domain is less accessible in a proportion of the VAMP2 immobilised on the chip surface. In order to establish whether this is the case, a different method of ligand immobilisation could be used. Amine coupling was chosen due to the high efficiency of the method, however it would be possible to immobilise the VAMP2 via the GST tag at the C-terminus using an antibody capture method, resulting in a uniform orientation of the ligand.

Finally, the phospho-isoforms of *in vitro* phosphorylated Sx4 were investigated. A Phos-tag based mobility shift assays suggests, for the first time, that both Sx4 Y115 and Y251 can be phosphorylated on a single molecule of Sx4 (figure 3.16). This is important as data presented in this chapter suggests the Sx4-Y115,251E phospho-mutant has the biggest impact on the interactions of Sx4 *in vitro*. In order to confirm that both these residues are phosphorylated, whole protein electrospray-based mass spectrometry could be used (Compton et al., 2011). Using *in vitro* phosphorylated Sx4 it would be possible to show either a mass shift corresponding to one or two phosphate groups present on a single molecule of Sx4.

In summary, data presented in this chapter suggests that phosphorylation of Sx4 at Y115 and Y251 affects SNARE protein interactions. I have shown that Sx4-Y115,251E increases SNARE complex assembly in an *in vitro* assay, and that this may be due to a conformational change in the protein. In addition, analysis of the binary interactions of the protein suggests that phosphorylation may differentially effect the interactions of Sx4 with SNAP23 and VAMP2. Finally, I have provided evidence that one molecule of Sx4 can be phosphorylated on both Y115 and 251. Further characterisation of the

interactions of Sx4 mutants and SNAP23 and VAMP2 could be carried out to attempt to elucidate the mechanisms by which phosphorylation of the protein increases SNARE complex assembly. In addition, the effect of Sx4 phosphorylation on GLUT4 translocation should be determined; I will address this in the next chapter.

Chapter Four

Analyses of the effects of phospho-mimetic Sx4 on GLUT4 translocation

4 Analyses of the effects of phospho-mimetic Sx4 on GLUT4 translocation

4.1 Introduction

4.1.1 Regulation of GLUT4 translocation

Insulin stimulation results in a 10-20 fold increase in cell surface GLUT4 in adipocytes and muscle cells (Bryant and Gould, 2011). This increase is predominantly due to an upregulation of the rate of exocytosis from GSVs (Yang et al., 1992). The current model for GLUT4 trafficking is that the protein is trafficked through multiple intracellular compartments, including endosomes, the *trans*-Golgi network and GSVs (Larance et al., 2008) (section 1.5.4). Although this pathway has been heavily studied, dissecting and identifying the points at which GLUT4 translocation is actively regulated has proved challenging.

One important development in identifying regulators of GSV fusion at the plasma membrane has been in the characterisation of the protein AS160. The protein contains GTPase activating domains for Rab proteins (Sano et al., 2003). AS160 is phosphorylated by Akt in response to insulin and mutation of the phosphorylated sites to alanine results in impaired insulin-stimulated GLUT4 translocation (Sano et al., 2003). Thus a model has been proposed whereby phosphorylation of AS160 inactivates its Rab GAP function and that this event is necessary for GLUT4 translocation (Larance et al., 2005; Sano et al., 2003).

Improvements in microscopy techniques have also gone some way to aid in the dissection of events leading to GSV fusion at the plasma membrane. Total internal reflection microscopy (TIRF) allows examination of fluorescent events that occur within 150 nm of the plasma membrane (Axelrod et al., 1983). High resolution TIRF microscopy has been used in studies investigating the frequency of fusion of GFP-GLUT4 vesicles at the plasma membrane in 3T3-L1 adipocytes (Bai et al., 2007; Huang et al., 2007). These

studies demonstrated that insulin-treated cells display an increased rate of fusion frequency when compared to basal, and that the docking/tethering time of GSVs is reduced upon insulin stimulation. In addition, the study by Bai and colleagues showed that inhibition of AS160 decreases docking frequency of GSVs at the plasma membrane, under both basal and insulin stimulated conditions (Bai et al., 2007). This suggests that AS160 plays a role in GSV docking at the plasma membrane rather than in fusion of vesicles at this step.

The development of cell free fusion assays has also been an important step in elucidating the mechanisms regulating GSV docking and fusion. Koumanov and colleagues carried out an important study that investigated GSV fusion at the plasma membrane in 2005. They developed a cell free assay which they used to show that GSV fusion with the plasma membrane is not constitutively active but is stimulated by insulin (Koumanov et al., 2005). GSVs and plasma membrane, in the form of plasma membrane liposomes, were isolated from rat adipose cells in either the basal or insulin stimulated state. A fluorescence resonance energy transfer (FRET) based content mixing fusion assay was then carried out. The study found that insulin stimulation increases fusion by 8 fold. Moreover they concluded that the insulin-regulated fraction is the plasma membrane, as insulin stimulated cytosol or GSVs are not sufficient to drive fusion with basal plasma membrane liposomes.

Taken together, the research to date shows that GSV fusion at the plasma membrane is an activated rather than constitutive trafficking event (Bryant and Gould, 2011; Larance et al., 2008). What is known about the regulation of GSV tethering/docking/fusion at the plasma membrane thus far is discussed in more detail in section 1.5.6.

4.1.2 Cell systems used to study GLUT4 translocation

Much of the work into elucidating GLUT4 trafficking mechanisms has been carried out in mouse 3T3-L1 adipocytes. However, transiently expressing transfected proteins in

differentiated 3T3-L1 adipocytes is very challenging as most commercial transfection protocols require sub-confluent cells and the expression of the protein declines with time. 3T3-L1 cells must be confluent to differentiate to adipocytes; moreover differentiation takes up to two weeks and so expression levels of any DNA transfected prior to differentiation would likely no longer be detectable.

Therefore, in order to manipulate the trafficking machinery required for GLUT4 translocation, a readily transfectable and insulin responsive, cell line must be used. Both HeLa (Hernandez et al., 2001) and CHO (Wei et al., 1998) cells have been shown to be insulin responsive. For this study HeLa cells have been used. Insulin stimulation of HeLa cells has been shown to result in the translocation of GLUT4 to the PM (Haga et al., 2011), and is known to induce PI3K signalling (Dubois et al., 2009). These results suggest that HeLa cells possess the basic machinery required for GLUT4 trafficking. Indeed, HeLa cells express the insulin-like growth factor-I receptor (IGFR), which binds to insulin with a low affinity (Dubois et al., 2009; Entingh-Pearsall and Kahn, 2004). It is likely that insulin works through this cell surface receptor to elicit a response in HeLa cells.

HeLa cells however, do not express GLUT4 (Rodríguez-Enríquez et al., 2009). Therefore a HA-GLUT4-GFP reporter construct was used in this study, allowing for quantitative analysis of GLUT4 translocation. The construct contains a HA tag in the first exofacial loop and a GFP tag at the C-terminus. This construct is widely used in the field and been characterised in numerous studies. Importantly, the protein has been shown to be trafficked in a manner that is indistinguishable from endogenous GLUT4 (Lampson et al., 2000; Martin et al., 2006).

4.2 Aims of this chapter

The data presented in the previous chapter suggest that tyrosine phosphorylation of Sx4, at residues 115 and 251, effects its interactions with the SNARE proteins SNAP23 and VAMP2 *in vitro*. The translocation of GLUT4 is a regulated membrane trafficking event

facilitated at the plasma membrane by a SNARE complex consisting of Sx4, SNAP23 and VAMP2. This chapter aims to examine the impact of Sx4 phosphorylation on GLUT4 translocation to the plasma membrane. In order to do this I have utilised a HeLa cell line expressing GLUT4 that harbours an HA tag in the first exofacial loop and a C-terminal GFP tag. I have used a combination of confocal microscopy and flow cytometry to assess the effect on GLUT4 translocation of overexpressing phosphomimetic mutant Sx4 proteins on GLUT4 translocation in the presence of the endogenous protein. Ultimately it will be important to extend these studies into adipocytes and/or muscle cells and so have concomitantly used CRISPR-Cas9 technology to create Sx4 knockout cell lines in 3T3-L1 fibroblasts, with the view of differentiating these into 3T3-L1 adipocytes lacking endogenous Sx4. Using a combination of approaches to study the effects of phosphorylation of Sx4 on GLUT4 translocation, in the presence or absence of endogenous Sx4, will allow for a more complete picture of the mechanisms that regulate the process to emerge.

4.3 Results

4.3.1 Characterising a Myc tagged Sx4 construct

In order to assess the impact of Sx4 phosphorylation at Y115 and Y251, full length phosphomimetic Sx4 constructs were created, as opposed to the truncated versions lacking the trans-membrane domain used in the previous chapter. It was important to introduce an epitope tag to the constructs in order to distinguish them from endogenous Sx4 expressed in the HeLa cells. An internal Myc tag was introduced to the protein, between the N-terminus and the Habc domain (Figure 4.1A). The tag was introduced here so as to confer as little disruption to the function of the protein as possible, as both the N and C terminals of the protein are important to its function (D'Andrea-Merrins et al., 2007; Latham et al., 2006). For example, analysis of the interactions of Sx4 proteins containing point mutations or truncations have shown that both the N- and C-terminus are required for Munc18c binding (D'Andrea-Merrins et al., 2007; Latham et al., 2006).

Full length Sx4(Myc) WT, Y115E, Y251E and Y115,251E constructs were generated using the custom gene synthesis service from GenScript (NJ, USA). Before the constructs were expressed in cells I carried out some *in vitro* characterisation to determine whether the Myc tag has any discernable effect on the protein's behaviour. In order to do this a version of Sx4(Myc) lacking the transmembrane domain and tagged at the C-terminus with GST was created. Primers were designed (table 2.5) and the cytosolic portion of Sx4 from the Sx4(Myc) plasmid was amplified by PCR (section 2.2.4), before being cloned into the pETDuet vector, used for the bacterially expressed Sx4 proteins discussed in chapter 3 (section 2.2.5 and 2.2.6). Cytosolic Sx4(Myc) (residues 1-273), with a C-terminal GST tag was then expressed and purified from *E. coli* as described in section 2.3.2. In order to test the function of Sx4(Myc) an *in vitro* binding assay was set up with the SM protein Munc18c. Sx4-GST has been shown to bind to Munc18c *in vitro* (Aran et al., 2009). Sx4(Myc)-GST, Sx4-GST and GST were immobilised to glutathione Sepharose beads and incubated with Munc18c-WT and a phospho-mimetic mutant Munc18c-Y521E tagged at

the N-terminus with His (For purification details see section 5.3.1). Following incubation for 60 minutes at 4 °C, beads were collected and washed extensively (section 2.5). Samples were then subject to SDS-PAGE and immunoblot analysis. Figure 4.1B shows a representative immunoblot and Coomassie stained gel showing protein input. Both Sx4-WT and Sx4(Myc) bind to Munc18c WT and Y521E. Sx4(Myc)-GST exhibited more binding to Munc18c than Sx4-GST alone. This gave me confidence to proceed with the Myc-tagged constructs as it indicates that the gross structure of the protein is not detrimentally affected by the presence of the tag.

The expression of full length Sx4(Myc) was next examined. HeLa cells were transfected with Sx4(Myc)-WT, Y115E, Y251E and Y115,251E, as described in section 2.9.6. The protein was then detected by either immunofluorescence (section 2.10)(figure 4.2A) or immunoblotting (section 2.11)(figure 4.2B). Figure 4.2B shows all Sx4(Myc) constructs are expressed in HeLa cells and can be detected by immunoblot using an anti Myc antibody. Two bands can be detected in cells expressing Sx4(Myc), this may be due to protein truncations. The ratio of the two bands is the same for each of the mutants and so this should not affect any future experiments comparing the effects of expressing the mutants. Figure 4.2A shows Sx4(Myc) is also detected by immunofluorescence.

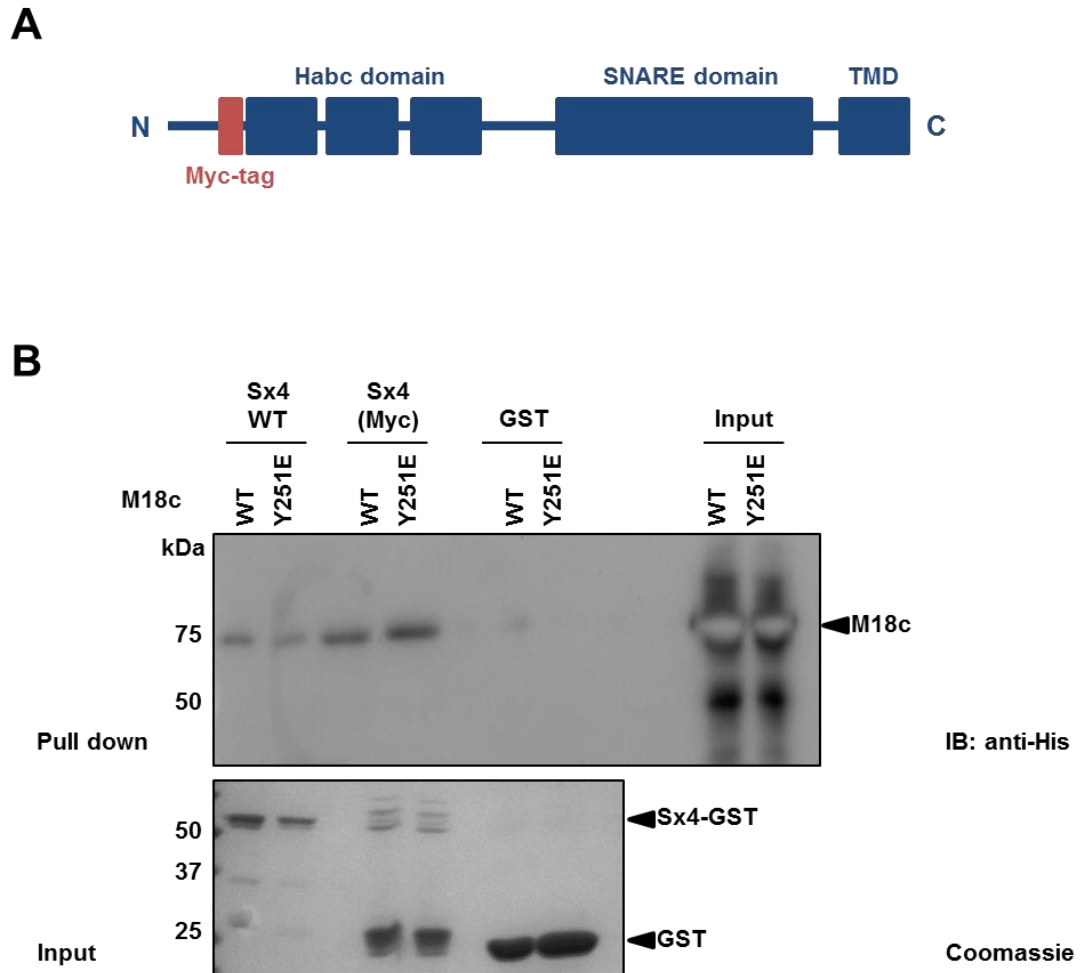


Figure 4.1 Sx4(Myc) characterisation

A Domain structure of Sx4, showing the location of the Myc tag. Sx4 comprises of an N-terminal domain, a Habc domain, SNARE domain and transmembrane domain (TMD). A Myc tag has been placed between the N-terminus and the Habc domain, a site that has been predicted to have minimal impact on the structure and function of the protein. **B** Pull down assay showing comparison of Sx4(Δ TMD)-GST and Sx4(Myc)(Δ TMD)-GST binding to Munc18c. Sx4-GST, Sx4(Myc)-GST and GST were immobilised to glutathione Sepharose beads before being incubated with His-Munc18c-WT or His-Munc18c-Y521E for 60 minutes at 4 °C. The beads were then collected and washed before being analysed by SDS-PAGE and immunoblot (section 2.5). Representative immunoblot and coomassie stained gels from three experiments are shown.

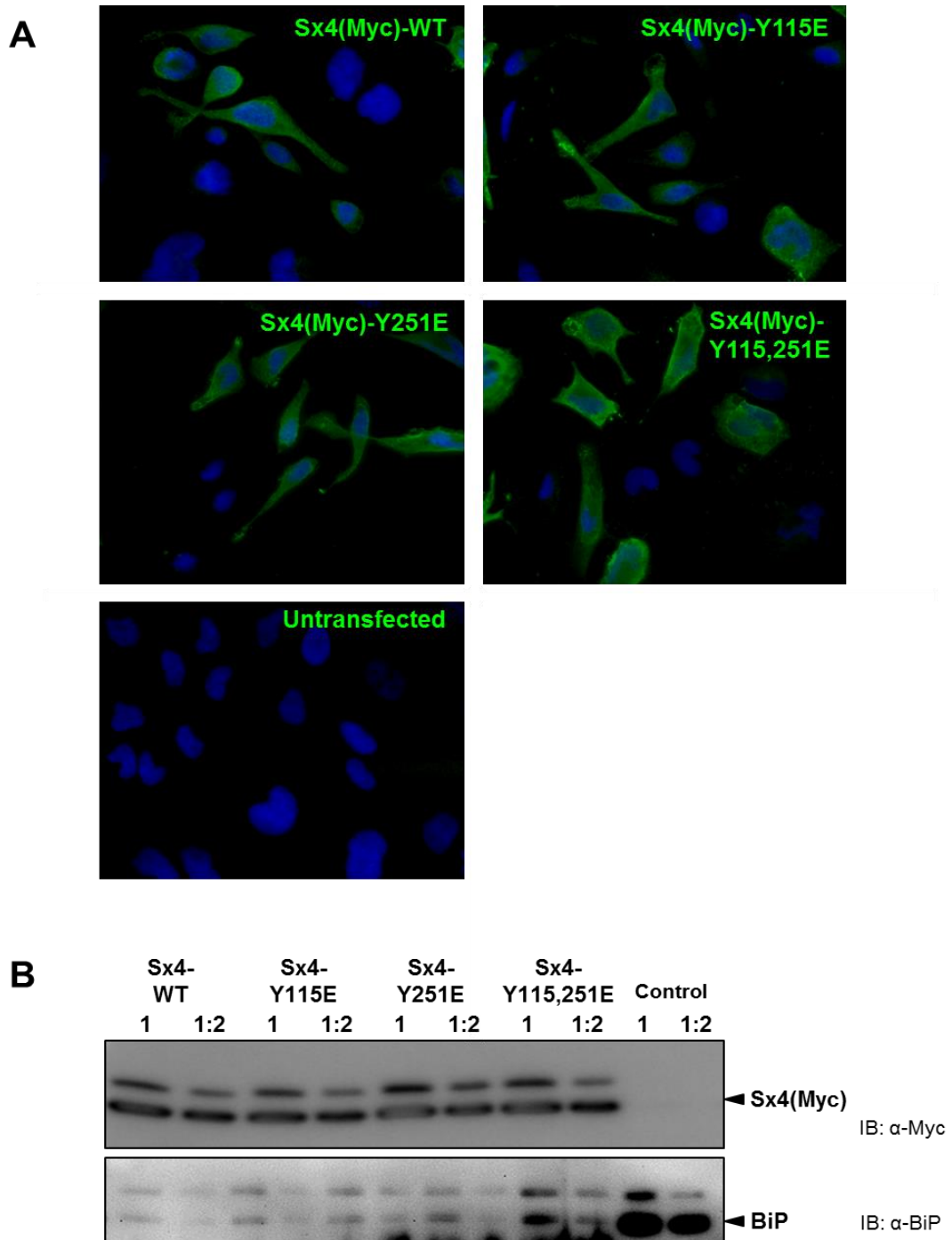


Figure 4.2: Expression of Sx4(Myc) in HeLa cells

A HeLa cells were plated onto glass cover slips in a 24 well plate before being transfected with 0.5 μ g Sx4(Myc) (section 2.9.6). Cells were fixed, permeabilised and stained for Sx4(Myc) using an anti-Myc antibody (section 2.10) (Green). Cell nuclei were stained with DAPI (Blue). **B** HeLa cells were plated in 6 well plates before being transfected with 2 μ g of Sx4(Myc) (section 2.9.6). Cells were then lysed into PBS plus sample buffer and lysates analysed by SDS-PAGE and immunoblotting (section 2.11). Upper gel shows Sx4(Myc) as detected by an anti-Myc antibody. BiP was used as a loading control. Untransfected cells were used as a negative control.

4.3.2 The effect of Sx4(Myc) phospho-mimetic mutants on GLUT4 translocation in HeLa cells

In order to examine the effects of Sx4 phosphorylation on GLUT4 translocation, a HeLa cell line expressing HA-GLUT4-GFP was used. The GLUT4 expressed in these cells contains a HA tag in the first exofacial loop of the protein, and a GFP tag at the C terminus (Dawson et al., 2001). This allows the translocation of GLUT4 to be examined, with the GFP signal equating to total GLUT4 levels and surface stained HA detecting the GLUT4 that has been inserted into the plasma membrane (Dawson et al., 2001). This construct has been previously characterised and has been shown to exhibit insulin stimulated translocation in a manner indistinguishable from endogenous GLUT4 (Lampson et al., 2000; Martin et al., 2006). Figure 4.3 shows confocal microscopy images of HA-GLUT4-GFP HeLas that have been treated with or without (basal) insulin, prior to surface staining with an anti-HA antibody in the absence of cell permeabilisation (section 2.9.8 and 2.10). An increase in the surface staining of HA-GLUT4-GFP was seen in insulin-stimulated cells (bottom panel). In addition, the localisation of GLUT4 (GFP) changed upon insulin stimulation. Under basal conditions (top panel) the GFP signal was in intracellular puncta, whereas upon insulin stimulation (bottom panel) the GFP signal was largely redistributed to the cell periphery.

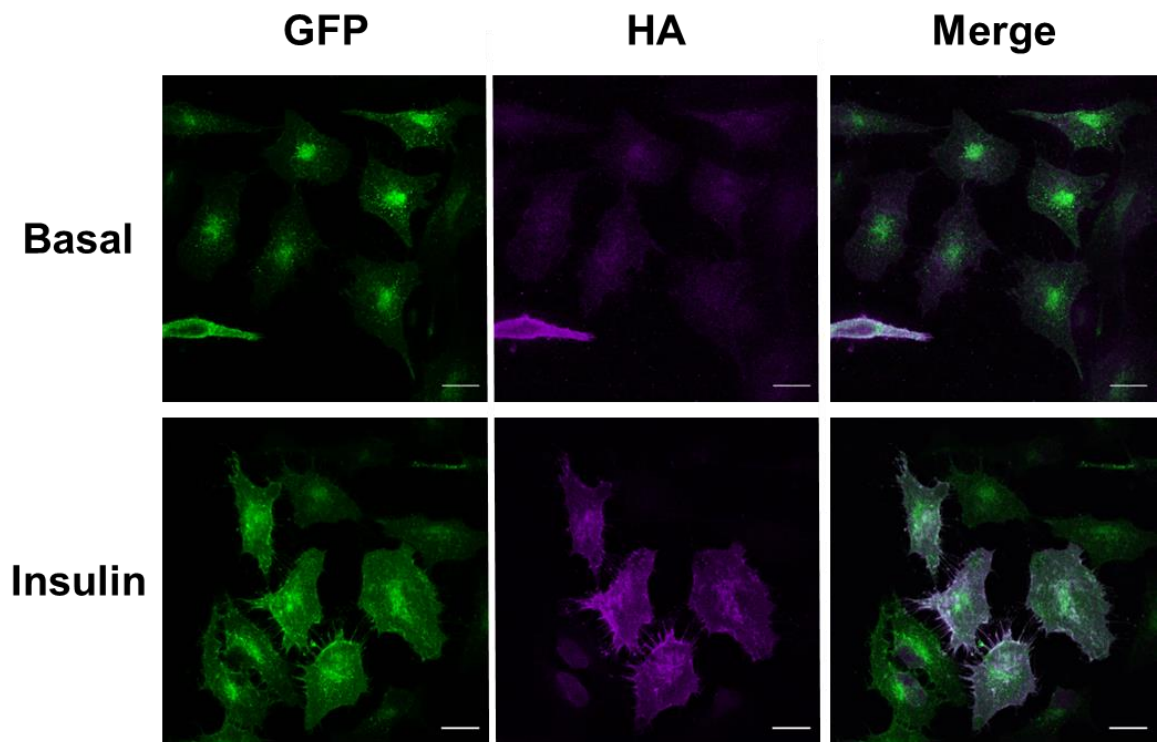


Figure 4.3: Insulin stimulates GLUT4 translocation in HeLa cells

HA-GLUT4-GFP HeLa cells were plated onto glass coverslips before either being treated with 170nM insulin for 20 minutes (insulin) or not (basal) (section 2.9.8). GLUT4 at the cell surface was then detected by surface staining for HA (purple) (section 2.10). Total GLUT4 is visualised using GFP (green). Upon insulin stimulation a change in cellular location and an increase in cell surface signal of GLUT4 can be seen. Scale bar = 20 μ m

Figure 4.3 shows that HA-GLUT4-GFP is translocated to the cell surface upon insulin stimulation in HeLa cells. This HeLa cell line was therefore utilised in order to examine the effect of over expression of Myc tagged phosphomimetic Sx4. Cells transfected with Sx4(Myc) WT, Y115E, Y251E, Y115,251E or an empty vector control (pCR3.1)(section 2.9.6). 24 hours after transfection, cells were treated with or without insulin (sections 2.9.8). The cells were then stained for cell surface HA-GLUT4-GFP, prior to permeabilisation and staining for Sx4(Myc) (Section 2.10). Immunofluorescence was imaged using a Zeiss LSM 880 invert confocal microscope.

Figure 4.4 suggests that overexpression of Sx4(Myc) phosphomutants affected GLUT4 localisation under basal conditions. The intracellular localisation and insulin response in cells overexpressing Sx4(Myc)-WT was comparable to that of untransfected cells and the empty plasmid control. Similarly, no distinguishable change can be seen in the localisation of GLUT4 (GFP) under basal conditions when Sx4(Myc)-Y115E is overexpressed. Although high levels of basal cell surface HA staining can be seen in all samples, changes in the total GLUT4 localisation (GFP) in cell expressing Sx4(Myc)-Y251E or Sx4(Myc)-Y115,251E were noted under basal conditions. When either of these mutants was expressed total GLUT4 (GFP) localisation resembled that of insulin-stimulated cells.

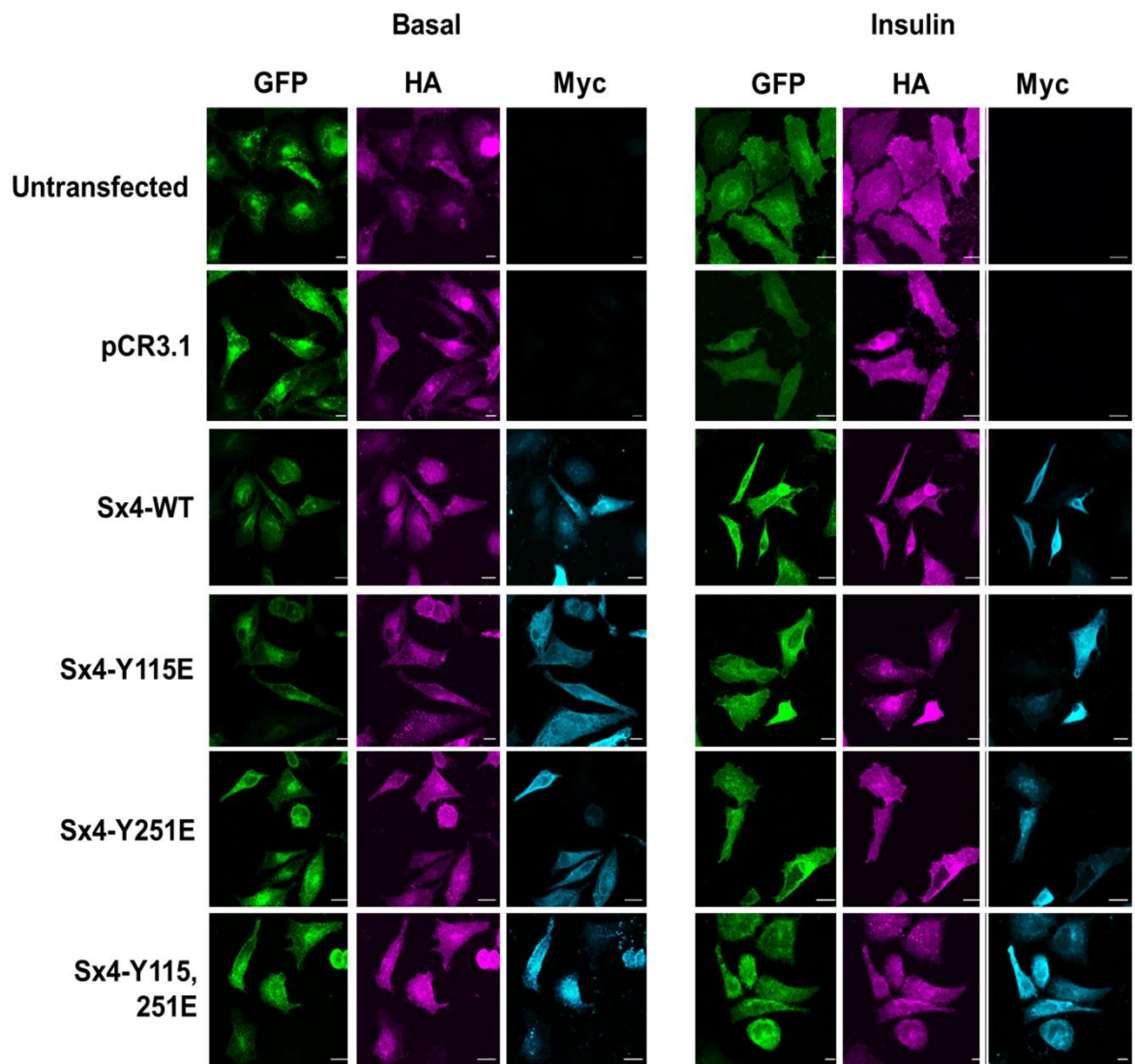


Figure 4.4 Effect of Sx4 phosphomutant over expression in HA-GLUT4-GFP HeLa cells

HeLa cells expressing HA-GLUT4-GFP were grown on glass cover slips and transfected with 0.5 µg per well of Sx4(Myc) WT, Y115E, Y251E or Y115,251E or an empty pCR3.1 plasmid (section 2.9.6). 24 hours later cells were serum starved and treated with (insulin, right) or without (basal, left) 170 nM insulin (section 2.9.8). Cells were then surface stained for HA in the absence of cell permeabilisation, before being permeabilised and stained for Myc (section 2.10). Immunofluorescence images were taken using a Zeiss 880 invert confocal microscope. Panels show GFP (total GLUT4, green), surface stained AlexaFluor 647 HA (cell surface GLUT4, magenta) and Sx4(Myc) stained with anti-Myc and DyLight 405 (cyan). Scale bar = 20 µm.

4.3.3 Quantification of HA-GLUT4-GFP translocation in HeLa cells by flow cytometry

Overexpression of Sx4 phosphomimetic mutants, Y251E and Y115,251E, in HA-GLUT4-GFP HeLa cells showed a change in the subcellular localisation of GLUT4 under basal conditions. Whilst immunofluorescence and microscopy can be used to observe changes in proteins, data from these experiments are hard to quantify. I next sought to quantify the translocation of HA-GLUT4-GFP in HeLa cells using flow cytometry.

In order to optimise conditions for quantification of surface stained of HA by flow cytometry an antibody titration was carried out. HA-GLUT4-GFP HeLa cells were treated with or without (basal) insulin. Cells were then fixed and surface stained for HA before being lifted from the culture dish and analysed by flow cytometry (section 2.12). Figure 4.5 shows flow cytometry data represented in bar graphs (for raw data see appendix III). The median GFP fluorescence intensity, and therefore total GLUT4, was unchanged upon insulin stimulation (Figure 4.5A). Figure 4.5B shows an increase in the median fluorescence intensity of cell surface GLUT4 (HA) could be detected upon insulin stimulation. The ratio of basal/insulin median fluorescence intensity of cell surface HA was calculated. Figure 4.5C shows that a primary antibody dilution of 1:200 (500 ng/ml) was optimum for detecting insulin stimulated GLUT4 translocation.

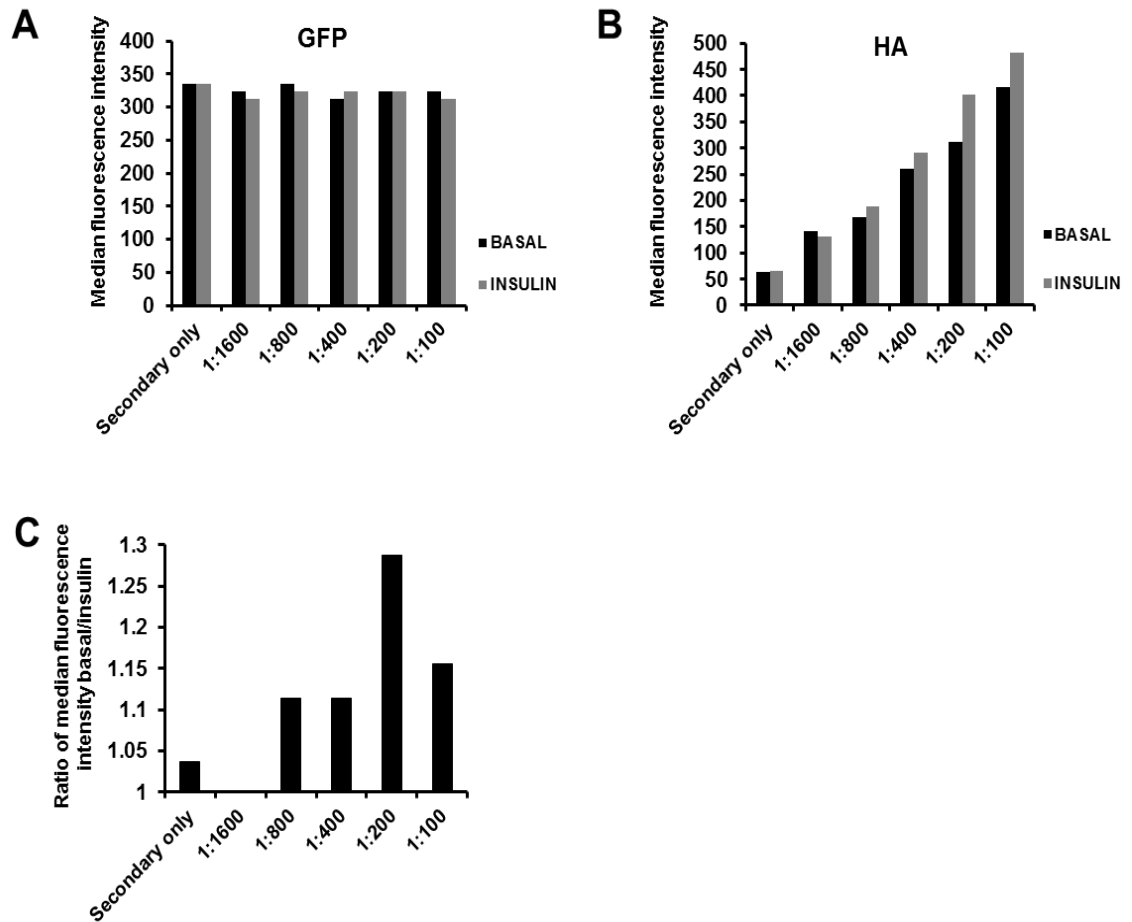


Figure 4.5 Quantification of HA-GLUT4-GFP translocation in HeLa cells by flow cytometry

HA-GLUT4-GFP HeLa cells were serum starved before being treated with or without (basal) 170 nM insulin for 20 minutes. Cells were then fixed and surface stained using an anti HA antibody (section 2.12). Cells were lifted and analysed using a Beckman Coulter CyAn ADPs flow cytometer. Data was collected and graphs show the median fluorescence intensity (For raw data see appendix III) **A** GFP shows total GLUT4 levels were unchanged upon insulin stimulation. **B** An increase in the median fluorescence intensity of surface HA staining was seen upon insulin stimulation. **C** The ratio of the median fluorescence intensity of insulin compared to basal cell surface HA signal. An antibody dilution of 1:200 showed the biggest fold change of cell surface HA signal upon insulin stimulation

Figure 4.5 shows that an insulin response in HA-GLUT4-GFP HeLa cells was detected by flow cytometry. The effect of overexpressing Sx4(Myc) phospho-mutants on HA-GLUT4-GFP translocation was then examined. HA-GLUT4-GFP HeLa transfected with Sx4(Myc) WT and phospho-mimetic mutants, along with an empty vector control and an untransfected control treated with transfection reagent only (section 2.9.6). Cell surface HA-GLUT4-GFP was stained using an anti-HA antibody, before cells were permeabilised and stained for Sx4(Myc) expression. The fluorescence intensity of total (GFP) and cell surface (HA) HA-GLUT4-GFP was measured in cells that were positive for Sx4(Myc) (transfected) in addition to those that had no Sx4(Myc) signal (untransfected) in each sample (For raw data see appendix IV).

Figure 4.6A shows the median fluorescence intensity of surface stained HA in transfected and untransfected cells under basal or insulin-stimulated conditions. Over expression of Sx4-WT increased cell surface HA-GLUT4-GFP under basal conditions. This is likely due to the high level of expression of Sx4(Myc). Over expression of Sx4-Y115E or Sx4-Y251E increased basal cell surface GLUT4 by a factor of 2.5 and 2.4 fold respectively when compared to untransfected cells. Moreover, overexpression of Sx4-Y115,251E increased basal cell surface HA-GLUT4-GFP by 3.7-fold. Figure 4.6B shows the ratio of median fluorescence intensity of basal/insulin, and therefore the insulin response of HA-GLUT4-GFP in the cells. Cells that had no transfection treatment (untransfected) exhibited a 1.8 fold increase in surface stained HA in insulin-treated cells compared to basal. Cells that had been transfected with an empty pCR3.1 control plasmid (control) displayed a slightly reduced insulin response of a 1.3 fold increase of basal/insulin cell surface HA-GLUT4-GFP. Untransfected cells from Sx4-WT, Sx4-Y115E and Sx4-Y115,251E samples showed a similar increase in cell surface GLUT4 in response to insulin (1.43, 1.34 and 1.43 fold respectively). Cells that had been transfected with Sx4-WT (positively stained for Myc) showed a reduced insulin response, with a 1.16 fold increase in cell surface HA staining of insulin stimulated cells compared to basal. Whereas, the insulin response in cells that

were Myc positive, and expressing Sx4-Y115E, Sx4-Y251E or Sx4-Y115,251E, was eradicated (with a basal/insulin cell surface HA ratio of 0.86, 0.65 and 0.7 respectively) due to the increase in cell surface HA-GLUT4-GFP under basal conditions. Figure 4.6C shows that GFP fluorescence intensity, and therefore total HA-GLUT4-GFP, is similar across all samples, demonstrating that the changes in cell surface HA staining were not due to changes in HA-GLUT4-GFP expression.

Figure 4.7 shows histograms representing the fluorescence intensity of cell surface HA of cells that are Sx4(myc) negative (untransfected, green) and those that are expressing Sx4(myc) (transfected, blue) under basal conditions. An increase in the number of cells with high fluorescence intensity (greater than 10^3) was seen when Sx4-Y115E, Sx4-Y251E and Sx4-Y115,251E were overexpressed. Figure 4.7 also shows the ratio of the median HA fluorescence intensity of untransfected/transfected cells. This ratio increases in cells expressing Sx4 phospho-mimetic mutants, again showing that expression of the phospho mutants increases cell surface GLUT4 under basal conditions.

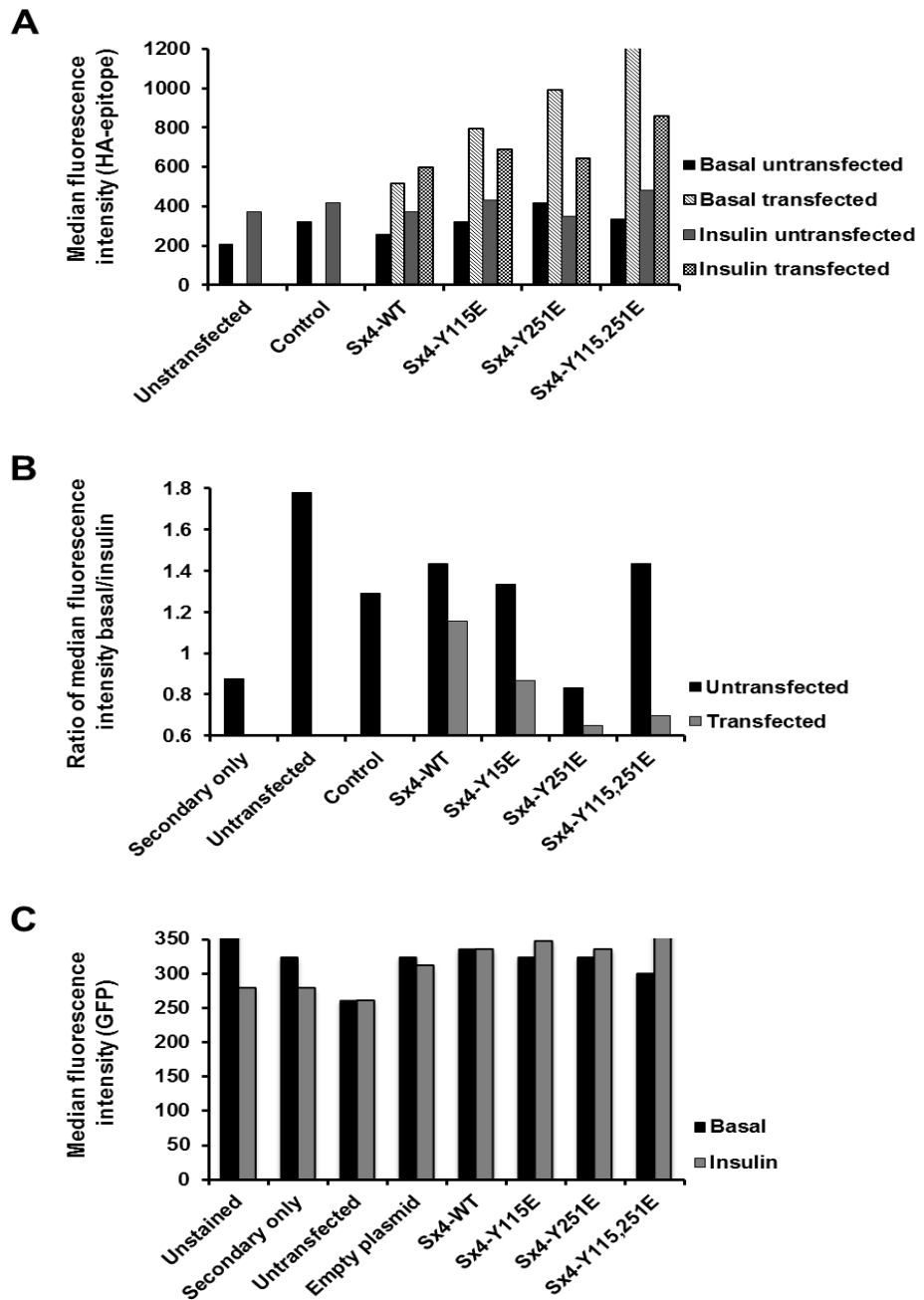


Figure 4.6 Expression of Sx4 phospho-mutants increases cell surface GLUT4

HA-GLUT4-GFP HeLa cells were transfected with Sx4(Myc) WT, Y115E, Y251E, Y115,251E or empty plasmid control (section 2.9.6). 24 hours after transfection cells were treated with or without insulin for 20 minutes (section 2.9.8) before being surface stained for HA. Cells were then stained for transfected syntaxin using a Myc antibody and analysed using flow cytometry (section 2.12). **A** Median fluorescence intensity for the HA epitope of basal and insulin treated transfected (Myc positive) and untransfected (Myc negative) cells. Expression of Sx4 phospho-mutants increases cell surface HA. **B** Ratio of median fluorescence intensity (HA epitope) basal/insulin for untransfected (Myc negative) and transfected (Myc positive). Ratio shows insulin response in cells is decreased in transfected cells due to high levels of basal cell surface HA. **C** Median fluorescence intensity of GFP signal for basal and insulin stimulated cells. GFP fluorescence intensity (representing total GLUT4) remains similar across all samples. A total of ~5000 cells were analysed for each sample. For raw data see Appendix IV.

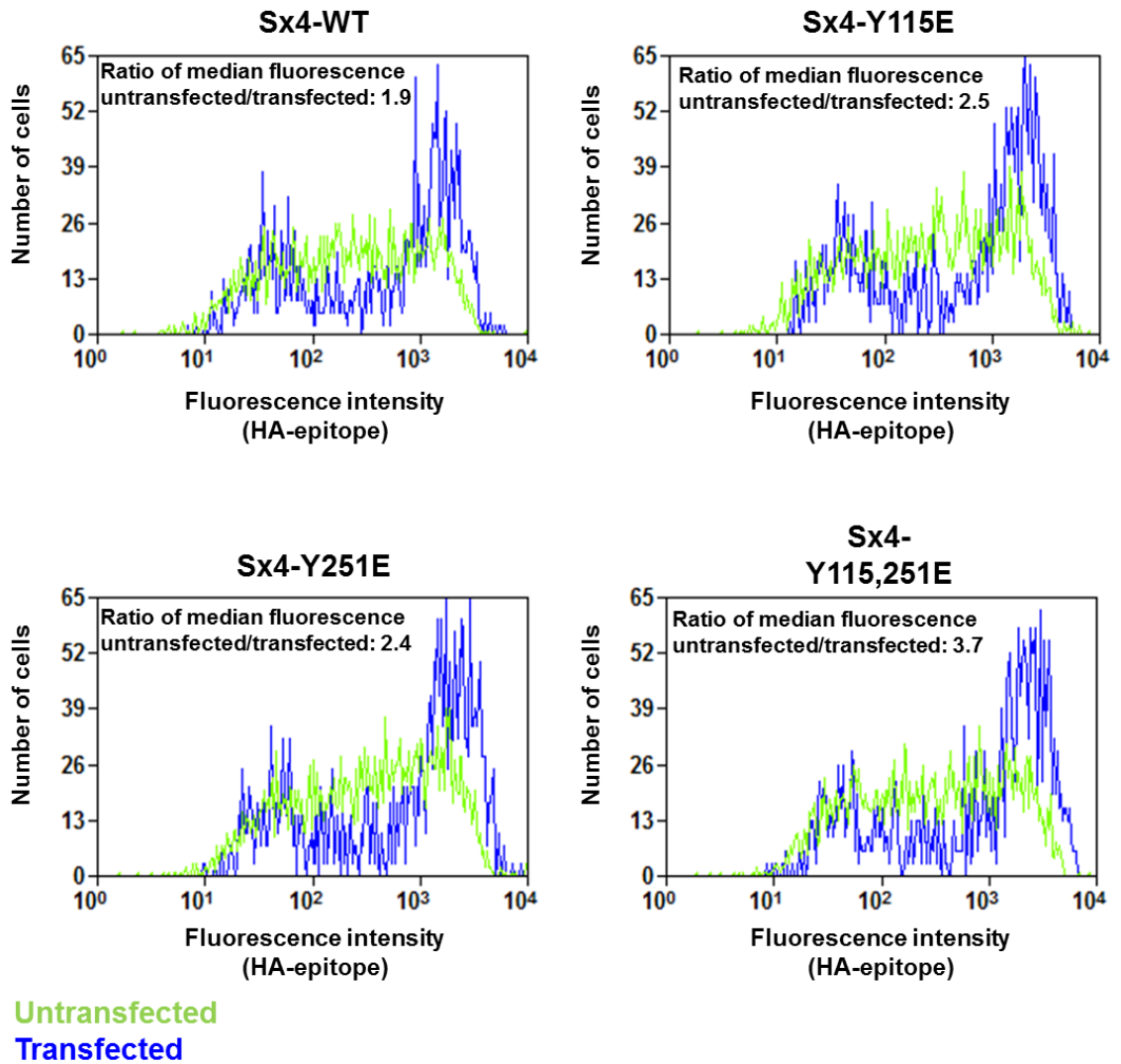


Figure 4.7 Histograms showing increase in basal cell surface GLUT4 in Sx4 phospho-mutant expressing HA-GLUT4-GFP HeLa cells

HA-GLUT4-GFP HeLa cells were transfected with Sx4(Myc) WT, Y115E, Y251E, Y115,251E or empty plasmid control (section 2.9.6). Cells were stained for transfected syntaxin using a Myc antibody and analysed using flow cytometry (section 2.12). Shown are histograms of the fluorescence intensity (HA epitope) comparing untransfected (green) and transfected (blue) cells under basal condition. A total of ~5000 cells were analysed from each sample. The ratio of the median fluorescence of cell surface HA-staining of untransfected/transfected cells is shown. Expression of Sx4 phospho-mimetic mutants increases the ratio of cell surface HA-GLUT4-GFP of untransfected/transfected cells.

4.3.4 Generating Sx4 knockout 3T3 cell lines using CRISPR-Cas9 technology

Previous data presented in this chapter shows that phosphorylation of Sx4 at Y115 and/or Y251 increases cells surface GLUT4 under basal condition in HeLa cells in the presence of endogenous Sx4. Expressing Sx4 phosphomutants in cells that lack endogenous Sx4 would allow more detailed examination of the consequences of phosphorylation and eliminate competition of the endogenous and transfected proteins. A Sx4 knock out cell line was then generated using CRISPR-Cas9 technology.

The CRISPR-Cas9 technology is based on CRISPRs (clustered regularly interspaced palindromic repeats) found in the genomes of bacteria and archaea (Horvath & Barrangou 2010). The CRISPRs along with *cas* (CRISPR associated) genes encode proteins as part of an adaptive defence mechanism to provide immunity from viruses (Barrangou et al., 2007). Increased understanding of CRISPR in bacteria led to the development of CRISPR-Cas technology for mammalian genome editing. Cas9 is an endonuclease that, when used in conjunction with CRISPR guide RNA, introduces a site-specific double strand break in the target gene (Doudna & Charpentier 2014). This results in an easy to use genome editing tool, whereby a single plasmid can encode the guide RNA and Cas9 to knock out expression of the target gene.

3T3-L1 fibroblasts were chosen to generate the knock out cell lines as these can be differentiated into adipose cells, which are insulin responsive and are important regulators of glucose homeostasis in mammals (Bryant and Gould, 2011). Before generating the knockout cell lines the transfection efficiency of 3T3-L1 fibroblasts was investigated. In order to do this a construct expressing cellugyrin harbouring an N-terminal td-Tomato tag was transfected into both 3T3-L1 cells and 3T3-L1 cells stably expressing HA-GLUT4-GFP at varying concentrations (section 2.9.6). Figure 4.8 shows that both cell lines were successfully transfected. Furthermore, 0.5 µg of plasmid resulted in the best transfection efficiency.

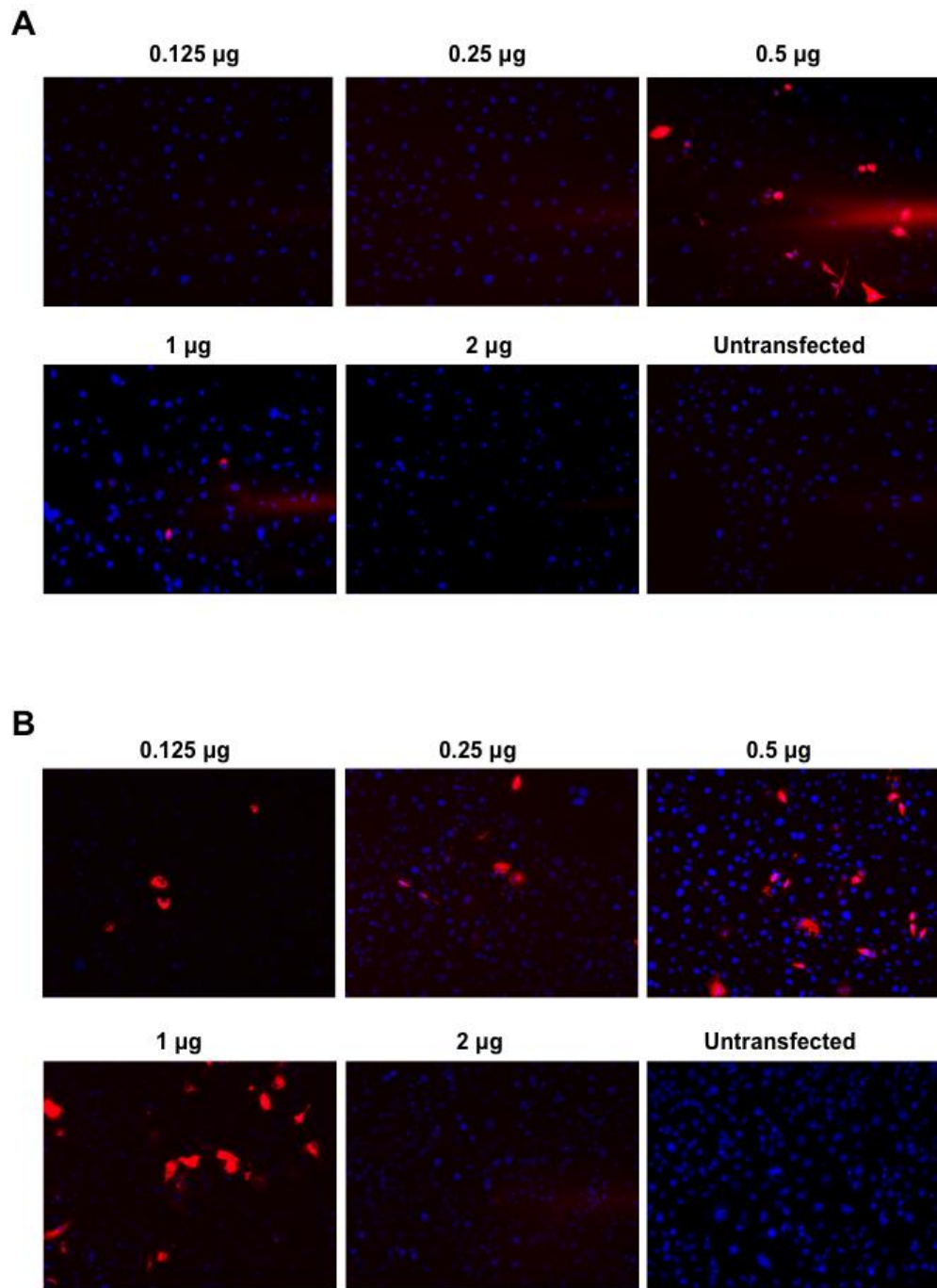


Figure 4.8 3T3-L1 and HA-GLUT4-GFP 3T3-L1 fibroblasts are successfully transfected

3T3-L1 (**A**) and HA-GLUT4-GFP 3T3-L1 (**B**) fibroblasts were plated on glass cover slips before being transfected with 0.125, 0.25, 0.5, 1 or 2 μg of plasmid expressing tdTomato-cellugyryn (section 2.9.6). After 24 hours in transfection media the transfection efficiency of the cells was examined by microscopy. Nuclei were stained using DAPI (blue). Td-Tomato-cellugyryn is shown in red. Both cell lines were successfully transfected.

A CRISPR plasmid with guide RNA targeting a region of exon 2 of Sx4 was purchased from Sigma-Aldrich (Sigma-Aldrich Ltd., Gillingham, Dorset, UK). The plasmid also expressed an RFP marker, allowing for rapid sorting of transfected cells by fluorescence-activated cell sorting (FACS).

3T3-L1 and HA-GLUT4-GFP 3T3 cells were transfected with Sx4 CRISPR plasmid. After 24 hours, transfected cells were sorted using a Beckman Coulter MoFlo Astrios flow cytometer. Figure 4.8 shows dot plots of FACS analysis of both 3T3-L1 (Figure 4.8A) and HA-GLUT4-GFP 3T3-L1 (Figure 4.8B) cells. The fluorescence intensity of RFP is plotted against that of GFP for both cell lines. HA-GLUT4-GFP 3T3 cells show a positive shift in GFP signal demonstrating that they are expressing the tagged GLUT4. Each event plotted corresponds to a cell. Cells from region R2 in each sample were sorted and kept for further culture. FACS analysis revealed that both cell lines had good transfection efficiency, at 49% for 3T3-L1 cells and 48% for HA-GLUT4-3T3 cells.

RFP positive cells were cultured to allow single colonies to form, before a number of colonies were selected and expanded (section 2.13). Immunoblot analysis was carried out on the selected colonies to screen for Sx4 knock out. Cell lysates were then run on 12 % SDS-PAGE gels and analysed by immunoblot detection of Sx4 and tubulin (loading control). Positive controls of WT 3T3-L1 or HA-GLUT4-GFP 3T3-L1 cell lysates were also run. Figure 4.9 shows that Sx4 knock down was successful in several colonies in both 3T3-L1 and HA-GLUT4-GFP 3T3-L1 cells. Colonies that showed no Sx4 signal but a strong tubulin loading control signal were then chosen to be characterised. Colonies 7, 8, 13 and 14 were selected from the 3T3-L1 cells (Figure 4.9A). Colonies 2, 3 5 and 8 were chosen from HA-GLUT4-GFP 3T3-L1 cells (Figure 4.9B).

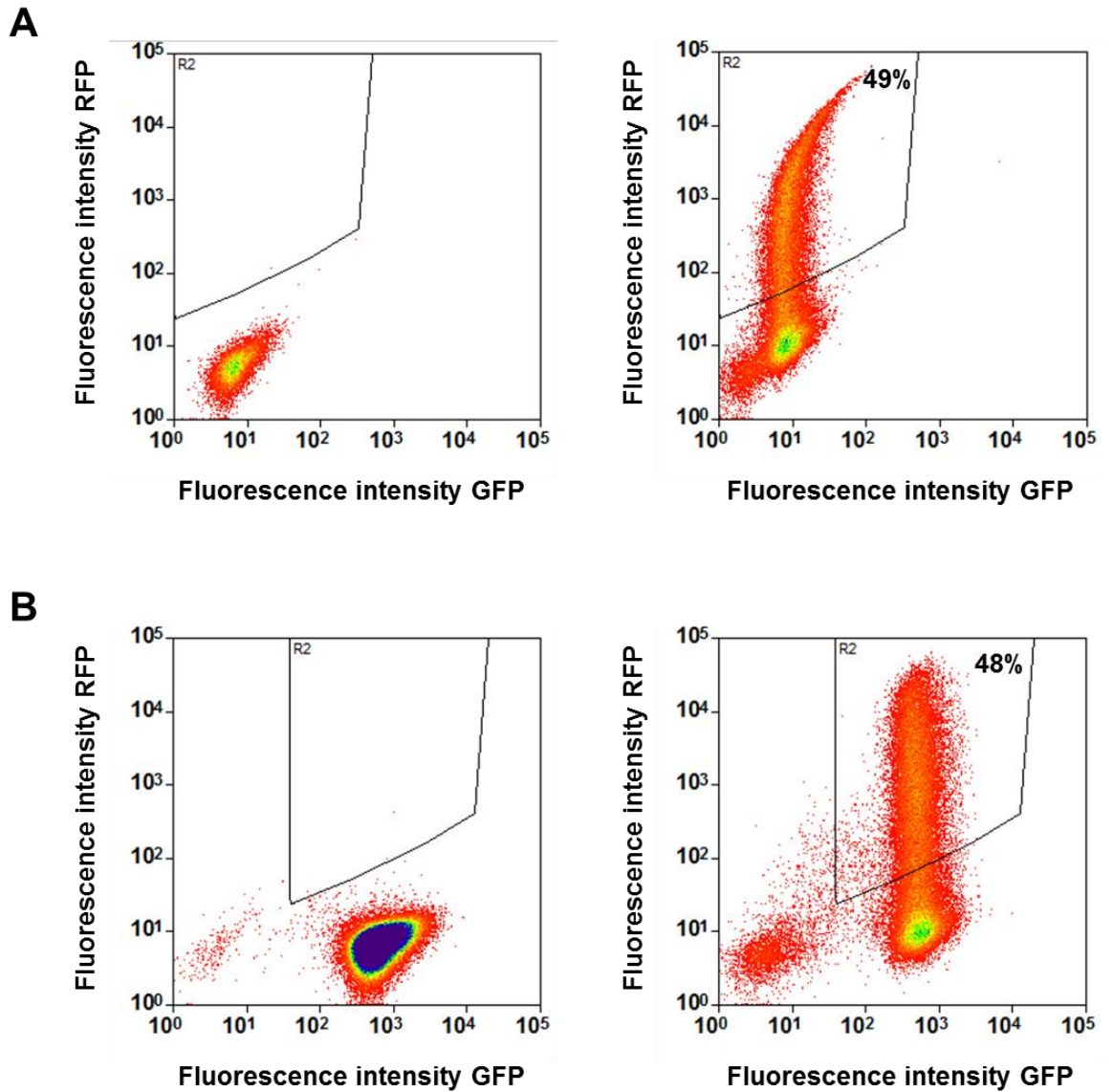


Figure 4.9 Fluorescence-activated cell sorting of CRISPR-Cas9 transfected 3T3-L1 cells

3T3-L1 (A) and HA-GLUT4-GFP 3T3-L1 (B) were plated before being transfected with a CRISPR plasmid targeting Sx4. 24 hours after transfection cells were lifted and analysed by fluorescence-activated cell sorting (FACS) (section 2.13). Shown are dot plots representing fluorescence intensity of RFP plotted against the fluorescence intensity of GFP. Each dot represents one event (cell). Cells in box R2 represent RFP positive cells that were kept for further culture.

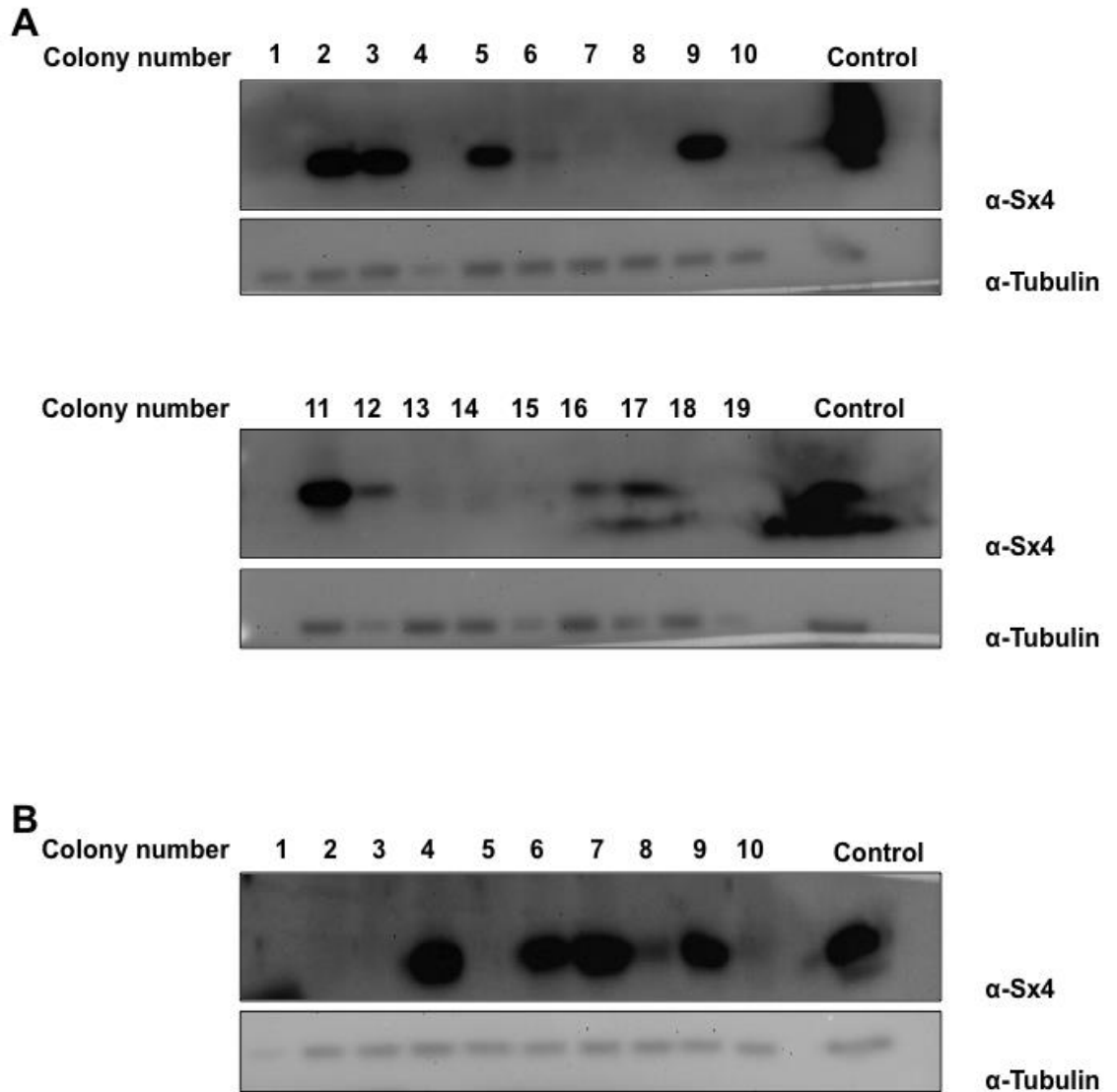


Figure 4.10 Immunoblots of 3T3-L1 Sx4 CRISPR knockout cell lines

3T3-L1 and HA-GLUT4-GFP 3T3-L1 cells were transfected with an Sx4 CRISPR plasmid before transfected cells were sorted using flow cytometry. Cells were then cultured until single colonies formed. Colonies were selected and expanded before being lysed and subject to immunoblot analysis (section 2.13). **A** 3T3-L1 CRISPR colonies. **B** HA-GLUT4-GFP 3T3-L1 CRISPR colonies. Lysates were blotted with an anti-tubulin antibody as a loading control. Anti-Sx4 blots show numerous colonies have been successfully depleted of Sx4.

4.3.5 Characterising Sx4 CRISPR knockout 3T3-L1 cell lines

Figure 4.9 shows that Sx4 was successfully knocked out of 3T3-L1 and HA-GLUT4-GFP 3T3-L1 cells. Colonies that were negative for Sx4 expression were then chosen to continue to culture and characterise.

The propensity for the Sx4 knockout cells to differentiate was first examined. Sx4 knockout 3T3-L1 and HA-GLUT4-GFP 3T3-L1 along with WT cells were plated and treated with adipocyte differentiation media (section 2.9.7). The cells were then examined by microscopy to assess their differentiation. Figure 4.11 shows differentiation of 3T3-L1 (A) and HA-GLUT4-GFP 3T3-L1 (B) cells to adipocytes. WT cells exhibit the morphological features expected when cells are differentiated (Armani et al., 2010). The cells become spherical and lipid droplets can be seen. Figure 4.11A shows that, with the exception of C13, Sx4 knockout 3T3-L1 fibroblasts are capable of differentiating. In contrast, none of the HA-GLUT4-GFP 3T3-L1 knockout cells showed the morphological changes associated with differentiation.

The insulin-response in Sx4 knockout HA-GLUT4-GFP 3T3-L1 cells was then examined. Cells were plated before being differentiated (section 2.9.7) and treated with insulin (section 2.9.8). Cells were surface stained for HA and imaged using confocal microscopy (section 2.10). Figure 4.12 shows that HA-GLUT4-GFP in WT 3T3-L1 adipocytes translocated to the PM in response to insulin. Although Sx4 depleted cells did not differentiate (Figure 4.11 and 4.12), ectopically expressed GLUT4 has been shown to translocate in response to insulin in 3T3-L1 fibroblasts (Huang et al., 2013). Figure 4.12 shows that no change was seen in the intracellular localization (GFP) or surface staining (HA) of HA-GLUT4-GFP in Sx4 depleted cells.

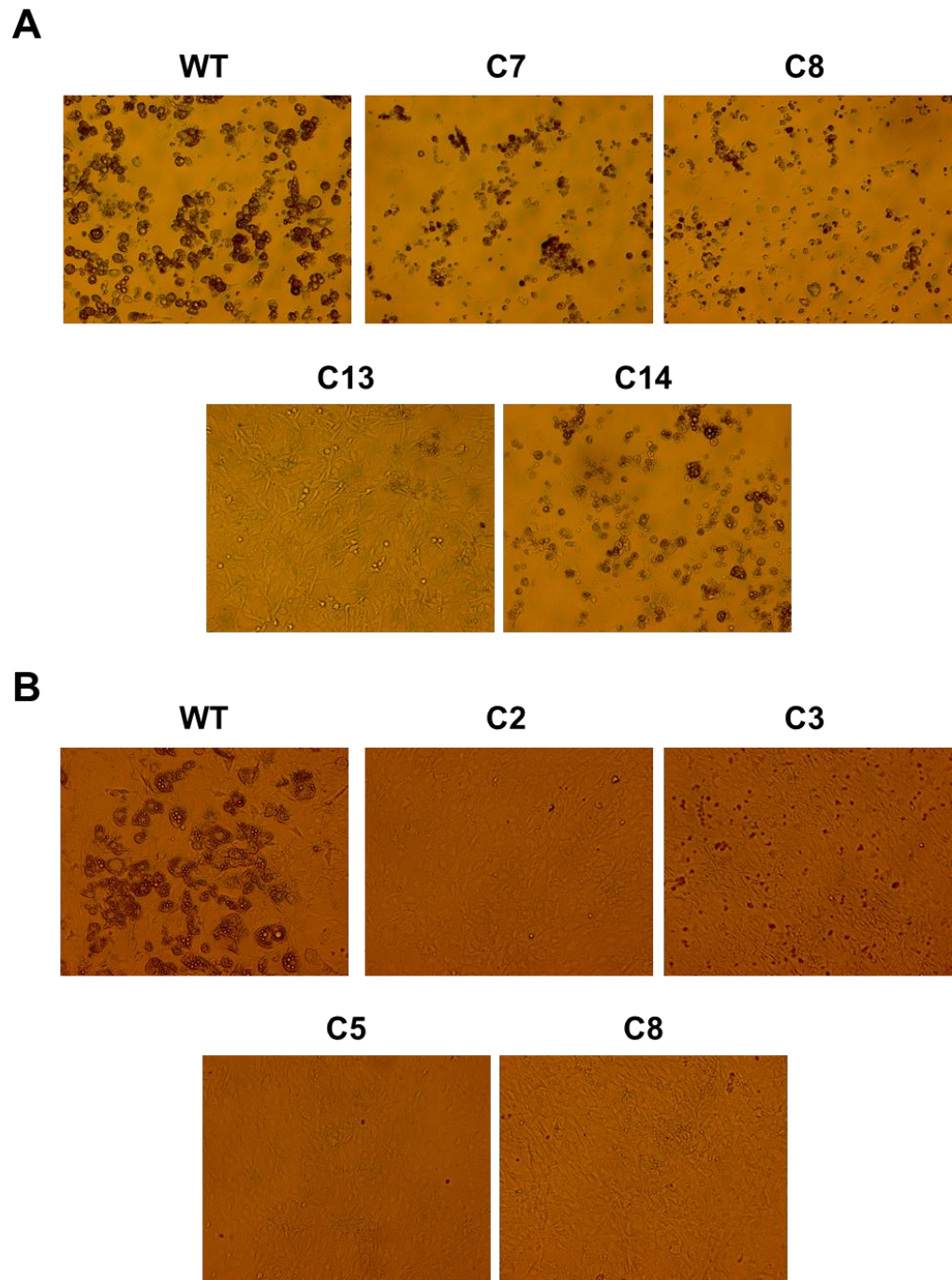


Figure 4.11 Differentiation of Sx4 knockout 3T3-L1 fibroblasts to adipocytes

3T3-L1 fibroblasts were plated and treated with adipocytes differentiation media (section 2.9.7). Cells were then imaged using a light microscope. **A** WT 3T3-L1 cells along with Sx4 knockout colonies C7, C8, C13 and C14. **B** WT and Sx4 knockout C2, C3, C5 and C8 HA-GLUT4-GFP 3T3-L1 cells. Images show WT cells were successfully differentiated whereas cells depleted of Sx4 showed a varied response to the differentiation treatment.

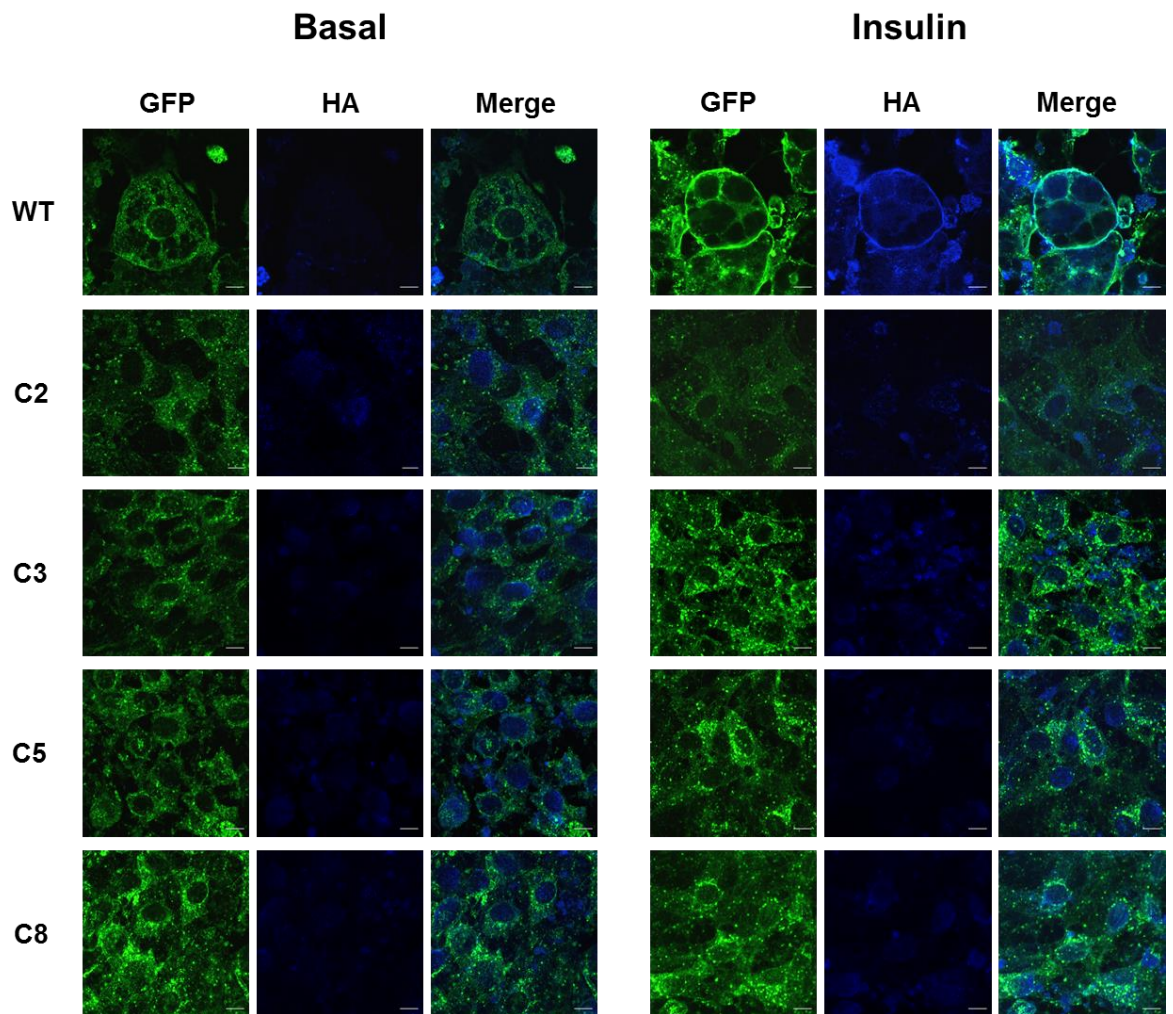


Figure 4.12 HA-GLUT4-GFP does not translocate to the cell surface in insulin-stimulated cells depleted of Sx4

HA-GLUT4-GFP 3T3-L1 cells were plated and treated with adipocyte differentiation media (section 2.9.7). Following differentiation, cells were serum starved and stimulated with 170 nM insulin for 20 minutes (section 2.9.8). The cells were then fixed and surface stained for GLUT4 using an anti-HA antibody (section 2.10). Cells were analysed using confocal microscopy. Images show that Sx4 knockout cells (C2, C3, C5 and C8) failed to differentiate and were not insulin responsive. Whereas WT 3T3-L1 adipocytes (top panel) showed a robust relocalisation of HA-GLUT4-GFP following insulin treatment. Scale bar = 10 μ m.

4.4 Discussion

GLUT4 is a glucose transporter protein that, upon insulin-stimulation, is rapidly translocated from its intracellular stores to the plasma membrane in fat and muscle cells (Bryant et al., 2002). This regulated membrane trafficking event is controlled by a SNARE complex consisting of Sx4, SNAP23 and VAMP2 at the PM (Kawanishi et al., 2000; St-Denis et al., 1999). Sx4 has been shown to be phosphorylated at tyrosine residues 115 and 251 in 3T3-L1 adipocytes in response to insulin (Schmelzle et al., 2006). This chapter therefore aimed to examine the effect of Sx4 phosphorylation on the translocation of GLUT4 to the PM.

In order to study the effect of Sx4 phosphorylation at Y115 and Y251 on GLUT4 translocation Myc tagged phospho-mimetic Sx4 mutants were generated. An *in vitro* pull down assay using the cytosolic domain of recombinant purified Sx4(Myc)-GST and Sx4-GST was carried out (Figure 4.1). The assay showed that Sx4(Myc)-GST bound to more Munc18c than Sx4-GST. This increase may be due to slight structural changes in the protein due to the presence of the Myc tag. The tag was introduced between the N-terminal domain and the Habc domain in an attempt to cause as little disruption to the function of Sx4 as possible. As the protein was still functional the slight increase in binding to Munc18c was not concerning as any effect of phosphorylation of Y115 and Y251 when expressing phospho-mimetic mutants should be seen in addition to the effects of expressing the WT protein.

I then examined the effect of over expressing Myc-tagged phospho-mimetic Sx4 mutants, in the presence of the endogenous protein, in HeLa cells expressing a HA-GLUT4-GFP reporter protein (figure 4.4). Over expression of phospho-mimetic mutants appeared to have an effect on the localisation of HA-GLUT4-GFP when compared to cells expressing Sx4(Myc) WT or no Sx4(Myc). However, quantifying this change is particularly hard in

HeLa cells as they show fairly high levels of cell surface GLUT4 under basal conditions, and a smaller insulin response than adipocytes or muscle cells.

Given that it proved hard to analyse the effect of overexpressing phospho-mimetic Sx4(Myc) in HA-GLUT4-GFP HeLa cells, I sought to study this using a more quantitative technique. Figure 4.5 shows that flow cytometry was an effective way of quantifying cell surface GLUT4 and that an insulin-induced increase in the levels of the protein at the cell surface was detected. This method also allowed for rapid quantification of roughly 5000 cells per sample. Analysing this many cells by microscopy would not be possible. The effect of over expressing Sx4(Myc) phospho-mimetic mutants on HA-GLUT4-GFP translocation was then analysed using flow cytometry (figure 4.6 and 4.7). Expression of the phospho-mimetic mutants increased cell surface GLUT4 under basal conditions, this is consistent with data from the previous chapter showing that phospho-mimetic Sx4 forms more SNARE complexes when compared to Sx4-WT (figure 3.3). It is tempting to speculate that insulin-induced phosphorylation of Sx4 at Y115 and/or Y251 regulates GLUT4 translocation by increasing the propensity of Sx4 to form SNARE complexes and therefore increasing the rate of GSV fusion. However, more detailed analysis of GSV fusion in the presence of phospho-mimetic Sx4 is needed to elucidate whether GSV fusion frequency is increased. For example, TIRF microscopy could be used to resolve the discrete steps of GLUT4 trafficking at the plasma membrane (Bai et al., 2007).

It will also be important to examine the effect of phosphorylation of Sx4 in adipocytes and/or muscle cells. In addition, analysis of the effect of Sx4 phospho-mutants in the absence of endogenous Sx4 will be important. Depleting endogenous Sx4 will remove the competition for any phospho-mutants expressed, this may be especially important when analysing phospho-resistant mutants where WT endogenous Sx4 may rescue and mask the effects of the mutants. I therefore sought to generate knockout cell lines in 3T3-L1 fibroblasts that will be differentiated into adipocytes lacking endogenous Sx4. The cell lines were generated using CRISPR-Cas9 technology that allowed for rapid and accurate

targeting of Sx4 (figures 4.9 and 4.10). Interestingly, when the Sx4 depleted cells were characterised a difference in their propensity to differentiate was observed (figure 4.11). 3T3-L1 cells that were depleted of Sx4 were capable of differentiating, however the morphology of 3T3-L1 fibroblasts that were expressing HA-GLUT4-GFP and depleted of Sx4 did not change following treatment with differentiation media. Sx4 is up-regulated upon differentiation of 3T3-L1 fibroblasts to adipocytes (Torrejón-Escribano et al., 2002). So it is logical that the morphological changes seen in Sx4 knockout 3T3-L1 cells were not as striking and those seen in WT 3T3-L1 cells. It has been noted from observations in the laboratory that HA-GLUT4-GFP expressing 3T3-L1 cells do not differentiate as well as those not expressing the reporter protein (unpublished observations). These cells are a higher passage number than the 3T3-L1 cells normally used for differentiation experiments. It may therefore be that the cells have a reduced propensity to differentiate and so depletion of Sx4 has a greater negative effect on these cells than it does on 3T3-L1s not expressing HA-GLUT4-GFP. One way to test whether any differentiation response occurs in the Sx4 knockout cells would be to blot for markers of adipocyte differentiation. Several molecular markers have been identified in adipogenesis, such as PPAR γ , C/EBPs, lectin and FABP4 (Baxa et al., 1989; Hwang et al., 1997; Rosen and MacDougald, 2006). Immunoblot analysis of cells that had been treated with differentiation media would indicate whether the cells show the molecular markers of differentiation but no morphological changes. Additionally, analysis of the glucose uptake of the cells would be important for characterisation of Sx4 knockout cells not expressing the HA-GLUT4-GFP reporter construct. Sx4 is required for GLUT4 translocation to the plasma membrane (Tellam et al., 1997; Volchuk et al., 1996), therefore successful knockout of Sx4 would reduce the amount of insulin-stimulated glucose uptake in the cells. Indeed, figure 4.12 shows that HA-GLUT4-GFP does not translocate to the plasma membrane in Sx4 knockout cells.

In summary, this data shows that Sx4 phosphorylated at Y115 and Y251 increases cell surface GLUT4 in HeLa cells. Further analysis is needed to elucidate the precise mechanism by which this phosphorylation regulates GLUT4 trafficking. In order to do this Sx4 knockout 3T3-L1 cells have been generated which can be used in the future to examine the effects of Sx4 phospho-mutants in adipocytes depleted of the endogenous proteins.

Chapter Five

***In vitro* analyses of the interactions of phospho- mimetic Sx4 and Munc18c**

5 In vitro analyses of the interactions of phospho-mimetic Sx4 and Munc18c

5.1 Introduction

5.1.1 SM proteins

Although SNARE proteins have been shown to be the minimal machinery required for fusion (Weber et al., 1998), a number of other proteins have been implicated in regulating SNARE proteins and membrane trafficking (Jahn et al., 2003)(see section 1.4 for more detail). The Sec1/Munc18 (SM) family of proteins are amongst those that regulate membrane fusion. SM proteins bind to syntaxins with high affinity and through a number of different binding modes (section 1.4.1) (Rizo and Südhof, 2012). Inhibition or depletion of SM proteins in cells generally leads to a reduction in membrane fusion, however elucidating the mechanisms by which SM proteins regulate membrane fusion has proved challenging and contradictory (Carr and Rizo, 2010; Toonen and Verhage, 2003).

5.1.2 Sx4 and Munc18c interaction

The SM protein that interacts with Sx4 is Munc18c. Munc18c binds to both monomeric syntaxin, binary SNARE complex intermediates and the tertiary SNARE complex of Sx4, SNAP23 and VAMP2 (Latham et al., 2006). However, the effect of Munc18c on SNARE complex assembly and membrane fusion has been hard to elucidate. Munc18c has been shown to both enhance (Latham et al., 2006) and inhibit (Kioumourtoglou et al., 2014) SNARE complex assembly *in vitro*. Munc18c was found to be inhibitory to membrane fusion mediated by Sx4, SNAP23 and VAMP2 in an *in vitro* assay using artificial liposomes (Brandie et al., 2008). Moreover, in adipocytes derived from mice embryonic fibroblasts of Munc18c knockout mice insulin-induced GLUT4 translocation is enhanced (Kanda et al., 2005). Contrastingly another study reported that heterozygous Munc18c knockout mice show reduced insulin sensitivity (Oh et al., 2005). These data present a complex picture of the role of Munc18c in regulating GLUT4 translocation and suggest that there may be other factors regulating function of the protein.

5.1.3 Munc8c phosphorylation

Two studies in 2006 reported that Munc18c is phosphorylated (Oh and Thurmond, 2006; Schmelzle et al., 2006). The study by Thurmond's laboratory showed an increase in Munc18c phosphorylation in insulin-stimulated MIN6 pancreatic beta cells and 3T3-L1 adipocytes. They identified the residue that is phosphorylated as tyrosine 219. Meanwhile, Schmelzle and colleagues carried out quantitative mass spectrometry on insulin-treated 3T3-L1 adipocytes in order to identify changes in the phosphorylation state of protein in the cells. They identified that Munc18c phosphorylation at tyrosine 521 increases >10 fold following insulin-stimulation.

As with Sx4 (section 3.3.6), Munc18c can be phosphorylated directly by CIRK *in vitro* (Aran et al., 2011) and this phosphorylation occurs only on Y521 not Y219 *in vitro* (Aran-Ponte, 2009). In an *in vitro* pull down assay both phosphomimetic and CIRK phosphorylated Munc18c no longer bind to Sx4, suggesting that phosphorylation of Munc18c relieves its inhibitory effect on SNARE complex formation (Aran et al., 2011). Moreover, preassembly of the Sx4/Munc18c-Y521E complex has a stimulatory effect on SNARE complex assembly (Kioumourtzoglou et al., 2014).

Further investigations into the effect of phosphorylation of Munc18c at tyrosine 219 showed that phosphorylation at this residue causes the protein to dissociate from Sx4 (Oh and Thurmond, 2006). Interestingly, phosphorylation Y219 phosphorylation of Munc18c causes a switch in binding specificity from Sx4 to the protein Doc2 β (Jewell et al., 2008). Doc2 β is a ubiquitously expressed C2 domain-containing protein (Sakaguchi et al., 1995). Immunoprecipitation experiments from 3T3-L1 adipocytes revealed the protein binds to Munc18c (Ke et al., 2007). The Doc2 β /Munc18c complexes showed no interaction with Sx4, suggesting the two proteins bind in a mutually exclusive manner (Ke et al., 2007). Moreover, increased expression of Doc2 β enhanced insulin-stimulated GLUT4 translocation, whereas inhibition of the protein decreased it (Ke et al., 2007). These data

suggest that the switch in binding of Munc18c from Sx4 to Doc2 β may be an important regulatory mechanism in the trafficking of GLUT4 (Jewell et al., 2008).

5.2 Aims of this chapter

The data presented thus far in this study suggests that phosphorylation of Sx4 affects its interactions with the SNARE proteins VAMP2 and SNAP23 and that this in turn effects GLUT4 translocation to the PM. The SM protein Munc18c has also been shown to be phosphorylated in response to insulin, on tyrosine residue 521 (Schmelzle et al., 2006). The aim of this chapter was to dissect the effect of both Sx4 and Munc18c phospho-mimetic mutants on their interactions *in vitro*. In order to do this a number of pull down assays and complex assembly assays have been carried out using recombinant purified proteins.

5.3 Results

5.3.1 Purification of His tagged Munc18c

In order to assess the effect of both Sx4 and Munc18c phosphorylation *in vitro* WT and phospho-mimetic mutants of both proteins were expressed and purified (section 2.3.2). Sx4-WT, Sx4-Y115E, Sx4-Y251E, Sx4-Y115,251E and Sx4-Open tagged at the C-terminus with GST were expressed and purified from *E. coli* (see figure 3.1). Munc18c tagged at the N-terminus with His was also expressed and purified from *E. coli* (2.3.2). Figure 5.1 shows representative Coomassie stained gels and anti-His immunoblots of Munc18c-WT and Munc18c-Y521E. Anti-His immunoblots were used in addition to Coomassie staining to visualise Munc18c as a contaminating protein of 75 kDa was purified with Munc18c and so using Coomassie staining alone to compare the amount of the protein was inaccurate.

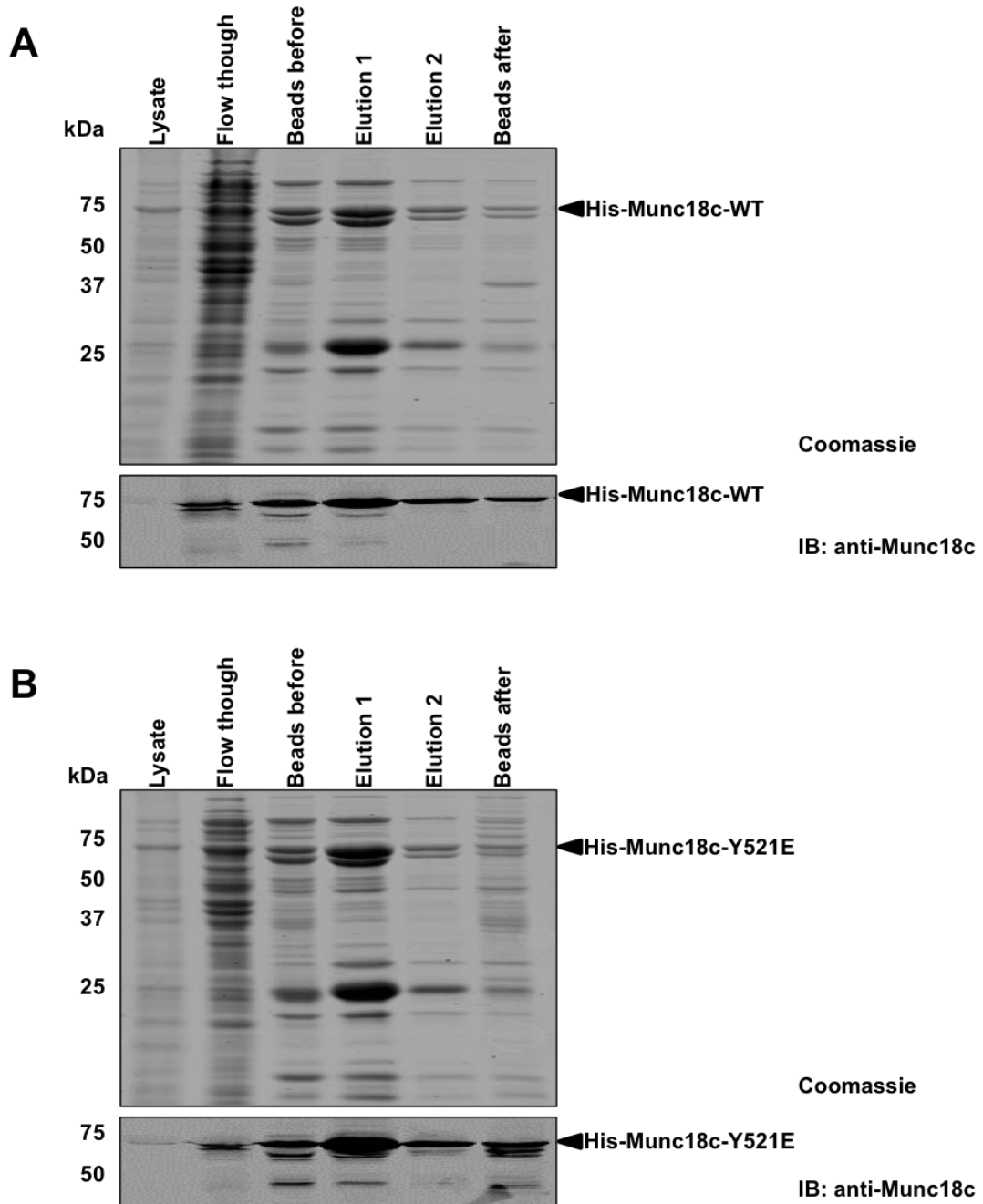


Figure 5.1: Expression and purification of His-Munc18c.

Munc18c tagged at the N-terminus with His was expressed in and purified from BL21 (DE3) *E. coli* as described in methods section 2.3.2. 10 μ l of samples taken during purification were analysed by SDS-PAGE and either coomassie stained or immunoblotted with anti-Munc18c antibody. **A** Representative Munc18c-WT purification. **B** Representative His-Munc18c Y521E purification. Elution samples represent 0.12 % of the total elution (see appendix I for details). Samples corresponding to bacterial lysate (lysate), unbound proteins following incubation with nickel beads (flow through), protein bound to beads (beads before), each of the two elutions and proteins that remained bound to beads following elution (beads after) were run.

5.3.2 The effect of Sx4 and Munc18c phospho-mimetic mutants on SNARE complex assembly

The effect of both Sx4 and Munc18c phosphorylation on SNARE complex assembly was then assessed. A complex assembly assay was carried out in the presence or absence of Munc18c-WT or -Y521E phospho-mimetic mutant (section 2.4). Samples were analysed by SDS-PAGE and immunoblot. Figure 5.2 shows the amount of complex formed with Sx4-WT or Sx4-Y115E in the presence or absence of Munc18c-WT or Munc18c-Y521E. The presence of Munc18c did not affect the amount of complex formed in samples containing Sx4-WT (lanes 1-3). Sx4-Y115,251E in the absence of Munc18c formed 23 % more SNARE complex than Sx4-WT in the absence of Munc18c as expected. In the presence of both Munc18c-WT and Munc18c-Y521E, Sx4-Y115,251E formed more complex than in the absence of the SM protein (22 % and 13 % increase respectively). Sx4-Y115,251E in the presence of WT Munc18c also was seen to form 39 % more complex than Sx4-WT in the presence of Munc18c-WT.

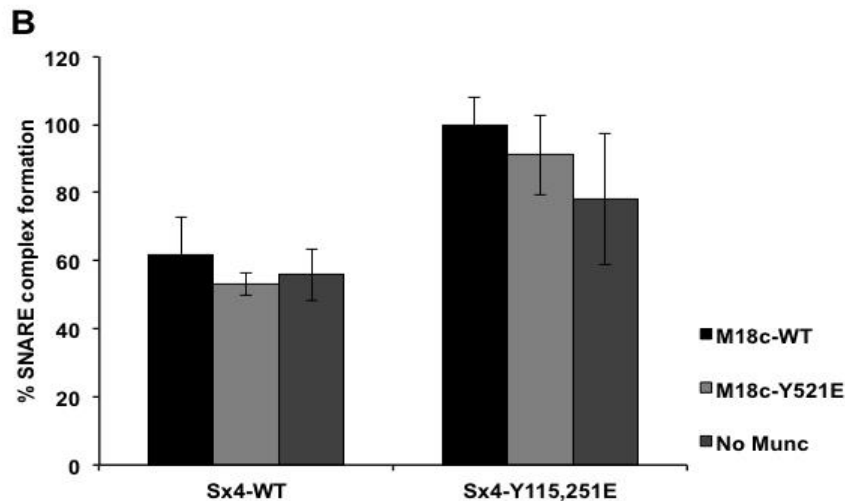
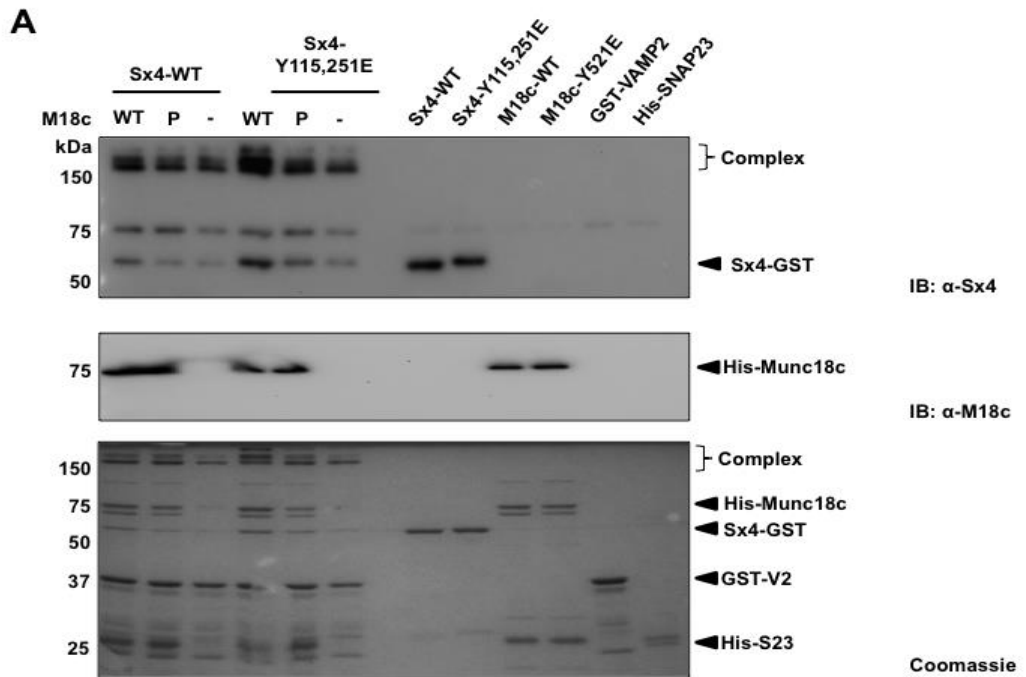


Figure 5.2 Sx4-Y115,251E pre-incubated with Munc18c-WT or -Y521E forms more SNARE complex than Sx4-WT

GST tagged Sx4 (Sx4-GST) WT or Y115,251E phospho-mutant was pre-incubated with either WT or Y521E phospho-mimetic Munc18c tagged at the N-terminus with His, for 1 hour at 4 °C. His-SNAP23 and GST-VAMP2 were then added and all proteins were incubated for 15 minutes at 4 °C. The reaction was then stopped and analysed by SDS-PAGE and immunoblot analysis (section 2.4). Input samples were run to show the amount of each protein used in the assay. **A** Representative Coomassie stained gels and immunoblots. Top panel shows the amount of complex formed in an anti-Sx4 immuno blot. Middle panel shows equal Munc18c input. Coomassie stained gel (bottom panel) shows the amount of complex formed and the protein input. **B** Densitometry analysis of the amount of complex formed using anti-Sx4 immunoblot. Sx4-Y115,251E forms more complex than the Sx4-WT in the absence or presence of Munc18c. Munc18c WT and phospho-mimetic mutants show little difference in the amount of complex formed. n=3, error bars show standard error of the mean.

5.3.3 Binary interactions of phosphomimetic Sx4 and Munc18c

The effect of Sx4 and Munc18c phosphorylation on their binary interactions was then investigated. Purified Sx4-GST was immobilised to glutathione Sepharose beads before being incubated with purified His-Munc18c for 60 minutes at 4 °C (section 2.5). Samples were analysed by SDS-PAGE and immunoblot. Figure 5.3A shows a representative immunoblot of the amount of Munc18c pulled down by Sx4 and a panceau stained membrane showing Sx4 input. Figure 5.3B shows quantification of the data. In contrast to previously reported data (Aran et al., 2011), Sx4-WT bound to both Munc18c-WT and the phospho-mimetic mutant. Contrastingly, Sx4-Open pulled down very little Munc18c-WT or Munc18c-Y521E. Sx4 phospho-mimetic mutants showed reduced binding to Munc18c; however no difference was seen in between their interaction with Munc18c-WT or Munc18c-Y521E.

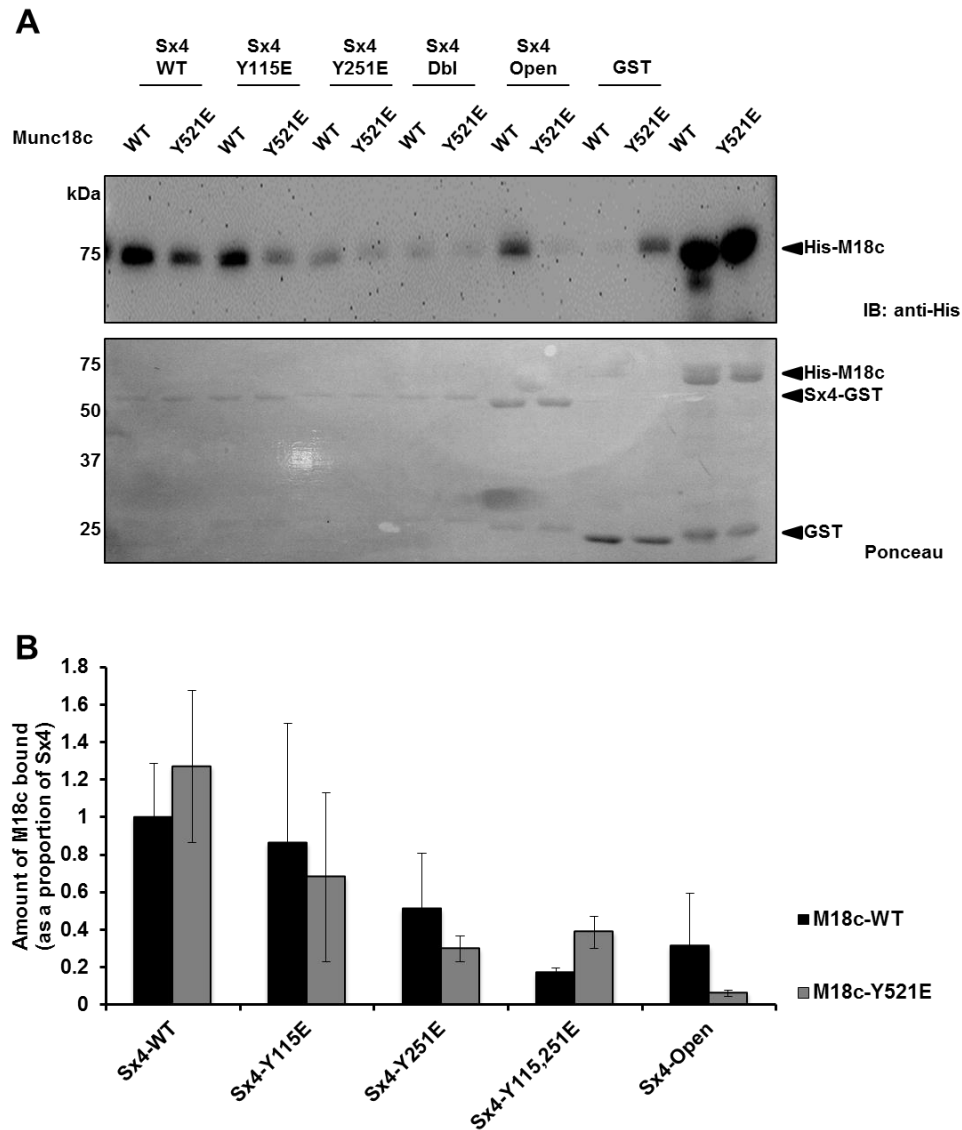


Figure 5.3 Sx4-WT pulls down more Munc18c than Sx4 phospho-mimetic mutants
 Sx4 tagged at the C-terminus with GST was immobilised to glutathione Sepharose beads before being incubated with Munc18c tagged at the N-terminus with His for 60 minutes at 4 °C. Beads were washed extensively before being analysed by SDS-PAGE and immunoblot (section 2.5). **A** Representative anti-His immunoblot and ponceau stained membrane showing Sx4-GST loading. **B** Densitometry quantification of the amount of Munc18c pulled down as a proportion of Sx4. Sx4-WT pulled down more Munc18c WT and Y521E than other Sx4 phospho-mutants.

5.4 Discussion

SM proteins are important regulators of SNARE complex assembly *via* their interaction with syntaxin proteins (Toonen and Verhage, 2003). The SM protein that regulates Sx4 is Munc18c (Tamori et al., 1998). Both Sx4 and Munc18c are phosphorylated in response to insulin (Schmelzle et al., 2006). In this chapter I aimed to investigate the effects of phosphorylation of Munc18c and Sx4 on binary and ternary SNARE interactions.

Phospho-mimetic Munc18c tagged at the N-terminus with His was expressed and purified from *E. coli* (Figure 5.1). Bacterial expression and purification of Munc18 proteins is notoriously challenging (Hu et al., 2003). Problems with contaminants and with low yields are common and so the construct used in this study had been codon optimised for bacterial expression. Never the less, it was noted that a contaminant of the same molecular weight as Munc18c was purified and so distorted the amount of protein seen by coomassie. Anti-His immunoblots were therefore used as a more reliable method of ensuring equal Munc18c-WT and -Y521E loading in experiments.

First an *in vitro* complex assembly, like that used in chapter 3, was carried out (Figure 5.2). Sx4-WT or Y115,251E was incubated with SNAP23 and VAMP2 in the presence or absence of Munc18c-WT, -Y521E or no Munc18c. Sx4-Y115,251E showed an increased ability to form SNARE complex, in both the presence and absence of Munc18c, consistent with data from figure 3.3. However, no change was seen in the amount of SNARE complex formed by Sx4-WT or Sx4-Y115,251E, in the presence of either Munc18c-WT or the phospho-mimetic mutant. This is in contrast to previously published results (Kioumourtzoglou et al., 2014). This study found that Munc18c has an inhibitory effect on SNARE complex assembly, whereas Munc18c-Y521E stimulates formation of the complex. The chief difference between the assay from this publication and the assay performed here is that they pre-incubated Munc18c with Sx4 immobilised to beads, and then removed any unbound Munc18c before the other components of the complex were

added. Here, Sx4 and Munc18c were preincubated, however unbound Munc18c was not removed from the assay before SNAP23 and VAMP2 were added. It is therefore possible that, in the assay using immobilised Sx4, the Sx4/Munc18c complexes formed are inhibitory and that this inhibition is not relieved during the time allowed for SNARE complex assembly. Whereas in the assay carried out in this study, free Munc18c may be able to interact with either binary Sx4/SNAP23 complexes or with VAMP2, in a manner that is not inhibitory for SNARE complex assembly. Repeating the assay carried out by Kioumourtzoglou et al, with Sx4-WT and Sx4-Y115,251E would resolve this difference.

The binary interactions between phospho-mimetic Sx4 and Munc18c were also examined (Figure 5.3). All phospho-mimetic Sx4 mutants, along with Sx4-Open mutants, bound to less Munc18c than Sx4-WT. Munc18c has been reported to be inhibitory for both SNARE complex assembly and GLUT4 translocation (Brandie et al., 2008; Kanda et al., 2005). In addition, data from chapters 3 and 4 suggests that phosphorylation of Sx4 may enhance GLUT4 translocation and SNARE complex assembly. A reduction in binding of phosphorylated Sx4 to Munc18c would therefore be consistent with both these observations. However, a previous study has reported that phosphorylated Munc18c can no longer bind to Sx4 *in vitro* (Aran et al., 2011). This contrasting data suggests differences in the protein purified or assay conditions.

The Munc18c construct used in this study has been codon optimised for expression in *E. coli*, in contrast to constructs used in the previously mentioned contrasting studies (Aran et al., 2011; Kioumourtzoglou et al., 2014). Codon optimisation aims to overcome low protein yield by optimising rare codons in the target gene to mirror those that are more commonly used in the host (Burgess-Brown et al., 2008). However, limitations in protein expression are not always solely down to the limited availability of rare tRNAs. mRNA sequence and structure are important for proper translation and folding of proteins (Rosano and Ceccarelli, 2014). Changes in the codons used may have an effect on mRNA structure and therefore effect the folding of the translated protein. It would

therefore be beneficial to compare the structures of both codon optimised Munc18c and Munc18c used in the aforementioned studies in order to confirm their overall structure is the same. In order to optimise purification of Munc18c, some studies have used Sf9 insect cells (Hu et al., 2003; Yu et al., 2013). However, whilst they may provide improved protein folding they are also capable of more complex posttranslational modifications, such as phosphorylation, and so would present another complication when studying the effect of Y521 phosphorylation on Munc18c interactions.

The data presented in this chapter suggests that phosphorylation of Sx4 Tyr-115 and Tyr-251 and Munc18c Tyr521 may effect interactions of the proteins. However, like with the data in chapter three, assessing the statistical significance of the data presented in this chapter showed was difficult. Future work investigating the structure and function of purified Munc18c will be crucial in order to understand this data in the context of previously published results. In addition, analysis of the binary interactions of the two proteins using a more quantitative technique would help to elucidate the effect of phosphorylation of both proteins on the formation of the inhibitory Sx4/Munc18c complex, such as SPR that has been used previously in this study (section 3.3.5). In addition, it will be important to assess the effect of these phosphorylation events on GLUT4 translocation in a cell based system.

Chapter Six

Discussion

6 Discussion

6.1 Discussion of results

The translocation of GLUT4 from intracellular stores to the PM in response to insulin is a regulated membrane trafficking event (Bryant et al., 2002). Fusion of GLUT4 storage vesicles with the PM is mediated by a SNARE complex consisting of Sx4, SNAP23 and VAMP2 (Bryant and Gould, 2011). One important regulator of this SNARE complex is the SM protein Munc18c (Jewell et al., 2010). Both Sx4 and Munc18c are tyrosine phosphorylated in response to insulin (Schmelzle et al., 2006), however the consequences of these phosphorylation events are not fully understood. One aim of this study was therefore to dissect the effects of Sx4 and Munc18c phosphorylation of SNARE complex assembly and insulin-stimulated GLUT4 translocation.

Chapter three examined the effects of phospho-mimetic Sx4 mutants on *in vitro* SNARE protein interactions. Using a complex assembly assay I found that Sx4-Y115,251E had an increased ability to form SNARE complexes than WT Sx4 (Figure 3.3). Furthermore, I demonstrated that this may be due to a conformational change in the protein. Sx4-open has previously been shown to be digested more quickly than Sx4-WT in a limited proteolysis assay (Aran et al., 2009). A similar assay I carried out showed that Sx4-Y115,251E was digested at a comparable rate to Sx4-open (Figure 3.5). The conformational change of syntaxins from 'closed' to 'open' is an important regulatory mechanism in SNARE complex assembly (Dulubova et al., 1999; MacDonald et al., 2010). These data suggests that phosphorylation of Sx4 at tyrosine residues 115 and 251 potentially represents an important regulatory feature, facilitating the switch between the open and closed conformation of the protein and increasing SNARE complex assembly. It would be interesting to perform further structural analysis of both phospho-mimetic and *in vitro* phosphorylated Sx4. NMR spectroscopy would provide more detail of any structural changes observed in the protein following phosphorylation.

The binary interactions of Sx4 phospho-mimetic mutants with the SNARE proteins SNAP23 and VAMP2 were then investigated. *In vitro* pull down assays suggested that Sx4 phosphorylation increased binding to both S23 and VAMP2 (Figures 3.6 and 3.8). These interactions were then investigated using SPR. I showed that Sx4 mutants bound to SNAP23 and VAMP2 with differing affinities to Sx4-WT and Open (Figure 3.10 and 3.11). Moreover, SPR experiments suggested that Sx4 phospho-mutants exhibited different affinities for SNAP23 and VAMP2. The binary interactions of Sx4 with SNAP23 and VAMP2 have been shown to be important for regulating SNARE complex assembly (Kawanishi et al., 2000; Kioumourtzoglou et al., 2014; St-Denis et al., 1999). Phosphorylation may regulate the affinity of Sx4 to form binary complexes with SNAP23 and VAMP2 differently, which in turn could regulate SNARE complex assembly. However, it is important to note that more work is needed to characterise the effect of phosphorylation on these binary complexes. Further SPR experiments using less immobilised ligand and lower concentrations of analyte would be needed to obtain more accurate equilibrium dissociation constants (Hulme and Trevethick, 2010).

Finally, in this chapter I presented data demonstrating that Sx4 could be phosphorylated on two residues simultaneously, using a Phos-tag based mobility shift assay (Figure 3.16). Analyses of the interactions of phospho-mimetic Sx4 in chapter three showed that Sx4-Y115,251E increases SNARE complex assembly, alters conformation of the protein and has an effect on binary interactions with SNAP23 and VAMP2. However, although mass spectrometry analysis has shown that both these residues are phosphorylated in response to insulin (Schmelzle et al., 2006), it was not yet known whether both can be phosphorylated on one molecule of syntaxin at the same time. In order to ascertain whether Sx4 is phosphorylated on both Y115 and Y251 simultaneously, I first used an *in vitro* phosphorylation assay with cytosolic insulin receptor kinase (CIRK). Sx4 is phosphorylated by CIRK *in vitro* (Aran-Ponte, 2009)(Figure 3.14). I then used a Phos-tag based mobility shift assay to show that a phospho-isoform that likely corresponds to Sx4

phosphorylated at both Y115 and Y251 was detected (Figure 3.16). Electrospray-based mass spectrometry (Compton et al., 2011) on non-fragmented Sx4, phosphorylated *in vitro* by CIRK, could be carried out to provide definitive proof that both residues can be phosphorylated on one residue.

Having investigated the interactions of phospho-mimetic Sx4 proteins *in vitro*, their effect on GLUT4 translocation was then examined. In order to do this I generated full length Sx4 WT and phospho-mimetic mutants harbouring an internal Myc tag (Figure 4.1). By overexpressing these proteins in the presence of endogenous Sx4, I showed that cell surface GLUT4 levels increased under basal conditions upon expression phospho-mimetic mutants compared to WT (Figure 4.4, 4.6 and 4.7). One study in 2014 provided evidence that insulin stimulates the formation of SNARE complexes containing Sx4, SNAP23 and VAMP2 in 3T3-L1 adipocytes (Kioumourtzoglou et al., 2014). This study used a proximity ligation assay (PLA) to show that insulin stimulation of adipocytes results in an increase in SNARE complex formation and that this increase is likely due to the mobilisation of a pool of Sx4 that is inactive under basal conditions. Phosphorylation of Sx4, which is increased following insulin-stimulation, may represent an important point of regulation in this model. It is tempting to hypothesise that insulin-stimulated phosphorylation of this pool of inactive Sx4 could activate the protein, potentially *via* a conformational change (Figure 3.5) and increase SNARE complex assembly (Figure 3.3) therefore increasing fusion of GSVs at the plasma membrane. The observation that expression of Sx4 phospho-mimetic mutants increases cell surface HA-GLUT4-GFP in HeLa cells (Figure 4.6 and 4.7) is consistent with this hypothesis.

To date, relatively little is known about the mechanisms by which insulin signalling regulates GLUT4 trafficking. AS160 has been identified as an important regulatory factor (Larance et al., 2005; Sano et al., 2003) and the protein directly interact with the insulin signalling pathway through its phosphorylation by Akt (Sano et al., 2003). However, AS160 has been implicated in regulating GSV docking at the PM (Bai et al., 2007)

whereas the fusion frequency of GLUT4 containing vesicles is known to increase in response to insulin (Huang et al., 2007). Data presented in chapters three and four of this study suggest that phosphorylation of Sx4 could play a role in increasing the fusion frequency of GSVs at the plasma membrane. More direct investigations into the effect of Sx4 phosphorylation on GSV fusion at the plasma membrane could be carried out using TIRF microscopy or by studying fusion of isolated GSVs and plasma membrane liposomes from cells expressing Sx4 phospho-mutants, similar to the assay developed by Koumanov and colleagues (see section 4.1.1 (Koumanov et al., 2005)).

Carrying out assays such as those mentioned above would require Sx4 phospho-mutants to be expressed in the absence of endogenous Sx4, so as to be sure all fusion events observed would be regulated by the mutant of interest. With this in mind I also created Sx4 knockout cell lines using CRISPR-Cas9 technology. Sx4 knockout HA-GLUT4-GFP 3T3-L1 and 3T3-L1 fibroblasts were made (Figure 4.10). Following confirmation of the depletion of Sx4 the cells were treated with adipocyte differentiation media (Figure 4.11). Interestingly whilst 3T3-L1 Sx4 knockout cells showed some morphological differentiation those expressing HA-GLUT4-GFP did not. It is likely that this difference is due to the HA-GLUT4-GFP 3T3-L1 cell line differentiating poorly, even in the presence of Sx4, as discussed in more detail in section 4.4. Although further characterisation of these Sx4 knockout cell lines is needed (see section 4.4), they could prove a very useful tool in dissecting the effect of Sx4 phosphorylation on GSV fusion at the plasma membrane.

Data discussed thus far suggests that phosphorylation of Sx4 may represent an important regulatory step in GLUT4 trafficking. The SM protein that regulates Sx4, Munc18c, is also phosphorylated in response to insulin on tyrosine residue 521 (Schmelzle et al., 2006). It is therefore important to understand the effect of this phosphorylation on the Munc18c/Sx4 interaction and the implications for SNARE complex assembly. In chapter five I aimed to investigate the effect of phosphorylation of Sx4 and Munc18c on their interactions *in vitro*. However, analysing the effect of phosphorylation of both proteins proved to be challenging.

In a complex assembly assay the presence of either Munc18c-WT or phospho-mimetic mutant had no effect on the amount of SNARE complex formed by either Sx4-WT or Sx4-Y115,251E (Figure 5.2). However, in an *in vitro* pull down assay, Sx4 phospho-mimetic mutants bound to less Munc18c than Sx4-WT (Figure 5.3). Moreover, Munc18c-Y521E showed no difference in binding to Sx4 than Munc18c-WT. On one hand, as the Munc18c/Sx4 interaction has been shown to be inhibitory to SNARE complex assembly (Brandie et al., 2008; Kioumourtzoglou et al., 2014), relief of this inhibition by Sx4 phosphorylation would make sense. However, Sx4 can also bind to Munc18c *via* its N-terminus in a manner that is complimentary to Sx4 being in an open and active conformation (Hu et al., 2007; Latham et al., 2006). Furthermore, Sx4-Open has been shown to bind to Munc18c in an *in vitro* assay at levels comparable to Sx4-WT (Aran et al., 2009). It is therefore confusing that binding of Sx4-open to Munc18c is reduced in this assay (Figure 5.3). In a similar contrasting manner, phosphorylated Munc18c has been reported to no longer bind to Sx4 (Aran et al., 2011) and to stimulate SNARE complex assembly (Kioumourtzoglou et al., 2014). One main reason for the discrepancies in the published data and the data presented in chapter 5 is that the Munc18c used in this study was produced using a codon-optimised plasmid. Whilst optimising the codon usage for expression in *E. coli* should ultimately result in the same protein being produced, it is possible that some structural differences could occur during translation (discussed in more detail in section 5.4). SM proteins are notoriously difficult to purify. Indeed previous studies have co-purified the protein with a chaperone to improve solubility (Scott et al., 2004) or used different cell lines for purification (Hu et al., 2003). Therefore, optimisation and characterisation of purified recombinant Munc18c from both codon-optimised and non-optimised plasmids is required before any conclusions can be drawn from this data.

6.2 Proposed model and future work

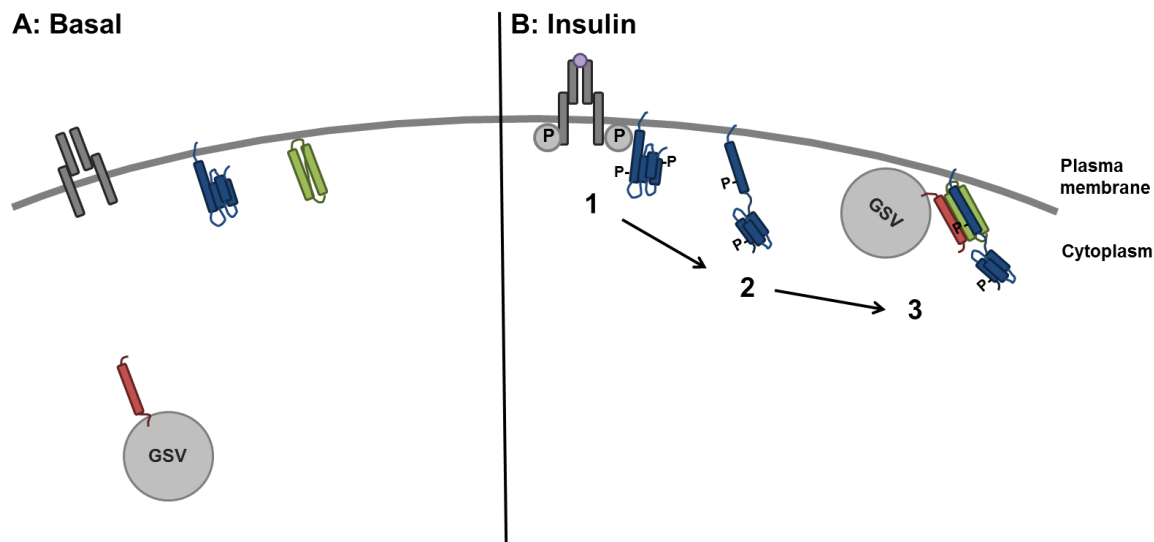


Figure 6.1: Proposed model of the effects of insulin stimulated Sx4 phosphorylation at Y115 and Y251

A Under basal conditions Sx4 (blue) is unphosphorylated and in a closed conformation that is incompatible with SNARE complex formation, SNAP23 (green) is also localised to the PM. VAMP2 (red) is shown on GSVs. **B** Upon insulin (purple spot) binding, the insulin receptor (grey) directly phosphorylates Sx4 at Y115 and Y251 (1). Following phosphorylation Sx4 favours a more open conformation (2). This results in the increased formation of SNARE complexes with SNAP23 and VAMP2 (3) and leads to an increase in the amount of GLUT4 at the PM.

The data presented in this thesis suggests that phosphorylation of Sx4 at tyrosine residues 115 and 251 in response to insulin may be an important point of regulation of GLUT4 trafficking. Figure 6.1 shows a summary of the proposed model of Sx4 phosphorylation based on the data presented in this study. Under basal conditions the majority of unphosphorylated Sx4 is in the closed conformation and is unable to form SNARE complexes (Dulubova et al., 1999)(Figure 6.1A). Upon activation, the insulin receptor then directly phosphorylates Sx4, this results in Sx4 adopting a more open conformation and the increased formation of SNARE complexes. This increase in SNARE complex formation leads to an increase of GLUT4 at the PM (Figure 6.1B). It is likely that this phosphorylation event represents a switch, whereby transient phosphorylation of Sx4 leads to an increase in cell surface GLUT4 allowing the rapid uptake of glucose in a

controlled manner. It would therefore be intriguing to examine the kinetics of the phosphorylation and dephosphorylation of the protein following insulin stimulation. Phosphorylation of Sx4 also affects the binary interactions between the protein and SNAP23 and VAMP2, however the precise mechanism by which this affects SNARE complex formation and the implication on GLUT4 trafficking is not yet clear.

Data presented in this study supports the hypothesis that phosphorylation of Sx4 at tyrosine residues 115 and 251, and potentially Munc18c at Tyr-521, represents an important feature in the regulation of SNARE complex assembly and insulin-stimulated GLUT4 translocation. Nevertheless, there is more work that can be done to identify the precise mechanisms by which this phosphorylation regulates GLUT4 trafficking.

In an *in vitro* complex assembly assay Sx4-Y115,251E formed more complex than Sx4-WT. However, quantifying the amount of complex formed by densitometry analysis of immunoblots is relatively indirect and more prone to error. Assessing the amount of complex formed by Sx4 phospho-mimetic mutants by a more quantitative method would therefore be desirable. Both *in vitro* membrane fusion assays (Brandie et al., 2008; Yu et al., 2013) and surface plasmon resonance (Rea et al., 1998) could be used in order to achieve this.

Similarly, systematic analysis of the interactions of both phospho-mimetic Sx4 and Munc18c will need to be carried out. Initially, structural comparisons of both codon optimised and non-optimised Munc18c could be carried out. Circular dichroism experiments would establish whether the secondary structure of the protein has changed with the optimisation. Similarly, the binding of both forms of the protein to Sx4 or VAMP2 would be systematically assessed. Once the codon optimised Munc18c has been fully characterised, interactions with Sx4-phosphomutants could be analysed, again using quantitative techniques such as SPR or ITC (isothermal titration calorimetry).

It would also be informative to quantify the interactions of phosphorylated Sx4 and Munc18c in adipocytes and/or muscle cells. Development of phospho-specific antibodies for both proteins would allow immunoprecipitation experiments to be carried out on insulin-stimulated cells. Immunoprecipitation of phosphorylated Sx4 or Munc18c following insulin-stimulation, and therefore phosphorylation, may reveal changes in the interactome of the proteins and build on data obtained in this study by SPR (Figure 3.9 and 3.10) that phosphorylation of Sx4 has differing effects on interactions with SNAP23 and VAMP2.

Finally, a crucial experiment would be to express phospho-resistant Sx4 in either HeLa cells or Sx4 depleted 3T3-L1 adipocytes to analyse the effect of this mutation on insulin-stimulated GLUT4 translocation. Data obtained in this study would lead to the hypothesis that expression of Sx4 that is unable to be phosphorylated would reduce insulin-stimulated GLUT4 translocation to the PM. It will be important to address this point to assess the importance of phosphorylation and whether it is necessary for an increase in GLUT4 exocytosis following insulin-stimulation.

Elucidating the mechanisms by which the insulin signalling pathway acts on the machinery required for trafficking of GLUT4 is a challenging but important step in understanding this regulated trafficking event. Understanding the mechanisms that lead to GLUT4 exocytosis may help to understand other regulated trafficking events. Moreover, new insights into the regulation of GLUT4 trafficking machinery may provide novel treatment targets for patients with Type II diabetes and insulin resistance.

Appendices

Appendix I: Summary of purified recombinant proteins used in this study

Table I: Summary of purified recombinant proteins used in this study

Protein	Size (kDa)	Culture volume (L)	Elution method	Elution volume (ml)	Typical yield (mg/ml)
Sx4-GST (WT)	57	3	Reduced glutathione	6	1
Sx4-GST (Y115E)	57	3	Reduced glutathione	6	1
Sx4-GST (Y251E)	57	3	Reduced glutathione	6	1
Sx4-GST (Y115,251E)	57	3	Reduced glutathione	6	1
His-SNAP23	24	3	Imidazole	6	2
GST-VAMP2	36	4	Reduced glutathione	6	1
VAMP2	10	4	Thrombin cleaved	3	0.5
GST	26	1	Reduced glutathione	3	2
His-Munc18c (WT)		6	Imidazole	4	n/a
His-Munc18c (Y521E)		6	Imidazole	4	n/a

Appendix II: Raw SPR data

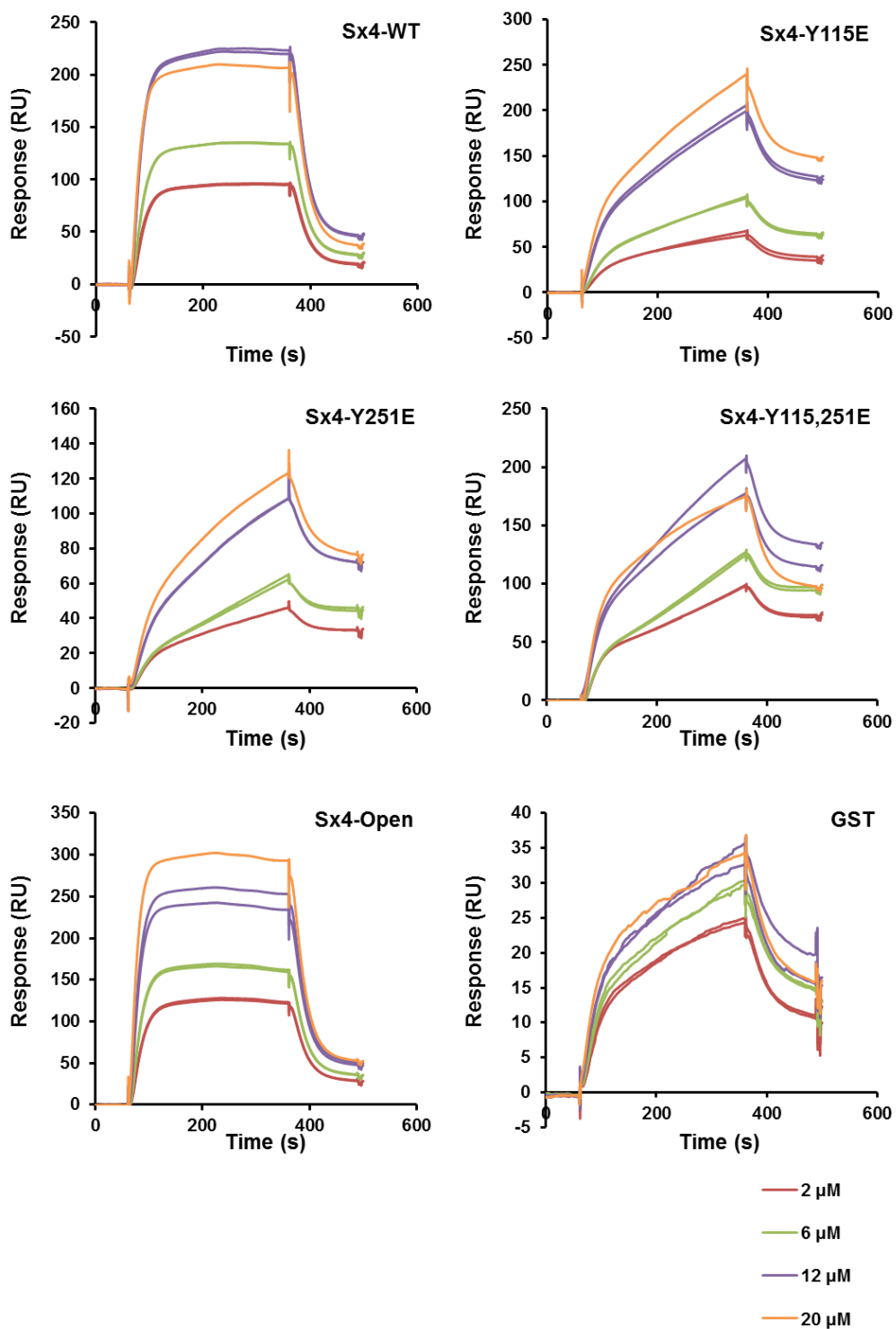


Figure II.1 Raw data showing repeats of Sx4 binding to SNAP23 by SPR

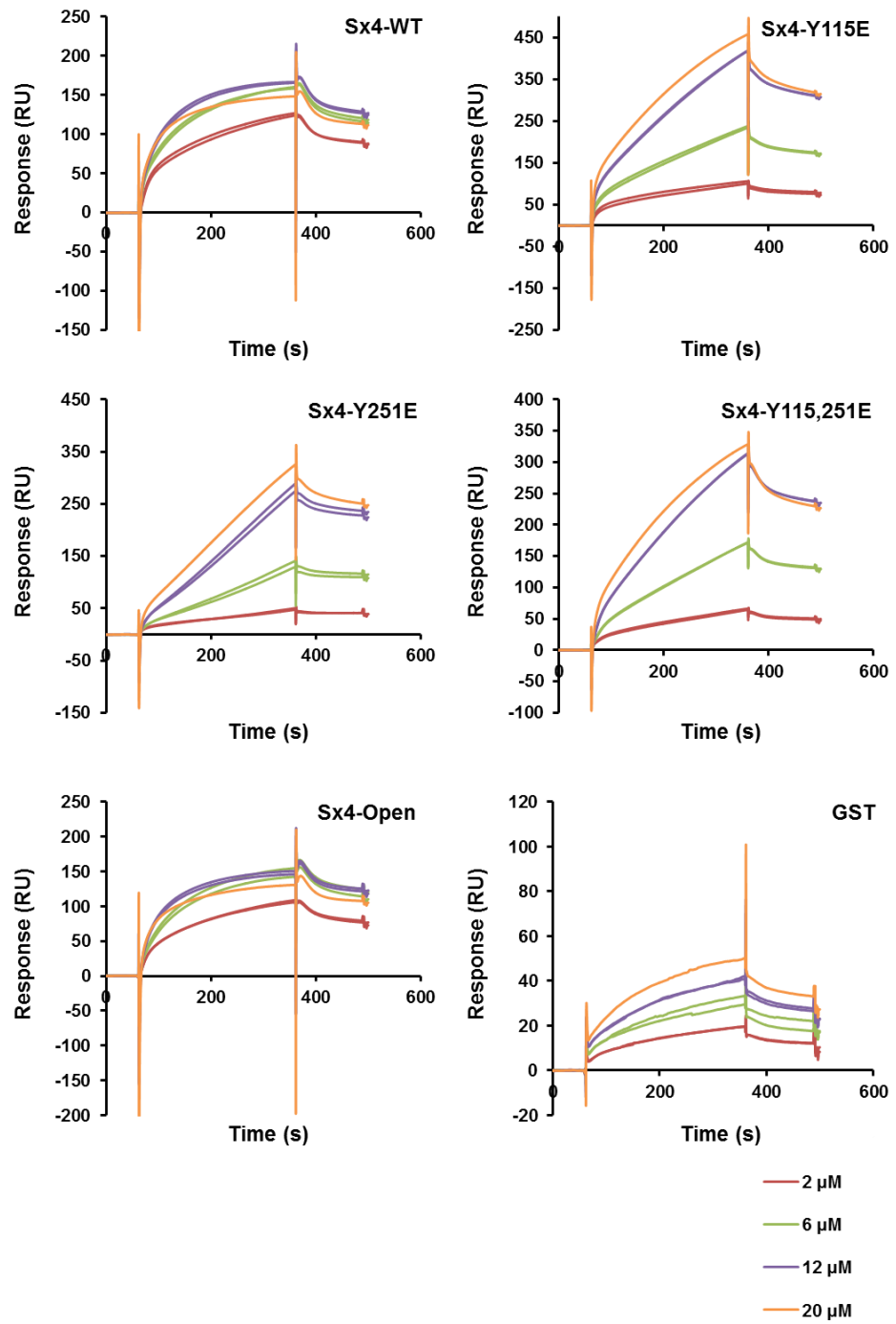


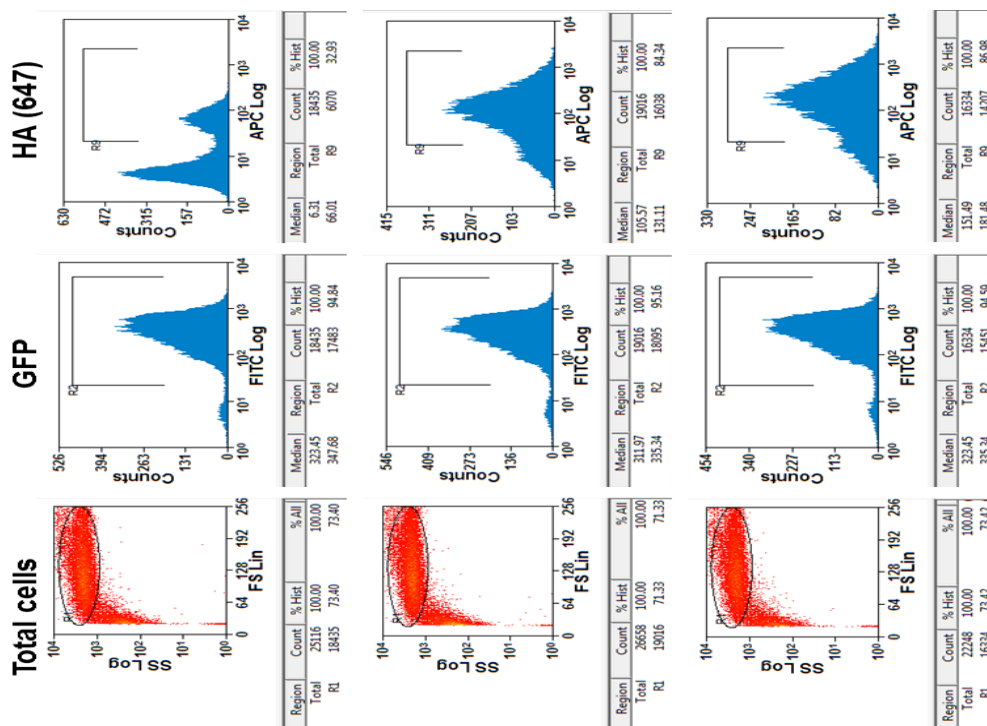
Figure II.2 Raw data showing repeats of Sx4 binding to VAMP2 by SPR

Table II Summary of K_D values of Sx4 binding to VAMP2/SNAP23 obtained by SPR

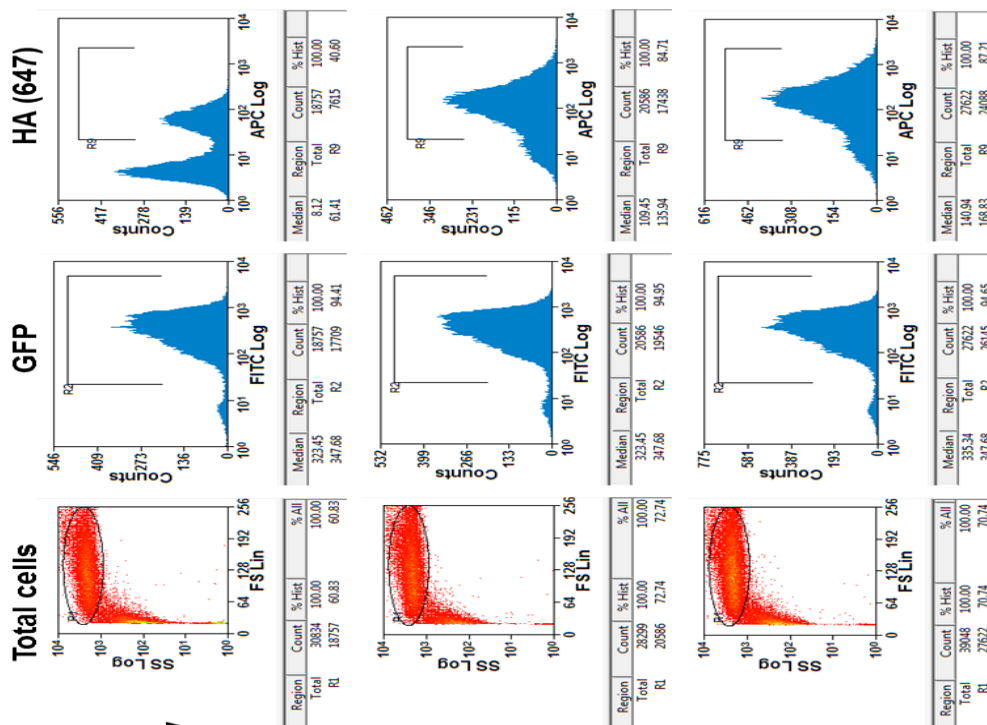
VAMP2		SNAP23	
Sx4	K_D (μM)	Sx4	K_D (μM)
WT	7.6	WT	0.14
Y115E	25.2	Y115E	13.2
Y251E	16.6	Y251E	19.7
Y115,251E	4.3	Y115,251E	10.6
Open	23.5	Open	0.26

Appendix III: Raw data from flow cytometry analysis of cell surface HA-GLUT4-GFP antibody titration

Insulin



Basal



Secondary only

1:1600

1:800

Insulin

Basal

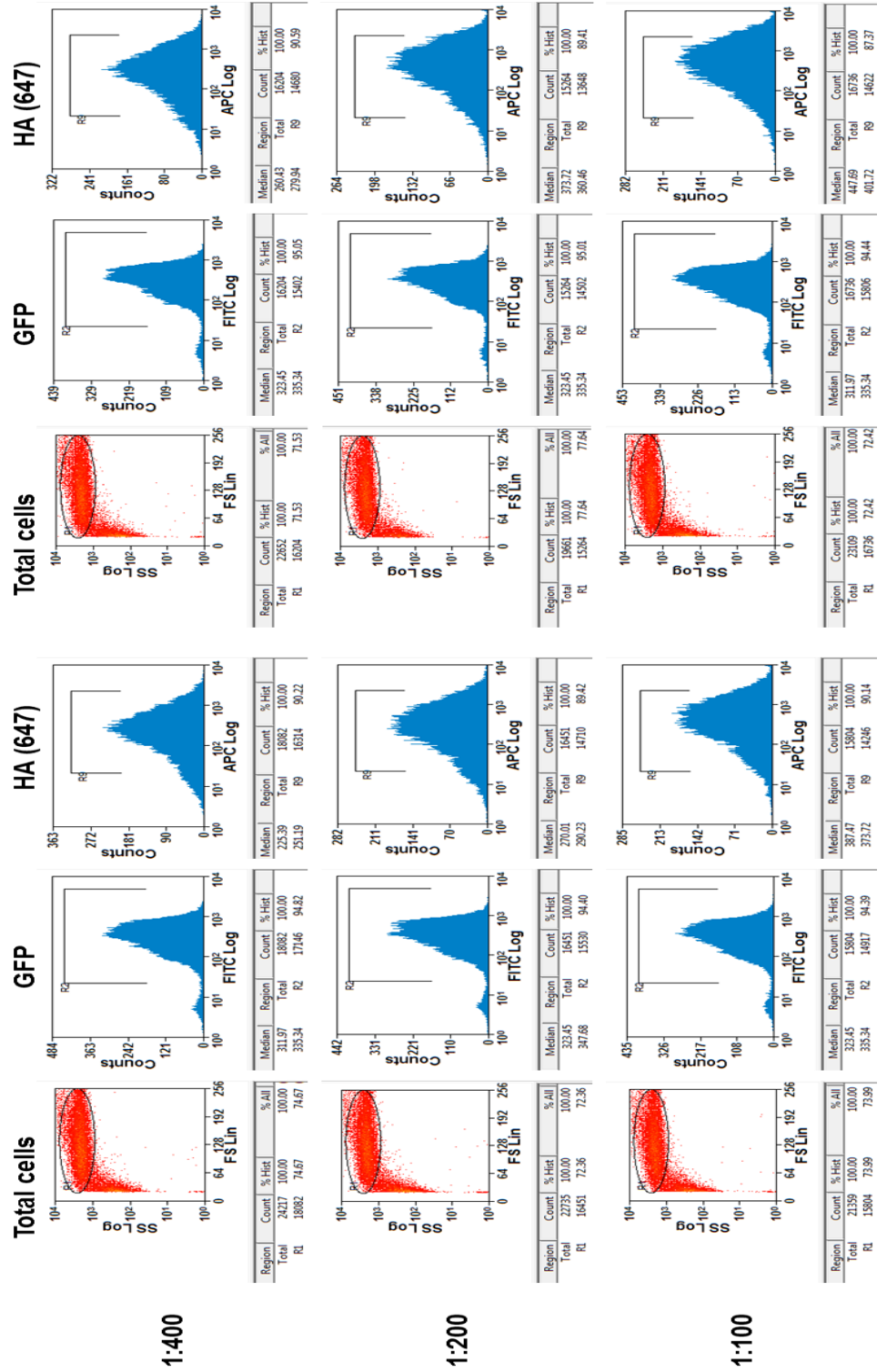


Figure III.1 Summary of raw data from analysis of antibody titration of cell surface HA-GLUT4-GFP by flow cytometry

Appendix IV: Raw data of the flow cytometry analysis of the effect of overexpressing Sx4 on cell surface HA-GLUT4-GFP levels

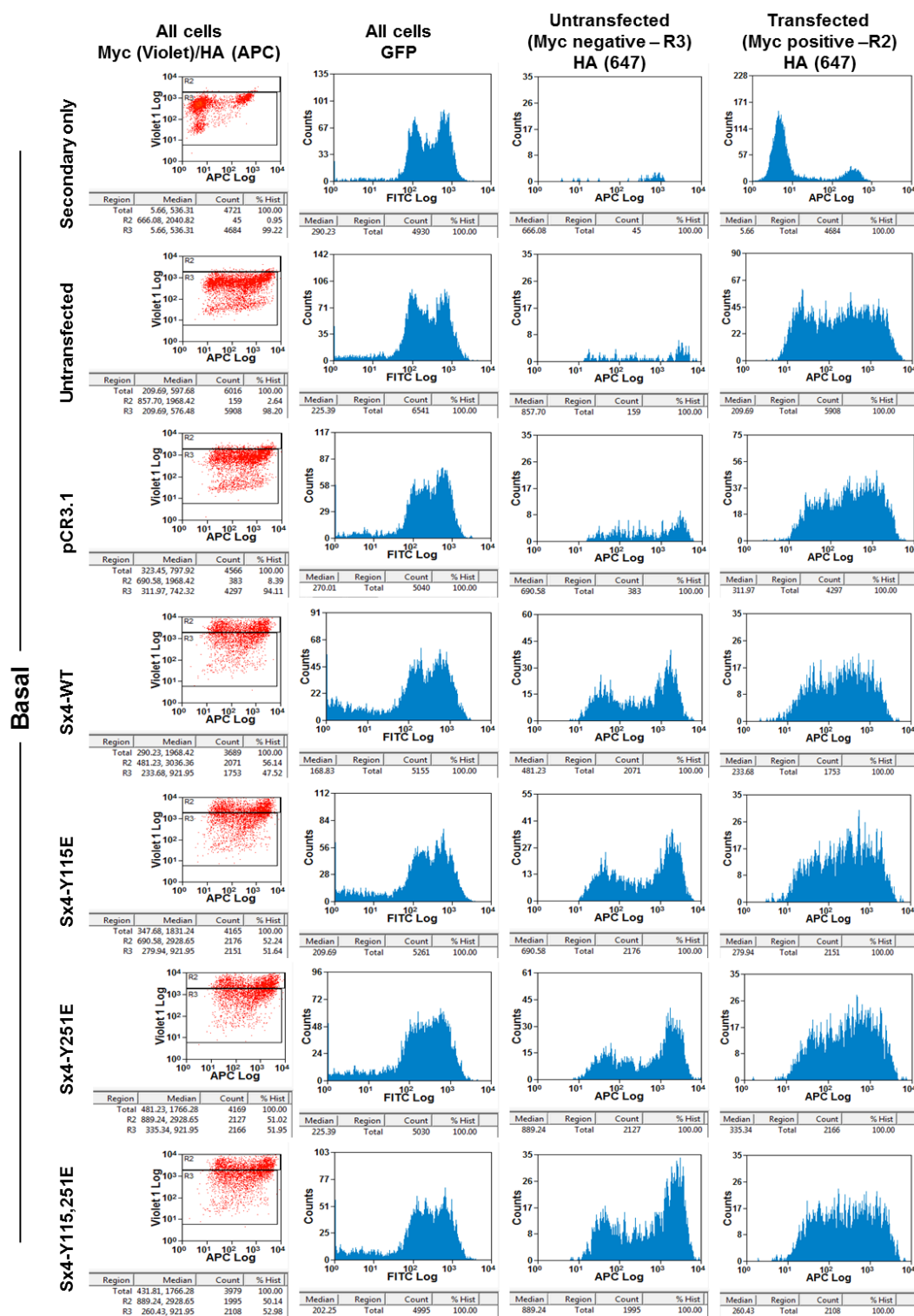


Figure IV.1 Summary of quantification of basal cell surface HA-GLUT4-GFP in cells expressing Sx4(Myc) phospho-mimetic mutants by flow cytometry

Insulin

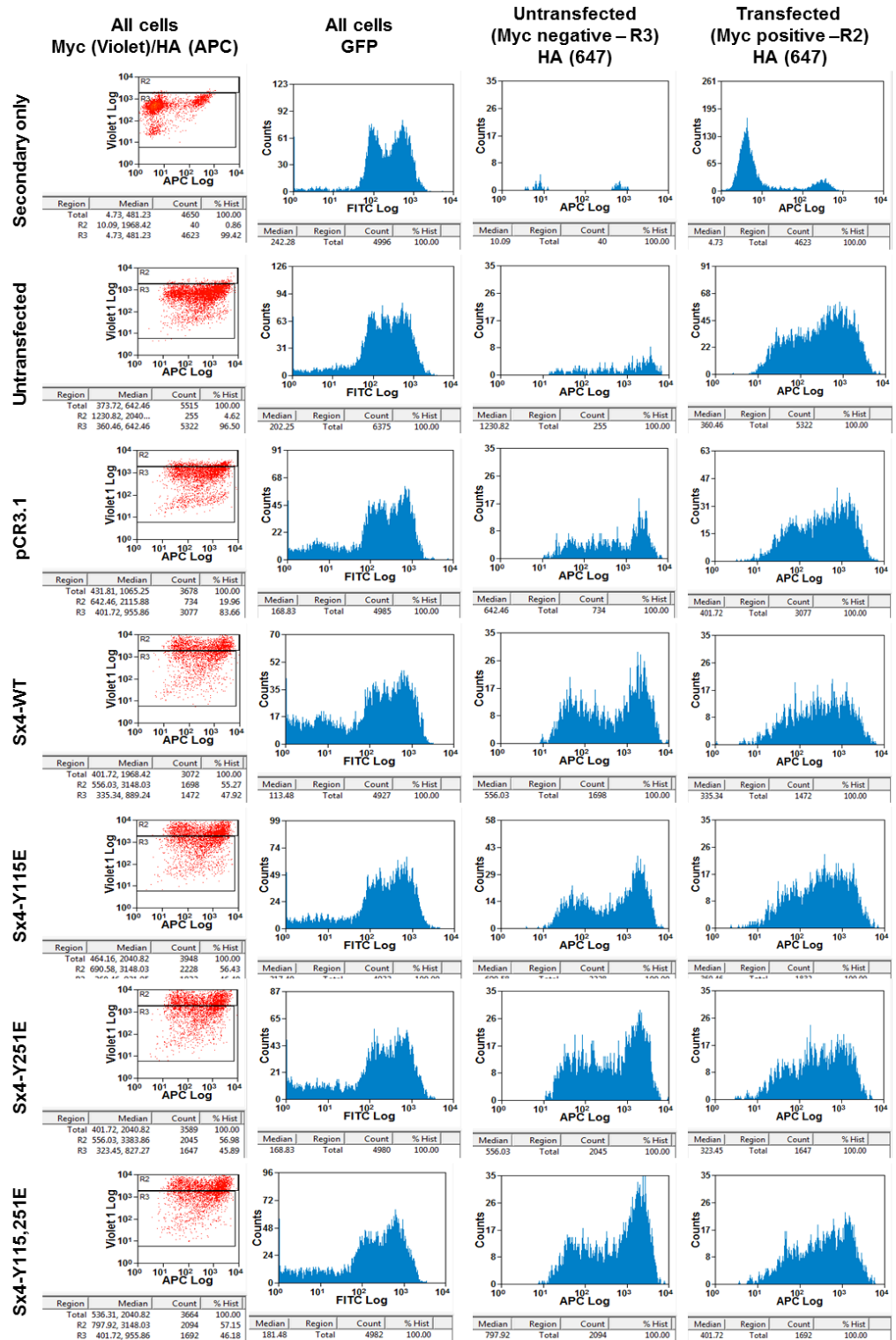


Figure IV.2 Summary of quantification of cell surface HA-GLUT4-GFP in insulin-stimulated cells expressing Sx4(Myc) phospho-mimetic mutants by flow cytometry

List of References

- Abel, E. D., Peroni, O., Kim, J. K., Kim, Y.-B., Boss, O., Hadro, E., Minnemann, T., Shulman, G. I. and Kahn, B. B.** (2001). Adipose-selective targeting of the GLUT4 gene impairs insulin action in muscle and liver. *Nature* **409**, 729–733.
- Advani, R. J., Yang, B., Prekeris, R., Lee, K. C., Klumperman, J. and Scheller, R. H.** (1999). VAMP-7 Mediates Vesicular Transport from Endosomes to Lysosomes. *J. Cell Biol.* **146**, 765–775.
- Antonin, W., Fasshauer, D., Becker, S., Jahn, R. and Schneider, T. R.** (2002). Crystal structure of the endosomal SNARE complex reveals common structural principles of all SNAREs. *Nat. Struct. Biol.* **9**, 107–111.
- Aran, V., Brandie, F. M., Boyd, A. R., Kantidakis, T., Rideout, E. J., Kelly, S. M., Gould, G. W. and Bryant, N. J.** (2009). Characterization of two distinct binding modes between syntaxin 4 and Munc18c. *Biochem. J.* **419**, 655–60.
- Aran, V., Bryant, N. J. and Gould, G. W.** (2011). Tyrosine phosphorylation of Munc18c on residue 521 abrogates binding to Syntaxin 4. *BMC Biochem.* **12**, 19.
- Aran-Ponte, V.** (2009). Regulation of SNARE-dependent fusion in an in vitro system. *PhD Thesis, Univ. Glas.*
- Armani, A., Mammi, C., Marzolla, V., Calanchini, M., Antelmi, A., Rosano, G. M. C., Fabbri, A. and Caprio, M.** (2010). Cellular models for understanding adipogenesis, adipose dysfunction, and obesity. *J. Cell. Biochem.* **110**, 564–572.
- Armstrong, J.** (2000). Minireview Membrane traffic between genomes. *Genome Biol.* 1–4.
- Axelrod, D., Thompson, N. L. and Burghardt, T. P.** (1983). Total Internal Reflection Fluorescent Microscopy. *J. Microsc.* **129**, 19–28.

- Bai, L., Wang, Y., Fan, J., Chen, Y., Ji, W., Qu, A., Xu, P., James, D. E. and Xu, T.** (2007). Dissecting Multiple Steps of GLUT4 Trafficking and Identifying the Sites of Insulin Action. *Cell Metab.* **5**, 47–57.
- Barrangou, R., Fremaux, C., Deveau, H., Richards, M., Boyaval, P., Moineau, S., Romero, D. A. and Horvath, P.** (2007). CRISPR Provides Acquired Resistance Against Viruses in Prokaryotes. *Science (80-)*. **315**, 1709–1712.
- Baxa, C. A., Sha, R. S., Buelt, M. K., Smith, A. J., Matarese, V., Chinander, L. L., Boundy, K. L. and Bernlohr, D. A.** (1989). Human adipocyte lipid-binding protein: purification of the protein and cloning of its complementary DNA. *Biochemistry* **28**, 8683–8690.
- Beckers, C. J. M., Block, M. R., Glick, B. S., Rothman, J. E. and Balch, W. E.** (1989). Vesicular transport between the endoplasmic reticulum and the Golgi stack requires the NEM-sensitive fusion protein. *Nature* **339**, 397–398.
- Bell, G. I. and Polonsky, K. S.** (2001). Diabetes mellitus and genetically programmed defects in beta-cell function. *Nature* **414**, 788–791.
- Bell, G. I., Murray, J. C., Nakamura, Y., Kayano, T., Eddy, R. L., Fan, Y., Byers, M. G. and Shows, T. B.** (1989). Polymorphic Human Insulin-Responsive Glucose-Transporter Gene on Chromosome 17p13. *Diabetes* **38**, 1072–75.
- Bennett, M. K., Calakos, N. and Scheller, R. H.** (1992). Syntaxin: a synaptic protein implicated in docking of synaptic vesicles at presynaptic active zones. *Science (80-)*. **257**, 255–259.
- Bennett, M. K., Garcia-Ararras, J., Elferink, L. A., Peterson, K., Fleming, A. M., Hazuka, C. D. and Scheller, R. H.** (1993). The syntaxin family of vesicular transport receptors. *Cell* **74**, 863–873.

- Birnbaum, M. J.** (1989). Identification of a novel gene encoding an insulin-responsive glucose transporter protein. *Cell* **57**, 305–315.
- Blot, V. and McGraw, T. E.** (2006). GLUT4 is internalized by a cholesterol-dependent nystatin-sensitive mechanism inhibited by insulin. *EMBO J.* **25**, 5648–5658.
- Bock, J. B., Lin, R. C. and Scheller, R. H.** (1996). A new syntaxin family member implicated in targeting of intracellular transport vesicles. *J. Biol. Chem.* **271**, 17961–17965.
- Bock, J. B., Matern, H. T., Peden, A. A. and Scheller, R. H.** (2001). A genomic perspective on membrane compartment organization. *Nature* **409**, 839–841.
- Bracher, A. and Weissenhorn, W.** (2002). Structural basis for the Golgi membrane recruitment of Sly1p by Sed5p. *EMBO J.* **21**, 6114–6124.
- Brandie, F. M., Aran, V., Verma, A., McNew, J. A., Bryant, N. J. and Gould, G. W.** (2008). Negative regulation of syntaxin4/SNAP-23/VAMP2-mediated membrane fusion by Munc18c In Vitro. *PLoS One* **3**, 1–7.
- Brenner, S.** (1974). The genetics of *Caenorhabditis elegans*. *Genetics* **77**, 71–94.
- Bryant, N. J. and Gould, G. W.** (2011). SNARE Proteins Underpin Insulin-Regulated GLUT4 Traffic. *Traffic* **12**, 657–664.
- Bryant, N. J. and James, D. E.** (2003). The Sec1p/Munc18 (SM) protein, Vps45p, cycles on and off membranes during vesicle transport. *J. Cell Biol.* **161**, 691–696.
- Bryant, N. J., Govers, R. and James, D. E.** (2002). Regulated transport of the glucose transporter GLUT4. *Nat. Rev. Mol. Cell Biol.* **3**, 267–277.
- Burgess-Brown, N. A., Sharma, S., Sobott, F., Loenarz, C., Oppermann, U. and**

- Gileadi, O.** (2008). Codon optimization can improve expression of human genes in *Escherichia coli*: A multi-gene study. *Protein Expr. Purif.* **59**, 94–102.
- Burgoyne, R. D. and Morgan, A.** (2007). Membrane Trafficking: Three Steps to Fusion. *Curr. Biol.* **17**, 255–258.
- Burkhardt, P., Hattendorf, D. A., Weis, W. I. and Fasshauer, D.** (2008). Munc18a controls SNARE assembly through its interaction with the syntaxin N-peptide. *Embo J* **27**, 923–933.
- Cain, C. C., Trimble, W. S. and Lienhard, G. E.** (1992). Members of the VAMP family of synaptic vesicle proteins are components of glucose transporter-containing vesicles from rat adipocytes. *J. Biol. Chem.* **267**, 11681–11684.
- Carr, C. M. and Rizo, J.** (2010). At the junction of SNARE and SM protein function. *Curr. Opin. Cell Biol.* **22**, 519–527.
- Carr, C. M., Grote, E., Munson, M., Hughson, F. M. and Novick, P. J.** (1999). Sec1p binds to SNARE complexes and concentrates at sites of secretion. *J. Cell Biol.* **146**, 333–344.
- Cheatham, B., Vlahos, C. J., Cheatham, L., Wang, L., Blenis, J. and Kahn, C. R.** (1994). Phosphatidylinositol 3-kinase activation is required for insulin stimulation of pp70 S6 kinase, DNA synthesis, and glucose transporter translocation. *Mol. Cell. Biol.* **14**, 4902–11.
- Chen, Y. A. and Scheller, R. H.** (2001). SNARE-mediated membrane fusion. *Nat. Rev. Mol. Cell Biol.* **2**, 98–106.
- Chernomordik, L. V. and Kozlov, M. M.** (2003). Protein-Lipid interplay in fusion and fission of biological membranes. *Annu. Rev. Biochem.* **72**, 175–207.

- Christie, M. P., Whitten, A. E., King, G. J., Hu, S.-H., Jarrott, R. J., Chen, K.-E., Duff, A. P., Callow, P., Collins, B. M., James, D. E., et al.** (2012). Low-resolution solution structures of Munc18:Syntaxin protein complexes indicate an open binding mode driven by the Syntaxin N-peptide. *Proc. Natl. Acad. Sci. U. S. A.* **109**, 9816–21.
- Clary, D. O., Griff, I. C. and Rothman, J. E.** (1990). SNAPs, a family of NSF attachment proteins involved in intracellular membrane fusion in animals and yeast. *Cell* **61**, 709–721.
- Compton, P. D., Zamdborg, L., Thomas, P. M. and Kelleher, N. L.** (2011). On the scalability and requirements of whole protein mass spectrometry. *Anal. Chem.* **83**, 6868–6874.
- Cushman, S. W. and Wardzala, L. J.** (1980). Potential mechanism of insulin action on glucose transport in the isolated rat adipose cell. *J. Biol. Chem.* **255**, 4758–62.
- D’Andrea-Merrins, M., Chang, L., Lam, A. D., Ernst, S. A. and Stuenkel, E. L.** (2007). Munc18c interaction with syntaxin 4 monomers and SNARE complex intermediates in GLUT4 vesicle trafficking. *J. Biol. Chem.* **282**, 16553–16566.
- Dacks, J. B. and Field, M. C.** (2007). Evolution of the eukaryotic membrane-trafficking system: origin, tempo and mode. *J. Cell Sci.* **120**, 2977–85.
- Dawson, K., Aviles-Hernandez, A., Cushman, S. W. and Malide, D.** (2001). Insulin-Regulated Trafficking of Dual-Labeled Glucose Transporter 4 in Primary Rat Adipose Cells. *Biochem. Biophys. Res. Commun.* **287**, 445–454.
- Diaz, R., Mayorga, L. S., Weidman, P. J., Rothman, J. E. and Stahl, P. D.** (1989). Vesicle fusion following receptor-mediated endocytosis requires a protein active in Golgi transport. *Nature* **339**, 398–400.

- Doudna, J. A. and Charpentier, E.** (2014). The new frontier of genome engineering with CRISPR-Cas9. *Science (80-.)*. **346**, 1258096–1258096.
- Douen, A. G., Ramlal, T., Cartee, G. D. and Klip, A.** (1990). Exercise modulates the insulin-induced translocation of glucose transporters in rat skeletal muscle. *FEBS Lett.* **261**, 256–260.
- Dubois, F., Vandermoere, F., Gernez, A., Murphy, J., Toth, R., Chen, S., Geraghty, K. M., Morrice, N. a and MacKintosh, C.** (2009). Differential 14-3-3 affinity capture reveals new downstream targets of phosphatidylinositol 3-kinase signaling. *Mol. Cell. Proteomics* **8**, 2487–2499.
- Dubuke, M. L. and Munson, M.** (2016). The Secret Life of Tethers: The Role of Tethering Factors in SNARE Complex Regulation. *Front. Cell Dev. Biol.* **4**, 1–8.
- Dulubova, I., Sugita, S., Hill, S., Hosaka, M., Fernandez, I., Südhof, T. C. and Rizo, J.** (1999). A conformational switch in syntaxin during exocytosis: Role of munc18. *EMBO J.* **18**, 4372–4382.
- Dulubova, I., Yamaguchi, T., Gao, Y., Min, S., Huryeva, I., Su, T. C. and Rizo, J.** (2002). How Tlg2p / syntaxin 16 ` snares ` Vps45. *EMBO J.* **21**, 3620–3631.
- Dulubova, I., Khvotchev, M., Liu, S., Huryeva, I., Südhof, T. C. and Rizo, J.** (2007). Munc18-1 binds directly to the neuronal SNARE complex. *Proc. Natl. Acad. Sci. U. S. A.* **104**, 2697–702.
- Eguez, L., Lee, A., Chavez, J. A., Miinea, C. P., Kane, S., Lienhard, G. E. and McGraw, T. E.** (2005). Full intracellular retention of GLUT4 requires AS160 Rab GTPase activating protein. *Cell Metab.* **2**, 263–272.
- Entingh-Pearsall, A. and Kahn, C. R.** (2004). Differential roles of the insulin and insulin-

like growth factor-I (IGF-I) receptors in response to insulin and IGF-I. *J. Biol. Chem.* **279**, 38016–38024.

Fasshauer, D., Otto, H., Eliason, W. K., Jahn, R. and Brünger, a T. (1997). Structural changes are associated with soluble N-ethylmaleimide-sensitive fusion protein attachment protein receptor complex formation. *J. Biol. Chem.* **272**, 28036–28041.

Fasshauer, D., Sutton, R. B., Brunger, A. T. and Jahn, R. (1998). Conserved structural features of the synaptic fusion complex: SNARE proteins reclassified as Q- and R-SNAREs. *Proc. Natl. Acad. Sci. U. S. A.* **95**, 15781–6.

Fernandez, I., Ubach, J., Dulubova, I., Zhang, X., Sudhof, T. C. and Rizo, J. (1998). Three-dimensional structure of an evolutionarily conserved N-terminal domain of syntaxin 1A. *Cell* **94**, 841–849.

Fiebig, K. M., Rice, L. M., Pollock, E. and Brunger, A. T. (1999). Folding intermediates of SNARE complex assembly. *Nat. Struct. Biol.* **1**,.

Foletti, D. L., Lin, R., Finley, M. A. F. and Scheller, R. H. (2000). Phosphorylated syntaxin 1 is localized to discrete domains along a subset of axons. *J. Neurosci.* **20**, 4535–44.

Foster, L. J., Yeung, B., Mohtashami, M., Ross, K., Trimble, W. S. and Klip, A. (1998). Binary interactions of the SNARE proteins syntaxin-4, SNAP23, and VAMP-2 and their regulation by phosphorylation. *Biochemistry* **37**, 11089–11096.

Fujita, Y., Shirataki, H., Sakisaka, T., Asakura, T., Ohya, T., Kotani, H., Yokoyama, S., Nishioka, H., Matsuura, Y., Mizoguchi, A., et al. (1998). Tomosyn: A syntaxin-1-binding protein that forms a novel complex in the neurotransmitter release process. *Neuron* **20**, 905–915.

- Fukuda, M.** (2008). Membrane traffic in the secretory pathway: Regulation of secretory vesicle traffic by Rab small GTPases. *Cell. Mol. Life Sci.* **65**, 2801–2813.
- Gagescu, R.** (2000). SNARE hypothesis 2000. *Nat. Rev. Mol. Cell Biol.* **1**, 2000.
- Gerst, J. E.** (2003). SNARE regulators: Matchmakers and matchbreakers. *Biochim. Biophys. Acta - Mol. Cell Res.* **1641**, 99–110.
- Glick, B. S. and Rothman, J. E.** (1987). Possible role for fatty acyl-coenzyme A in intracellular protein transport. *Nature* **326**, 309–12.
- Gonzalo, S. and Linder, M. E.** (1998). SNAP-25 palmitoylation and plasma membrane targeting require a functional secretory pathway. *Mol. Biol. Cell* **9**, 585–597.
- Grant, B. D. and Donaldson, J. G.** (2009). Pathways and mechanisms of endocytic recycling. *Nat. Rev. Mol. Cell Biol.* **10**, 597–608.
- Gual, P., Le Marchand-Brustel, Y. and Tanti, J.-F.** (2005). Positive and negative regulation of insulin signaling through IRS-1 phosphorylation. *Biochimie* **87**, 99–109.
- Guo, W., Grant, A. and Novick, P.** (1999). Exo84p is an exocyst protein essential for secretion. *J. Biol. Chem.* **274**, 23558–23564.
- Haga, Y., Ishii, K. and Suzuki, T.** (2011). N-glycosylation is critical for the stability and intracellular trafficking of glucose transporter GLUT4. *J. Biol. Chem.* **286**, 31320–31327.
- Hajdуч, E., Aledo, J. C., Watts, C. and Hundal, H. S.** (1997). Proteolytic cleavage of cellubrevin and vesicle-associated membrane protein (VAMP) by tetanus toxin does not impair insulin-stimulated glucose transport or GLUT4 translocation in rat adipocytes. *Biochem. J.* **321 (Pt 1)**, 233–8.

- Hata, Y., Slaughter, C. A. and Südhof, T. C.** (1993). Synaptic vesicle fusion complex contains unc-18 homologue bound to syntaxin. *Nature* **366**, 347–351.
- Hatakeyama, H. and Kanzaki, M.** (2011). Molecular Basis of Insulin-Responsive GLUT4 Trafficking Systems Revealed by Single Molecule Imaging. *Traffic* **12**, 1805–1820.
- Hayashi, T., McMahon, H., Yamasaki, S., Binz, T., Hata, Y., Südhof, T. C. and Niemann, H.** (1994). Synaptic vesicle membrane fusion complex: action of clostridial neurotoxins on assembly. *EMBO J.* **13**, 5051–5061.
- Hayashi, T., Yamasaki, S., Nauenburg, S., Binz, T. and Niemann, H.** (1995). Disassembly of the reconstituted synaptic vesicle membrane fusion complex in vitro. *EMBO J.* **14**, 2317–2325.
- Hernandez, R., Teruel, T. and Lorenzo, M.** (2001). Akt mediates insulin induction of glucose uptake and up-regulation of GLUT4 gene expression in brown adipocytes. *FEBS Lett.* **494**, 225–231.
- Hirshman, M. F., Goodyear, L. J., Wardzala, L. J., Horton, E. D. and Horton, E. S.** (1990). Identification of an intracellular pool of glucose transporters from basal and insulin-stimulated rat skeletal muscle. *J. Biol. Chem.* **265**, 987–991.
- Hohl, T. M., Parlati, F., Wimmer, C., Rothman, J. E., Söllner, T. H. and Engelhardt, H.** (1998). Arrangement of subunits in 20 S particles consisting of NSF, SNAPs, and SNARE complexes. *Mol. Cell* **2**, 539–548.
- Holt, M., Varoqueaux, F., Wiederhold, K., Takamori, S., Urlaub, H., Fasshauer, D. and Jahn, R.** (2006). Identification of SNAP-47, a novel Qbc-SNARE with ubiquitous expression. *J. Biol. Chem.* **281**, 17076–17083.
- Hong, W.** (2005). SNAREs and traffic. *Biochim. Biophys. Acta* **1744**, 120–144.

- Horvath, P. and Barrangou, R.** (2010). CRISPR/Cas, the immune system of bacteria and archaea. *Science* (80-.). **327**, 167–170.
- Hu, S. H., Gee, C. L., Latham, C. F., Rowlinson, S. W., Rova, U., Jones, A., Halliday, J. A., Bryant, N. J., James, D. E. and Martin, J. L.** (2003). Recombinant expression of Munc18c in a baculovirus system and interaction with syntaxin. *Protein Expr. Purif.* **31**, 305–310.
- Hu, S.-H., Latham, C. F., Gee, C. L., James, D. E. and Martin, J. L.** (2007). Structure of the Munc18c/Syntaxin4 N-peptide complex defines universal features of the N-peptide binding mode of Sec1/Munc18 proteins. *Proc. Natl. Acad. Sci. U. S. A.* **104**, 8773–8778.
- Huang, S., Lifshitz, L. M., Jones, C., Bellve, K. D., Standley, C., Fonseca, S., Corvera, S., Fogarty, K. E. and Czech, M. P.** (2007). Insulin stimulates membrane fusion and GLUT4 accumulation in clathrin coats on adipocyte plasma membranes. *Mol. Cell. Biol.* **27**, 3456–3469.
- Huang, G., Buckler-Pena, D., Nauta, T., Singh, M., Asmar, A., Shi, J., Kim, J. Y. and Kandror, K. V** (2013). Insulin responsiveness of glucose transporter 4 in 3T3-L1 cells depends on the presence of sortilin. *Mol. Biol. Cell* **24**, 3115–22.
- Hubbard, S. J.** (1998). The structural aspects of limited proteolysis of native proteins. *Biochim. Biophys. Acta* **1382**, 191–206.
- Hulme, E. C. and Trevethick, M. A.** (2010). Ligand binding assays at equilibrium: Validation and interpretation. *Br. J. Pharmacol.* **161**, 1219–1237.
- Hutagalung, A. H. and Novick, P. J.** (2011). Role of Rab GTPases in membrane traffic and cell physiology. *Physiol. Rev.* **91**, 119–149.

- Hwang, C. S., Loftus, T. M., Mandrup, S. and Lane, M. D.** (1997). Adipocyte differentiation and leptin expression. *Annu. Rev. Cell Dev. Biol.* **13**, 231–259.
- Inoue, M., Chang, L., Hwang, J., Chiang, S.-H. and Saltiel, A. R.** (2003). The exocyst complex is required for targeting of Glut4 to the plasma membrane by insulin. *Nature* **422**, 629–633.
- Jahn, R., Lang, T. and Sudhof, T. C.** (2003). Membrane fusion. *Cell* **112**, 519–533.
- James, D. E., Brown, R., Navarro, J. and Pilch, P. F.** (1988). Insulin-regulatable tissues express a unique insulin-sensitive glucose transport protein. *Nature* **333**, 183–185.
- James, D. E., Strube, M. and Muecdler, M.** (1989). Molecular cloning and characterization of an insulin-regulatable glucose transporter. *Nature* **338**, 83–87.
- Jedrychowski, M. P., Gartner, C. A., Gygi, S. P., Zhou, L., Herz, J., Kandror, K. V. and Pilch, P. F.** (2010). Proteomic analysis of GLUT4 storage vesicles reveals LRP1 to be an important vesicle component and target of insulin signaling. *J. Biol. Chem.* **285**, 104–114.
- Jewell, J. L., Oh, E., Bennett, S. M., Meroueh, S. O. and Thurmond, D. C.** (2008). The tyrosine phosphorylation of Munc18c induces a switch in binding specificity from syntaxin 4 to Doc2beta. *J. Biol. Chem.* **283**, 21734–46.
- Jewell, J. L., Oh, E. and Thurmond, D. C.** (2010). Exocytosis mechanisms underlying insulin release and glucose uptake: conserved roles for Munc18c and syntaxin 4. *Am. J. Physiol. Regul. Integr. Comp. Physiol.* **298**, R517–R531.
- Kahn, S. E., Hull, R. L. and Utzschneider, K. M.** (2006). Mechanisms linking obesity to insulin resistance and type 2 diabetes. *Nature* **444**, 840–846.

- Kanda, H., Tamori, Y., Shinoda, H., Yoshikawa, M., Sakaue, M., Udagawa, J., Otani, H., Tashiro, F., Miyazaki, J. and Kasuga, M.** (2005). Adipocytes from Munc18c-null mice show increased sensitivity to insulin-stimulated GLUT4 externalization. *J. Clin. Invest.* **115**, 291–301.
- Kandror, K. V., Coderre, L., Pushkin, A. V. and Pilch, P. F.** (1995). Comparison of glucose-transporter-containing vesicles from rat fat and muscle tissues: evidence for a unique endosomal compartment. *Biochem. J.* **307**, 383–390.
- Kawaguchi, T., Tamori, Y., Kanda, H., Yoshikawa, M., Tateya, S., Nishino, N. and Kasuga, M.** (2010). The t-SNAREs syntaxin4 and SNAP23 but not v-SNARE VAMP2 are indispensable to tether GLUT4 vesicles at the plasma membrane in adipocyte. *Biochem. Biophys. Res. Commun.* **391**, 1336–1341.
- Kawanishi, M., Tamori, Y., Okazawa, H., Araki, S., Shinoda, H. and Kasuga, M.** (2000). Role of SNAP23 in insulin-induced translocation of GLUT4 in 3T3-L1 adipocytes: Mediation of complex formation between syntaxin4 and VAMP2. *J. Biol. Chem.* **275**, 8240–8247.
- Ke, B., Oh, E. and Thurmond, D. C.** (2007). Doc2B is a novel Munc18c-interacting partner and positive effector of syntaxin 4-mediated exocytosis. *J. Biol. Chem.* **282**, 21786–21797.
- Keller, S. R., Davis, A. C. and Clairmont, K. B.** (2002). Mice deficient in the insulin-regulated membrane aminopeptidase show substantial decreases in glucose transporter GLUT4 levels but maintain normal glucose homeostasis. *J. Biol. Chem.* **277**, 17677–17686.
- Khvotchev, M., Dulubova, I., Sun, J., Dai, H., Rizo, J. and Südhof, T. C.** (2007). Dual modes of Munc18-1/SNARE interactions are coupled by functionally critical binding

to syntaxin-1 N terminus. *J. Neurosci.* **27**, 12147–55.

Kinoshita, E., Kinoshita-Kikuta, E., Takiyama, K. and Koike, T. (2006). Phosphate-binding Tag, a New Tool to Visualize Phosphorylated Proteins. *Mol. Cell. Proteomics* **5**, 749–757.

Kioumourtzoglou, D. (2012). Investigations into insulin-regulated trafficking of the facilitative glucose transporter GLUT4 in adipocytes; novel insights from in situ studies.

Kioumourtzoglou, D., Gould, G. W. and Bryant, N. J. (2014). Insulin stimulates syntaxin4 SNARE complex assembly via a novel regulatory mechanism. *Mol. Cell. Biol.* **34**, 1271–9.

Kloepper, T. H., Kienle, C. N. and Fasshauer, D. (2007). An Elaborate Classification of SNARE Protein Sheds Light on the Conservation of the Eukaryotic Endomembrane System. *Mol. Biol. Cell* **18**, 3463–3471.

Koumanov, F., Jin, B., Yang, J. and Holman, G. D. (2005). Insulin signaling meets vesicle traffic of GLUT4 at a plasma-membrane-activated fusion step. *Cell Metab.* **2**, 179–189.

Kraegen, E. W., James, D. E., Jenkins, a B. and Chisholm, D. J. (1985). Dose-response curves for in vivo insulin sensitivity in individual tissues in rats. *Am. J. Physiol.* **248**, E353–E362.

Kuhné, M. R., Zhao, Z., Rowles, J., Lavan, B. E., Shen, S.-H., Fischer, E. H. and Lienhard, G. E. (1994). Dephosphorylation of insulin receptor substrate 1 by the tyrosine phosphatase PTP2C. *J. Biol. Chem.* **269**, 15833–15837.

Lampson, M. A., Racz, A., Cushman, S. W. and McGraw, T. E. (2000). Demonstration

of insulin-responsive trafficking of GLUT4 and vpTR in fibroblasts. *J. Cell Sci.* **113**, 4065–4076.

Larance, M., Ramm, G., Stockli, J., Van Dam, E. M., Winata, S., Wasinger, V., Simpson, F., Graham, M., Junutula, J. R., Guilhaus, M., et al. (2005). Characterization of the role of the Rab GTPase-activating protein AS160 in insulin-regulated GLUT4 trafficking. *J. Biol. Chem.* **280**, 37803–37813.

Larance, M., Ramm, G. and James, D. E. (2008). The GLUT4 code. *Mol. Endocrinol.* **22**, 226–233.

Latham, C. F., Lopez, J. A., Hu, S.-H., Gee, C. L., Westbury, E., Blair, D. H., Armishaw, C. J., Alewood, P. F., Bryant, N. J., James, D. E., et al. (2006). Molecular dissection of the Munc18c/syntaxin4 interaction: implications for regulation of membrane trafficking. *Traffic* **7**, 1408–1419.

Leto, D. and Saltiel, A. R. (2012). Regulation of glucose transport by insulin: traffic control of GLUT4. *Nat. Rev. Mol. Cell Biol.* **13**, 383–396.

Lin, R. C. and Scheller, R. H. (2000). Mechanisms of synaptic vesicle exocytosis. *Annu. Rev. Cell Dev. Biol.* **16**, 19–49.

Lipka, V., Kwon, C. and Panstruga, R. (2007). SNARE-ware: the role of SNARE-domain proteins in plant biology. *Annu. Rev. Cell Dev. Biol.* **23**, 147–174.

Littleton, J. T., Chapman, E. R., Kreber, R., Garment, M. B., Carlson, S. D. and Ganetzky, B. (1998). Temperature-sensitive paralytic mutations demonstrate that synaptic exocytosis requires SNARE complex assembly and disassembly. *Neuron* **21**, 401–13.

Livingstone, C., James, D. E., Rice, J. E., Hanpeter, D. and Gould, G. W. (1996).

Compartment ablation analysis of the insulin-responsive glucose transporter (GLUT4) in 3T3-L1 adipocytes. *Biochem. J.* **315**, 487–95.

MacDonald, C., Munson, M. and Bryant, N. J. (2010). Autoinhibition of SNARE complex assembly by a conformational switch represents a conserved feature of syntaxins. *Biochem. Soc. Trans.* **38**, 209–12.

Malhotra, V., Orci, L., Glick, B. S., Block, M. R. and Rothman, J. E. (1988). Role of an N-ethylmaleimide-sensitive transport component in promoting fusion of transport vesicles with cisternae of the Golgi stack. *Cell* **54**, 221–227.

Malsam, J., Kreye, S. and Söllner, T. H. (2008). Membrane fusion: SNAREs and regulation. *Cell. Mol. Life Sci.* **65**, 2814–2832.

Marash, M. and Gerst, J. E. (2001). t-SNARE dephosphorylation promotes SNARE assembly and exocytosis in yeast. *EMBO J.* **20**, 411–21.

Marash, M. and Gerst, J. E. (2003). Phosphorylation of the Autoinhibitory Domain of the Sso t-SNAREs Promotes Binding of the Vsm1 SNARE Regulator in Yeast. *Mol. Biol. Cell* **14**, 3114–3125.

Martin, L. B., Shewan, A., Millar, C. A., Gould, G. W. and James, D. E. (1998). Vesicle-associated membrane protein 2 plays a specific role in the insulin-dependent trafficking of the facilitative glucose transporter GLUT4 in 3T3-L1 adipocytes. *J. Biol. Chem.* **273**, 1444–1452.

Martin, O. J., Lee, A. and McGraw, T. E. (2006). GLUT4 distribution between the plasma membrane and the intracellular compartments is maintained by an insulin-modulated bipartite dynamic mechanism. *J. Biol. Chem.* **281**, 484–490.

McNew, J. A., Parlati, F., Fukuda, R., Johnston, R. J., Paz, K., Paumet, F., Söllner, T.

- H. and Rothman, J. E.** (2000). Compartmental specificity of cellular membrane fusion encoded in SNARE proteins. *Nature* **407**, 153–159.
- Miinea, C. P., Sano, H., Kane, S., Sano, E., Fukuda, M., Peränen, J., Lane, W. S. and Lienhard, G. E.** (2005). AS160, the Akt substrate regulating GLUT4 translocation, has a functional Rab GTPase-activating protein domain. *Biochem. J.* **391**, 87–93.
- Millar, C. A., Shewan, A., Hickson, G. R., James, D. E. and Gould, G. W.** (1999). Differential regulation of secretory compartments containing the insulin-responsive glucose transporter 4 in 3T3-L1 adipocytes. *Mol. Biol. Cell* **10**, 3675–88.
- Min, J., Okada, S., Kanzaki, M., Elmendorf, J. S., Coker, K. J., Ceresa, B. P., Syu, L. J., Noda, Y., Saltiel, A. R. and Pessin, J. E.** (1999). Synip: A novel insulin-regulated syntaxin 4-binding protein mediating GLUT4 translocation in adipocytes. *Mol. Cell* **3**, 751–760.
- Misura, K. M., Scheller, R. H. and Weis, W. I.** (2000). Three-dimensional structure of the neuronal-Sec1-syntaxin 1a complex. *Nature* **404**, 355–362.
- Muppirala, M., Gupta, V. and Swarup, G.** (2012). Tyrosine phosphorylation of a SNARE protein, Syntaxin 17: Implications for membrane trafficking in the early secretory pathway. *Biochim. Biophys. Acta* **1823**, 2109–2119.
- Nieler, H. B., Onofri, F., Valtorta, F., Schiavo, G., Montecucco, C., Greengard, P. and Benfenati, F.** (1995). Phosphorylation of VAMP/synaptobrevin in synaptic vesicles by endogenous protein kinases. *J. Neurochem.* **65**, 1712–1720.
- Novick, P. and Schekman, R.** (1979). Secretion and cell-surface growth are blocked in a temperature-sensitive mutant of *Saccharomyces cerevisiae*. *Proc. Natl. Acad. Sci. U. S. A.* **76**, 1858–1862.

- Oh, E. and Thurmond, D. C.** (2006). The stimulus-induced tyrosine phosphorylation of Munc18c facilitates vesicle exocytosis. *J. Biol. Chem.* **281**, 17624–17634.
- Oh, E., Spurlin, B. A., Pessin, J. E. and Thurmond, D. C.** (2005). Munc18c heterozygous knockout mice display increased susceptibility for severe glucose intolerance. *Diabetes* **54**, 638–647.
- Ohya, T., Miaczynska, M., Coskun, U., Lommer, B., Runge, A., Drechsel, D., Kalaidzidis, Y. and Zerial, M.** (2009). Reconstitution of Rab- and SNARE-dependent membrane fusion by synthetic endosomes. *Nature* **459**, 1091–1097.
- Okada, T., Kawano, Y., Sakakibara, T., Hazeki, O. and Ui, M.** (1994). Essential role of phosphatidylinositol 3-kinase in insulin-induced glucose transport and antilipolysis in rat adipocytes. *J. Biol. Chem.* **269**, 3568–3573.
- Olson, A. L. and Pessin, J. E.** (1996). Structure, function, and regulation of the mammalian facilitative glucose transporter gene family. *Annu. Rev. Nutr.* **16**, 235–256.
- Olson, A. L., Knight, J. B. and Pessin, J. E.** (1997). Syntaxin 4 , VAMP2 , and / or VAMP3 / Cellubrevin Are Functional Target Membrane and Vesicle SNAP Receptors for Insulin-Stimulated GLUT4 Translocation in Adipocytes. *Mol. Cell. Biol.* **17**, 2425–2435.
- Oyler, G. A., Higgins, G. A., Hart, R. A., Battenberg, E., Bloom, F. E., Wilson, M. C., Oyler, A., Higgins, A., Hart, A. and Bloom, F.** (1989). The Identification of a Novel Synaptosomal-associated Protein, SNAP25, Differentially Expressed by Neuronal Subpopulations. *J. Cell Biol.* **109**, 3039–3052.
- Palade, G.** (1975). Intracellular aspects of the process of protein synthesis. *Science* (80-). **189**, 867.

- Parkar, N. S., Akpa, B. S., Nitsche, L. C., Wedgewood, L. E., Place, A. T., Sverdlov, M. S., Chaga, O. and Minshall, R. D.** (2009). Vesicle formation and endocytosis: function, machinery, mechanisms, and modeling. *Antioxid. Redox Signal.* **11**, 1301–12.
- Paumet, F., Rahimian, V. and Rothman, J. E.** (2004). The specificity of SNARE-dependent fusion is encoded in the SNARE motif. *Proc. Natl. Acad. Sci. U. S. A.* **101**, 3376–3380.
- Peck, G. R., Ye, S., Pham, V., Fernando, R. N., Macaulay, S. L., Chai, S. Y. and Albiston, A. L.** (2006). Interaction of the Akt substrate, AS160, with the glucose transporter 4 vesicle marker protein, insulin-regulated aminopeptidase. *Mol. Endocrinol.* **20**, 2576–83.
- Perera, H. K. I., Clarke, M., Morris, N. J., Hong, W., Chamberlain, L. H. and Gould, G. W.** (2003). Syntaxin 6 regulates GLUT4 trafficking in 3T3-L1 adipocytes. *Mol. Biol. Cell* **14**, 2946–2958.
- Pfeffer, S. R.** (1999). Transport-vesicle targeting: tethers before SNAREs. *Nat. Cell Biol.* **1**, E17-22.
- Poirier, M. A., Xiao, W., Macosko, J. C., Chan, C., Shin, Y.-K. and Bennett, M. K.** (1998a). The synaptic SNARE complex is a parallel four-stranded helical bundle. *Nat. Struct. Biol.* **5**, 765–769.
- Poirier, M. A., Hao, J. C., Malkus, P. N., Chan, C., Moore, M. F., King, D. S. and Bennett, M. K.** (1998b). Protease Resistance of Syntaxin. SNAP-25 .VAMP Complexes. *J. Biol. Chem.* **273**, 11370–11377.
- Polgar, J., Chung, S.-H. and Reed, G. L.** (2002). Vesicle-associated membrane protein 3 (VAMP-3) and VAMP-8 are present in human platelets and are required for granule

secretion. *Blood* **100**, 1081–1083.

Proctor, K. M., Miller, S. C. M., Bryant, N. J. and Gould, G. W. (2006). Syntaxin 16 controls the intracellular sequestration of GLUT4 in 3T3-L1 adipocytes. *Biochem. Biophys. Res. Commun.* **347**, 433–8.

Randhawa, V. K., Bilan, P. J., Khayat, Z. A., Daneman, N., Liu, Z., Ramlal, T., Volchuk, A., Peng, X. R., Coppola, T., Regazzi, R., et al. (2000). VAMP2, but not VAMP3/cellubrevin, mediates insulin-dependent incorporation of GLUT4 into the plasma membrane of L6 myoblasts. *Mol. Biol. Cell* **11**, 2403–17.

Ravichandran, V., Chawla, A. and Roche, P. A. (1996). Identification of a Novel Syntaxin- and Synaptobrevin/VAMP-binding Protein, SNAP-23, Expressed in Non-neuronal Tissues. *J. Biol. Chem.* **271**, 13300–13303.

Rea, S., Martin, L. B., McIntosh, S., Macaulay, S. L., Ramsdale, T., Baldini, G. and James, D. E. (1998). Syndet, an adipocyte target SNARE involved in the insulin-induced translocation of GLUT4 to the cell surface. *J. Biol. Chem.* **273**, 18784–18792.

Rickman, C. and Duncan, R. R. (2010). Munc18/syntaxin interaction kinetics control secretory vesicle dynamics. *J. Biol. Chem.* **285**, 3965–3972.

Risinger, C. and Bennett, M. K. (1999). Differential phosphorylation of syntaxin and synaptosome-associated protein of 25 kDa (SNAP-25) isoforms. *J. Neurochem.* **72**, 614–624.

Rizo, J. and Südhof, T. C. (2012). *The Membrane Fusion Enigma: SNAREs, Sec1/Munc18 Proteins, and Their Accomplices—Guilty as Charged?*

Rodríguez-Enríquez, S., Marín-Hernández, A., Gallardo-Pérez, J. C. and Moreno-Sánchez, R. (2009). Kinetics of transport and phosphorylation of glucose in cancer

cells. *J. Cell. Physiol.* **221**, 552–559.

Ros-Baro, A., Lopez-Iglesias, C., Peiro, S., Bellido, D., Palacin, M., Zorzano, A. and Camps, M. (2001). Lipid rafts are required for GLUT4 internalization in adipose cells. *Proc. Natl. Acad. Sci. U. S. A.* **98**, 12050–12055.

Rosano, G. L. and Ceccarelli, E. A. (2014). Recombinant protein expression in *Escherichia coli*: Advances and challenges. *Front. Microbiol.* **5**, 1–17.

Rosen, E. D. and MacDougald, O. A. (2006). Adipocyte differentiation from the inside out. *Nat. Rev. Mol. Cell Biol.* **7**, 885–96.

Rossi, G., Salminen, A., Rice, L. M., Brunger, A. T. and Brennwald, P. (1997). Analysis of a yeast SNARE complex reveals remarkable similarity to the neuronal SNARE complex and a novel function for the C terminus of the SNAP-25 homolog, Sec9. *J. Biol. Chem.* **272**, 16610–16617.

Rossi, V., Banfield, D. K., Vacca, M., Dietrich, L. E. P., Ungermann, C., D'Esposito, M., Galli, T. and Filippini, F. (2004). Longins and their longin domains: Regulated SNAREs and multifunctional SNARE regulators. *Trends Biochem. Sci.* **29**, 682–688.

Sadler, J. B. A., Bryant, N. J. and Gould, G. W. (2015). Characterization of VAMP isoforms in 3T3-L1 adipocytes: implications for GLUT4 trafficking. *Mol. Biol. Cell* **26**, 530–6.

Sakaguchi, G., Orita, S., Maeda, M., Igarashi, H. and Takai, Y. (1995). Molecular cloning of an isoform of Doc2 having two C2-like domains. *Biochem. Biophys. Res. Commun.* **217**, 1053–1061.

Sanderfoot, A. A., Assaad, F. F. and Raikhel, N. V (2000). The Arabidopsis genome. An abundance of soluble N-ethylmaleimide-sensitive factor adaptor protein receptors.

Plant Physiol. **124**, 1558–1569.

- Sano, H., Kane, S., Sano, E., Miinea, C. P., Asara, J. M., Lane, W. S., Garner, C. W. and Lienhard, G. E.** (2003). Insulin-stimulated Phosphorylation of a Rab GTPase-activating Protein Regulates GLUT4 Translocation. *J. Biol. Chem.* **278**, 14599–14602.
- Sapperstein, S. K., Lupashin, V. V., Schmitt, H. D. and Waters, M. G.** (1996). Assembly of the ER to Golgi SNARE complex requires Uso1p. *J. Cell Biol.* **132**, 755–767.
- Schmelzle, K., Kane, S., Gridley, S., Lienhard, G. E. and White, F. M.** (2006). Temporal dynamics of tyrosine phosphorylation in insulin signaling. *Diabetes* **55**, 2171–2179.
- Scott, B. L., Van Komen, J. S., Irshad, H., Liu, S., Wilson, K. A. and McNew, J. A.** (2004). Sec1 p directly stimulates SNARE-mediated membrane fusion in vitro. *J. Cell Biol.* **167**, 75–85.
- Shen, J., Tareste, D. C., Paumet, F., Rothman, J. E. and Melia, T. J.** (2007). Selective Activation of Cognate SNAREpins by Sec1/Munc18 Proteins. *Cell* **128**, 183–195.
- Shepherd, P. R. and Kahn, B. B.** (1999). Glucose Transporters and Insulin Action: Implications for Insulin Resistance and Diabetes Mellitus. *N. Engl. J. Med.* **341**, 248–257.
- Shewan, A. M., Van Dam, E. M., Martin, S., Luen, T. B., Hong, W., Bryant, N. J. and James, D. E.** (2003). GLUT4 Recycles via a trans-Golgi Network (TGN) Subdomain Enriched in Syntaxins 6 and 16 But Not TGN38: Involvement of an Acidic Targeting Motif. *Mol. Biol. Cell* **14**, 973–986.
- Shi, J. and Kandrор, K. V.** (2005). Sortilin is essential and sufficient for the formation of Glut4 storage vesicles in 3T3-L1 adipocytes. *Dev. Cell* **9**, 99–108.

- Shigematsu, S., Watson, R. T., Khan, A. H. and Pessin, J. E.** (2003). The adipocyte plasma membrane caveolin functional/structural organization is necessary for the efficient endocytosis of GLUT4. *J. Biol. Chem.* **278**, 10683–10690.
- Shimazaki, Y., Nishiki, T., Omori, A., Sekiguchi, M., Kamata, Y., Kozaki, S. and Takahashi, M.** (1996). Phosphorylation of 25-kDa Synaptosome-associated Protein. *J. Biol. Chem.* **271**, 14548–14553.
- Slot, J. W., Geuze, H. J., Gigengack, S., Lienhard, G. E. and James, D. E.** (1991). Immuno-localization of the insulin regulatable glucose transporter in brown adipose tissue of the rat. *J. Cell Biol.* **113**, 123–135.
- Smyth, A. M., Duncan, R. R. and Rickman, C.** (2010). Munc18-1 and syntaxin1: Unraveling the interactions between the dynamic duo. In *Cellular and Molecular Neurobiology*, pp. 1309–1313.
- Snyder, D. A., Kelly, M. L. and Woodbury, D. J.** (2006). SNARE complex regulation by phosphorylation. *Cell Biochem. Biophys.* **45**, 111–123.
- Söllner, T., Whiteheart, S. W., Brunner, M., Erdjument-Bromage, H., Geromanos, S., Tempst, P. and Rothman, J. E.** (1993). SNAP receptors implicated in vesicle targeting and fusion. *Nature* **362**, 318–324.
- Spurlin, B. A., Park, S.-Y., Nevins, A. K., Kim, J. K. and Thurmond, D. C.** (2004). Syntaxin 4 transgenic mice exhibit enhanced insulin-mediated glucose uptake in skeletal muscle. *Diabetes* **53**, 2223–2231.
- St-Denis, J.-F., Cabaniols, J.-P., Cushman, S. W. and Roche, P. A.** (1999). SNAP-23 participates in SNARE complex assembly in rat adipose cells. *Biochem. J.* **338**, 709–715.

- Steedmaier, M., Yang, B., Yoo, J., Huang, B., Shen, M., Yu, S., Luo, Y. and Scheller, R. H.** (1998). Three Novel Proteins of the Syntaxin / SNAP-25 Family. *J. Biol. Chem.* **273**, 34171–34179.
- Stenmark, H.** (2009). Rab GTPases as coordinators of vesicle traffic. *Nat. Rev. Mol. Cell Biol.* **10**, 513–25.
- Struthers, M. S., Shanks, S. G., MacDonald, C., Carpp, L. N., Drozdowska, A. M., Kioumourtzoglou, D., Furgason, M. L. M., Munson, M. and Bryant, N. J.** (2009). Functional homology of mammalian syntaxin 16 and yeast Tlg2p reveals a conserved regulatory mechanism. *J. Cell Sci.* **122**, 2292–2299.
- Sutton, R. B., Fasshauer, D., Jahn, R. and Brunger, A. T.** (1998). Crystal structure of a SNARE complex involved in synaptic α resolution exocytosis at 2 . 4 Å. *Nature* **395**, 347–353.
- Suzuki, K. and Kono, T.** (1980). Evidence that insulin causes translocation of glucose transport activity to the plasma membrane from an intracellular storage site. *Proc. Natl. Acad. Sci. U. S. A.* **77**, 2542–2545.
- Takeda, H., Kawasaki, A., Takahashi, M., Yamada, A. and Koike, T.** (2003). Matrix-assisted laser desorption/ionization time-of-flight mass spectrometry of phosphorylated compounds using a novel phosphate capture molecule. *Rapid Commun. mass Spectrom.* **17**, 2075–2081.
- Tamori, Y., Kawanishi, M., Niki, T., Shinoda, H., Araki, S., Okazawa, H. and Kasuga, M.** (1998). Inhibition of insulin-induced GLUT4 translocation by Munc18c through interaction with syntaxin4 in 3T3-L1 adipocytes. *J. Biol. Chem.* **273**, 19740–19746.
- Tellam, J. T., McIntosh, S. and James, D. E.** (1995). Molecular identification of two novel Munc-18 isoforms expressed in non-neuronal tissues. *J. Biol. Chem.* **270**, 5857–5863.

- Tellam, J. T., Macaulay, S. L., McIntosh, S., Hewish, D. R., Ward, C. W. and James, D. E.** (1997). Characterization of Munc-18c and Syntaxin-4 in 3T3-L1 Adipocytes. *J. Biol. Chem.* **272**, 6179–6186.
- TerBush, D. R., Maurice, T., Roth, D. and Novick, P.** (1996). The Exocyst is a multiprotein complex required for exocytosis in *Saccharomyces cerevisiae*. *EMBO J.* **15**, 6483–6494.
- Toonen, R. F. G. and Verhage, M.** (2003). Vesicle trafficking: Pleasure and pain from SM genes. *Trends Cell Biol.* **13**, 177–186.
- Torrejón-Escribano, B., Gómez de Aranda, I. and Blasi, J.** (2002). SNARE expression and distribution during 3T3-L1 adipocyte differentiation. *FEBS Lett.* **512**, 275–281.
- Torreri, P., Ceccarini, M., Macioce, P. and Petrucci, T. C.** (2005). Biomolecular interactions by Surface Plasmon Resonance technology. *Ann. Ist. Super. Sanita* **41**, 437–41.
- Trimble, W. S., Cowan, D. M. and Scheller, R. H.** (1988a). VAMP-1: a synaptic vesicle-associated integral membrane protein. *Proc. Natl. Acad. Sci. U. S. A.* **85**, 4538–42.
- Trimble, W. S., Cowan, D. M. and Scheller, R. H.** (1988b). VAMP-1: a synaptic vesicle-associated integral membrane protein. *Proc. Natl. Acad. Sci. U. S. A.* **85**, 4538–42.
- Van Vliet, C., Thomas, E. C., Merino-Trigo, A., Teasdale, R. D. and Gleeson, P. A.** (2003). Intracellular sorting and transport of proteins. *Prog. Biophys. Mol. Biol.* **83**, 1–45.
- Verhage, M., Maia, A. S., Plomp, J. J., Brussaard, A. B., Heeroma, J. H., Vermeer, H., Toonen, R. F., Hammer, R. E., van den Berg, T. K., Missler, M., et al.** (2000). Synaptic assembly of the brain in the absence of neurotransmitter secretion. *Science*

(80-). **287**, 864–869.

- Villalba, M., Wente, S. R., Russell, D. S., Ahn, J. C., Reichelderfer, C. F. and Rosen, O. M.** (1989). Another version of the human insulin receptor kinase domain: expression, purification, and characterization. *Proc. Natl. Acad. Sci. U. S. A.* **86**, 7848–7852.
- Volchuk, A., Sargeant, R., Sumitani, S., Liu, Z., He, L. and Klip, A.** (1995). Cellubrevin is a resident protein of insulin-sensitive GLUT4 glucose transporter vesicles in 3T3-L1 adipocytes. *J. Biol. Chem.* **270**, 8233–8240.
- Volchuk, A., Wang, Q., Ewart, H. S., Liu, Z., He, L., Bennett, M. K. and Klip, A.** (1996). Syntaxin 4 in 3T3-L1 adipocytes: regulation by insulin and participation in insulin-dependent glucose transport. *Mol. Biol. Cell* **7**, 1075–82.
- Watanabe, T., Smith, M. M., Robinson, F. W. and Kono, T.** (1984). Insulin action on glucose transport in cardiac muscle. *J. Biol. Chem.* **259**, 13117–22.
- Watson, R. T., Khan, A. H., Furukawa, M., Hou, J. C., Li, L., Kanzaki, M., Okada, S., Kandror, K. V. and Pessin, J. E.** (2004). Entry of newly synthesized GLUT4 into the insulin-responsive storage compartment is GGA dependent. *EMBO J.* **23**, 2059–2070.
- Watson, R. T., Hou, J. C. and Pessin, J. E.** (2008). Recycling of IRAP from the plasma membrane back to the insulin-responsive compartment requires the Q-SNARE syntaxin 6 but not the GGA clathrin adaptors. *J. Cell Sci.* **121**, 1243–1251.
- Weber, T., Zemelman, B. V., McNew, J. A., Westermann, B., Gmachl, M., Parlati, F., Sollner, T. H. and Rothman, J. E.** (1998). SNAREpins: Minimal machinery for membrane fusion. *Cell* **92**, 759–772.
- Wei, M. L., Bonzelius, F., Scully, R. M., Kelly, R. B. and Herman, G. A.** (1998). GLUT4

and transferrin receptor are differentially sorted along the endocytic pathway in CHO cells. *J. Cell Biol.* **140**, 565–575.

Whyte, J. R. C. and Munro, S. (2002). Vesicle tethering complexes in membrane traffic. *J. Cell Sci.* **115**, 2627–2637.

Widberg, C. H., Bryant, N. J., Girotti, M., Rea, S. and James, D. E. (2003). Tomosyn interacts with the t-SNAREs syntaxin4 and SNAP23 and plays a role in insulin-stimulated GLUT4 translocation. *J. Biol. Chem.* **278**, 35093–35101.

Williams, D. and Pessin, J. E. (2008). Mapping of R-SNARE function at distinct intracellular GLUT4 trafficking steps in adipocytes. *J. Cell Biol.* **180**, 375–387.

Wimmer, C., Hohl, T. M., Hughes, C. A., Muller, S. A., Sollner, T. H., Engel, A. and Rothman, J. E. (2001). Molecular Mass, Stoichiometry, and Assembly of 20 S Particles. *J. Biol. Chem.* **276**, 29091–29097.

Wong, S. H., Xu, Y., Zhang, T. and Hong, W. (1998). Syntaxin 7, a novel syntaxin member associated with the early endosomal compartment. *J. Biol. Chem.* **273**, 375–380.

World Health Organization (2016). Global Report on Diabetes. 1–88.

Xu, Y., Zhang, F., Su, Z., McNew, J. a and Shin, Y.-K. (2005). Hemifusion in SNARE-mediated membrane fusion. *Nat. Struct. Mol. Biol.* **12**, 417–422.

Yamada, E., Okada, S., Saito, T., Ohshima, K., Sato, M., Tsuchiya, T., Uehara, Y., Shimizu, H. and Mori, M. (2005). Akt2 phosphorylates Synip to regulate docking and fusion of GLUT4-containing vesicles. *J. Cell Biol.* **168**, 921–928.

Yamada, E., Saito, T., Okada, S., Takahashi, H., Ohshima, K., Hashimoto, K., Satoh,

- T., Mori, M., Okada, J. and Yamada, M.** (2014). Synip phosphorylation is required for insulin-stimulated GLUT4 translocation and glucose uptake in podocyte. *Endocr. J.* **61**, 523–527.
- Yamaguchi, T., Dulubova, I., Min, S.-W., Chen, X., Rizo, J. and Sudhof, T. C.** (2002). Sly1 binds to Golgi and ER syntaxins via a conserved N-terminal peptide motif. *Dev. Cell* **2**, 295–305.
- Yamakawa, H., Seog, D.-H., Yoda, K., Yamasaki, M. and Wakabayashi, T.** (1996). Uso1 protein is a dimer with two globular heads and a long coiled-coil tail. *J. Struct. Biol.* **116**, 356–365.
- Yang, J., Clark, A. E., Harrison, R., Kozka, I. J. and Holman, G. D.** (1992). Trafficking of glucose transporters in 3T3-L1 cells trafficking proteins. *Biochem J* **281**, 809–817.
- Yang, C., Coker, K. J., Kim, J. K., Mora, S., Thurmond, D. C., Davis, A. C., Yang, B., Williamson, R. A., Shulman, G. I. and Pessin, J. E.** (2001). Syntaxin 4 heterozygous knockout mice develop muscle insulin resistance. *J. Clin. Invest.* **107**, 1311–1318.
- Yeaman, C., Grindstaff, K. K., Wright, J. R. and Nelson, W. J.** (2001). Sec6/8 complexes on trans-Golgi network and plasma membrane regulate late stages of exocytosis in mammalian cells. *J. Cell Biol.* **155**, 593–604.
- Yeh, T.-Y. J., Sbodio, J. I., Tsun, Z.-Y., Luo, B. and Chi, N.-W.** (2007). Insulin-stimulated exocytosis of GLUT4 is enhanced by IRAP and its partner tankyrase. *Biochem. J.* **402**, 279–290.
- Yokoyama, S., Shirataki, H., Sakisaka, T. and Takai, Y.** (1999). Three splicing variants of tomosyn and identification of their syntaxin-binding region. *Biochem. Biophys. Res. Commun.* **256**, 218–22.

Yu, H., Rathore, S. S., Lopez, J. a, Davis, E. M., James, D. E., Martin, J. L. and Shen, J. (2013). Comparative studies of Munc18c and Munc18-1 reveal conserved and divergent mechanisms of Sec1/Munc18 proteins. *Proc. Natl. Acad. Sci. U. S. A.* **110**, E3271-80.

Zeigerer, A., Lampson, M. A., Karylowski, O., Sabatini, D. D., Adesnik, M., Ren, M. and McGraw, T. E. (2002). GLUT4 retention in adipocytes requires two intracellular insulin-related transport steps. *Mol. Biol. Cell* **13**, 2421–2435.

Zerial, M. and McBride, H. (2001). Rab proteins as membrane organizers. *Nat. Rev. Mol. Cell Biol.* **2**, 107–117.

Zhao, P., Yang, L., Lopez, J. A., Fan, J., Burchfield, J. G., Bai, L., Hong, W., Xu, T. and James, D. E. (2009). Variations in the requirement for v-SNAREs in GLUT4 trafficking in adipocytes. *J. Cell Sci.* **122**, 3472–3480.